Antimicrobial Aggregates for the In-Situ Control of Microbially Induced Concrete Corrosion

By Alejandro Caicedo-Ramirez

B.S. Chemical Engineering, Universitat Politècnica de Catalunya, 2010

M.S. Molecular Biotechnology, Universitat de Barcelona, 2011

M.S. Environmental Engineering, University of Colorado Boulder, 2014

A thesis submitted to the

Faculty of the Graduate School of the

University of Colorado in partial fulfillment

of the requirement for the degree of Doctor of Philosophy

Department of Civil, Environmental, and Architectural Engineering

2018

Signature page:

This thesis entitled:
Antimicrobial Aggregates for the In-Situ Control of Microbially Induced Concrete Corrosion
written by Alejandro Caicedo-Ramirez
has been approved for the Department of Civil, Environmental, and Architechtural Engineering

_____
Mark Hernandez, Committee chair

_____
Sherri Cook, Committee member

Date_____

The final copy of this thesis has been examined by the signatories, and we
find that both the content and the form meet acceptable presentation standards
of scholarly work in the above mentioned discipline.

Abstract

Alejandro Caicedo-Ramirez (Ph.D., Civil Engineering)

Antimicrobial Aggregates for the In-Situ Control of Microbially Induced Concrete Corrosion

Thesis directed by Professor Mark T. Hernandez

Concrete is the most common material used to transport storm water and sewage in the world. It is used for pipes, culverts, tunnels and variety of other subterranean appurtenances. Municipalities, water utilities, and many agencies recognize that concrete corrosion is emerging as one of the most serious problems plaguing this critical infrastructure. The dominant form of concrete deterioration in wastewater conveyance systems is microbially mediated (Microbial Induced Concrete Corrosion: MICC). This type of corrosion occurs as a result of ubiquitous microbiological sulfur cycling within sewers: Below the waterline, sulfate present in wastewater is reduced to sulfide (H_2S) under anoxic conditions; this partitions into the headspace of pipes and other wastewater structures as H_2S gas, which serves as a substrate for biofilms of acidogenic sulfur-oxidizing bacteria (SOBs) above the waterline. These biofilms produce sulfuric acid, which chemically dissolve the cement binder and compromise the concrete structure. While current mitigation technologies focus their attention on developing acid resistant materials, little research has been done on limiting acidophile development in these environments. In response to the current research gaps in this arena, the central aim of my work was to study the effects of substituting metal-impregnated sorbents for a fraction of the fine aggregates traditionally used in cements – for the express purpose of inhibiting the bacterial communities responsible for the corrosion in sewer systems. Laboratory investigations evaluated the inhibition potential of selected heavy metals against SOB communities, and resolved minimum inhibitory concentrations, individually and in combinations. Parallel studies characterized different sorbents along with their metal desorption

profiles in response to biogenic acid. Field studies in the Denver Metropolitan wastewater collection system, then assessed anti-corrosion performance of cement mortar formulations with different loads of metal-impregnated sorbents.

Acknowledgements:

First and foremost, I would like to express my sincere gratitude to my advisor Prof. Mark T. Hernandez for his support throughout this journey. His guidance greatly contributed to the successful completion of this work, as well as my personal and professional growth. Thank you for continuously challenging my mind, for your patience, understanding, and empathy. I would not have pursued a PhD under any other mentorship. Be afraid not! Your cars are now safe.

I would also like to thanks my thesis committee: Prof. Sherri Cook, Prof., Prof. Zhiyong "Jason" Ren, Prof. Joseph Ryan, Prof. Wil V. Srubar, and Dr. Dennis Grubb. I was fortunate to expand and improve this work through the comments and observations of these outstanding academics and professionals.

My gratitude also goes to the funding sources that made this work possible. To the Balsells Fellowship Fund, the Generalitat de Catalunya, and specially, Mr. Pere Balsells i Jofre for giving me the unique opportunity to pursue a PhD in the USA. To the Civil, Environmental, and Architectural Engineering Department at the University of Colorado Boulder for awarding me with the Doctoral Assistantships for Excellence. To the state of Colorado for its Advanced Industries Accelerator Program grant, and to Phoenix Services LLC. for its economic support and material's supply.

Many people have contributed to the completion of this thesis. Dr. Alina Handorean who gave me the necessary skills for microbial extractions. Dr. Alison Ling who introduced me to the concept of microbial concrete corrosion and guided me during my first year as a graduate student. Dr. Natalie Hull who helped me in the analysis of DNA sequences. Dr. Fred Luiszer's excellent skills in the analysis of elements were an important contribution to this work. Enjoy Hawaii, you deserve it. My talented friend Dr. Juan Pablo Gevaudan who helped me to better understand cementitious materials. Dr. Ismael Justo-

Reinoso, my research teammate, a good friend (and excellent neighbor). Thank you for contributing to this work, for sharing ideas, and for helping me all these years. Mark Hofmeister and Metro Wastewater Reclamation District, whose collaboration (and patience) made possible the accelerated field test. Finally, many thanks to Dr. Ronald Harvey, Jennifer Underwood, and Paul Bilznik at USGS for training me in qPCR-related techniques.

I am grateful to have lived these years in Boulder surrounded by amazing people. Past and present Hernanditos who I could share lab experiences and engage in productive discussions. The Spanish crew who made me feel a little closer from home. My futbol teammates, running, and climbing companions. In this little town I had the immense luck to make friends from people from all around the globe. A thesis-long acknowledgement section would be needed to mention you all. Moving further away, I also want to thank the unconditional and ever-lasting friendship of the DiMaria and the Esplugues crews, whom I can always count on despite the distance.

I finish with the people I will always have in my heart: my family. My uncle Jorge, my aunt Maruja, and all my family in the USA. I cannot thank you enough for your love, care, and generosity. Nicollette, my love and partner in life. You make me a better human being, every day. Mamá and Papá, Juli and Quique, you are always in my thoughts with every important decision that I make. Your unconditional love and support is the reason why I have achieved this goal. This thesis is yours too.

Table of Contents

List of Tables

List of Figures

Chapter 1 Introduction and Scope

1.1 Rationale

Concrete is the most common material used to transport stormwater and sewage in the world. It is the primary material used in pipe, culverts, tunnels and variety of other appurtenances (e.g. manholes, lift stations, siphons). Municipalities, water utilities, and many agencies recognize that concrete corrosion is emerging as one of the most serious problems impacting this critical infrastructure. Wastewater collection systems in the United States consist of about 800,000 miles of sewers and 12 million wastewater manholes. Nearly a quarter of this infrastructure is over 40 years old, and over 80% is made entirely of concrete [1]. In 2016, The US Environmental Protection Agency (EPA) estimated the capital investment necessary to meet the quality standards on the Clean Water Act for new conveyance systems and existing conveyance system repair to be $44.5B and $51.2B, respectively [1]. Annual maintenance required for approximately 8,000 miles of wastewater sewers, costs $4.5B [2], $3.4B of which is spent on sewer rehabilitation [3]. These numbers are only expected to increase with projected construction estimates, the maintenance of aging pipes and improvements in infrastructure performance diagnosis. The dominant form of concrete deterioration in wastewater conveyance systems is microbially mediated (e.g. Microbially Induced Concrete Corrosion or MICC). Corrosion occurs as a result of ubiquitous microbiological sulfur cycling within wastewater collection systems. Sulfate present in wastewater is reduced to sulfide (H_2S) in anoxic biofilms below the waterline. This sulfur species can partition into the headspace of pipes and other wastewater structures as H_2S gas, which serves as a substrate for biofilms of acidogenic sulfur-oxidizing bacteria (SOB) above the waterline, most often on the crowns of sewer pipes. These biofilms produce sulfuric acid, the latter of which chemically attacks the cement binder and weaken the concrete structure [4, 5].

Current material-based mitigation solutions for this type of corrosion can be divided in four main types: a) use of corrosion-resistant pipe materials; b) surface coatings and linings; c) concrete binder additives; and, d) antimicrobial additives. The most common approaches are trenchless technologies, which do not require excavation and pipe replacement (e.g. sprayed cast concrete coatings, sprayed polymer coatings, casting new internal lining using an acid-resistant material) [2]. However, these mitigation strategies for MICC are neither long-term, cost-effective, and universal, nor do they address the root cause of this problem: acidogenic microbial activity. For example, cured-in-place acid resistant resins can have significant costs ($130-290 per linear feet), will require special curing conditions, and may not completely avoid gas infiltration and further corrosion beyond the polymeric layer [6].

Some researchers and concrete manufacturers have focused their attention on limiting acidophilic bacterial growth by superficially treating concrete with special admixtures or coatings, such as metal-loaded zeolites, with limited success for long term exposures and/or under aggressive corrosive environments [7-9]. For this approach to be cost-effective, inhibition must be sustained for years and not require external activation.

In response to the current research gaps in this arena, the central aim of this work was to evaluate the effects of substituting metal-impregnated sorbents (activated carbon and steel slag) for a fraction of the fine aggregates traditionally used in cements to intentionally inhibit the bacterial communities responsible for the corrosion in sewer systems. As a sustainable infrastructure approach, this mitigation strategy must meet two conditions: 1) be cost-effective compared to current practices; and, 2) it must incorporate recycled or upcycled materials.

In recent years, many investigations have been published on the development of low cost activated carbon from a broad range of source materials (e.g. agricultural wastes, fecal matter) [10, 11].

Activated carbon, with its high specific surface area, micro porous character, superficial chemical nature, and controlled grain size distribution, is a sorbent that can be used for the removal of heavy metals from different industrial wastewaters [12-14]. Similarly, steel slags have been studied as potential sorbents for heavy metals. These materials are an abundant granular byproduct of steel making worldwide. Historically considered a waste with little value, its alkaline composition and buffering capacity make it an excellent heavy metal sorbent through oxide-hydroxide complexation and surface precipitation [15-17].

Recent studies have focused their attention on the inhibitory effect some heavy metals can have on different acidophilic bacteria. There are some indications that acidophilic SOBs from sewer crowns are susceptible to relatively low concentrations of selected heavy metals – notably copper and cobalt [18, 19]. Collectively, this studies point to an opportunity where inhibitory metals spiked media (GAC, Slag) strategically incorporated into cement could inhibit acidophilic bacterial growth on concrete infrastructure surfaces.

1.2 Hypotheses

The overarching hypothesis driving this research is that **specific metals sorbed to activated carbon or steel slag grains entrained in cement, can significantly inhibit acidophilic bacteria growth responsible for MICC in sewer headspaces, thus increasing the functional life of sewer infrastructure in severely corrosive environments**. To this end, the following sub-hypotheses will be tested as proposed below:

Hypothesis I. Different metal ions have different inhibitory potential against acidophilic Sulfur Oxidizing Bacteria (SOB) present in sewer systems.

Hypothesis I a. A dose-response relationship can be established for selectively inhibiting acidophilic SOB. This manifests as dominance of neutrophilic communities sustaining a neutral pH range, when challenged under conditions that favor biogenic acid production.

Hypothesis I b. Metal association and release is a function of sorbent type and can be engineered to harbor a range of inhibitory metal species and host concentrations effective against the activities of planktonic and sessile SOB.

Hypothesis II. Metals laden sorbents will remain immobilized when mixed and cured with Portland cements such that no metal will leach in into virgin cement mixtures at the pH of cement. However, inhibitory metal doses will be locally available - on a microscale - in response to biogenic acid production on cement surfaces, and metal exposures can be engineered to be pH responsive, locally bioavailable as pH drops below predetermined levels.

Hypothesis II a. Acid functionalized activated carbon will be more efficient at mediating inhibitory metal doses in pH ranges relevant to acidophilic microbial activities (pH<5) but have a similar sorption capacity than its virgin activated carbon. Acid-modified activated carbon, impregnated with select metal ions, will bind/release metals in a pH dependent manner, preferably when acidophilic SOBs become active, acting as long-term metal reservoir for antimicrobial, and thus anti-corrosive effect.

Hypothesis II b. Steel slag of similar grain size distribution as fine aggregates, can also host metals when entrained in cement and exposed to biogenic acid, although its specific metal loading profile will be different than activated carbons, regardless of their modifications.

1.3 Research Approach

These hypotheses were challenged at three different scales of observation (Figure 1-1):

i) Laboratory scale, where metal toxicity was evaluated against acidophilic mixed cultures extracted from corroded sewers and grown in liquid and solid (agar).

ii) Pilot bioreactor scale, simulating corrosive environments typically found in sewer systems.

iii) Full Field in continuously operating sewers that presented an aggressively corrosive environment [4].

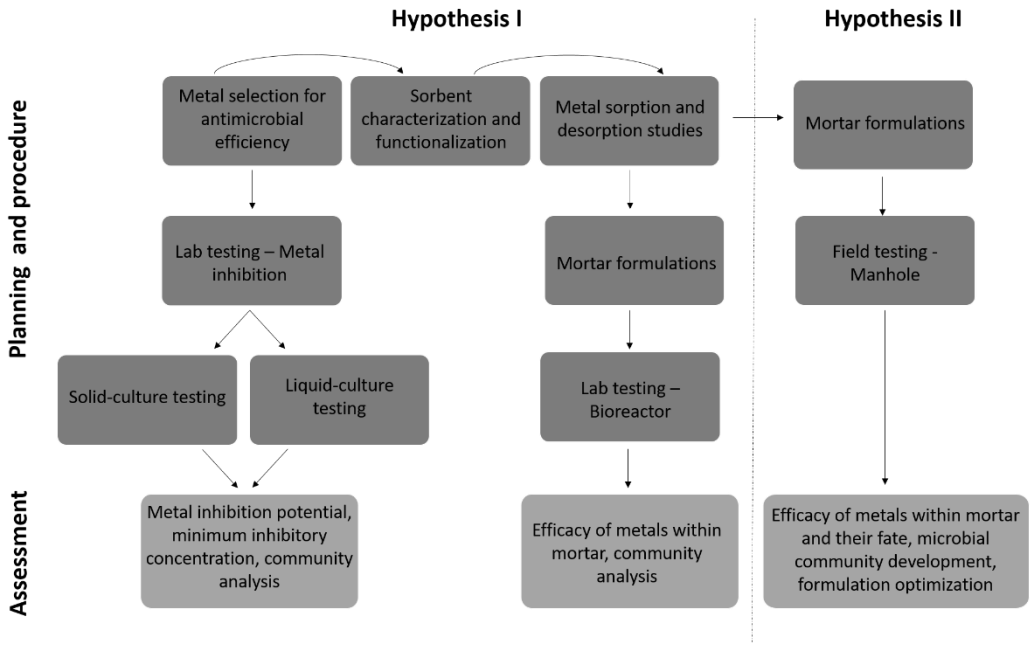

Figure 1-1. Flow chart of research approach and hypothesis testing.

1.3.1 Approach for Hypothesis I

Hypothesis I: **Different metal ions have different inhibitory potential against acidophilic Sulfur Oxidizing Bacteria present in sewer systems.**

The following objectives were used to challenged hypothesis I:

1) A set of heavy metals sorbed onto activated carbon were investigated for their inhibition potential against acidophiles enriched from sewer systems in agar formats.

2) The minimum inhibitory concentration and metal synergy of selected metals was observed in liquid enrichment cultures; microbial community composition was evaluated in response to different metal dosages.

3) Selected metal carriers, activated carbons and steel slag, were evaluated for their capacity to sorb-desorb heavy metals in solution and when entrained in cement. In the case of activated carbon, the effect of acid functionalization on heavy metal immobilization was studied.

1.3.2 Approach for Hypothesis II

Hypothesis II. **Metal laden sorbents will remain immobilized when mixed and cured with Portland cements such that no metal will leach in into virgin cement mixtures at the pH of cement. However, inhibitory metal doses will be locally liberated in response to biogenic acid production on microgram levels as engineered to be pH responsive, increasing local metal exposure as pH drops below predetermined levels.**

The following objectives were used to challenged hypothesis II:

1) Mortar formulations were prepared by replacing sand fractions for similarly-sized metal-sorbent grains. Micro-scale elemental study of cured formulations, chemical speciation, and mobilization studies were used to determine the fate of the antimicrobial metal within the cured mortar.

2) Acidification of activated carbon was designed to favor ionic metal adsorption at circumneutral pH, favoring desorption at a pH levels relevant to the onset of acidophilic growth.

3) Antimicrobial effect of mortar formulations was assessed in a lab scale reactor simulating the conditions found in severely corrosive environments.

4) A field study was executed by exposing mortar formulations to an actual corrosive environment in the field. Performance of each formulation was determined through microbiological, chemical, and physical assays.

Chapter 2 Review of Relevant Literature

2.1 Overview of Microbially Induced Concrete Corrosion

Microbially Induced Concrete Corrosion (MICC) is a well-documented, yet persistent problem that affects sewer systems around the globe. Its extent can be devastating; different investigators have studied the degree of surface deterioration on affected pipes, manholes and other appurtenances, reporting degradation rates between 1-10 mm per year [20-22]. The general degradation pathway starts with surface acidification by gases (H_2S and CO_2) partitioned from the wastewater and dissolved in the condensed water on the pipe crown. This enables surface acidification and conditioning for microbial colonization, which eventually succeeds towards acidophilic communities that produce significant amounts of sulfuric acid (H_2SO_4). The acid reacts with the cement matrix generating soft and structurally compromising products, gypsum ($CaSO_4$) being the predominant byproduct [20]. The overall process can be defined as a biologically-mediated sulfur oxidation spanning the complete sulfur cycle from H_2S to H_2SO_4 (Figure 2-1). A special characteristic about this type of corrosion is the lack of microbial diversity responsible for the accelerated production of H_2SO_4. Independently of the geographical location, as judged by both culture and phylogenetics, the dominant genus in corroded sewer systems has been consistently observed to be *Acidithiobacillus* [23, 24]. This genus is composed of obligate chemolithoautotrophic aerobes able to fix gaseous CO_2 and use reduced sulfur species and/or Fe^{2+} as electron donors. *Acidithiobacillus* has been extensively studied as they play a key role in biologically-mediated acid mine drainage, as well as corroding petroleum transport and wastewater infrastructures [25-27].

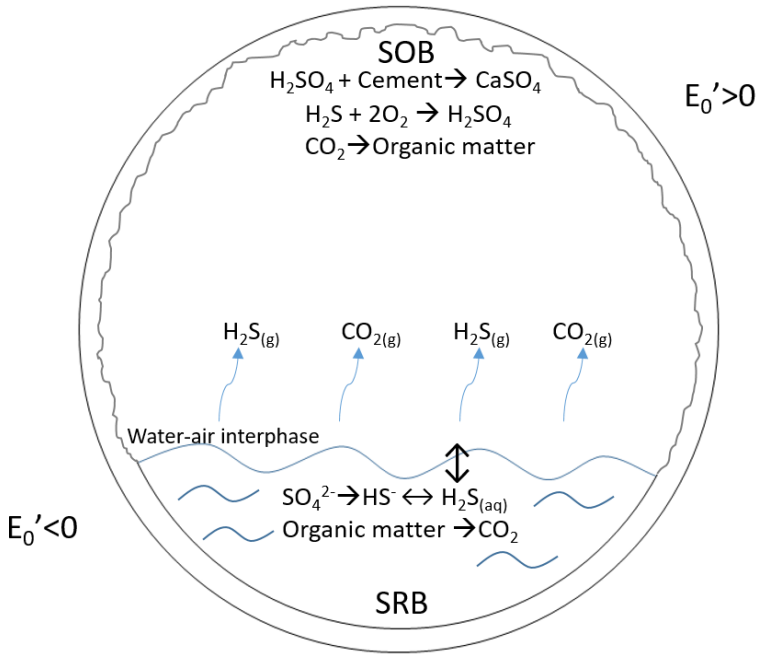

Figure 2-1. Schematic of MICC process on a cross-section of a concrete sewer pipe. Sulfur-reducing bacteria (SRB) are active in the sewage as biofilms; Sulfur-oxidizing bacteria (SOB) are active on the pipe surface above the water line; E_0' indicates the favorable redox potential for the reactions to occur.

2.2 Microbially Induced Concrete Corrosion in Sewer Systems

2.2.1 Biological Sulfur cycle

Sulfur is an essential element for all domains of life. It exists in various oxidation states taking part in critical organic and inorganic reactions (Table 2-1). Biologically-mediated sulfur transformations occur by assimilatory or dissimilatory mechanisms, depending on the metabolic role of sulfur within the cell (i.e. synthesis of sulfur-containing biomolecules or energy production) [28, 29].

Table 2-1. Oxidation state of inorganic sulfur compounds. Adapted from [30].

Oxidation state				
-II	**0**	**+II**	**+IV**	**+VI**
H_2S Hydrogen sulfide	S Elemental sulfur	(SO) Sulfur monoxide	SO_2 Sulfur dioxide	SO_3 Sulfur trioxide
HS^- Bisulfide	S_8 S^0	(H_2SO_2) Sulfoxylic acid	H_2SO_3 Sulfurous acid	H_2SO_4 Sulfuric acid
			SO_3^{2-} Sulfite	SO_4^{2-} Sulfate
	S----------SO_3^{2-} Thiosulfate			
H_2S----------SO_3 Thiosulfuric acid				
	S----------SO_3^{2-} | S----------SO_3 Tetrathionate			
H_2S----------S_n Polysulfane				
S^{2-}----------S_n Polysulfide				

The different sulfur species relevant to major metabolic pathways in bacteria is shown in Figure 2-2. Microbial transformations of sulfur are highly dependent on the redox potential and pH of the system. Under aerobic conditions, chemolitoautotrophy is the dominant mechanism for sulfur oxidation. In this context, microbes rely on inorganic carbon sources for substrate and oxidize reduced sulfur species to obtain energy. Well characterized wastewater bacteria that mediate sulfur chemolitoautotrophy, include *Beggiatoa* and *Thiotrix spp.*, and all *Thiobacillus* and *Acidithiobacillus spp.* Anoxic sulfur oxidation is a different oxidation pathway mediated by some photolitotrophic and chemolitotrophic species, including *Cyanobacteria* and *Chlorobiaceae spp*., and *Thiobacillus denitrificans* [31]. This metabolism is not considered a significant factor toward MICC.

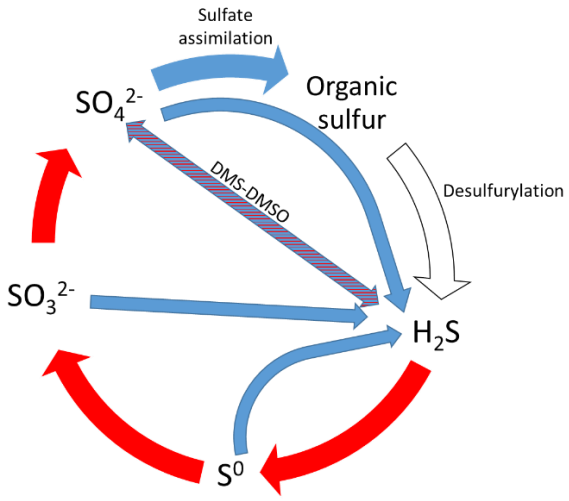

Figure 2-2. Simplified redox cycle for sulfur showing major species. Oxidations are shown in red arrows and reductions in blue. Transformations with no redox changes are in white. DMSO, dimethylsulfoxide; DMS, dimethylsulfide. Adapted from [28, 29].

At a global scale, Dimethyl sulfide (DMS) is an important molecule in the microbial sulfur cycle (Figure 2-3). It is produced from decomposition of dimethylsulfoniopropionate (DMSP) produced by algae. DMS can be chemically or biologically oxidized to dimethyl sulfoxide (DMSO), which in turn serves as a terminal electron acceptor in anaerobic environments, leading to reduction of DMSO to volatile DMS. When DMS is released to the atmosphere it can be photochemically oxidized to methyl sulfonates and sulfates, which serve as cloud condensation nuclei. This mechanism is relevant to the marine environment, accounting for global scale surface water temperature regulation [32]. In anoxic environments, DMS can be degraded in three ways: 1) methanogenesis (yielding CH_4 and H_2S), 2) as electron donor for photosynthetic CO_2 fixation in phototrophic purple bacteria (yielding DMSO), and 3) as an electron donor in for some chemoorganotrophs and chemolitotrophs (yielding DMSO) [28].

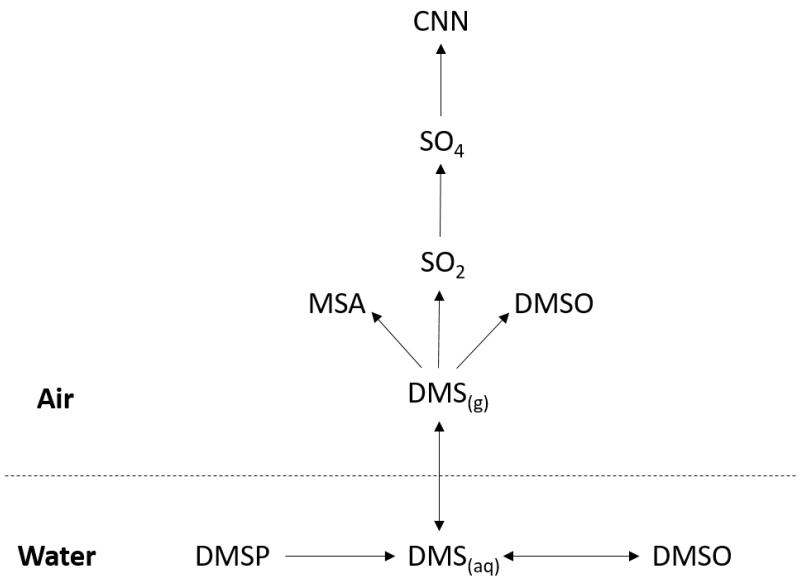

Figure 2-3. Simplified schematic of major transformations involved in the production of Dimethyl sulfide (DMS) and consequent cloud condensation nuclei (CNN). Algae-produced Dimethylsulfopropionate (DMSP) is decomposed to DMS, which in turn may be oxidize to Dimethyl sulfoxide (DMSO) in marine environments. DMS can partition and further decompose in Methyl sulfonates (MSA), DMSO, and Sulfur dioxide (SO_2). SO_2 further oxidizes to sulfate (SO_4), which promotes CNN formation.

In anoxic environments, oxidized sulfur species can be microbially reduced through respiration. Sulfur reducing microbes obtain energy by oxidizing organic compounds, or H_2, while using oxidized sulfur species as electron acceptors [28, 29, 31]. Examples of sulfur reducing bacteria include *Desulfolobus*, *Desulfovibrio*, and *Desulfobacter spp*. A ubiquitous mechanism of sulfur reduction is sulfate/sulfide assimilation. This is a basic mechanism of sulfur intake for the synthesis of proteins and other molecular sulfur-containing machinery, with the specific pathways varying according to the environmental redox potential (i.e. oxic or anoxic), and the organism involved (i.e. bacteria, archaea, fungi, plants) [31].

Sulfur disproportionation is a chemolitotrophic process in which some intermediate sulfur compounds serve as both electron donor and acceptors, yielding H_2S and SO_4^{2-}. Due to its similarity to carbon fermentation processes, this mechanism is described as inorganic fermentation. Bacteria able to disproportionate sulfur include sulfur reducing-related species like *Desulfovibrio*, *Desulfobacter*, and

Desulfococcus spp. [33]. Finally, desulfurylation is a common process in which organic reduced sulfur is decomposed into sulfide species without redox transformations [28, 29].

2.2.2 Sulfur fate and transport in sewer systems

Sewer infrastructure is a unique example of a built environment in which sulfur species undergo a complete redox cycle. The most abundant sulfur input to these systems is in the form of sulfates. For domestic wastewater, sources include drinking water and drinking water treatment byproducts, soaps and detergents, food waste, and excreted products. Dissolved sulfate is typically found in wastewater at concentrations between 24-72 mg/L [34]. Microbial sulfate transformations and kinetics depend on the wastewater composition and sewer design, and can be estimated through analysis of parameters such as the oxidation-reduction potential (ORP), dissolved oxygen (DO), dissolved nitrate (NO_3^-), pH, COD, and temperature along the sewer [35, 36]. Under aerobic conditions, sulfate concentration does not vary significantly, as existing microbial communities will use more energetically efficient electron acceptors for respiration purposes. This dominates when enough substrates are available and the oxidation potential is above +300 mV (Table 2-2). However, under anoxic conditions and in the absence of nitrate, existing sulfate undergoes microbially-mediated reductive transformations (Section 2.2.1). These redox conditions are met in sewer appurtenances with high residence time and/or low flow, which facilitate rapid DO consumption (i.e. storage tanks, pressurized sewers, low slope-gradient pipes) and sulfur reducing bacteria proliferation [20].

Table 2-2. Redox potential of representative electron donors and electron acceptors involved in electron transfer processes. E'_0 indicates the standard potential for the presented half-cell reactions at pH=7. Adapted from [37].

Redox couple	E'_0 (mV)
SO_4^{2-}/HSO_3^-	-516
CO_2/formate$^-$	-432
H^+/H_2	-414
$S_2O_3^{2-}/HS^- + HSO_3^-$	-402
CO_2/acetate$^-$	-290
S^0/HS^-	-270
CO_2/CH_4	-244
Acetaldehyde/ethanol	-197
Pyruvate$^-$/lactate$^-$	-190
$HSO_3^-/S_3O_6^{2-}$	-173
Oxaloacetate^{2-}/malate^{2-}	-172
HSO_3^-/HS^-	-116
Glycine/acetate$^-$ + NH_4^+	-10
$S_4O_6^{2-}/S_2O_3^{2-}$	+24
Fumarate/succinate	+33
$S_3O_6^{2-}/S_2O_3^{2-} + HSO_3^-$	+225
NO_2^-/NO	+350
NO_3^-/NO_2^-	+433
Fe^{3+}/Fe^{2+}	+772
O_2/H_2O	+818

A study by Tanaka et al. modeled the carbon and sulfur transformation occurring in different sewer lines. The authors concluded that under anaerobic conditions present in pressure sewers, the readily biodegradable substrates change little, an important factor to ensure denitrification and biological phosphorous removal at the wastewater treatment plant [36]. However, this also allows for increased sulfide formation and later partitioning, in response to pH and local hydrodynamic conditions. Persistence of hydrogen sulfide in the wastewater phase is highly dependent on dissolved oxygen (DO), pH, metal concentration, temperature, salinity, and the interfacial area between the liquid and air phases. When DO is above 0.5 mg/L, H_2S can be chemically oxidized [38]. If not enough oxygen is available, aqueous sulfide concentration can persist. Sulfide speciation in wastewater is pH- and pE-dependent. Of the three sulfide species (H_2S, HS^-, S^{2-}) only hydrogen sulfide can partition to the gaseous

phase. The equilibrium constant, or pKa, driving the formation of H_2S or HS^- is close to 7. At typical pH values for municipal wastewater, the equilibrium between hydrogen sulfide and bisulfide is significantly influenced by even moderate pH variations [35]. The dominance of sulfur species in aqueous phases at different at different pH/Eh is shown in Figure 2-4.

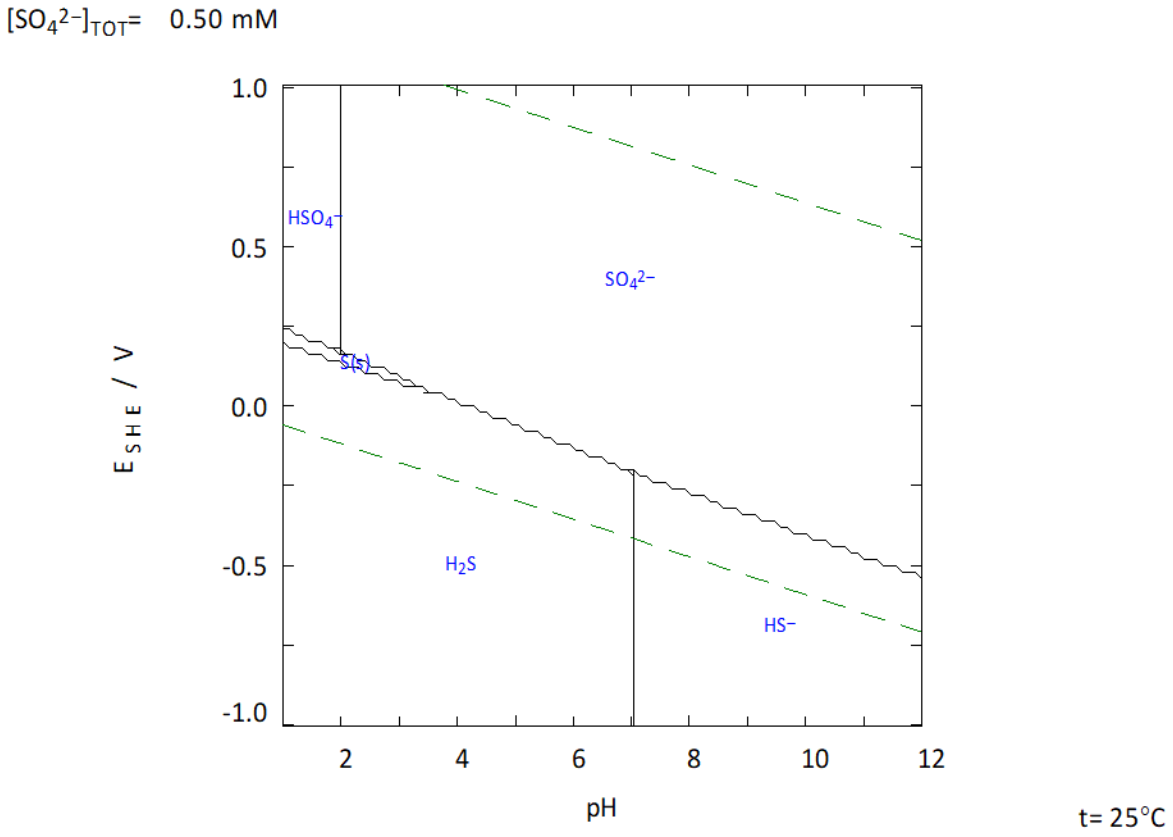

Figure 2-4. Pourbaix diagram for sulfur speciation in wastewater (0.5 mM) showing high dependence on both pH and E_{SHE}. Potential as measured with a standard hydrogen electrode (SHE).

The presence of heavy metals in wastewater can also limit the amount of dissolved sulfide through complexation and precipitation of highly insoluble metal sulfides. Due to current US regulations for wastewater discharge, metal-sulfur interactions are limited in domestic wastewater and does not contribute significantly to the overall sulfur transformations in collection systems [20]. Increased wastewater temperature not only drives accelerated microbial activity and consequent sulfide production, but also reduces aqueous solubility of H_2S. Additionally, H_2S partitioning is enhanced if the

sewer hydraulic design allows for increased turbulence and interfacial area between the liquid and the air phase. This typically occurs in manhole drops, or after wastewater is pumped from a lift station. Once released to the gaseous phase, H_2S can be transported out of the sewer through pressure differential, leading to harmful exposure and odor problems. Being dense gases, H_2S, and CO_2 can also remain within the sewer and dissolve into the condensate above the water line. This facilitates abiotic acidification and conditioning for subsequent SOB colonization. SOB are aerobic microbes that fix CO_2 and oxidize sulfur species to sulfuric acid as the end-product, completing the sulfur cycle initiated in the wastewater.

2.3 Concrete and Biogenic Corrosion Chemistry

2.3.1 Concrete and cement hydration

Concrete is the most common material used in sewer infrastructure. It is composed of a mixture of coarse and fine aggregates bonded together with a hardened mixture of water and cement [39]. Typical coarse aggregates include stone, recycled construction material, and slags, while fine aggregates include sand, and crushed gravel. Generally considered inert fillers, these aggregates are added in order to decrease the amount of cement used without compromising structural properties. The component responsible for most of the structural and durability properties is the binder, cement. Unhydrated cement can be considered as a mixture of simple oxides, CaO being quantitatively the most important [39]. Table 2-3 shows the major cations reported on an oxide and compound basis present in Portland cement, which is the most common type of cementitious material used in sewers.

Production of cement starts with the manufacture of the “clinker”. The clinker is generated by mixing raw materials (i.e. limestone, clay) to optimal proportions. This grinded mixture is then passed through a kiln where temperatures of 1,400-1,500 ◦C are reached. The process dehydrates the mixture, removes carbonates, and produces the major mineral forms in cement: alite, belite, tricalcium aluminate, and tetracalcium aluminoferrite. After cooling, pulverization of the formed nodules occurs

and a small fraction of gypsum is added to regulate the setting time, shrinkage, and strength development. The result is a powder of <45 μm particle size known as Portland cement [40].

Table 2-3. Composition of Portland cement expressed as oxide and compound mass percentage (wt%).

Oxide	*wt %*	Compound	wt%
CaO	*61-67*	$3CaO.SiO_2$	13-34
SiO_2	*18-24*	$2CaO.SiO_2$	45-75
Al_2O_3	*2.5-7*	$3CaO.Al_2O_3$	3-15
Fe_2O_3	*0-6*	$4CaO.Al_2O_3.Fe_2O_3$	0-18
MgO	*0-4.5*		
SO_3	*1.5-5*		

While a variety of Portland cement types exist, the general hydration reactions are the same. When water is added to the cement powder, hydration reactions are initiated (Table 2-4). Tricalcium silicate, the most abundant compound, reacts rapidly to form the hardened products calcium silica hydrate (C-S-H) and calcium hydroxide. This reaction is responsible for the early strength gain of the paste. Dicalcium silicate hydration is slower, also producing C-S-H and calcium hydroxide. The reaction is responsible for paste strength increase after one week. Tricalcium aluminate hydration releases significant heat during the firsts days of reaction. This compound reacts with gypsum, producing ettringite. Formation of ettringite delays solid phase setting that would otherwise occur from the fast hydration kinetics of tricalcium aluminate. In addition, sulfate helps control drying shrinkage which could otherwise generate internal pressures and cracking. Once sulfate is depleted, remaining tricalcium aluminate starts to react with ettringite, yielding monosulfoaluminates. Tetracalcium aluminoferrite hydration generates calcium hydroxide and hydrated forms of the same compound. It contributes little to the material's strength. As previously stated, major hydration products include C-S-H, calcium hydroxide, ettringite and monosulfoaluminate [39-41]. Figure 2-5 shows the time-dependent variation in relative volume of the major hydrated products in Portland cement.

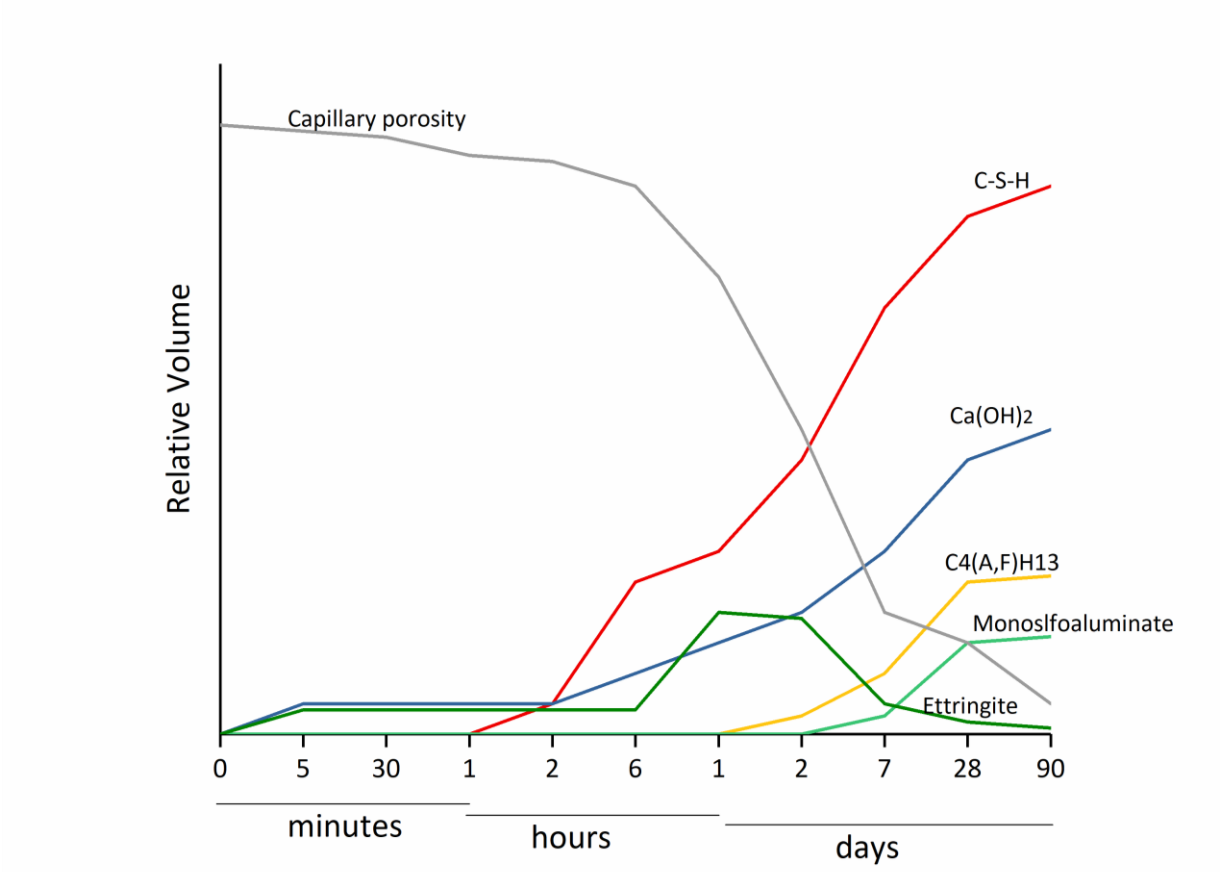

Figure 2-5. Relative volumes of most common hydration products of Portland cement pastes as a function of time. C-S-H refers to calcium silicate hydrate, and C4(A,F)H13 refers to tertacalcium aluminoferrite hydrated compounds as for cement nomenclature. Adapted from[40].

C-S-H is an amorphous calcium silica based gel of general formula $xCaO.SiO_2.yH_2O$, where subscripts x and y may vary significantly. It acts as the main binding phase and provides cohesiveness to the matrix. Its structure is not well understood, and is hypothesized to be similar to that of tobermorite and jennite [39, 41], both calcium silicate-based minerals. This configuration is thought to be achieved through increasing polymerization of SiO_4 units with increasing hydration [39]. The average chain length of mature pastes is in the range 2.5−3.0 SiO_4 units [42]. Calcium hydroxide [$Ca(OH)_2$] is evenly precipitated in the form of crystals of Portlandite. These compounds do not provide strength properties to the matrix and reactions with external agents can lead to deleterious effects on the hardened paste, but provide significant pH buffering. Calcium sulfoaluminate phases in hydration products include

ettringite and monosulfoaluminate. Ettringite is a needle shaped mineral with the general formula $6CaO.Al_2O_3.3SO_3.32H_2O$. This mineral is formed in the firsts days of hydration until all $CaSO_4$ is depleted. Then, unhydrated tricalcium aluminate starts to react with ettringite, dissolving the latter and generating calcium monosulfoaluminate. This hexagonal-shaped mineral has a general formula $4CaO.Al_2O_3.SO_3.12H_2O$. Neither ettringite or monosulfoaluminate contribute significantly to the paste's strength. Moreover, external sulfates can react with these cement phases creating expansive reactions that lead to increased internal pressures and ultimate cracking [39-41].

Table 2-4. Major hydration reactions in Portland cement (oxide notation). Adapted from [40].

$2(3CaO.SiO_2) + 11\ H_2O$ Alite	→ $3CaO.2SiO_2.8H_2O + 3\ (CaO.H_2O)$ C-S-H + Calcium hydroxide
$2(2CaO.SiO_2) + 9\ H_2O$ Belite	→ $3CaO.2SiO_2.8H_2O + CaO.H_2O$ C-S-H + Calcium hydroxide
$3CaO.Al_2O_3 + 3\ (CaO.SO_3.2H_2O) + 26\ H_2O$ Tricalcium aluminate + Gypsum	→ $6CaO.Al_2O_3.3SO_3.32H_2O$ Ettringite
$2(3\ CaO.Al_2O_3) + 6\ CaO.Al_2O_3.3SO_3.32H_2O + 4\ H_2O$ *Tricalcium aluminate + Ettringite*	→ $3\ (4CaO.Al_2O_3.SO_3.12H_2O)$ Calcium monosulfoaluminate
$3CaO.Al_2O_3 + CaO.H_2O + 12\ H_2O$ *Tricalcium aluminate + Calcium hydroxide*	→ $4CaO.Al_2O_3.13H_2O$ Tetracalcium aluminate hydrate
$4CaO.Al_2O_3.Fe_2O_3 + 2\ (CaO.H_2O) + 10\ H_2O$ *Tetracalcium aluminoferrite + Calcium hydroxide*	→ $6CaO.Al_2O_3.Fe_2O_3.12H_2O$ Calcium aluminoferrite hydrate

The volume of water added to the cement's paste is replaced by hydration products over time. The presence of water beyond that required for these reactions leads to increased capillary porosity, negatively affecting the strength of the hardened paste and increasing the diffusivity of detrimental chemicals, including biogenic acids, if exposed [40].

2.3.2 Biogenic sulfate attack on concrete

Once concrete sewer pipes enter service, the corrosion process is initiated. Progressive surface acidification results by exposure from H_2S and CO_2 gases, which eventually lower pH from 12-13 to 9-7. This is a slow abiotic process that has little impact on the material's integrity, and superficial deposition of sulfites, elemental sulfur and carbonates occur [43]. At circumneutral pH, microbial colonization occurs. The dominant SOB communities during this phase are neutrophilic sulfur oxidizing microorganims (NSOM) that oxidize the reduced sulfur species to partially oxidized forms (i.e. S^0 and $S_2O_3^{2-}$), but can also produce sulfate (SO_4^{2-}). This, coupled with the excretion of organic acids by bacteria, suppress the pH below 4, inducing a shift in the microbial ecology. At this stage, acidophilic sulfur oxidizing microorganisms (ASOM) become the dominant microbial group. These SOBs are responsible for accelerated SO_4^{2-} production in the form of sulfuric acid, which readily reacts with the cement matrix in a process called biogenic sulfate attack. This type of microbially-mediated deterioration is characterized by the deleterious reactions of SO_4^{2-} and hydronium ions (H^+) with the hydration products of cement. Chemical sulfate attack is characterized by the reaction of external sulfate sources with cement (Table 2-5). For example, sodium and calcium sulfates can penetrate pores and react with monosulfoaluminates to reproduce undesirable amounts of ettringite, causing swell, cracking and opening up porosity. Sodium sulfate can also react with calcium hydroxide to produce additional calcium sulfate and sodium hydroxide. When local monosulfoaluminate is depleted, SO_4^{2-} ions can react with calcium and water to produce gypsum. This reaction uses calcium from remnant $Ca(OH)_2$ and through decalcification of the C-S-H [44, 45]. Unhydrated remaining compounds are also susceptible to sulfate attack. Alite can react with sulfates and produce gypsum while unreacted tricalcium aluminate will lead to the same end products as attacked monosulfoaluminates [44, 45]. Overall, these reactions change the internal pressure of the material (leading to cracking), decalcification of the C-S-H binder, and production of granulated and structurally weak products (i.e. gypsum). Interestingly, these reactions are

associated to chemical shrinkage, rather than the local expansion of the corroded products. This is because sulfated products formed after curing can have a bigger spatial configuration than their unhydrated counterparts; crystal growth causes unwanted internal pressures, and ion mobilization from uncorroded to corroded areas generate expansive osmotic pressures [46].

Table 2-5. External sulfate attack reactions on major hydrated cement compounds. Adapted from [39].

<u>Sodium sulfate reactions</u>	
$Ca(OH)_2 + Na_2SO_4.10H_2O$ Calcium hydroxide + Sodium Sulfate	$\rightarrow CaSO_4.2H_2O + 2\ NaOH + 8\ H_2O$ Calcium sulfate + Sodium hydroxide + water
$3CaO.Al_2O_3.12H_2O + 3\ (CaSO_4.2H_2O) + 14\ H_2O$ Tricalcium aluminate hydrate + calcium sulfate + water	$\rightarrow 3CaO.Al_2O_3.3CaSO_4.32H_2O$ Ettringite
$2(3CaO.Al_2O_3.12H_2O) + 3\ (Na_2SO_4.10H_2O)$ Tricalcium aluminate hydrate + Sodium sulfate	$\rightarrow 3CaO.Al_2O_3.3CaSO_4.32H_2O + 2\ Al(OH)_3 + 6\ NaOH + 17\ H_2O$ Ettringite + Aluminum hydroxide + Sodium hydroxide + water
<u>Magnesium sulfate reactions</u>	
$Ca(OH)_2 + MgSO_4$ *Calcium hydroxide + Magnesium sulfate*	$\rightarrow CaSO_4 + Mg(OH)_2$ Calcium sulfate + Magnesium hydroxide
$3CaO.Al_2O_36H_2O + 3MgSO_4$ *Tricalcium aluminate hydrate + Magnesium sulfate*	$\rightarrow 3CaSO_4 + 2\ Al(OH)_3 + 3\ Mg(OH)_2$ Calcium sulfate + Aluminum hydroxide + Magnesium hydroxide
$3CaO.SiO_2.2H_2O + 3MgSO_4.7H_2O$ *C-S-H + Magnesium sulfate*	$\rightarrow 3(CaSO_4.2H_2O) + 3\ Mg(OH)_2 + 2\ SiO_2$ Calcium sulfate + Magnesium hydroxide + Silicon oxide
<u>Sulfuric acid reactions</u>	
$Ca(OH)_2 + H_2SO_4$ *Calcium hydroxide + Sulfuric acid*	$\rightarrow CaSO_4.2H_2O$ Calcium sulfate
$3CaO.Al_2O_3.12H_2O + 3\ (CaSO_4.2H_2O) + 14H_2O$ Tricalcium aluminate hydrate + Calcium sulfate + water	$\rightarrow 3CaO.Al_2O_3.3CaSO_4.32H_2O$ Ettringite
$3CaO.Al_2O_3.3CaSO_4.32H_2O$ Ettringite	$\rightarrow CaSO_4 + Al_2(SO_4)_3$ (pH<10) Calcium sulfate + Aluminum sulfate
$3CaO.SiO_2.2H_2O + H_2SO_4$ *C-S-H + sulfuric acid*	$\rightarrow CaSO_4 + Si(OH)_4 + H_2O$ Calcium sulfate + silicic acid + water

Biogenic sulfate attack couples these sulfate-based reactions with acidification by hydronium ions. H^+ can easily penetrate concrete and dissolve solid hydration products within the binder. Hydroxyl ions contained in the hydration products are, in effect, neutralized by the protons. Calcium, iron, aluminum as well as sulfate ions enter the pore solution and diffuse toward the concrete surface. A highly porous corroded layer then develops, consisting of hydrated silicates, ettringite, and gypsum [47]. In contrast to chemical tests of sulfuric acid attack on concrete, in which a passivation layer of gypsum is formed, biological production of the acid leads to the formation of a porous gypsum layer which allows for acidophilic microbial colonization at further concrete depths (as far as oxygen and sulfide can diffuse), which in turn leads to increased production of sulfuric acid and increased corrosion penetration [48]. In this way, the progressive failure of concrete occurs. It is therefore strategic to inhibit the proliferation of acidophilic bacteria, and the release of heavy metals in the vicinity of pH=4, thus pre-emptying their dominance.

2.4 Current Mitigation Technologies

Since it was first detected in sewer systems, effective mitigation solutions against MICC have been the focus of many investigations. Strategies to reduce the corrosion impact are divided in three major groups according to the targeted phase: wastewater, gaseous space, and solid surfaces. Common strategies are summarized in Table 2-6.

Table 2-6. General strategies to limit the extent of MICC according to the targeted phase (wastewater, headspace, surfaces).

Wastewater	Headspace	Surfaces
Preventive – Limit influent SO_4^{2-} sources Preventive – Improve hydraulic design of sewer lines (low turbulence)	Forced ventilation to reduce H_2S concentration and improve aeration	H_2SO_4 resistance – OPC* Concrete mix design optimization H_2SO_4 resistance – Use of SCM* blends
H_2S oxidation – Addition of oxidants		H_2SO_4 resistance – Use of alternative cementitious materials
H_2S partitioning – pH adjustment		H_2SO_4 resistance – Use of synthetic polymeric materials
H_2S precipitation – Addition of metals		Antimicrobial – Use of antimicrobial sprays
Antimicrobial – Addition of oxidants to limit SRB growth		Antimicrobial – Use of antimicrobial admixtures or aggregates
Antimicrobial – pH shock treatment		

* OPC: Ordinary Portland Cement
* SCM: Supplementary Cementitious Materials

2.4.1 Sulfide production prevention and strategies at the wastewater level

Preventive solutions can be applied based on the wastewater composition and conveyance system design. A study by Pikaar and coworkers [49] attributed a significant fraction of the dissolved sulfate in domestic wastewater to aluminum sulfate (alum) addition used for drinking water treatment. Alum is the most common coagulation agent used in drinking water treatment in countries with developed economies. The study revealed that as much as 52% of the total sulfate in wastewater originated from the use of this coagulant. Transition to non-sulfate based coagulants can have a significant impact in the total sulfate concentration, therefore limiting H_2S produced in sewers and ultimately slowing biogenic corrosion rates.

Improved hydraulic design of new and existing sewer infrastructure, is another preventive measure to minimize sulfide generation and partitioning. H_2S production is favored under anaerobic conditions – low flow velocity, long residence time, and low dissolved oxygen (DO). Designing pipe slopes to induce turbulence favors sewage aeration and reduces solids deposition which contributes to sulfate reducing conditions. Limiting the use of force mains and siphons, and avoiding excessive detention times in wet wells and holding tanks can help limit sulfide concentrations in the water and pipe headspace [20, 22].

Other strategies for sulfide mitigation focus on limiting sulfur-reducing bacteria (SRB) activity and/or oxidizing H_2S before it partitions into the gaseous phase. Direct addition of chemicals into wastewater can be used to prevent the activity of SRB, which are responsible for the transformation of sulfate into sulfide. Air or oxygen injection to increase oxygen levels above DO > 0.5 mg/L can limit SRB activity, therefore mitigating sulfide production in sewers [20]. Addition of nitrate salts is another sulfide mitigation method which leverages redox control to favor nitrate reducing conditions [22]. pH shock can also be used to inhibit SRB activity. According to the EPA, this guidance procedure involves adding sodium hydroxide to increase wastewater pH above 12 for a period of 20-30 minutes, significantly inhibiting SRB activity up to 2 weeks; however, the alkaline wastewater has to be isolated and diluted back into the main collection system to avoid potential disruptions to normal WWTP operations [20]. Other approaches to contain sulfide which is already present in wastewater include dosing oxidants, enhancing sulfide precipitation, and adjusting wastewater pH. O_2, $KMnO_4$, NaOCl are common oxidants applied in order to change the oxidation-reduction potential (ORP) of the system to values above that of the redox couple SO_4/H_2S (-0.22 mV) [22]. This leads to chemical oxidation of sulfide to sulfate, preventing the latter from reaching the gas phase. Addition of iron salts has been commonly practiced to precipitate insoluble sulfides *in situ*. This approach relies on the fact that most metal-sulfide complexes can be rapidly formed and are highly insoluble. Both ferric (III) and ferrous (II) forms of iron

are practical and effective for this purpose [22, 50]. However, these approaches carry formidable reagent costs. Implementation of the Water Quality Act of 1987 resulted in a substantial drop in wastewater metal concentration across the USA. The unintended consequence was that dissolved sulfide concentrations increased in sewers and promoted concrete corrosion. Two factors account for this effect: 1) the existing metal concentrations prior implementation of the Act were sufficient to complex and/or precipitate dissolved sulfide in sewers; and/or, 2) the elevated metal concentrations provided an inhibitory effect against SRB communities [20]. Iron salts, especially ferric chloride, are used to supplement the metal load required to immobilize sulfide species present in sewers, that might have been otherwise precipitated by other metals before strict regulations for wastewater discharge were implemented in 1987. Additional approaches to control sulfide partitioning in sewers are through adjusting wastewater pH. Aqueous sulfide speciation is pH dependent (Figure 2-4). The pKa_1 of hydrogen sulfide ($H_2S \leftrightarrow HS^- + H^+$) is close to 7; therefore, adjusting wastewater above pH 8 can limit the amount of hydrogen sulfide partitioning into the gas phase. Combination of the above strategies is advantageous for long lasting effects to be realized [51]. However, each approach requires continuous chemical addition into the wastewater and can result in significant operational costs depending on sewage flows to be treated.

Ventilation can also remove hydrogen sulfide gas from sewer headspaces. This approach is used in WWTP where air is withdrawn from the headspace and either treated separately or piped to an existing biological processes [20]. Ventilation for conveyance systems is limited by the costs associated to mechanical ventilation, relatively short term effectiveness, and the discharge of H_2S to the ambient surroundings.

2.4.2 Materials used to mitigate corrosion in exposed surfaces

Hydrogen sulfide gasses in sewer headspaces cannot always be controlled; thus corrosion mitigation strategies of exposed pipe surfaces are often applied. The simplest and least expensive approach is to optimize the concrete's mix design to resist MICC. Concrete characteristics that influence the extent of sulfuric acid attack include: cement content, water/cement ratio, cement type, and aggregate type, and pH buffering capacity [52]. As cement content increases, more calcium is available to react with sulfuric acid to form gypsum and ettringite, resulting in increased corrosion rates [53]. It is generally accepted that a low water-to-cement ratio (w/c) reduces porosity and permeability, making ion diffusion through the cement matrix more difficult. However, conflicting results on the use of low and high w/c ratios for sulfuric acid resistance have been reported [53-57]. Some studies indicate better performance against sulfuric acid when using a w/c >0.4. Two reasons can account for this behavior: a lower w/c ratio, by increasing cement content, may result in more available reactive calcium, which in turn could lead to increased corrosion rates; and, a higher w/c may result in relatively more space for expansive products (i.e. gypsum) to relocate, avoiding internal pressures and creating a passivation barrier, upon exposure to sulfates [53-55]. Nevertheless, other studies and field applications indicate that low w/c ratios can be effective as well, and are commonly used to limit the extent of biological sulfuric acid corrosion in sewer pipes [56, 57]. Using different types of Portland cement, can also improve corrosion resistance. ASTM C150 specifies two types of Portland cement for moderate and severe sulfate attack, type II and V respectively [58]. These cements are characterized by having a low tricalcium aluminate content: <8% for type II, and <5% for type V. Sulfates react with hydrated tricalcium aluminate resulting in expansion and cracking of concrete. Therefore, limiting its content results in lower amounts of expansive sulfated products [39, 40].

Improvements on Ordinary Portland Cement (OPC) mixture's design can mitigate corrosion to a limited extent. Additional resistance can be gained by adding supplementary cementitious materials

(SCM), or by replacing the use of Portland cement as the major cementitious binder. Other cementitious materials used for biogenic corrosion resistance include: fly ash, silica fume, metakaolin, ground granulated blast furnace slag (GGBFS), and calcium aluminate cement (CAC) (Table 2-3).

Table 2-7 Composition of common cementitious materials and SCMs expressed as oxide mass percentage (%) [59-62].

Type	SiO_2	Al_2O_3	CaO	Fe_2O_3	MgO	$Na_2O + K_2O$	SO_3
OPC	23.4	5.1	63.4	1.9	1.3	0.8	2.1
Fly ash	54.7	22.8	8.9	7.4	1.8	1.3	-
Silica fume	86.5	0.4	0.3	3.6	0.4	1.0	-
Metakaolin	52.0	43.0	0.2	2.2	0.1	0.6	-
GGBFS	35.5	15.4	34.0	1.0	9.4	1.0	2.5
CAC	4.4	39.5	37.6	15.1	0.7	0.2	-

Fly ash is the most often used SCM in Portland cement infrastructure. This fine byproduct from coal combustion is composed of spherical-like particles of SiO_2, Al_2O_3, and in some cases fractions of CaO. Replacement of OPC with fly ash leads, upon hydration, to formation of a dense matrix of C-S-H and calcium aluminosilicate gels (C-A-S-H) with lower free $Ca(OH)_2$ content due to hydration reactions between the two pozzolans. This results in increased resistance to sulfuric acid attack [59, 63, 64]. Similarly, silica fume reduces the deleterious effects of sulfuric acid exposure. This byproduct of the silicon and ferrosilicon alloy production is also based on spherical particles composed mostly of SiO_2. Its high surface area allows for high reactivity when mixed with Portland cement, resulting in a lower Ca/Si ratio C-S-H gel [59, 63, 64]. Another commonly used pozzolan is metakaolin. This SCM results from the calcination of kaolinite-rich soils. Al_2O_3 and SiO_2 are the major constituents and hydration reactions with OPC result in C-S-H and C-A-S-H gels, similarly to the use fly ash [59, 65]. A slightly different SCM used in the cement industry is ground granulated blast furnace slag (GGBFS). GGBFS is the major byproduct of the steel making industry. More similar in composition to OPC than previously described SCMs, it provides some level of corrosion protection while offering improvement to some structural properties.

GGBFS induces some hydrated products similar to those from fly ash and silica fume, but due to the higher CaO content, these products are realized only at higher supplement levels [64]. However, its lower efficacy against sulfuric makes its use limited [61]. The nature of the dominant structural gels formed during cement hydration can be predicted by the proportion of SiO_2, Al_2O_3, and CaO in the cementitious blend (Figure 2-5). A rational blend design can maximize acid resistance by formation of durable gels while maintaining reasonable structural properties. More recently, this includes the combination of different SCMs in ternary and quaternary blends. It is argued that improved durability can be achieved through optimal design of such blends, as observed by improved performance against sulfuric acid [66].

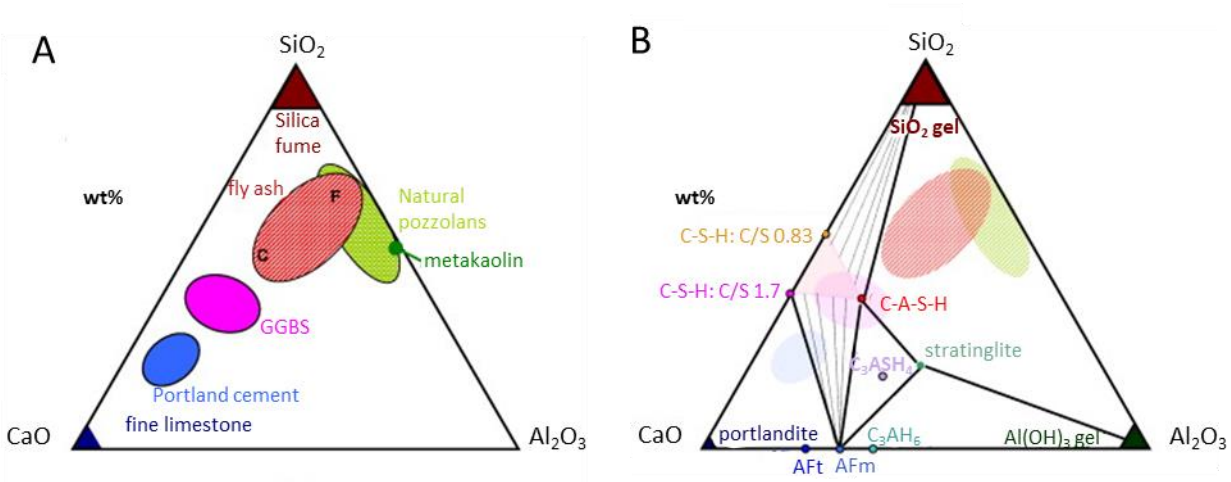

Figure 2-6. A) $CaO–Al_2O_3–SiO_2$ ternary diagram of cementitious materials, B) hydrate phases in the $CaO–Al_2O_3–SiO_2$ system with OPC. Aft and AFm correspond to ettringite and monosulfoaluminate, respectively. C_3AH_6 and C_3ASH_4 account for trialcium aluminate hydrate and tricalcium sulfoaluminate hydrate according to widely-accepted cement nomenclature, respectively. Adapted from [64].

A special case for enhancing cement corrosion resistance is the use of calcium aluminate cements (CAC). CAC contain CaO and Al_2O_3 as the major oxides, with little to no silica content. Major hydration products include tricalcium aluminate hydrate and aluminum hydroxide. When exposed to acid, tricalcium aluminate hydrate dissolves into Ca^{2+} and highly insoluble aluminum hydroxide. Below pH 3-4, aluminum hydroxide dissolves, releasing Al^{3+}. Initial aluminum hydroxide deposition and

formation of sulfate salts, resulting from H_2SO_4 attack, can lead to formation of a passivation barrier, which in-turn limits diffusion of additional acid deeper into the matrix [67]. Laboratory and field studies have shown better durability than OPC under biogenic acid attack conditions [7, 67].

Advances in the study of geopolymers, have led to the development of alkali-activated cements (AAC). AACs are made by mixing solid aluminosilicate powders such as fly ash, blast furnace slag, metakaolin, or combinations of these materials with an alkaline activating solution, typically of alkali metal hydroxides or silicates [68, 69]. If designed properly, AACs can offer significantly better structural and durability performance than regular OPC. With AACs, the polymeric nature of the hydrated gel depends on the powdered precursors and activators, but often consists of polymeric bonds of Si-O-Si and Si-O-Al units charged-stabilized by alkali metals (i.e Na^+) or alkali earths (i.e. Ca^{2+}). The resulting gels are either sodium dominant (N-A-S-H) or calcium dominant (C-A-S-H) [68, 70]. According to Allahverdi et al. [71], the corrosion mechanism of geopolymeric pastes at relatively high concentrations of sulfuric acid starts with an ion exchange reaction between the charge-compensating cations of the framework (Na^+, Ca^{2+}) and H_3O^+ ions from the solution, along with an electrophilic attack by protons on polymeric Si−O−Al bonds. This process results in dealumination: ejection of tetrahedral aluminum from the aluminosilicate framework. The second step of the corrosion process varies depending on the nature of the dominant gel formed. For N-A-S-H gels, acid diffusion will increase the degree of dealumination. For C-A-S-H gels, the exchanged Ca^{2+} diffusing toward the acid solution will react with SO_4^{2-} resulting in the formation and deposition of gypsum inside a corroding layer, providing a protective effect which can inhibit the deterioration process. N-A-S-H gels appear to degrade less when confronted with sulfuric acid than their C-A-S-H counterparts, mostly due to their low calcium content. However, at least some calcium content is desired to help form a passivation barrier that limits ion diffusion into the interior cement matrix. Further, hydrated C-A-S-H gels generate a denser matrix and offer improved structural properties over N-A-S-H gels. Ultimately, a durable and strong AAC binder will include an optimal ratio of

the two gels, have an advanced degree of polymerization, as well as a smaller pore size distribution [69, 71-73]. Overall, development of cementitious materials intended to increase resistance to sulfuric acid is through using materials that: 1) are highly alkaline; 2) generate dense, acid impermeable byproducts; and/or, 3) have a low reactivity against H_2SO_4. However, no AAC material is completely immune to continuous acid exposures and will eventually succumb to corrosion problems if *in-situ* acid production is not controlled.

Historically, development of new cementitious materials has focused on creating acid-resistant binders. While the nature of the acid produced during MICC is biogenic, few studies have focused in developing admixtures that can provide a lasting inhibitory effect against acidophilic microorganisms responsible for MICC. Among these, different approaches have been tested but few have reached commercialization. Sun et al. [74] sprayed free nitrous acid on an active acidophilic biofilm growing on concrete samples in a controlled chamber. After treatment, they observed H_2S uptake decrease 84% - 92% after 15 days, without any obvious recovery of SOB activity after 12 months. Other material-based studies focused their attention in the effect of adding specific chemicals to cement formulations. Negishi et al. [75] evaluated the effect of adding calcium tungstate (0.075 wt%) and metal nickel (0.075 wt%) to OPC samples exposed to the atmosphere of different sludge tank manhole of 3 WWTPs. After 2 years, they reported that samples containing both agents exhibited improved durability than samples only containing elemental nickel or no inhibitory agent. These samples showed weight loss of 0.2 % in an atmosphere of 28 ppm H_2S, 1% in an atmosphere of 42 ppm H_2S, and 22% in an atmosphere of 82 ppm H_2S, indicating poor durability under moderate-to-high H_2S atmospheres. Kong et al. [76] studied the effect of adding different antimicrobial agents (and amounts) to an OPC concrete mixture, including NaBr, Na_2WO, ZnO, Copper phtahlocyanine (CPC), and Dodecyl dimethyl benzyl ammonium chloride (DDC). He submerged the concrete samples in artificially intensified sewage for 120 days and analyzed changes in the overall microbial content through DNA quantification and sequencing techniques. Among

these antimicrobials, concrete mixtures containing CPC not only offered the biggest reduction in sewage bacterial content (90.82% of Bacteriodete and 64.25% Proteobacteria) but also retained most of the active compound (99.69 wt%) while CPC also improved workability and compressive strength of original hydrated mixtures. Although this study did not simulate the corrosion environment characteristic of sewer crowns, it shows the potential of antimicrobial admixtures in reducing overall microbial content, and microbes related to sulfate reduction in wastewater systems. De Muynck et al. [7] studied the antimicrobial effectiveness of a variety of admixtures including polymeric fibers and copper/silver zeolites complexes on a liquid SOB mixture. The authors observed a decrease in microbial activity when inoculating SOB cultures on acclimated mortar surfaces containing 1% of each antimicrobial compounds (polymeric fibers and metal-zeolites), metal-zeolites being more effective than polymeric fibers. However, when submerging concrete specimens in SOB liquid cultures, no inhibitory effect was observed. The authors argued the reasons for this might have included: 1) a low volume-to-surface area for the specimens too exert substantial biocidal effect; and, 2) the relatively large amount of liquid might have resulted in a dilution of the antimicrobial component below the minimal inhibitory concentration. This reflects the importance of proper experimental design and simulation of corrosion environments in laboratory settings. Metal-zeolite admixtures are among the most studied antimicrobial admixtures for MICC. Haile and Nakhla [77] studied the effect of acclimated cement coated with zeolites and epoxy on microbial abundance after immersion in *Acidithiobacillus thiooxidans* liquid cultures. The authors observed absence of *A. thiooxidans* 10 days after inoculation on coupons coated with epoxy-silver zeolite-cured cement in the following weight ratios of 2-2-1 and 1-3-1, while high cell abundance was observed on coupons with little or no antimicrobial content. Additionally, they observed no inhibitory impact from coupon leachates on the metabolic activities of communities typically found in activated sludge. The authors expanded and confirmed the inhibitory effect of silver-zeolite coated specimens against *A. thiooxidans* in both planktonic and biofilm cultures [78]. They ultimately showed

the effectiveness of the zeolite coating along with electrochemically deposited copper oxide coatings on lab scaled pipes submerged in *A. thiooxidans* cultures [9].

Few material-based antimicrobial technologies for MICC applications are currently available. ConBlock MIC and Con^{Mic}Shield® are liquid additives based on silicone quaternary ammonium (SQA) salts commercialized by ConSeal™ (www.conseal.com) and ConShield (www.conshield.com), respectively. The companies claim that their products are able to mitigate corrosion through long lasting growth inhibition of several microbial species, including *A. thiooxidans*, while remaining active within the cement matrix. SQAs are part of the quaternary ammonium compound group (QAC), cationic surfactants extensively studied due to their high antibacterial activity by cell membrane impairment [79]. SQAs are of special interest due to the fact that they can provide an antimicrobial effect while bounded to different types of surfaces [80, 81]. Zeomighty® is a different antimicrobial additive developed by the Japanese company Sinanen Zeomic (www.zeomic.co.jp). The product is based on zeolite powder, in which some Si groups are substituted by Al, similarly to a geopolymer. This generates negative charges that are compensated by addition of antimicrobial cations, Ag^{+} and Cu^{2+}. Functionalized zeolite powder is then mixed with cement and applied as a coating in sewer pipes. According to the company, application of only 1 wt% in mortar suppresses proliferation of sulfur oxidizing bacteria for long periods of time without compromising structural integrity. However, the scope of application are environments with an annual average hydrogen sulfide concentration of 10 ppm or less.

Overall, selection of antimicrobial admixtures has to consider a holistic approach: have a high antimicrobial potential, minimum cost, long-term efficacy, and cannot negatively affect structural properties. In addition, the active ingredients should offer specificity against *A. thiooxidans* in order to avoid disruption of microbial communities associated with relevant processes of wastewater treatment.

A different approach to mitigate the extent of corrosion relies in the use of synthetic polymers, generally considered chemically inert against biogenic acids produced in corrosive environments. Commonly used materials include: Polyvinyl chloride (PVC), Polyethylene (PE), High density polyethylene (HDPE), polybutylene(PB), Acrylonitrile-butadiene-styrene (ABS), polymer concrete, fiberglass, and epoxy resins among other [2, 20, 82]. Material selection is based on application (e.g. pipe, lining, coating), design needs, economics, and space availability at the installation working area [20, 82].

2.4.3 Rehabilitation techniques for corrosion-affected infrastructure

Rehabilitation techniques are diverse, all of which aim to extend the service life of affected infrastructure while avoiding the elevated costs associated with pipe replacement; the most popular are trenchless techniques. Many mature and emerging rehabilitation techniques exist, and they can be classified in the following groups: pipe bursting, slip-lining, cured-in-place, formed-in-place and grout-in-place pipes, and coatings (Table 2-8).

Table 2-8. General trenchless techniques for pipe rehabilitation. Adapted from [2].

Technique	ID diam. Range (in)	Length (ft)	Flow bypass	Excavation required	Curing time	Cross section change
Pipe bursting	2-54	<750	Yes	Yes	No	Same/Increase
Slip-lining	4-150	<5,000	No	Yes	No	Decrease
Cured-in-place	8-96	<2,500	Yes	No	Yes	Decrease
Formed-in-place	3-59	<1,500	Yes	No	No	Decrease
Grout-in-place	6-144	<525	Yes	No	Yes	Same/Decrease
Coatings	Type-dependent	Type-dependent	Yes	No	Yes	Same/Decrease

Pipe bursting, or in-line expansion, involves outward forced expansion of an existing pipe by a bursting tool. During the process, a bursting head uses the existing pipe shape as insertion guide. As the bursting tool advances, a new pipeline (attached to the bursting head) with increased diameter is left behind. PE, HDPE, PVC, and ductile iron are commonly used materials used for the new pipe installation.

Typical internal diameters range between 2” and 54”. During the pipe bursting process, the segment must be taken out of service and flow needs to be bypassed. Additionally, pit excavation is required for accessing the original pipe and for laterals reopening. However, this technique offers improved structural integrity with increased flow capacity [2, 82, 83].

Slip-lining is a mature technology used with a wide variety of available materials. It involves inserting a new continuous length of pipe of smaller diameter into an existing pipe. Segments of pipes are joined together by heat fusion or by use of bell and spigots joints, and the space between the existing pipe and the liner are grouted with a cementitious material. Three types of slip-lining are used: continuous, segmental, and spiral wound. Materials used include: PVC, PE, HDPE, PB, fiberglass-reinforced polyesters, and other reinforced thermosetting resins. The installation is relatively fast, no flow needs to be bypassed, and a wide range of sizes for internal diameter (4-150’’) are available. Pit excavation for pipe access, cleaning and conditioning of the original pipe prior slip-lining is required, and reduction of flow capacity are among the major issues on the use of this technology [2, 82, 83].

Cured-in-place pipe (CIPP) involves the installation of a flexible fabric liner tube that has been impregnated with a thermosetting resin into an existing pipe. The resin impregnated tube is cured using the original pipe as shape, creating a liner that fits tightly against the existing pipe internal diameter through the use of water or air pressure. Installation can be done through manholes, therefore minimizing disruption above ground. This technology requires thorough cleaning of the original pipe prior liner insertion to avoid irregularities in the cured liner, and flow bypass is necessary as the insertion process blocks flow through. Typical internal diameters used range between 8” and 96”. These liners are advantageous as they are able to fit different pipe shapes, and offer increased durability against corrosion. Additionally, minimal flow capacity is lost and infiltration can be eliminated. Disadvantages include the need to bypass flow, monitor the curing process and possible leachates into

the water stream, and the elevated cost compared to similar technologies. Additionally, defective installations are time consuming and expensive to fix, since in most cases the entire segment has to be excavated and replaced using open cut methods [2, 82, 83]. Formed in place pipes, or close fit lining, are technologies that fall between slip-lining and CIPP. Basically, a folded flexible pipe is deformed and inserted into a host pipe. After the liner is pulled through the existing pipe, the material is heated and pressurized to fit the original pipe's shape. Unlike CIPP, these methods do not make use of resins, therefore no curing time is necessary. However, this rehabilitation method offers less versatility when compared to CIPP. In addition to smaller diameter ranges and installation lengths, only slight bends and path offsets can be negotiated. Also, with this type of rehabilitation, achieving a leak-proof seal at manholes has proven to be challenging, because the installation of hydrophilic rubber seals or chemical seals must be used. Another significant problem has been observed with polyethylene systems due to shrinkage. The liner may retract and prevent a proper seal with the original pipe walls, if an undersized liner is cut too short in the manholes. Sufficient liner protrusion into the manhole with an appropriate short-term relaxation period corrects this problem. PVC and HDPE are commonly used materials for this technology.

Grout-in-place liners are normally applied to control groundwater infiltration due to leaking joints or cracking of pipe walls. This technique is mostly considered for point repairs of structurally sound pipes over a wide range of diameters (6" to 144"). Common types of chemical grout include acrylamide, acrylic and acrylate, urethane grout, and urethane foams. Flood grouting is a similar technique used when significant leaking and infiltration occur in a wide length pipe length or when these cannot be easily located. The process involves sequential flooding of the pipe segment with two different liquid compounds that polymerize when mixed, sealing damaged areas. Regardless of type, no structural repair can be achieved with grouting and flow bypass is necessary [82, 83].

Coatings are used when the goal is to extent the service life of new or existing pipes or manholes. A coating has to meet two conditions: have a good adhesion to the pipe's surface, and high resistance against corrosive environments. The coating material can be applied by spray, trowel, or roller either as a patch or completely covering the affected structure. Novel application techniques include vertical spincast (for manholes), and horizontal spincast (for pipes). Necessary prerequisites for coating include cleaning the affected surface from corrosion products and debris prior application, and ensuring enough thickness for effective surface protection. Surface cleaning is typically done with pressurized air, while determination of minimum thickness depends on the coating material. Common coating compounds include polyurea, polyurethane, vinylesters, epoxy, and shotcrete. Generally, use of polymeric resins applies when the concrete is exposed to significant corrosion and no structural gain is necessary, while shotcrete (mortar applied through a hose at high velocity) is applied when structural integrity needs to be recovered or increased. Additionally, structural integrity can be enhanced through combination of materials, such as carbon fiber and fiberglass with mortar cements or resin coatings, or by installation of a steel cage to the pipe wall prior treatment. Advantages of coatings include a lower cost compared to existing rehabilitation technologies, a fast application of a few hours, no flow capacity loss, and with no required excavation. Disadvantages include the need to bypass flow while applying the coating (for pipes), the need to thoroughly clean the affected structure prior application, and the need for special curing [2, 82, 83].

Selection of an appropriate technology for sewer rehabilitation is case-specific and based on several factors, and require a life cycle analysis. The impact of some these factors can be difficult to quantify, nevertheless can be driving forces on the selection of a rehabilitation method on the long term. Direct costs associated with different rehabilitation methods include: traffic disruption, environmental disturbances, commerce and industry disruption, costs associated to adjacent infrastructure, and health and safety issues [82].

2.5 Microbial Communities Associated to Microbially Induced Concrete Corrosion

2.5.1 Microbial Diversity and Succession

Detailed microbial identification from sewer systems is providing a better understanding of relevant biological processes and dynamics occurring in these built environments. Recent progress has been achieved thanks to the development of high throughput DNA sequencing techniques and analysis. An example of such is the phylogenetical indentification of the communities involved in the biologically-mediated sulfur cycle in sewer systems.

As previously described in Section 2.2.2, sulfur transformations can be divided into those occurring in the wastewater and those occurring at the pipe's crown, both of which are microbially-mediated. Below the water line, under anaerobic conditions, biofilms containing sulfate-reducing bacteria (SRB) often develop. SRBs use organic matter as a substrate and dissolved sulfate as an electron acceptor, reducing the latter to sulfide. SRBs that have been typically found in wastewater conveyance systems include *Desulfovibrio*, *Desulfolobus*, *Desulfobacter,* and *Desulfomicrobium* [84-86]. Common characteristics include their preference for anaerobic conditions, heterotrophy, and the possession of a dissimilatory sulfite reductase (*dsr*) system that has been a specific phylogenetical marker of SRB members [87]. Dissolved sulfate is typically found in wastewater in the concentration range between 24-72 mg/L [34]. SRBs can thrive at these levels and produce sulfide if conditions, such as low dissolved oxygen (DO) and low nitrate, are favorable. For example, if DO is less than 0.5 mg/L, biological sulfide production is favored and the reduced sulfur species persist in the wastewater. If DO is above this threshold, chemical reoxidation of sulfide species and biofilm communities that use oxygen as electron acceptors will be favored [88]; however, under high DO conditions SRBs can still persist as some are facultative and retain the ability to use oxygen and nitrate as electron acceptors in addition to sulfate [84, 89].

Biogenic sulfide partitions to the gas phase as hydrogen sulfide. Once released, H_2S (and CO_2) dissolve into the condensate layers on the sewer's crown. Abiotic concrete acidification results from this process, which in turn allows for initial microbial colonization.

Figure 2-7 illustrates a generalized microbial succession pattern and diversity changes associated with new concrete exposed to H_2S and CO_2 in sewers. Microbial colonization of SOB starts with growth of a highly diverse group of neutrophilic sulfur oxidizing microorganisms (NSOM) which include *Thiobacillus spp*., *Thiothrix spp*., *Thiomonas spp*., *Pseudomonas spp*., *Thiobacillus Thioparus*, *Halothiobacillus Neapolitanus*, and *Starkella Novella* among others [23, 24, 90]. These taxa are highly adaptable to different environmental conditions in the pH range between 9 and 5. Mixotrophic growth is common at this stage where the major sulfur species used for respiration are H_2S, S^0, and $S_2O_3^{2-}$. Microbial diversity is relatively high as selection pressures are minimal at this stage: circumneutral pH, high humidity, moderate dissolved salts, and mesophilic temperatures (20-30 ˚C). Chemolitoautotrophic growth and production of organic acids, which contribute to pH depression, lead to enrichment of a variety of neutrophilic heterotrophic communities able to use acids excreted by their syntrophic counterparts as substrate [90].

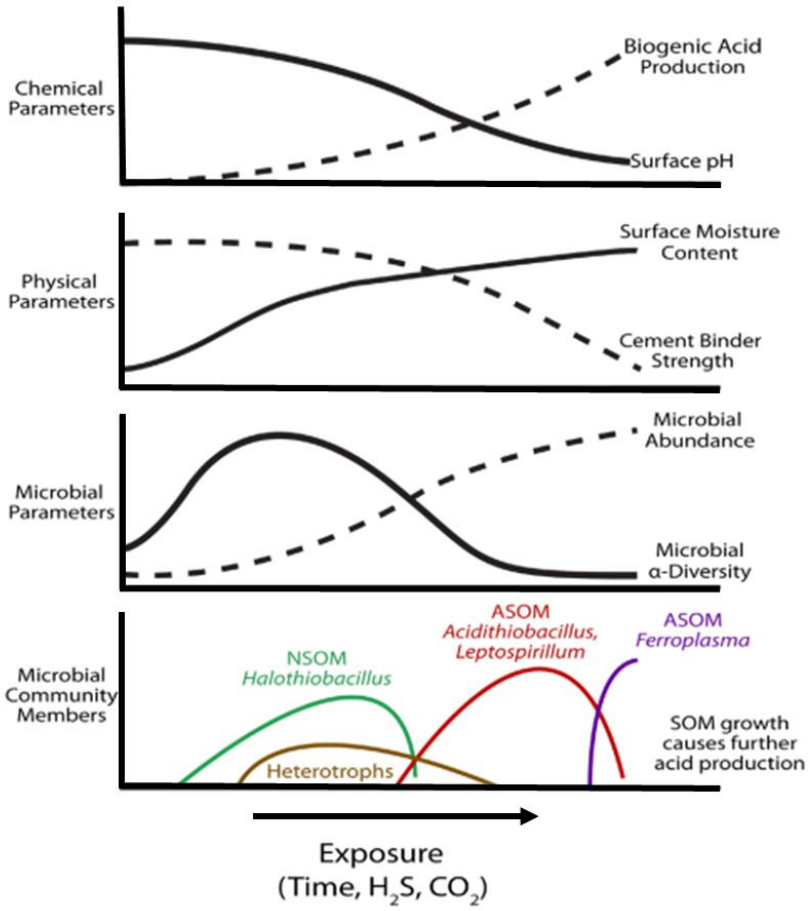

Figure 2-7. Juxtaposition of chemical, physical, and microbial changes associated with increased exposure (composite of time, H_2S, and CO_2) in microbially induced concrete corrosion. Adapted from [4].

Surface acidification continues due to accumulation of oxidized sulfur species and organic acids; microbial diversity then contracts towards acidophilic, halotolerant sulfur oxidizing microorganisms (ASOM). Below pH 4, the dominant acidophilic genus found in sewer's crown is *Acidithiobacillus*. The genus is comprised of 7 species, the most common in sewer systems being *Acidithiobacillus thiooxidans* [23, 24, 90]. These obligate chemolithoautotrophs thrive in (organic) carbon limited environments, with high levels of reduced sulfur species. They are responsible for increased sulfuric acid generation, and accelerated concrete deterioration. In this acidic environment, heterotrophs have also been cultured as well as characterized through DNA-based techniques. Although *Acidithiobacillus spp.* appear to dominate these environments, the following genera have also been recovered from acid biofilms on

sewer crowns: *Bacillus*, *Mycobacterium*, *Ochrobactrum*, *Acidiphilium*, *Burkholderiales*, *Sphingobacteriales*, and *Xanthomonadales* [91, 92]. Although less studied, fungi have also been observed in these acidic environments, such as sulfur oxidizing *Fusarium spp.* [93]. The role of the heterotrophs has also been hypothesized to be symbiotic: *A. thiooxidans* excretes organic acids, self-inhibitory if accumulated, that other heterotrophs can use as carbon sources [23]. It is also hypothesized that some of these microorganisms can mediate oxidation of hydrogen sulfide to intermediate sulfur species that can otherwise be used by *A. thiooxidans* as electron donors (i.e. S^0 and $S_2O_3^{2-}$)[94]. In advanced corrosion stages (pH <1), *Acidithiobacillus* remains reported as the dominant genus. However, the possibility of a late succession shift towards extreme acidophiles has been observed. Ling et al. [24] reported on the microbial succession associated with concrete corrosion in working manholes and the dominance of *Ferroplasma spp.* in severely corroded concrete (pH<1). Members of the Archaea domain have also been described in acid mine drainage environments. They are extremely acidophilic, facultative anaerobes with mixotrophic capabilities including the oxidation of reduced sulfur and iron species, as well as a broad capability to metabolize organic compounds [95, 96]. Succession towards this genus may be dependent on oxygen concentration in the pipe headspace, as well as oxygen penetration within the corrosion product.

2.5.2 Acidithiobacillus thiooxidans

MICC in sewer systems was first reported in the year 1900 after observing degraded mortar joints in bricks in the US. The authors concluded that sewer gases were responsible for the degradation through chemical reaction with mortar components [97]. In 1921, Waksman and Joffe [98] succeeded in isolating a bacterium from sulfur containing rocks, and named these isolates *Thiobacillus thiooxidans*. This new species was grouped with morphologically and physiologically similar microorganisms discovered in the early 20th century (i.e. *Thiobacillus thioparus*, *Thiobacillus denitrificans*). Later, in the year 1945, Parker [99] isolated strains of sulfur oxidizing bacteria from corroded concrete and reported

them as the major organism responsible for concrete deterioration. The author named this species *Thiobacillus concretivorous*. It was later found that this species had DNA that was homologous to *Thiobacillus thiooxidans*, and thus was removed from accepted taxonomic lists [100, 101]. In the year 2000, thanks to more comprehensive 16S rRNA gene sequencing and analysis, eight existing *Thiobacillus* species were reclassified into three new genera, namely *Acidithiobacillus*, *Halothiobacillus*, and *Thermithiobacillus*. Among these species, *Thiobacillus thiooxidans* was reclassified and renamed *Acidithiobacillus thiooxidans,* of which there are many strains [102].

The genus *Acidithiobacillus* belongs to the phylum *Proteobacteria* and currently circumscribes seven species (Figure 2-8) [103, 104]. They are obligate acidophilic, gram negative, rod-shaped bacteria (0.3-0.5 x 0.7-4 μm) with some motile representatives presenting flagella. These chemolithoautotrophs are able to fix gaseous CO_2 and obtain energy through the oxidation of reduced sulfur species [103]. They are ubiquitous around the globe and have been found on both natural and built environments. Typical habitats include marine, freshwater, and soils especially rich in reduced sulfur species (i.e. sulfur springs, sulfide ores, sewer conveyance systems) [103]. *Acidithiobacilli* are of special interest in the mining industry as they have been found to play an important role mobilizing metals in acid mine drainage, and innovative applications are being developed to mine ores by using these acidophiles (i.e. biomining applications) [102, 105].

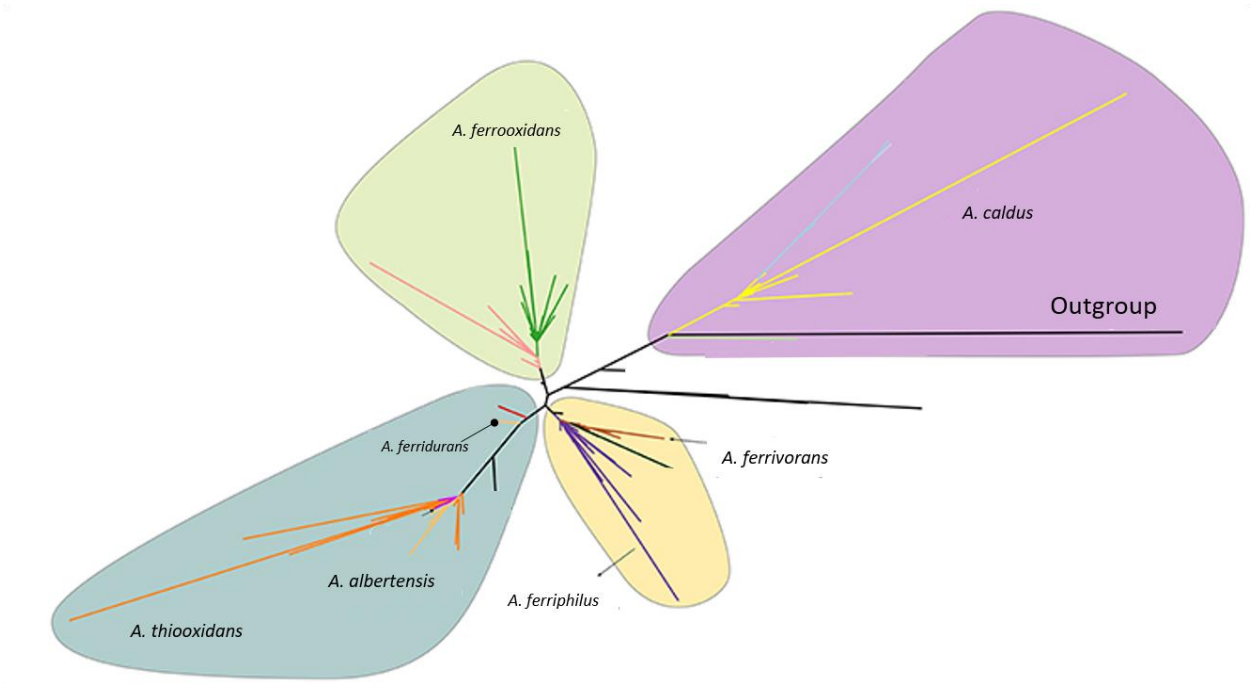

Figure 2-8. Major Acidithiobacillus species complex consensus phylogenetic tree built using maximum likelihood inference and 16S rRNA gene sequences of 580 strains and/or sequence clones. Colored areas represent clades while colored lines represent sub-clades. Adapted from [104].

As mentioned in Section 2.5.1, the dominant *Acidithiobacillus* species in sewer systems is *A.thiooxidans*. This mesophilic (~ 30 ˚C), acidophilic (<pH 4) autotroph is able to fix and assimilate CO_2 through the Calvin-Benson-Bassham cycle. Atmospheric CO_2 is sufficient for growth, although the higher concentrations typically found in sewer systems result in increased rates. No organic carbon compounds are used by this species for metabolic purposes [106, 107]. *A.thiooxidans* is an obligate aerobe, requiring oxygen as the final electron acceptor in sulfur respiration [102]. The sequenced genome of different strains has revealed common features in terms of sulfur metabolism, (Figure 2-9). All strains are found to possess the SOX system genes *soxXYZAB*, which allow for the partial oxidation of thiosulfate to sulfate. Additionally, genes associated with broad sulfur oxidation capabilities are prevalent, such as the ones encoding for tetrathionate hydrolase, thiosulfate quinone oxidoreductase, and sulfide quinone oxidoreductase [26, 108]. This species is known to oxidize a variety of sulfur compounds such as hydrogen sulfide (H_2S), elemental sulfur (S^0) and thiosulfate (S_2O_3). Mechanisms for sulfur oxidation have

been proposed and the associated pathways are described as follows: Extracellular elemental sulfur is mobilized by thiol groups of outer-membrane proteins and transported into the periplasm as persulfide. This sulfur species is then oxidized by periplasmic sulfur dioxygenase to sulfite, together with the formation of hydrogen sulfide. The latter reduced species can be oxidized to elemental sulfur by sulfide quinone oxydoreductase in the cytoplasmatic membrane. Elemental sulfur within the cytoplasm can be transformed into different products through catalysis by sulfur oxygenase oxidoreductase, namely sulfide, thiosulfate, and sulfite. Sulfite can be oxidized to sulfate by a sulfite acceptor oxidoreductase. Alternatively, it is proposed that sulfite can be catalyzed by the phosphoadenosine phosphosulfate (PAPS) reductase and the adenylyl-sulfate (APS) kinase to generate PAPS and APS. The latter can then produce sulfate via an unknown pathway. Additionally, sulfite and elemental sulfur within the cell can spontaneously form thiosulfate. Thiosulfate quinone oxydoreductase can then catalyze the formation of tetrathionate, which can be further hydrolyzed to thiosulfate and sulfate. Thiosulfate can also be directly oxidized to sulfate through the *sox* system. All these oxidation pathways lead to the transport of electrons, producing proton gradients or generating reducing power [108-110].

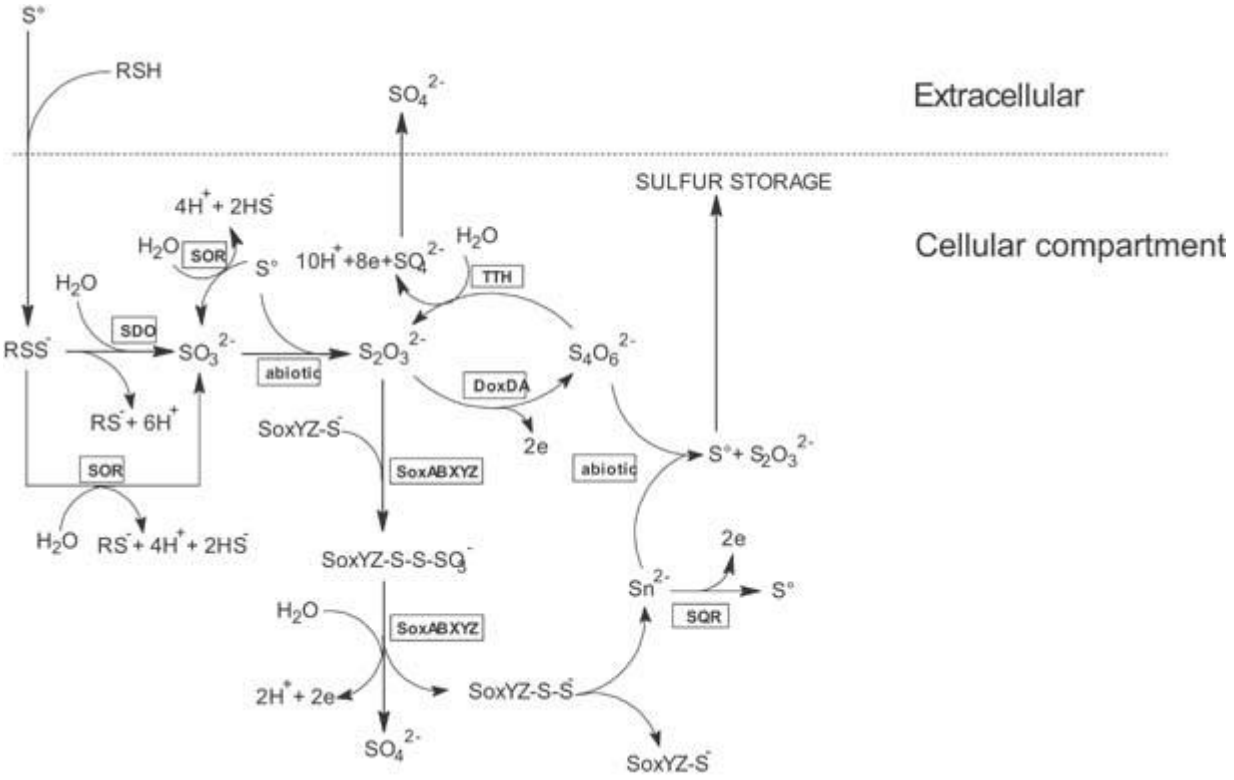

Figure 2-9. Schematic representation of reduced inorganic sulfur compounds oxidation model for Acidithiobacillus thiooxidans DSM 17318. SDO, sulfur dioxygenase; SOR, sulfur oxygenase reductase; TTH, tetrathionate hydrolase; DoxDA, Thiosulfate: quinol oxidoreductase; SoxABXYZ, sulfur-oxidizing operon; SQR, Sulfide:quinone oxidoreductase. Abiotic: spontaneous chemical reactions. From [109].

An interesting characteristic of *Acidithiobacillus spp.* is their evolutionary adaptation to different environments, especially those with presence of heavy metals. These species have been predominantly studied due to their role in bioleaching of heavy metals from different ores [111-113]. They have been isolated from natural environments associated with pyritic ores, and sulfide-rich caves and springs, where they can oxidize reduced sulfur species, lower pH, and mobilize metals. This process has exposed *Acidithiobacillus* to a selective pressure that led to high tolerance towards heavy metals. Table 2-9 reports the inhibitory concentration thresholds of common heavy metal cations against different *Acidithiobacillus* species extracted from sites with known heavy metal presence. In these ecological niches, acidophilic growth can develop under heavy metal concentrations in the order of dozens grams per liter. This remarkable characteristic is thought to be obtained through horizontal gene transfer of

plasmids, transposons and other mobile genetic material encoding for metal resistance genes, as evidence of genomic islands in the bacterial genome have been observed, although the specific mechanisms of acquisition in these environments are not well understood [112, 114].

Table 2-9. Observed inhibitory heavy metal concentrations against isolated Acidithiobacillus spp. All numbers are in mg/L.

Study	*Species*	Source	$[Cu^{2+}]$	$[Zn^{2+}]$	$[Cd^{2+}]$	$[Ni^{2+}]$	$[Fe^{3+}]$
[18]	*A. thiooxidans* BC1	Collection site for automobile batteries	400	> 10,000	300		
[115]	*A. thiooxidans* SFR01	Sewage sludge	1,270	13,000			
[111]	*A. ferrooxidans* D6	Uranium mine	> 10,000			> 9,400	
[112]	*A. ferrooxidans*	AMD/ARD sites	50,840	70,020	56,200	58,600	
[113]	*A. ferrooxidans*	Copper mine	> 25,000	> 40,000			> 10,000

Due to the high metal tolerance of some strains, few studies have focused their attention on using heavy metals to inhibit the growth of *Acidithiobacillus* from sewer crowns. However, unlike sulfide ores, the heavy metal content in sewer pipes is negligible; hence, resistance genes are not common nor necessary for these organisms. The metal susceptibility of these species have been scarcely evaluated, although consistently observed as significantly higher than their resistant counterparts [77, 116, 117].

2.6 Materials Aspects Relevant to Test Formulation

2.6.1 Antibacterial activity of heavy metals and their resistance

All living organisms require of essential heavy metals for vital biochemical processes. Some metal ions are necessary to maintain the cell membrane and DNA structure; others are important catalytic centers and co-factors for a variety of protein functions. However, when these metals are

found in excess or there is a significant amount of non-essential metals, microbial toxicity can result. The first step in this process involves transport of the heavy metals through the cell membrane. Transport is accomplished through either constitutively expressed or induced transporters found in the cell membrane. Non-essential metals may enter the cell using ion or molecular mimicry. Additionally, toxic heavy metals can be transported through association with small ligands (i.e. amino acids, phosphates, organic acids, siderophores) [118]. Once inside the cell, several toxicity mechanisms can prevail (Table 2-10).

Table 2-10. Antibacterial mechanism of metal toxicity. Adapted from [118].

Mechanism	Examples
ROS formation and antioxidant depletion	Fenton reaction (Fe^{3+}, Cu^{2+}),oxyanion reduction (Cr^{6+},As^{3+},Te^{4+}), thiol depletion (Ag^{+},Cd^{2+},Co^{2+})
Protein dysfunction	Destruction of Fe-S cluster (Cu^{+}, Ag^{+}, Hg^{2+}), exchange of catalytic metal (Pb^{2+}, Zn^{2+}), exchange of structural metal (Ni^{2+}, Pb^{2+})
Membrane impairment	Lipid peroxidation (Cu^{2+}, Cd^{2+}), electron transport chain disruption (Ag^{+})
Nutrient assimilation interference	Inhibition of Fe^{3+} transporter gene expression (Ga^{3+})
Genotoxicity	Fe-induced oxidative damage (Fe^{2+}, Fe^{3+})

The first mechanism is the metal-induced formation of reactive oxygen species (ROS). The formation of oxidizing species, H_2O_2 and $O_2^{\bullet -}$, and $OH^{\bullet}$, leads to lipid, protein, and DNA damage. An example of such is the Cu-induced Fenton-like reaction. In the suggested mechanism, Cu^{2+} oxidizes H_2O_2 to $O_2^{\bullet -}$ with the consequent reduction to Cu^{+}. Cu^{+} can then react with excess H_2O_2 to form $OH^{\bullet}$ and OH^{-}. The hydroxyl radical is the compound responsible for direct cell damage [119]. Additional pathways for ROS formation have been proposed depending on the nature of the metal and the reactive species within the cell (i.e. thiol-mediated metal reduction). The second mechanism of toxicity involves the loss

of enzymatic activity. This can be induced by the metal-associated oxidative stress and destruction of the Fe-S clusters in proteins, and loss of catalytic activity through ion mimicry at both the active and non-catalytic sites. A third group of mechanisms focus on the cell membrane. The first is the disruption of the electron transport chain by inactivating key enzymes located in the membrane. The second, through induction of lipid peroxidation. A forth mechanism is through interference with nutrient assimilation. In this case metals can inactivate the proteins associated with the uptake of nutrients such as sulfate, or iron, leading to cell starvation. Lastly, certain metals can also induce direct DNA damage through the production of ROS [118].

Through continuous exposure and adaptation, bacteria have developed a number of strategies to avoid toxic effects. Specific enzymes and proteins associated to detoxification vary from organism to organism, but three major mechanisms can be observed. The first is the efflux of metal ions out of the cell through constitutively expressed proteins or specifically expressed ones. The second is the segregation of metal cations into complexes by thiol-containing molecules. The third is the metal reduction into less toxic species. A combination of the three mechanisms is typically found in cells, most of the time combining efflux with either of the other two [120]. As an example, the genome analysis of a strain of *Acidithiobacillus ferrooxidans (ATCC 2370)* isolated from an acid mine drainage site revealed a significant amount of heavy metal resistance genes: *copCD* copper extrusion system, resistance-nodulation-cell division (RND) family of transporters, cation diffusion facilitator (CDF) proteins, and copper translocating P-type ATPases are some examples of genes found in this strain. Additionally, arsenic- and mercury- specific gene clusters were also observed. Genes related to ROS detoxification were also observed, especially those related to the production of low molecular weight thiols in the cytoplasm that, in combination with specific disulfide reductases, provide a reducing intracellular environment and maintain the thiol/disulfide balance of other molecules [27].

An important aspect of heavy metal resistance involves the acquisition of resistance genes. Presence of plasmids, transposons, and genomic islands are ubiquitous in microbes adapted to metal-rich environments [121-123]. While significant research has been done on characterizing the genes associated to contaminated sites, very few have studied the temporal adaptation of microbial communities *in situ*. In this context, the development of a metal-based antimicrobial compound has to be able to deliver concentrations well above the minimum inhibitory concentration to minimize the possibility of heavy metal resistance gene transfer.

2.6.2 Activated Carbon

Production of activated carbon involves the pyrolytic carbonization of raw material and the subsequent or parallel activation. Commonly raw precursors include bituminous coal, peat, lignite, petrol coke, and wood, although there is an increase interest in the use of other sustainable sources like agricultural wastes or wastewater sludge [124, 125]. During carbonization, volatile components are released, and the carbon realigns to form a pore structure that is developed during the activation process. Both chemical and physical activation selectively removes carbon, resulting in an opening of closed porosity and an increased average size of the micropores. Chemical activation involves the use of dehydrating and oxidizing agents such as zinc chloride, potassium hydroxide, or phosphoric acid, prior heat treatment. Physical activation is an endothermic process that involves the contact of a gaseous activating agent, either steam, air or CO_2, with the carbon at elevated temperatures (850-1,000 C), leading to increased oxidation of the treated surface [124]. Once carbonized and activated, the material can be ground and sieved according to its specific application.

The internal structure of the final product is considered to be that of a disorganized graphite of trigonally covalent bonded carbons connected by tetragonally bonded carbon cross-links, the latter group containing more active sites and higher reactivity. The role of activated carbon as an adsorbent is mostly driven by the porous nature created by these configurations. Physical characterization of an

activated carbon is done through determination of pore shape, size, volume, and surface area. As an example, reported surface area values for activated carbons range between 500 to 1,500 m^2/g [124]. However, not only the porous structure dictates the adsorption capabilities, but also the chemical properties of the surface. The most common functional groups are oxygen-containing, which can be classified as acidic or basic groups (Figure 2-10). Carboxyl, hydroxyl, anhydride, lactone, and lactole groups are among the acidic groups. Basic groups include ether, alcohol, pyrone, quinone, and chromene groups. Although less abundant, nitrogen groups are also important. Unlike oxygen groups, which are formed spontaneously in the carbonization process, nitrogen groups depend on the source material and the activating agent used. Commonly, treatment with nitrogen-containing reagents at low temperatures result in the formation of lactams, imides, and amines, which exhibit a slight acidic nature. On the contrary, treatment at high temperatures result in an increase of N quaternary (N atoms incorporated in the graphitic layer in substitution of C-atoms) pyridine and pyrrole-type structures. Other minor groups include sulfur-, phosphorous-, and halogen- based [126, 127].

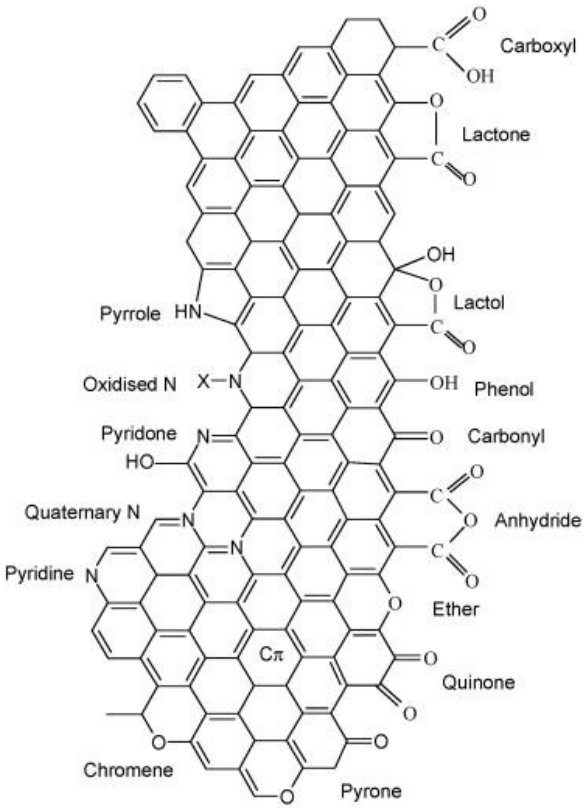

Figure 2-10. Oxygen and Nitrogen functional groups in activated carbons. From [127].

Carbon applications are conditioned by both their chemical characteristics and surface chemistry. A variety of techniques can be applied to investigate the presence/absence of specific functional groups. However, the most accurate picture of the surface functionalities is to be given when complementary techniques are applied (Table 2-11).

Table 2-11. Common techniques for chemical characterization of activated carbon. Adapted from [126].

Analysis	*Description*	*Examples*
Total composition	Quantification of the heteroatoms present in the carbon	Outgassed extraction/ICP-MS
Boehm titration	Characterization and quantification of functional groups based on the selective neutralization by equilibration with a series of bases of increasing strength	Back-titration of a nitrogen-spurged base-treated aliquot
Potentiometric titrations	Detailed characterization and quantification of pKas on activated carbon particles by potential changes through incremental titrant addition	Argentometric titration
pH, pH_{PZC},pH_{IEP}	Determination of the nature of the functional groups and amphoteric characteristics	Drift method for pHpzc
Spectroscopy	Qualitative description of physicochemical properties of carbon surfaces	FTIR, Raman, XPS, XRF, NMR
Calorimetry	Determination of the surface area and surface reactivity to elucidate adsorption mechanisms	Immersion, flow adsorption and gas-adsorption calorimetry
Inverse gas chromatography	Surface acid/base characterization through probe adsorption capacity	Chromatographic (dynamic) experiments
Temperature programmed desorption	Study of surface functionalities through carbon heating in a flowing carrier gas at a programmed heating rate to induce thermal desorption of adsorbed species from the carbon surface	TPD combined with IR spectroscopy

The versatility of activated carbon is based on the possibility to easily modify the functional groups on its surface. As discussed earlier, this can be accomplished by use of specific chemical agents during the activation process. However, surface modifications on the finished product are also commonly applied. The latter modification treatment strategies are divided in three major groups: chemical, physical, and biological. Chemical treatments include surface acidification, alkalinization, and impregnation [128]. Acidification involves treatment with acid and oxidizing agents to increase acid functional groups on the surface, leading to an increased chelation effect with dissolved metals in aqueous environments. Typically used agents include nitric acid, ammonium persulfate, and peroxide.

While improvement in ionic metal adsorption is enhanced, adsorption of organic compounds is reduced. This is thought to be due to loss of surface area and porosity, and the decrease of basic and hydrophobic groups. Alkali treated activated carbons are obtained through exposure with an alkali agent, typically NaOH and ammonia. The effects on the adsorption properties have been observed to be opposite to that of acidified activated carbons: organic adsorption is enhanced while ionic metal adsorption is reduced. Chemical impregnation includes those treatments that do not significantly alter the pH of activated carbon. The goal of impregnation is to homogeneously distribute a compound of interest on the carbon's internal surface area, creating a synergistic effect between AC and the impregnating agent to augment adsorption capacity as well as to boost the capacity of AC as inert porous carrier. Examples include impregnation with tetrabutyl ammonium for removal of aqueous copper, zinc, and chromium, impregnation with silver for removal of aqueous cyanide, or iron impregnated carbon for arsenic removal [128]. Physical surface modifications are mostly done through heat treatment. Heat-treated carbon is generally favorable for enhancing adsorption of organic molecules from aqueous solutions since basic characteristic of the carbon is amplified at high temperature conditions, and an increment in the internal surface area and the micro- and mesoporosity is achieved [128]. Lastly, biological modifications involve the use of activated carbon as a carrier of selected microbes for specific purposes. Examples include adsorption of *Pseudomonas* species for removal of phenol and benzene, or adsorption of *Rhodococcus* species for atrazine removal [128].

Relevant to this research, the use of activated carbon for metal adsorption is noteworthy. These materials are effective adsorbents of several dissolved heavy metal cations and oxyanions, reaching loads in the order of tenths milligrams of metal per gram of carbon. Sequestration from aqueous phases is achieved through two major mechanisms: surface precipitation, and electrostatic interactions [129-131]. Colloidal metal particles can be physically immobilized on the micropores when solution pH allows for metal hydroxide complexation or if the carbon's superficial pH is high enough to induce metal

complexation. The phenomenon of electrostatic interaction takes into account the charge and functional groups present in the carbon's surface. Cation adsorption is favored if the surface of the carbon is negatively charged. This occurs when the pH of the bulk solution is above the point of zero charge (pH_{PZC}) of the carbon. Conversely, when the pH is below the pH_{PZC} the surface can be neutral or positively charged, the latter allowing for oxyanions to be immobilized electrostatically [132]. This behavior is useful in developing functional modifications on the carbon surface to establish a specific adsorption/desorption pH threshold for specific metals.

2.6.3 Steel Slag

Steel slag is the major byproduct from the transformation of iron into steel. In the US only and for 2016, the processed slag sold (ex-plant) was estimated to be 15-20 million metric tons, with an associated value of $350 million [133]. However, a significant fraction of the produced slag (15-40 %) is initially stockpiled for indefinite periods of time until it can be sold or disposed of [134]. Therefore, utilization of steel slag in civil engineering applications can alleviate the need for their disposal, reduce the use of natural resources, and add economic value to this material [134]. The nature of steel slag depends on the steel making process used, and the cooling method. Table 2-12 shows the classification and oxide composition of the different types of slags.

Table 2-12. Composition as metal oxides for the major types of slag derived from the production of steel. From [134-136].

Type	Source	Composition (wt%)									
		CaO	SiO_2	Al_2O_3	FeO	Fe_2O_3	MgO	MnO	TiO_2	SO_3	P_2O_5
BF	Blast Furnace	32-45	32-42	7-16	0.1-1.5	0.1-1.5	5-15	0.2-1	0-3.7	1-2	0.5-1
BOF	Basic-oxygen furnace	30-60	8-20	1-9	10-35	3-38	0.8-15	0.3-8	0.4-2	0-0.3	0.2-3.3
EAF	Electric arc furnace	24-60	9-32	2-9	1-35	20-32.5	3-15	0.4-8	0.5-0.8	0-0.6	0-1.2
LF	Ladle furnace	30-60	2-35	5-35	0.1-15	0.2-3.3	1-12.5	0-5	0.3-0.9	0.1-1	0-0.4

Production of steel starts when iron ore or iron pellets, coke, and a flux (i.e. limestone, dolomite) are melted together in a blast furnace (BF). The end products are molten metal, BF slag, and carbon monoxide-rich gases. In integrated steel mills, the molten iron is directed to a basic-oxygen furnace (BOF), where it is mixed with steel scrap, alloying agents, and fluxes. Then, an oxygen lance blows pure oxygen on the charge at supersonic speeds inducing oxidation of impurities found in the charge, and lowering the carbon content through generation of carbon monoxide. The use of fluxes helps separating the oxidized impurities, later resulting in BOF slag. This byproduct floats on top of the molten steel and it can be separated by tilting the furnace in order to tap the steel into ladles. When all the steel has been poured, the furnace is tilted to the opposite side in order to pour the BOF slag into a ladle for further processing. Melted steel can be further refined in a ladle furnace (LF) or be sent to a continuous caster to produce billets, blooms, or slabs. A different steel production method is applied when steel scrap recycling is wanted: Electric arc furnace (EAF). Instead of using solid or gaseous fuels for heat production, electric arc furnaces use high power electric arcs generated through graphite electrodes. In this case, steel scraps and some pig iron are added to the furnace and an electric arc is applied. The electric resistance of the metals leads to heat production and consequent melting of the

scrap. Then, fluxes can be added (if not initially charged) and oxygen is blown to facilitate the oxidation and combination of the impurities with the fluxes. Additionally, carbon powder is also added through the slag phase to induce formation of carbon monoxide. After this process, the furnace is tilted to separate the molten steel from the slag in a similar way to the BOF. Independently of the method used, produced steel can be further refined in ladle furnaces. Ladle furnaces heat the steel through graphite electrodes, similarly to EAF. Additionally, inert gases, desulfurizing, and deoxidizing agents are also added in order to obtain high-grade steel. Lastly, amounts of metal (e.g. Ni, V, Cr) and carbon can be added to obtain specific alloys [134, 135]. Once separated from the molten steel, the slags can be cooled down through different processes. Natural air cooling only requires pouring the slag into a pit or on the ground. Water sprayed cooling involves the same process as natural air cooling with the additional spraying of water on the surface of the slag as soon as it solidifies. This allows cracking of slag particles due to temperature gradient, generating smaller and easier to handle particles. Water quenching is a method used to cool down molten slag, specifically BF slag. The method involves immersion of the molten slag into water, and may result in explosions through sudden water vapor formation within the slag cavities. Air-quenching involves the injection of pressurized air into molten slag, resulting in the ejection of small particles which fall into a water pond. This process increases the oxidation of the slag compounds and generates small and hard particles. Finally, the shallow box chilling involves pouring a thin layer of slag on a pan, followed by superficial water spraying. After this initial cooling process, the slag is transported to a spraying station to be gradually cooled down. The last step involves placing the slag into a water pool for further cooling and magnetic screening [135].

The wide variability in slags is a result of the original precursor composition (iron, fuel and flux sources), the melting process (BF, BOF, EAF, and LF), and the cooling method chosen (natural air cooling, water spray, water quenching, air quenching, and shallow chill box). This leads to highly alkaline particles with a specific elemental and mineral composition. The bulk oxide chemistry of slag can be

defined as a mixture of CaO, SiO_2, Al_2O_3, FeO, and MgO. Minor components include MnO, SO_3, TiO_2, and P_2O_5 among other traces. Generally speaking, mineral development is highly dependent on the cooling process applied. Slag that is cooled rapidly tends to form glassy, amorphous material, while slower cooling leads to increased crystallization [136]. Common minerals found in steel slags include Merwinite ($3CaO{\cdot}MgO{\cdot}2SiO_2$), Olivine ($2MgO{\cdot}2FeO{\cdot}SiO_2$), β-$C_2S$ ($2CaO{\cdot}SiO_2$), α-C_2S, C_4AF ($4CaO{\cdot}Al_2O_3{\cdot}FeO_3$), C_2F ($2CaO{\cdot}Fe_2O_3$), CaO (free lime), MgO (periclase and free MgO), Wustite (FeO), C_3S ($3CaO{\cdot}SiO_2$), and RO phase (solid solution of CaO-FeO-MnO-MgO) [134, 135]. The mineral content and distribution is key to determine the chemical reactivity and best application of the different types of slags. As an example, the presence of free lime in slag can lead to quick expansive reactions upon hydration, therefore limiting the use of high-free lime slags as construction materials.

Physical characterization of steel slag is typically done through determination of the specific gravity, grain size distribution, moisture content, surface area analysis, and micro-morphology. Chemical characterization, usually involves total composition analysis, natural pH, alkalinity, mineral phases, spectrophotometric analysis, and leaching tests. Other analysis can be made for application-specific purposes, but in general, very few heavy metals leach from slag products [137-139].

Steel making residuals have been traditionally recycled in order to maximize steel production. This is typically achieved by magnetic separation of the byproduct into a rich-iron phase and the residual slag. The iron-rich phase is fed back into the furnaces as cooling scrap while the residual slag can be partially used as recycled flux or sold as aggregate in pavement and construction works, railroad ballast, gabions, insulators, and as raw feed for cement manufacturing among other. Other recycling processes include the recovery of specific metals such as Pb, V, Zn, and Cr [140]. However, due to an increasing concern on the availability of natural resources coupled to an increasing demand, and the need to transition to a sustainable economy, some research has been done on the applicability of slags.

Consolidated research include the use of BF and steel slags as Portland cement substitutes and supplementary cementitious materials [135, 141]. Innovations in this arena are focused on the use of steel slags as precursors for alkali-activated cements [135]. In recent years, other studies have focused on environmental solutions through the use of slag such as CO_2 and H_2S scrubbing, phosphorous removal from water streams, heavy metal precipitation and pH neutralization of acid mine drainage, and silica and oligoelemental supplement for agriculture [140, 142-144]. Advanced research on the use of steel slag include, alkali-activated blends for durable infrastructure, soil stabilization, phosphorous removal and biogas upgrading from domestic wastewater, organic contaminant degradation, and the catalytic production of hydrogen [145-150].

Chapter 3 Materials and Methods

3.1 Microbial Characterization

3.1.1 Microbial cultures

Microbial biomass was aseptically collected from surfaces in a corroding sewer manhole in metropolitan Denver, Colorado. DNA was extracted and purified, and the 16S rRNA genes (V4-V5 region) sequenced on an Illumina Miseq platform identified that *Acidithiobacillus spp*. dominated these populations (>95% relative abundance) [24]. Enrichments from these extracts were grown on *Thiobacillus* media, developed by Starosvetsky et al. [151] and modified without agar or bromcresol green addition. This media is especially useful for chemoautotrophic growth of sulfur oxidizing acidophilic communities as no organic carbon source is added, while thiosulfate is supplemented as the major reduced sulfur species. pH was adjusted between 5.25-5.5 before inoculation. Cultures were incubated in the dark at 30 °C with occasional agitation until pH<2. Stock samples were prepared by mixing 1 mL of the grown culture with 1 mL 70 % (v/v) autoclaved glycerol. Samples were stored at - 80 °C until further use.

3.1.2 Bacterial enumeration

Aliquots from liquid cultures and suspended cells extracted from solid surfaces were used for determination of bacterial abundance. Quantification was completed using a widely accepted membrane filtration method [152] as adapted for direct epi-fluorescence microscopy of *Acidithobacillus spp*. recovered from sewer corrosion products [153].

3.1.3 Microbial activity

Microbial activity was measured through the NovaLUM ATP detection system (Charm Sciences Inc.). This luminometer is able to amplify ATP signals, expressed as relative light units (RLU), from swabbed surfaces using a calibrated Luciferine/Luciferase reaction [154]. PocketSwab® Plus (Charm

Sciences Inc.) swabs were used for all the ATP estimates reported here. After collecting the sample, the swabs were inserted in a sterile case which contained buffering agents and lyophilized enzymes to initiate the quantitative luciferin/luciferase reaction. The mixture was agitated for 30 seconds and the swab was inserted in the luminometer to obtain a define RLU value.

Adapting this technology for assessing the *in-situ* activity of *Acidithiobacillus spp.* cultures was enabled by the correlation of RLU values with cell density, growth, and pH observations of pure cultures. For this purpose, 25 mL of *Thiobacillus* liquid media was inoculated with 150 µl of pure culture (ATCC 19377). The culture was incubated in the dark at 30 ◦C with occasional agitation. Aliquots were taken at different days and assessed for microbial activity (RLU), cell abundance, and culture pH using methods previously described. Activity was measured by immersing the ATP swab in extracted aliquots following 30 seconds of agitation.

For cells sessile cells, activity was measured immediately after surface sampling and resuspended in a sterile saline solution. Details of this procedure are described in Section 3.6.1.

3.2 Phylogeny analysis

3.2.1 DNA recovery

Aliquots for DNA extraction were collected in 10 Mm Tris/1 Mm EDTA and serially diluted between 100 and 1,000 fold. DNA extraction, sequencing and analysis were performed as described by Ling et al. [24] with the following modifications: extraction was done by collecting 750 µL of the cell dilution. Then 500 mL NaCl/TE buffer with SDS, 250 mL phenol, 250 mL chloroform, and 0.1 mm silica/zirconium beads were added and the mixture bead-beaten for 1.5 minutes. DNA was precipitated from the supernatant using glycogen, ammonium acetate, and isopropanol, as previously described [155]. Pellets were washed with 70% ethanol and re-suspended in 25/50 µL sterile DNase/RNase-free water (Fisher Scientific). Extracted, eluted DNA was stored at -80 ◦C until further use.

3.2.2 16S clone libraries and gene quantification

Quantitative PCR (qPCR) was used to determine the abundance of the small subunit 16S rRNA genes isolated from DNA recovered in the field. qPCR was assessed with two different primer sets: a universal primer set 515F (5' GTGCCAGCMGCCGCGGTAA 3') and 1391R (5' GACGGGCGGTGTGTRCA 3') used for the identification of all Bacteria, Archaea, and Eukarya domains, which generates an amplicon of 890 bp [156], and the *Acidithiobacillus* genus specific primer set 27F (5' AGAGTTTGATCMTGGCTCAG 3') and THIO820R (5' ACCAAACATCTAGTATTCATCG 3'), which generates a 823 bp amplicon. The latter reverse primer was obtained from the development of FISH probes for enumeration of whole *Acidithiobacillus* cells [153]. Primer specificity was evaluated through use of the NCBI BLAST database [157] and carefully tested with comprehensive hybridization studies.

qPCR was conducted in 25 µL reaction volumes containing 10 µL Maxima SYBR Green/ROX qPCR Master Mix (2X) (Thermo Fisher Scientific), 1 µL of each primer (5 µM), 2 µL BSA (10 mg/mL), 9 µL of H_2O, and 2 µL of template DNA. Serial dilutions of linearized plasmids containing Universal and *Acidithiobacillus* 16S target were used to generate ct standards. 1 µL of yeast tRNA (100 ng/mL) was added to the standards to avoid template DNA from binding to plastic surfaces.

Cycling conditions included denaturation at 95 °C for 2 min; followed by 40 cycles of 95 °C for 30 s, 54.5 °C (*Acidithiobacillus*-specific primer set) or 56.5 °C (Universal primer set) for 30 s, 70 C for 60 s; fluorescence was then quantified. qPCR reactions were performed in triplicate for each sample and standard. A hybridization temperature (melting) curve was used in all assays to ensure amplification specificity. All assays were performed on a C1000 Touch™ Thermal Cycler with a CFX96™ Real-Time system (BioRad).

3.2.3 16S amplicon sequencing by Illumina MiSeq technology and analysis

Isolated DNA was used for analysis of bacterial profiles using the Illumina MiSeq platform using established methods [158, 159]. Amplicons used for sequencing were obtained by using primers that target approximately 375 base pairs of the V4-V5 variable region of the 16S rRNA gene. PCR products were normalized using a SequalPrep TM kit (Invitrogen), pooled, lyophilized, purified and concentrated using a DNA Clean and Concentrator Kit (Zymo). Amplicons were quantified using Qubit Fluorometer 2.0 (Invitrogen). The pool was diluted to 4 nM and denatured with 0.2 N NaOH at room temperature. The denatured DNA was diluted to 15 pM and spiked with 25 % of the Illumina PhiX control DNA prior to sequencer loading. Illumina paired-end sequencing was performed on the Miseq platform with versions v2.4 of the Miseq Control Software and of MiSeq Reporter, using a 600-cycle v3 reagent kit. Illumina MiSeq paired-end sequences were sorted by sample via barcodes in the paired reads with a python script. The sorted paired reads were assembled using phrap [160, 161]. Pairs that did not assemble were discarded. Assembled sequence ends were trimmed over a moving window of 5 nucleotides until average quality met or exceeded 20. Trimmed sequences with more than 1 ambiguity or shorter than 250 nt were discarded. Potential chimeras identified with Uchime (usearch6.0.203_i86linux32) [162] using the reference sequence of Schloss SILVA [163] were removed from subsequent analyses. Assembled sequences were aligned and classified with SINA (1.3.0-r23838) [164] using the 436028 bacterial and archaeal sequences in Silva 115NR99 [165] as reference configured to yield the Silva taxonomy. All unique sequences were taxonomically assigned, and operational taxonomic units (OTUs) were produced by clustering sequences with identical taxonomic assignments. Explicet v2.10.5 [166] was used for display, analysis, and figure generation of sequence data.

Bacterial compositions were visualized using non-metric multidimensional scaling (NMDS), which using multi-variate regressions, resolves genetic OTU assignment data into fewer dimensions, and can use any distance matrix [167]. Briefly, singleton OTUs (of which there is only one occurrence of any

given OTU) were removed and a Bray–Curtis dissimilarity matrix was calculated. The NMDS was run using the vegan package in Rstudio [168]. A three-dimensional model produced a goodness-of-fit value of <0.05 using Kruskal's stress formula, indicating that the ordination reasonably approximates the among-sample relationships [169]. A Shepard plot of calculated vs. raw dissimilarities showed strong nonmetric (R^2 = 0. 99) and linear (R^2 = 0.99) fits.

3.2.4 Limitations of 16S rRNA phylogenetic methods

While 16S rRNA methods have become the standard practice in the microbial ecology field, they are subject to a range of biases. DNA extraction efficiencies differ different organism types; DNA also experiences varying rates of decay during sample storage; and 16S rDNA copies vary across speciesand environmental conditions [163, 170-172]. Polymerase chain reaction (PCR) is used to copy targeted 16S rDNA genes prior to sequencing, but the process is subject to amplification biases that result from differing target sequence lengths and the specific DNA chemistry between organisms [173]; further different DNA sequences respond to different inhibiting compounds in the reaction mix such as calcium, iron, or organic acids [174, 175]. As a result, the abundance of some taxa may be over- or under-estimated. Several modifications to previously published DNA extraction and sequencing protocols were undertaken in this study to minimize these biases. Samples were collected into 1M Tris/0.01M EDTA buffer with the complimentary aims of complexing potential PCR inhibitors and minimizing pH-related DNA damage from acid hydrolysis. Samples were stored at 4 ◦C immediately upon collection and were extracted within 48 hours to further minimize the potential for DNA degradation post extraction. The DNA recovery protocol used here included bead-beating in a buffered phenol-chloroform solution, which has been shown to yield optimum DNA quantity and size when compared to other cell lysis methods that use only chemical approaches [172]. Bovine serum albumin was added to PCR reactions to facilitate amplification in the presence of inhibiting compounds [174].

In addition to biases introduced by DNA extraction and amplification, rRNA sequencing and subsequent analysis are also subject to a number of uncertainties [176]. The Illumina MiSeq sequencing method uses small cameras to detect fluorescence on DNA clusters arranged in a two-dimensional space that indicate which base is being added to a DNA strand. The optics of these detectors makes it difficult to distinguish between clusters exhibiting the same color. This can present resolution problems when a sequencer is reading the barcode and primer regions of the sequencing run or when the samples being sequenced contain relatively low diversity. To help ameliorate this problem, a random number of Ns (nucleotides of any type) are added before the primer sequence to de-phase the sequences; further known quantities of PhiX phage DNA and high diversity DNA samples are added to the sequencing reaction to provide appropriate genetic contrast.

Many sequence data analysis programs use Naive-Bayesian methods to compare the sequences recovered from field samples to curated databases to assign taxonomy calls. Many of these approaches leverage cluster analyses, and do not use full sequence alignments; nor do they consider secondary structure when assigning taxonomy; thus, the sequence data is treated as mathematical vectors instead of biological data. The method used to determinate taxonomy here, does not use cluster analyses, and considers rRNA secondary structure in 1:1 sequence alignments to the 50,000-character alignment curated by SINA [164]; this enables a more statistically robust and biologically sound phylogenetic characterization of the DNA recovered from field samples.

3.3 Inhibitory aggregates

3.3.1 Sorbent characterization and modifications

3.3.1.1 Activated carbon

Granular activated carbon (GAC), supplied by the Calgon Carbon Corporation and commercially sold as OL 20x50, was used as the raw carbon sorbent. This GAC was manufactured from bituminous

coal and was activated using superheated steam. The minimum iodine number (estimate for surface area and porosity) was 1,050 mg/g as reported by the supplier [177]. The particle size distribution was determined by standard sieve analysis (Table 3-1).

Table 3-1. Particle size distribution of GAC, BOF-S, and Ottawa sand used in this study.

		GAC Calgon OL20x50	BOF-S 20x50	Ottawa Sand
Sieve	Sieve size (mm)	Passing by mass (%)	Passing by mass (%)	Passing by mass (%)
10	2.000	100.00	100.00	100.00
20	0.850	99.56	99.89	100
40	0.425	2.08	1.98	69.5
60	0.250	0.61	0.32	14.79
100	0.150	0.51	0.10	2.86
200	0.075	0.32	0.05	0.03

The raw unmodified GAC (GAC-UNM) was used as received and as the precursor carbon for the production of acidified activated carbon (GAC-ACID). Acidification aimed to enhance the chelation effect between the negatively charged surface and the metal cations in solution by increasing the number of acidic functional groups. Optimization of the acidification process was based on the pH at the point of zero charge (pH_{PZC}) in order to favor cationic adsorption at circumneutral pH while favoring leaching at pH levels relevant to initial acidophilic growth. Initial evaluation of the acidification process was completed by adding GAC-UNM into solutions containing different concentrations of HNO_3 at a liquid-to-solid ratio of 2:1. The mixtures were homogenized and kept at room temperature for 30 min. Next, the beakers were placed in a furnace at 250 °C for 2.5 h. After heat treatment, the cooled GACs, now referred as GAC-ACID, were thoroughly washed with DI water to remove any excess of unreacted acid. Then, the obtained GAC-ACID were oven dried at 60 °C overnight and kept at room temperature and low humidity until further use. The GAC-ACID used for further studies was the one obtained after treatment with 5% HNO_3, which resulted in a pH_{PZC} between 4.5 and 5. For comparison, the pH_{PZC} of the unmodified counterpart was above pH 8.

Characterization of both GAC-UNM and GAC-ACID included the specific surface area and pore size distribution, specific bulk gravity, water saturation, pH and selected chemistry of surface functional groups.

Brunauer, Emmet and Teller (BET) surface area, micropore and mesopore volumes, and pore size distributions were determined from N_2 isotherm data collected using a Micromeritics Gemini V Surface Area and Pore Size Analyzer (Micromeritics). Prior to analysis, GAC samples were degassed under vacuum (2.0×10^{-1} mbar) at 100 °C for 24 hours prior to analysis. The degassed samples were then cooled and weighed. Surface area and pore size analysis was performed once the weighed samples were transferred to the analysis port. After analysis, samples were weighed again to give the final mass, which was used in the surface area and pore size calculations. Surface area of the samples were calculated using the BET equation, assuming the surface area occupied by each physisorbed nitrogen molecule was 0.162 nm^2 [178]. Mesopore volumes (pore diameter between 2 nm and 50 nm [178] and surface areas were calculated using the Barret-Joyner-Halenda (BJH) method with the Halsey:Faas correction. Micropore volumes (pore diameter smaller than 2 nm [178]) and surface areas were calculated using the t-plot method with the Harkins and Jura thickness equation.

The pH of point of zero charge (pH_{PZC}) was determined by the pH drift method [179, 180]. Batch polypropylene (50 mL) tubes, containing 25 mL of 0.1 M NaCl solution, were pH-adjusted with either NaOH or HCl solutions. The minimum difference between initial set points was 0.2 pH units. Next, 50 mg of GAC were added per batch. To eliminate the influence from dissolved and atmospheric CO_2, the solution was sparged with N_2. Then, the batches were mixed for 48 h and final pH was measured. The pH_{PZC} was found for the batch that experienced no changes from its initial pH.

The equilibrium pH of each carbon was determined by addition of 1 g of GAC into 5 mL of deionized water. The suspension was sparged with N_2 and mixed for 24 h to reach equilibrium prior pH measurement.

Oxygen-associated surface functionalities were determined through Boehm titration with the modifications reported by Goertzen et al. [181, 182]. Briefly, 0.75 g of GAC were placed in 25 mL of 0.05 M of either $NaHCO_3$, Na_2CO_3 or NaOH. The mixtures were sparged with N_2, sealed, and mixed for 24 h at room temperature. Then, 10 mL aliquots were centrifuged at 5,000 rpm for 10 min, and filtered through a 0.2 µm nylon membrane. HCl (0.05 M) was added to completely neutralize the bases on each batch. The volume of acid added was 20 mL for $NaHCO_3$ and NaOH, while the volume added for Na_2CO_3 batches was 30 mL. Next, the solutions were sparged with N_2 for 2 h, and back-titrated with 0.05 M of NaOH to obtain the contribution of the different functional groups on each GAC.

Fourier Transformed Infrared Spectroscopy (FTIR) spectra was obtained for each type of activated carbon using a Fourier Transform IR spectrophotometer (Nicolet iS10, Thermo Scientific, USA) in the range of 400-4,000 cm^{-1}. The samples were examined as KBr disks and the background spectrum of air was subtracted from their spectra. All samples were run by duplicate. Initial sample preparation used a mortar and pestle to crush the material into a fine powder (< 100 mesh). Next, a dry preparation of the powdered analyte was mixed with KBr powder to include a final mass concentration of 1 %. The mixture was then dried in a vacuum oven at 120˚C overnight and after that, pressed to obtain the KBr disks.

3.3.1.2 Steel slag

Basic oxygen furnace steel slag (BOF-S) 20x50 US mesh size, was obtained from the Indiana Harbor East Steel Mill complex in East Chicago (Indiana, USA). Characterization was done through determination of water absorption, specific gravity, pH, chemical and mineral composition.

Water saturation, specific bulk gravity were determined in accordance with ASTM standard C128-15 [183].

The equilibrium pH was determined by addition of 1 g of BOF-S into 5 mL of deionized water. The suspension was sparged with N_2 and mixed for 24 h to reach equilibrium prior pH measurement.

Chemical composition of the BOF-S was determined by Inductively Coupled Plasma – Optical Emission Spectroscopy (ICP-OES), on a calibrated ARL 3410+, using modifications to a widely accepted technique developed by Farrell et al. [184]. Five mL of a 7:3 mixtures of hydrochloric acid and hydrofluoric acid were combined with 2 mL of nitric acid and placed in digestion tubes that were maintained at 95 °C in a digestion block (HotBlock, Environmental Express) for approximately two hours. Samples were then cooled and brought to 50 mL with a 1.5 % boric acid solution (by mass). The samples were then reheated to 95 °C for 15 minutes and cooled for analysis. The samples were diluted 10x with deionized water and analyzed with the ICP-OES, as described above. An analytical blank, along with three standards that were made by accurately diluting certified standards, were used for calibration.

To determine the mineralogy of the sorbent, the BOF-S sample was first crushed into a powder with a mortar and pestle. The powder was then prepared for analysis using a modified method based on [185]. A Siemens D500 X-ray diffractometer was used to acquire the energy dispersion pattern. The sample was analyzed from 5 to 65 degrees 2θ using Cu Kα X-ray radiation, with a step size of 0.02 degrees and a dwell time of 2 seconds per step. Mineralogy was identified using Jade software (MDI, Version 9) and the International Centre for Diffraction Data (ICDD) 2003 database. Corundum was used to normalize peak heights between samples and align diffraction patterns.

A modified ethylene glycol method was used to evaluate the free lime content of the BOF slag [186]. Two types of slag were used for free lime determination: granular (20x50 US mesh size), and powdered (<100 US mesh size). Briefly, 1 gram of BOF slag was added into 50 mL preheated ethylene

glycol (80 °C). The solution was left in a water bath for 15 minutes with regular agitation. After the treatment, the solutions were centrifuged at 5,000 g for 10 minutes, and a 25 mL-aliquot was vacuum filtered. About 25 mL of deionized water and 1 ml of phenolphthalein indicator solution were added to the filtrate and then titrated to a colorless endpoint with 0.05 N HCl. The free lime content was calculated according to the next equation:

$$\%\ \boldsymbol{Free\ CaO} = \left(\frac{\boldsymbol{mL\ HCl \cdot normality\ of\ HCl}}{\boldsymbol{10 \cdot sample\ weight}}\right) \cdot \mathbf{28} \qquad \text{(Equation 1)}$$

3.3.2 Metal sorption/desorption tests

3.3.2.1 Sorption tests

For laboratory metal inhibition studies in solid media (Section 3.4.1), GAC-UNM was loaded with different metal species. Ten grams of GAC-UNM was added into 200 mL of DI water contained in each of 6 Erlenmeyer flasks where solutions were adjusted to a concentration of 50 mM using the following salts: $Cu(NO_3)_2$, $CoCl_2$, $CdSO_4$, $ZnSO_4$, and $NiCO_3$. Adsorption was facilitated by mixing at 120 rpm for 24 h at 20 °C. The metal laden GAC was then washed with DI water and placed in a furnace at 40 °C for 24 h. Once dried, the GAC was ground and sieved (< 0.1 mm), and referred as powdered activated carbon (PAC). Sorbed metal content was determined through ICP-OES of the digested powder, following the same protocol as in Section 3.3.1.2.

For the bioreactor and the field study (Sections 3.4.3 and 3.5), both GAC-UNM and GAC-ACID were loaded with Cu and Co as follows: Two 1-L glass bottles were prepared with 10 mM solutions of Cu ($Cu(NO_3)_2$), and 10 mM of Cu ($Cu(NO_3)_2$) and 10 mM Co ($Co(NO_3)_2$), respectively. GAC was added at a liquid-to-solid ratio of 20:1. For GAC-UNM, the metal solution was adjusted to pH 8 with NaOH 1M prior GAC addition. The batch was mixed overnight at 120 rpm and room temperature. For GAC-ACID, the metal solution was pH adjusted to the highest pH achievable where cationic Cu species were dominant in solution (pH 5.7-6), as estimated with a pH-dependent speciation diagram (Figure 3-1). Then, GAC-

ACID was added and mixed overnight at 120 rpm and room temperature. Next, the GAC-ACID was removed from solution and dried in an oven at 60 ˚C overnight. This partially loaded GAC-ACID was then added to a freshly prepared metal solution with the same conditions as the initial metal solution. This was done to ensure saturation of electrostatically sorbed Cu species onto GAC-ACID. After these process, both GAC-UNM and GAC-ACID were filtered using a filter paper (No.1 Whatman), and were washed with DI water, previously pH-adjusted to the final value of the batches in order to remove any non-sorbed or otherwise loosely-associated metal and avoid possible pH-dependent leaching. Next, the GAC was placed in an oven at 60 ˚C until dry. One gram of each GAC was used for metal load determination through ICP-OES, as previously described. The remaining GAC was stored until further use.

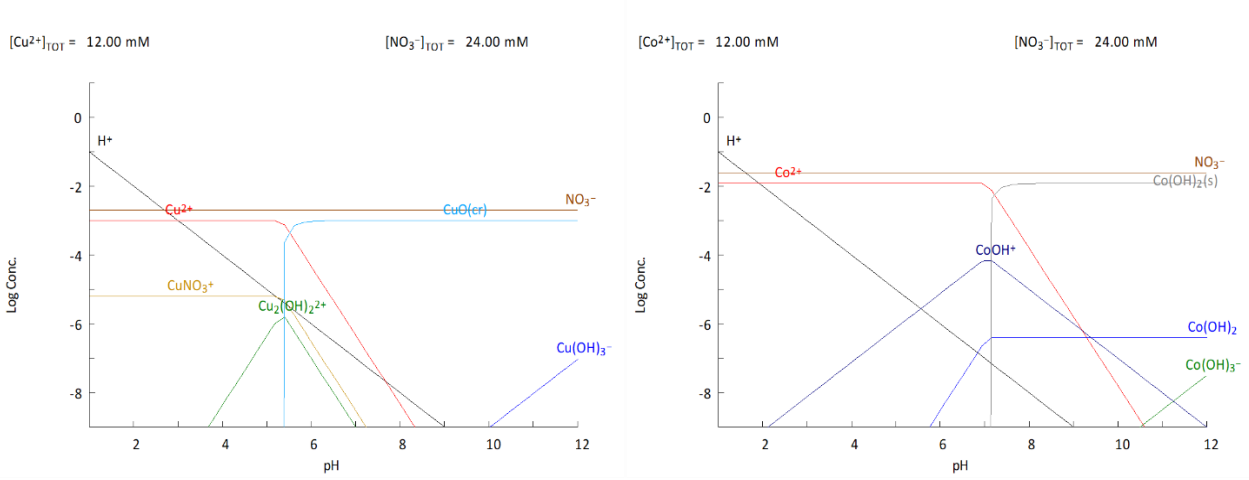

Figure 3-1. pH-dependent speciation of $Cu(NO_3)_2$ and $Co(NO_3)_2$ (12 mM each) in water. Only major species are shown.

BOF-S was loaded with Cu and Co as follows: 40 g of BOF-S was added into 1 L of deionized water contained in each of 2 1 L-glass bottles where solutions were adjusted to a concentration of 10 g/L $Cu(NO_3)_2$, and 10 g/L of both $Cu(NO_3)_2$ and $Co(NO_3)_2$. Next, batches were mixed at 120 rpm overnight. After adsorption, the BOF-S were processed identical to the GACs.

3.3.2.2 Desorption tests

The Acid Neutralization Capacity (ANC) and leaching profiles of the pure metal-laden sorbents, and the same embedded and cured in Portland cement, were assessed through batch leaching tests. One gram of powdered (<0.149 mm) pure Cu or Cu/Co laden sorbent was added to 20 mL aqueous solutions of HNO_3, in increasing H^+ equivalents, per kg of solid. The batches were mixed at 120 rpm for 24 h and room temperature. Next, the final pH of the solution was measured and the batches were centrifuged at 5,000 rpm for 10 minutes. The supernatant was recovered, filtered through a 0.2 µm filter, and aliquoted for cation analysis through ICP-OES. Additional ANC testing was performed for the same sorbents embedded and cured in Portland cement. Sample formulation and curing conditions were as described in Section 3.5.1 for the highest GAC and slag content. Leaching protocols and analyses were completed as described above for pure metal laden sorbents with some modifications. The acid used was changed to H_2SO_4 to reflect the dominant acid to which the samples were exposed in the field study, and increased equivalents of acid, per mass of solid, were used to account for the alkalinity provided by the Portland cement.

3.4 Laboratory metal inhibition studies

3.4.1 Metal inhibition potential in solid media

To assess the effectiveness of selected heavy metals in inhibiting acidophilic growth, a modified Kirby-Bauer assay was developed [187]. Rectangular polypropylene plates (14 cm × 5 cm) were autoclaved (pre-sterilized plastic may be substituted) and filled with 50 mL sterilized *Thiobacillus* agar (pH 5.5) previously described by Starosvetsky et al. [151], using thiosulfate ($S_2O_3^{2-}$) as a sole sulfur source; addition of Bromcresol green makes the agar change color from blue to yellow in response to biogenic sulfuric acid production (from inoculated acidophilic cultures), which drops the media pH below 4. Immediately following solidification, all agar was removed for a linear distance of 5 mm from one edge (long axis); this volume was replaced with a solution of liquid *Thiobacillus* agar and metal

impregnated activated carbon (10 mg/mL), by adding the different PACs prepared in Section 3.3.2 for laboratory metal inhibition studies in solid media. This resulted in triplicate rectangular plates containing a band of the following PAC-metal combinations: PAC-Cu, PAC-Co, PAC-Cd, PAC-Ni, PAC-Zn, and PAC-No metal as a control. Once dried, the plates were inoculated by evenly spreading 0.5 mL of an enriched SOB culture (Section 3.1.1) on each rectangular agar surface to facilitate monolayer growth. Control plates were prepared without inoculation to compare the pH-dependent leachability of the metals from the carbon particles. All plates were incubated at 30 °C in the dark for 10 days. After incubation, inhibition distances were measured by means of a caliper and divided based on the absence/presence of colonies. A small cylinder of agar (5.25 mm diameter) was extracted to the plates' depth at the interface between the inhibition area and the area containing dispersed colonies; this was digested by diluting the sample in DI H_2O and heating until the agar dissolved. Then three drops of concentrated HNO_3 (70 %) were added to facilitate determination of metal content through ICP-OES. For Cu and Cu/Co tests, agar samples from both inoculated and non-inoculated plates were extracted at different days and distances in order to describe the leaching behavior of the metal from the PAC. Distances selected for bacterial quantification were located in the center of the inhibition zone and the dispersed colonies distance, and 10 mm into bacterial monolayer. Using the same sampling approach as for the metals, cells were eluted from the agar surfaces of cylindrical punches into 300 µL of phosphate buffer saline (PBS) with 0.01 % Tween (Sigma-Aldrich). Cell counts, as described in Section 3.1.2, were normalized to the surface area from which they were eluted.

3.4.2 Metal inhibition in liquid media

Glass Erlenmeyer flasks were filled with 50 mL of *Thiobacillus* media and autoclaved at 121 °C for 15 min. Once media cooled to room temperature, acidophile cultures were inoculated by adding 150 µL of an enriched mixed culture extracted from a concrete corroded site. Metals used for acidophile growth inhibition included: Cu, Co, and Ag. Cu and Co were chosen as they have proven to be effective candidates

against sewer-crown acidophilic communities [116]. Ag was included as it is a broad-spectrum antibiotic metal used in a variety of formats and applications [188]. Metal stock solutions were prepared by dissolving metal salts in DI water. Salts used included: $Cu(NO_3)_2$, $Co(NO_3)_2$, and $AgNO_3$. Solutions were filtered through a 0.2 µm cellulose acetate filter before use. Volumes of the different metal stocks were added to establish a concentration gradient (Table 3-2). Next, flasks were incubated at 30 °C in the dark with occasional agitation. Acidophile metabolism was evaluated by measuring pH change over time with a pH meter (SympHony SP70P, VWR). To avoid contamination, the pH electrode was soaked in sterile 70% ethanol solution for 5 minutes and air dried prior immersion into each culture. Incubation lasted until pH dropped below 2.5 for batches were acidophilic metabolism was detected. This pH is indicative of *Acidithiobacillus spp.* exponential growth phase as demonstrated by different authors [189, 190]. Experimental endpoint for batches that did not experience pH drop was set based on the possibility of metal induced acidophile lag growth phase. Thirty to thirty-five days since inoculation was considered to be sufficient time to detect this effect, and set as the experimental endpoint for these cultures. Aliquots from each culture were extracted for total bacterial abundance and for analysis of bacterial profiles using the Illumina MiSeq platform (Section 3.2) at the end of the experiment.

Table 3-2. Heavy metal concentrations tested against acidophile development in thiosulfate-based media.

Metal	Concentration (mg/L)								
Cu	0	5	10	20	25	40	50	75	100
Ag	0	10	20	40	50	75			
Cu/Ag	0/0	10/5	20/10	30/15	40/20	50/25	60/30	100/50	
Co	0	10	20	30	40	50			
Cu/Co	0/0	5/5	10/10	15/15	20/20	25/25	40/40		

3.4.3 Mortar formulation tests in bioreactor settings

The effectivity of metal-laden sorbents incorporated in Portland cement was evaluated through laboratory simulation of the corrosion conditions that affect concrete infrastructure in sewer systems. The mortar samples challenged in laboratory studies are presented in Table 3-3 . Mix design, description

of the materials used, and rationale and is presented in Section 3.5.2. Cement, water, sand, and the different sorbents mixed were cast to form rectangles of 13x34x2.5 mm. The mortar samples were cured at 99% relative humidity for 7 days. Next, the samples were attached to polycarbonate slides and inserted into an annular biofilm reactor (Model 1100, BioSurface Technologies Corp.). To ensure elevated humidity through the experiment, 150 mL of water was added into the annular reactor prior gas addition. Moreover, the annular reactor was submerged into a heated water bath to ensure an internal water temperature between 28 and 30 ˚C. The reactor spun at 25 rpm for the duration of the experiment. Due to the elevated pH of fresh mortar, initial abiotic acidification of the mortar surfaces was facilitated by H_2S and CO_2 gases for 30 days. Gases were generated by addition of $NaHCO_3$ (1.5 g/L) and Na_2S (2.5 g/L) into a stirred 500 mL 5% HCl reservoir. Complete system design is shown in Figure 3-2. Next, the mortar samples were individually inoculated with 150 µL of acidophilic mixed culture once per week for 30 days. After inoculation, gas concentrations were measured with a gas monitor (GasAlert Micro5 IR, BW Technologies) and kept between ranges associated to severely corrosive environments (H_2S: 100-500 ppm_v, CO_2: 10,000-30,000 ppm_v). After 250 days, exposed mortar samples were recovered, and the corrosion product was removed with sterile stainless steel brushes. Samples were weighted before and after removal of the corrosion product. Next, the debris were diluted in 10 mL sterile saline solution and used as the solution for consecutive analysis.

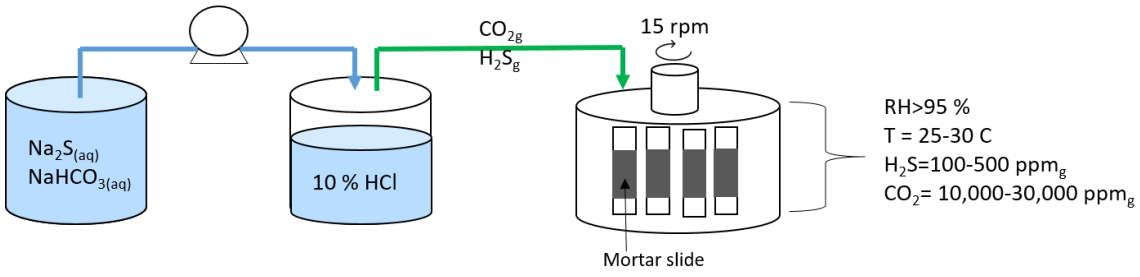

Figure 3-2. Diagram of annular reactor system used to simulate corrosive sewer environments. Blue line indicates the liquid transport of Na_2S and $NaHCO_3$ into the gas generator. Green lines indicate the transport of produced gases into the annular reactor.

Table 3-3.Formulations tested in simulated corrosion environments (Detailed rationale and mortar mix design is explained in Section 3.5.1 and Section 3.5.2).

Sorbent	Metal	Sand replacement (wt%)
N/A	N/A	0
GAC-UNM	N/A	10
GAC-UNM	Cu	10
GAC-UNM	Cu/Co	10
GAC-ACID	N/A	10
GAC-ACID	Cu	10
BOF-S	N/A	10-equivalent*
BOF-S	Cu	10-equivalent*
BOF-S	Cu/Co	10-equivalent*

*10-equivalent: Volumetric BOF-S grain distribution in the mortar equal to the 10% GAC formulations.

pH of the dilutions was measured with a calibrated pH-meter (SympHony SP70P, VWR). Microbial activity was measured as described in Section 3.1.3. Relative abundance of *Acidithiobacillus spp.* was evaluated through qPCR of the 16S rRNA gene as described in Section 3.2.2.

3.5 Field study

3.5.1 Mortar formulation rationale

The microbial inhibition effects of the metal-laden sorbents, incorporated as a substitute of fine aggregate in cement mortars, was evaluated in a sewer manhole exposed to moderate/severe corrosion. Addition of antimicrobial fine aggregates, and general cement mortar design, was based on the minimum inhibitory metal concentration (MIC) required to stop acidophilic growth in laboratory settings, while meeting the specifications for mortar mix design from ''AWWA C104-08: Cement-Mortar Lining for Ductile-Iron Pipe and Fittings" [191]. The goal was to incorporate enough aggregate to ensure a theoretical minimum metal concentration in the samples above the MIC. Additionally, the replacement of sand for metal impregnated aggregates minimized divergence from the particle size

distribution of the sand being replaced. Three different percentages (on a mass basis) of sand replacement for granular activated carbon were assessed: 2%, 5%, and 10%. For steel slag, the amount of sand replaced was the equivalent volumetric grain distribution equal to the 10% formulation containing GAC.

3.5.2 Mortar cement formulations

The cement used in this study was a commercial Portland cement (Type I/II) manufactured by Quikrete (USA) that complies with ASTM C150-16 [58]. The alkali- and metalloid-oxide content (obtained from X-ray fluorescence spectrometry (XRF)) as well as calculated Bogue composition of the cement used are summarized in Table 3-4. Ottawa test sand (U.S. Silica Company, USA) was used as the base fine aggregate. According to the manufacturer, this standardized aggregate is a clean natural sand with high silica content; it contains the following constituents on a percent basis: between 99.0-99.9% crystalline silica (quartz), < 1.0 aluminum oxide, < 0.1 iron oxide, and < 0.1 titanium oxide. The sand conforms to ASTM standard C778-17 [192]. The particle size distribution was also determined from standard sieve analysis, which is summarized in Table 3-1. Sorbents used as substitutes for sand are described in Section 3.3**.**

Table 3-4.Alkali- and metalloid-oxide content and Bogue composition analysis (% wt) of the cement.

Material	**CaO**	**SiO_2**	**Al_2O_3**	**Fe_2O_3**	**K_2O**	**MgO**	**Na_2O**	**SO_3**	**Loss on Ignition (LOI)**
Quikrete Type I/II	62.80	20.25	4.31	3.85	0.35	1.98	2.08	2.42	3.29
Calculated Bogue composition									
	C3S	**C2S**	**C3A**	**C4AF**					
Quikrete Type I/II	59.2	13.4	4.91	11.7					

The formulations tested are shown in Table 3-5 and the mortar mix was design used in Table 3-6. First, the cement, sand, and sorbents were dry mixed. Next, water was added and the mixture was thoroughly mixed for 90 seconds. Additional water was required to account for the water adsorption capacity of the

sorbent and to maintain the effective water-to-cement ratio between formulations. The resulting paste was cast in polypropylene cylinders (26.6 mm diameter, 40 mm height) avoiding the complete filling of the mold. The cast samples were tampered to release entrapped air and placed in a hydration chamber (99% RH) for a minimum of 7 days. Finally, samples were weight after curing (wet weight) and kept in a hydration chamber prior manhole installation. All formulations were prepared in quadruplicate. Three replicates were used for manhole installation while the remaining samples were kept in a hydration chamber for the duration of the experiment and used as unexposed controls. Sample classification and nomenclature used throughout the studies is shown in Figure 3-3.

Table 3-5. Formulations designed for field studies (based on sorbent used, metals sorbed, and percent of sorbent replacing sand within the mortar mix). All mortar formulations were prepared by quadruple.

Sorbent	Metal	Sand replacement (wt%)
N/A	N/A	0
GAC-UNM	N/A	2,5,10
GAC-UNM	Cu	2,5,10
GAC-UNM	Cu/Co	2,5,10
CAC-ACID	N/A	2,5,10
GAC-ACID	Cu	2,5,10
BOF-ACID	N/A	10-equivalent*
BOF-S	Cu	10-equivalent*
BOF-S	Cu/Co	10-equivalent*

*10-equivalent: Volumetric BOF-S grain distribution in the mortar equal to the 10% GAC formulations

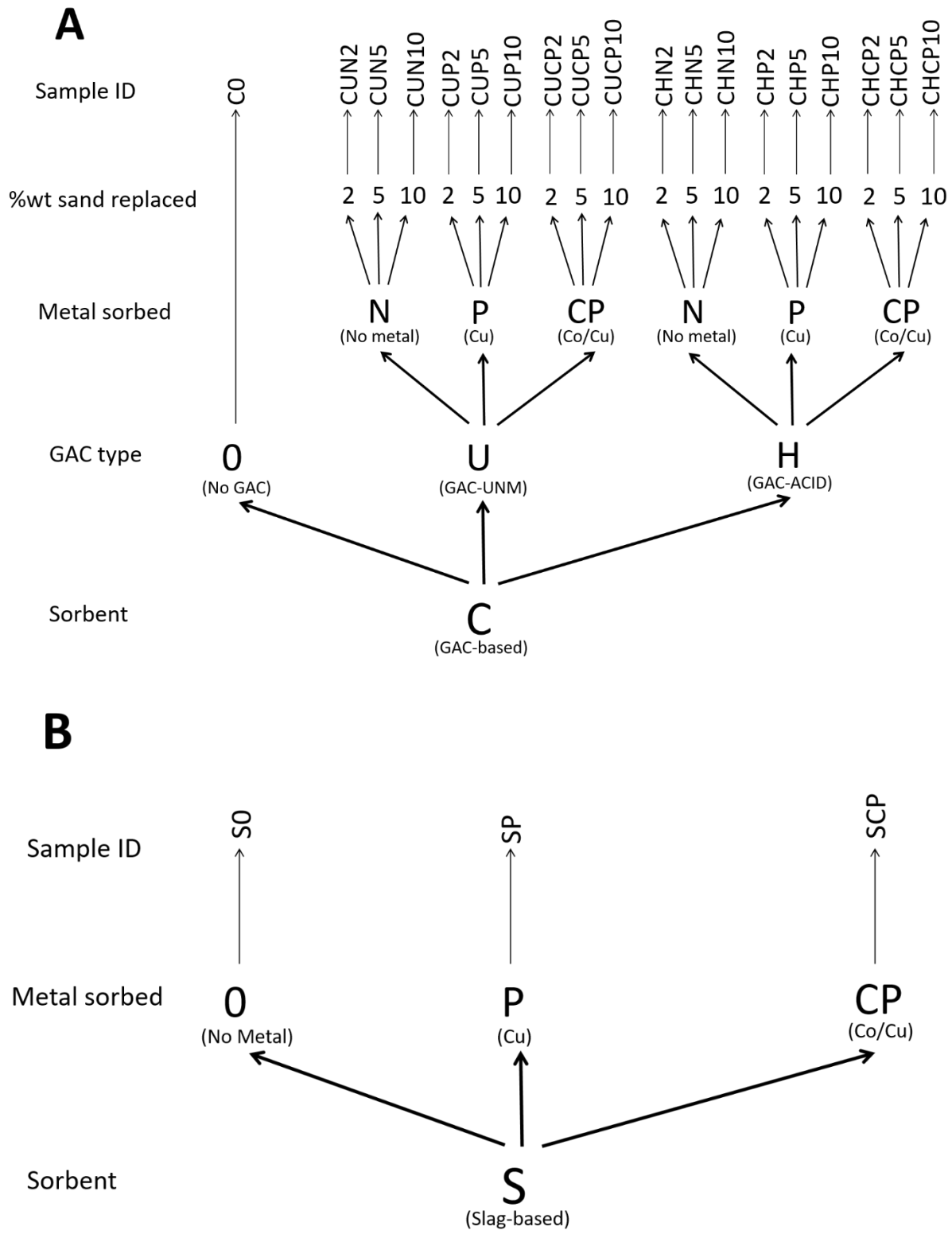

Figure 3-3. Classification nomenclature of the mortar formulations used in the studies. A) Mortars containing GAC. B) Mortars containing BOF-S.

Table 3-6. Mix design for the mortar formulations tested. GAC includes both acid-modified and unmodified of carbon. used as no significant differences in water absorption were seen. Ratios are given on a mass basis.

Formulation	W/C ratio	W/C ratio (effective)	C/S ratio
Mortar	0.4	0.4	0.43
GAC at 2%	0.44	0.4	0.44
GAC at 5%	0.49	0.4	0.45
GAC at 10%	0.58	0.4	0.48
BOF-S	0.4	0.4	0.72

*No significant differences in water absorption between GAC types.

3.5.3 Field test assessment and sample recovery

Cast mortar samples were inserted in polypropylene racks as shown in Figure 3-4. The inverted setup allowed for exposure of mortar surfaces to the manhole headspace environment while protecting them from exogenous acid sources and cross contamination.

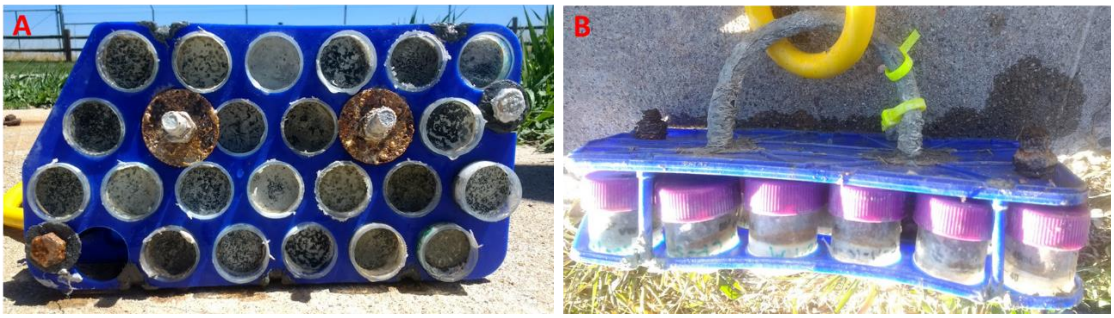

Figure 3-4. Example views of approximate volume and mass casted mortar samples installed in polypropylene racks secured with epoxy coated-stainless steel bolts and rods. A) bottom view. B) Front view.

The racks were hung on the steps in the manhole of a reclaimed metering station ladder located in Thornton, Colorado (Figure 3-5). This manhole receives domestic wastewater from a lift station, which causes the release of H_2S and CO_2 into the manhole. Due to the elevated concrete corrosion rates in this appurtenance, the Denver Metro Wastewater Reclamation District coated this and other manholes with a polymeric, acid resistant coating. These racks were left for a total of 11 months with periodic monitoring of the corrosion extent, and measurement of gas concentrations for the duration of the experiment.

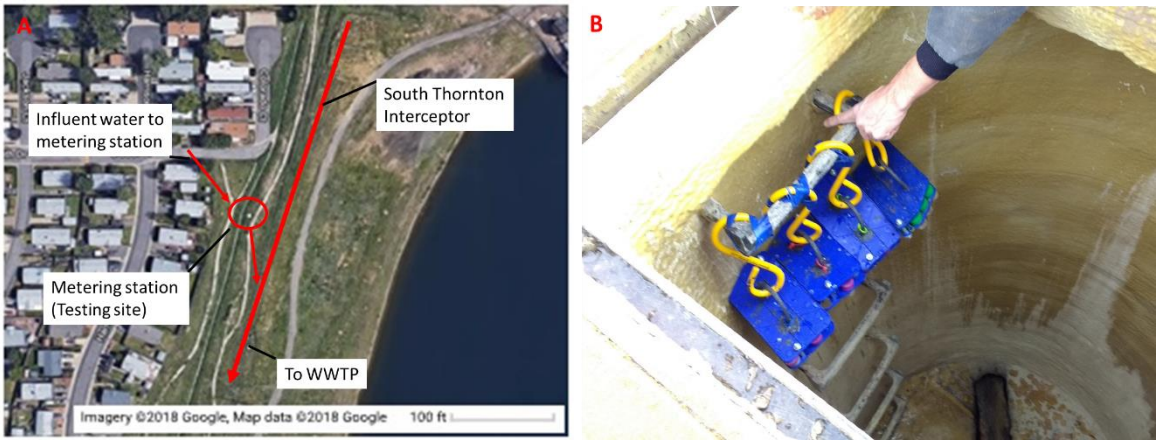

Figure 3-5. A) Map from the testing location. Red arrows indicate flow direction. The red circle shows the reclaimed metering station (LAT, LONG: 39.851046, -104.943181) used for accelerated corrosion studies. B) Photograph of the polypropylene racks installation in the manhole steps.

3.5.4 Experimental setup limitations

Specimens were exposed to the manhole's headspace environment with periodic visual inspections to assess their corrosion, and monitor H_2S and CO_2 concentrations. Experimental end-point was considered when significant differences between formulations were visually observed. This resulted in two important experimental limitations: 1) only point measurements of gas concentrations were recorded, as opposed to continuous monitoring and, 2) the results described the response of the formulations against biogenic corrosion for a total period of 11 months in a moderate-to-severe corrosive environment. Therefore, only projections on formulation performance can be made after that time.

Space availability and manhole accessibility limited the size and number of specimens tested. Sample dimensions were designed to maximize the number of formulations studied, with their respective controls and replicates, that resulted in a statistically representative data with the appropriate statistical power to resolve the anticorrosion response of the different formulations.

The polypropylene molds were designed to protect the specimens from contact with the manhole ceiling, wall or steps and their installation in the rack prevented them from falling into the

wastewater flow. However, biogenic acid production was uninhibited at the intersection of the interior polypropylene case wall where it contacted the mortar surface. As such, this resulted in corrosion patterns moving radially inward from the periphery of the circular mortar surfaces to the center.

3.6 Analysis of field samples

3.6.1 Extent of corrosion

All mortar samples were weighted prior to and post-removal of the corrosion product. Corrosion product was manually separated with a sterile scalpel. For samples presenting this type of corrosion, a fraction (10-70 mg) was saved and used for determination of the moisture content (Section 3.6.3). Complete corrosion product removal was achieved by wetting the corroded surface with a sterile saline solution and brushing the sample's surface with a sterile stainless steel brush. The total collected corrosion product was diluted in 10 mL saline and was referred as the "corrosion eluate".

Pictures of the exposed surfaces were taken and analyzed for corrosion extent of the exposed specimen area. Quantitation of the visible corrosion extent was completed using image J image processing capabilities [193, 194].

3.6.2 Microbial assays

Microbial activity of the dissolved corrosion product was measured on 1-to-10 dilutions of the corrosion eluate as previously described in Section 3.1.3. The assay was completed as soon as the corrosion eluate solution was prepared, to most accurately reflect the activity of the cells prior to their extraction from the coupon surfaces.

Sample preparation for microbial abundance started with the preparation of aliquots from the corrosion eluate in 4% paraformaldehyde. The preserved samples were kept at 4 °C until further use.

Before cell enumeration, the samples were diluted 1-to-10 in PBS with 0.1% Tween to facilitate cell detachment from biofilms. Next, the dilutions were sonicated with 80 W for 90 s to facilitate cell detachment from suspended solids. Then, the solutions were vortexed and the corrosion debris was allowed to settled for 20 min. Working solutions for cell counts were prepared by diluting the samples in water. Whole cell quantification was performed as described in Section 3.1.2.

Samples for DNA analysis were collected and diluted in 10 mM Tris/1 mM EDTA buffer to minimize DNA damage and to complex metal ions that could potentially inhibit DNA amplification. Samples were kept at 4 °C for a maximum of 48 hours before extraction (Section 3.2.1).

3.6.3 Moisture content

Fractions of corroded concrete from the field were dried at 60 C overnight. Samples were weighed before and after drying, and moisture content was calculated by dividing the mass lost by the original (wet) mass.

3.6.4 pH: Corrosion product and pore water

Due to the different corrosion performance of the formulations, samples were analyzed differently based on the presence or absence of a soft corrosion product. Superficial pH of samples that did not exhibit the external formation of a soft corrosion product were assessed by determining the pH of the original corrosion eluate (Section 3.6.1). Samples that presented external corrosion product were also analyzed for pore water pH. Pore water pH was estimated by adding a known amount of un-buffered saline solution (pH 6-8) to a fraction of the corrosion product. Hydrated samples were mixed and allowed to equilibrate for an hour, and pH was measured. Original pore water pH was estimated based on the volume of pore water in the sample (measured as described in Section 3.6.3), the volume of saline added, and the original pH of the water using Equation 2. This calculation was developed for

this thesis based on the assumption that pH is equal to the base-10 log of the hydronium ion concentration and the sum of pH and pOH is 14.

If $pH_m < pH_w$

$$\boldsymbol{pH = -log\left(\frac{(V_{sw}+V)\cdot 10^{-pH_m} - V_w \cdot 10^{-pH_w}}{V_{sw}}\right)} \qquad \text{(Equation 2)}$$

Where:

pH is calculated pH of sample water
pH_w is the pH of the saline solution
pH_m is the measured pH of equilibrated sample plus added water
V_{sw} is the volume of pore water in the original sample
V_w is the volume of saline solution

3.6.5 Chemistry evaluation of mortar formulations

To elucidate the corrosion response of the different formulations, the saline corrosion eluates, obtained in Section 3.6.1, were analyzed for calcium and total sulfur through, using ICP-MS by digesting aliquots from the corrosion eluate as described in Section 3.3.1.2.

Separately, intact, corrosion-exposed mortar cylinders were dehydrated by immersion in isopropanol at a 3: 1 liquid-to-solid ratio. After 7 days, the isopropanol solution was replaced and the samples were immersed for another 7 days. Next, the isopropanol was removed and the samples were vacuum dried for 48 hours. The dried mortar formulations were further processed for cation mobility assays and electron microprobe analysis (Section 3.6.6). Mobility of Ca, Cu, and Co before and after exposure to corrosive environments was assessed through sequential extractions of selected formulations. Sample preparation started with a cross sectional cut with a diamond blade (4" Trim Saw, Hi-Tech), on the y-axis of intact mortar cylinders exposed (or unexposed) to corrosion. One of the obtained halves was further cut at 3.5 mm depth from the corroded surface (or uncorroded for unexposed controls). The obtained half-thin disks were crushed and pulverized using a mortar and a pestle to pass a no. 100 mesh. The resulted powder was directly used for sequential cation extractions.

The extraction procedure was based on that of Tessier et al. for soils and sediments with the modifications developed by Li et al. for cement based solidified/stabilized waste materials [195, 196].

3.6.6 Electron Microprobe Analysis (EMPA)

Intact mortar cylinder "halves" not used for sequential extraction (Section 3.6.5) were analyzed for elemental mobility and relative elemental abundance through EMPA. Initial sample preparation required curing the dried samples in epoxy resin (EpoThin™ 2, Buehler) under vacuum to facilitate penetration of the resin into the void spaces. Once dried, the casted samples were cut with a diamond blade (4" Trim Saw, Hi-Tech) to expose the surface on interest. Next, sequential grinding was performed on the surface using silicon carbide abrasive sheets with increasing grit number (400, 600, 800, 1,000, and 1,500). Final sample polishing was done on a polisher (MetaServ™ 250 Grinder Polisher, Buehler), by use of diamond suspensions with decreasing size (9, 6, 1, and 0.25 microns). The quality of the grinding/polishing was visually assessed by use of a digital microscope (AM3111T, Dino-Lite). Final silver coating of the surface was added to improve sample electric conductivity prior EMPA (10 nm thickness).

The mobility and fate of elements of interest after exposure to corrosive environments was analyzed by compiling X-ray element maps of Si Kα, Al Kα, S Kα, Ca Kα, Fe Kα, Mg Kα, Co Kα, and Cu Kα obtained using a JEOL-8230 electron microprobe. In some cases, two maps for Cu Kα and Co Kα were tomographically assembled to enhance precision. An acceleration voltage of 15 keV and beam current of 50 nA was used for all maps. The electron beam was focused between 5 to 6 µm to match the pixel size, and a dwell time of 20 msec was used. Element maps were treated with CalcImage (ProbeSoftware, Inc.) to remove conflicting background using the mean atomic number (background) correction [197]. Results, expressed as net counts, are semi-quantitative since each pixel likely represents a mixture of two or more phases. The respective intensity scale bars differed for each element.

Chapter 4 Results

4.1 Metal inhibition potential in solid media

Inhibition potential of selected heavy metal ions was determined by a modified Kirby-Bauer diffusion susceptibility test [187]. As indicated by a pH-sensitive indicator dye, after 10 days, the agar pH dropped below 3 evenly across the plate, and the following three microbial growth zones distinctly emerged with different characteristic lengths, from the metal-laden powdered activated carbon (PAC): a clear inhibition zone, followed by a zone of dispersed macrocolonies, which then transitioned into a "lawn" of continuous bacterial growth (Figure 4-1). The control plate (Figure 4-1, A) containing PAC with no associated metals showed continuous growth along its length, and a small inhibition distance was measured (<5 mm). Different inhibition distances were measured based on the type of metal used and the amounts leached into the agar.

Table 4-1. Metal content as normalized by activated carbon mass (mg Metal/g PAC). Metal masses were determined by ICP-OES from the digested PAC.

PAC-Metal					
Cu	Co	Cd	Ni	Zn	(Cu/Co)
10.6	13.4	18.6	4.1	11.6	11/5.1

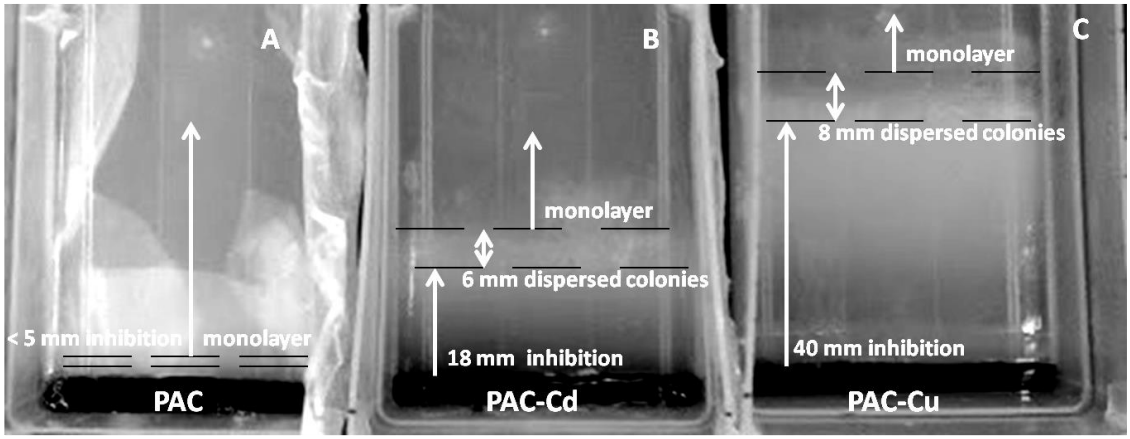

Figure 4-1. Photographs of inhibition response from sulfur oxidizing bacteria isolated from a corroding sewer grown on thiosulfate-containing agar after 240 hours (final pH≤ 3), in the presence of (A)-PAC alone; (B)-PAC+Cd (18.6 mg/g); and, (C)-PAC+Cu (10.6 mg/g).

After accounting for the inhibition distance observed on the control plates, and normalizing this characteristic distance by the metal concentrations leached, the "potential" of each metal in inhibiting acidophilic growth was indexed in Figure 4-2 .

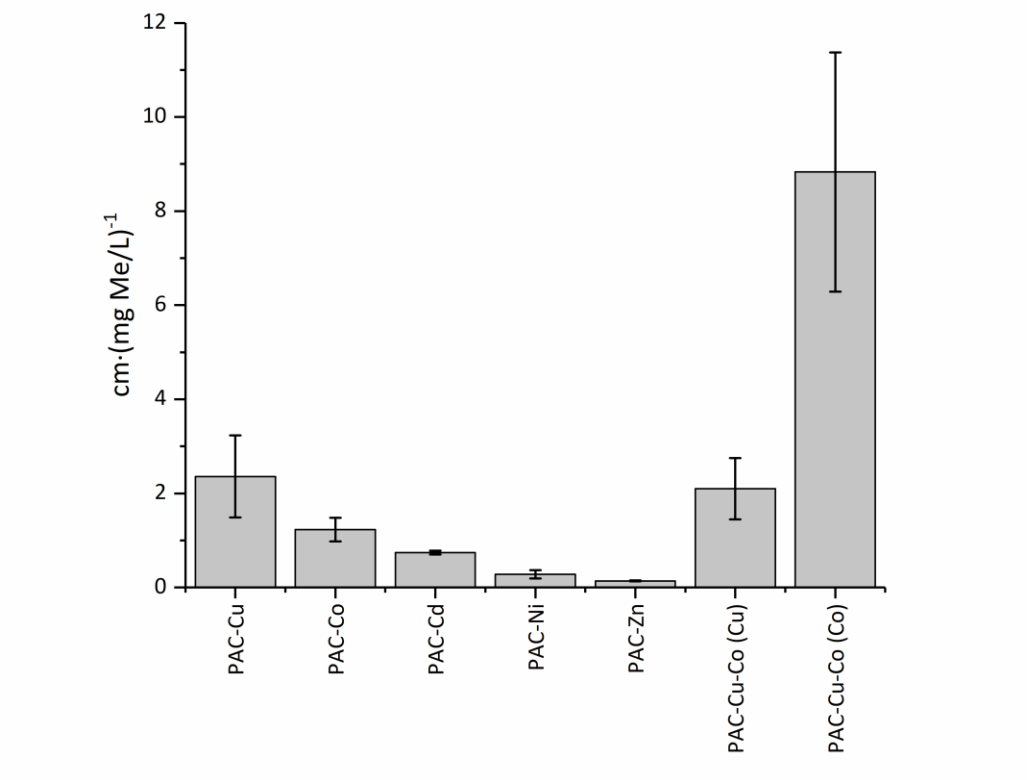

Figure 4-2. Characteristic inhibition lengths normalized by local metal concentration which had diffused to the end of the inhibition zones as compared to otherwise identical control plates not containing metal. Plates which were co-loaded with both copper and cobalt are on the right side of the plot; parentheticals below represent metal measured in co-loading scenario. (n=3).

Metal normalized inhibition lengths followed the series Cu>Co>Cd>Ni=Zn, where Zn and Ni displayed the least (relative) inhibitory potential. When Co and Cu were concomitantly loaded on activated carbon, the inhibition potential associated with Co increased 7.18 times over that of the Co alone, while Cu inhibition potential remained significantly unchanged. The correspondent average values on a normalized basis were: 2.36 cm·(mg Cu/L)$^{-1}$, 1.23 cm·(mg Co/L)$^{-1}$, 0.74 cm·(mg Cd/L)$^{-1}$, 0.28 cm·(mg Ni/L)$^{-1}$, 0.14 cm·(mg Zn/L)$^{-1}$, and 2.1 cm·(mg Cu/L)$^{-1}$ and 8.83 cm·(mg Co/L)$^{-1}$, the latter two values when concomitantly loaded.

Bacterial cell abundance on the different areas of the plate surfaces were quantified using the epifluorescence microscopy methods described in Section 3.1.2. Areas selected for representative analysis were located in the center of each inhibition zone and the dispersed colonies area, and 10 mm into the bacterial monolayer. For all metals, cell densities were consistently lower at the inhibition zone, averaging $1.67 \cdot 10^4$ cells/mm^2. Cell densities in the disperse colonies area were the highest, averaging $1 \cdot 10^7$ cells/mm^2. Finally, the cell densities found in the monolayer were slightly lower than in the previous area, averaging $1.87 \cdot 10^6$ cells/mm^2. The control plates without metals had consistent values along the plate, and presented minimum changes ($9.09 \cdot 10^5$ cells/mm^2). The cell densities in the inhibition area of the metal-containing plates increased when compared to the initial inoculated cell density (by a maximum factor of 3). Figure 4-3 shows the cell densities at the three different growth areas for triplicate Cu-containing plates.

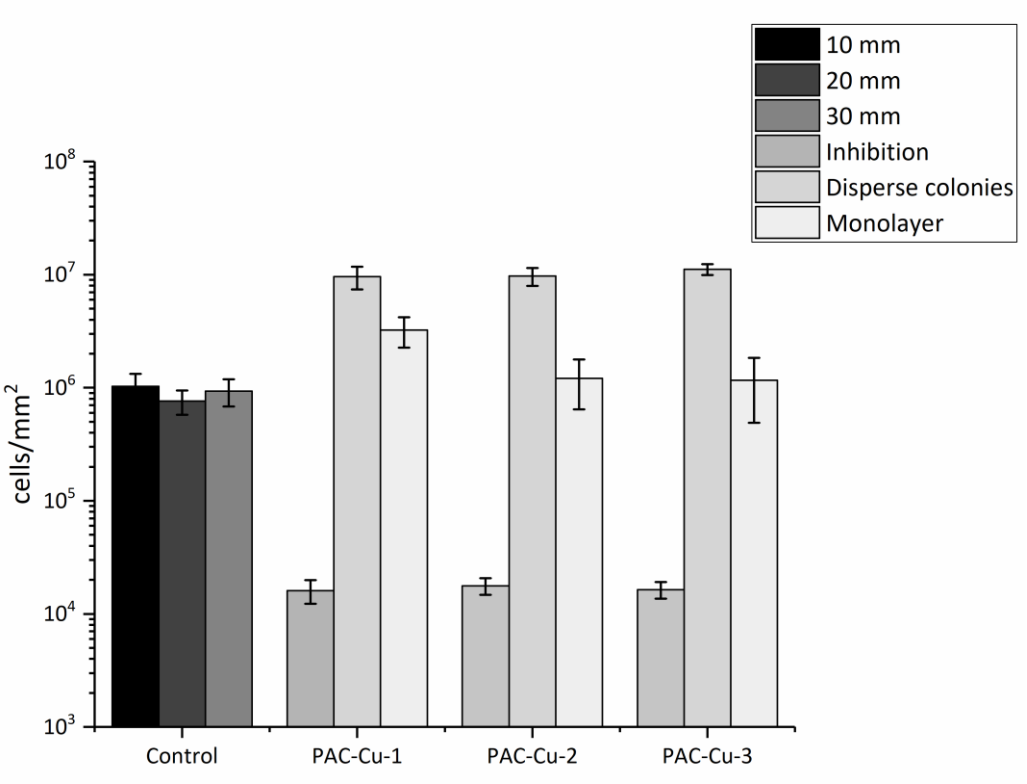

Figure 4-3. Cell density in the respective inhibition and growth zones on rectangular acidophilic agar plates incorporating copper laden activated carbon. (n=3).

4.2 Metal inhibition in liquid media

Because they represented the highest inhibitory potential in solid phase cultures, Cu and Co were chosen for further investigations in liquid settings. pH was monitored and used as an indicator for significant acidophilic SOB activity (Figure 4-4). *Thiobacillus* media, without any metal addition, was used as control for comparative analysis. In batches containing Cu, an increasing lag presented before pH drop occurred, in response to increasing Cu concentration, up to 40 mg Cu/L. All challenges below that threshold (40 mg Cu/L included) indicated significant acidophilic activity and had a common endpoint below pH 2. Above 40 mg Cu/L, no pH depression was observed; in contrast, pH increased and plateaued at values ranging between 6.5 and 6.7. Batches containing only Ag or Co, showed a similar lag effect; however, pH depression still resulted up to the highest challenge concentration (75 mg Ag/L, and 50 mg Co/L). Where only cobalt and silver were used, all challenges indicated some evidence of acidophilic activity.

Combinations of metals were also studied, including Cu/Ag and Cu/Co at mass ratios of 2:1 and 1:1, respectively. Where Cu/Ag were combined, thresholds for pH depression were observed at 40 mg Cu/L and 20 mg Ag/L. The same threshold was observed as for Cu alone, indicating no significant effect of silver on acidophile inhibition under these conditions. Thresholds for pH were also observed above 10 mg Cu/L and 10 mg Co/L, where copper and cobalt were combined. This challenge was monitored over 30 days, indicating significant acidophilic activity after 40 days of incubation.

All metal species used for the challenges were based on nitrate salts. Therefore, inhibition in the presence of counter ions, was also monitored. Challenges with increasing NO_3^- concentrations (up to 200 mg NO_3^-/L) where prepared with $NaNO_3$. All challenges indicated acidophilic activity and no lag effect was ever observed.

Aliquots for cell quantification and genetic analyses were extracted from each experiment when pH reached 2. If no pH drop was observed, aliquots were extracted after 30 days of incubation. Figure

4-5 illustrates the observed cell densities for all tests. Cell densities where pH dropped averaged: $1.06 \cdot 10^8$ cells/mL for Cu, $1.73 \cdot 10^8$ cells/mL for Ag, $3.81 \cdot 10^8$ cells/mL for Co, $5.06 \cdot 10^8$ cells/mL for Cu/Ag, and $6.47 \cdot 10^8$ cells/mL for Cu/Co. Cell densities for batches where pH did not drop were observed at an order of magnitude higher: $1.11 \cdot 10^9$ cells /mL for Cu, $2.10 \cdot 10^9$ cells /mL for Cu/Ag, and $1.16 \cdot 10^9$ cells/mL for Cu/Co.

Cu and Cu/Ag mixtures were chosen to investigate the microbial communities under conditions where a pH threshold was observed. 16S rRNA gene analysis of 17 samples generated over 4 million sequences, classified in 611 OTUs. After rarefaction analysis, the median Good's coverage was ≥99.9%, indicating enough sequencing data to confidently describe the diversity within these samples. Abundant OTUs consistently included 5 bacteria genera (Figure 4-6). Samples with metal concentration below the acidophilic inhibition threshold (40 mg Cu/L) indicated bacterial communities were dominated by *Acidithiobacillus spp*. Above that concentration, microbial composition significantly shifted to more diverse communities which were dominated by *Burkholderiaceae*. In Cu challenges, *Acidithiobacillus spp.* represented the dominant genus with >99% relative abundance under all conditions below the concentration threshold of 40 mg Cu/L. *Acidithiobacillus* accounted for less than 1% under any condition where Cu > 40 mg/L. In contrast, *Burkholderia* and *Ralstonia spp.* dominated communities where pH did not drop, while *Leifsonia* and *Methylobacterium* were found in smaller proportions. When copper and silver were both present, *Acidithiobacillus* represented the dominant genus below the concentrations of 40 mg Cu/L and 20 mg Ag/L. The same genus represented less than 1% in batches above these concentrations. Following the same pattern as in the presence of Cu alone, the enrichments were also dominated by *Burkholderia* and *Ralstonia spp.* with significant presence of *Sphingomonas spp., Leifsonia spp., Methylobacterium spp., and Microbacteriaceae spp.* (when Cu ≥ 40 mg/L).

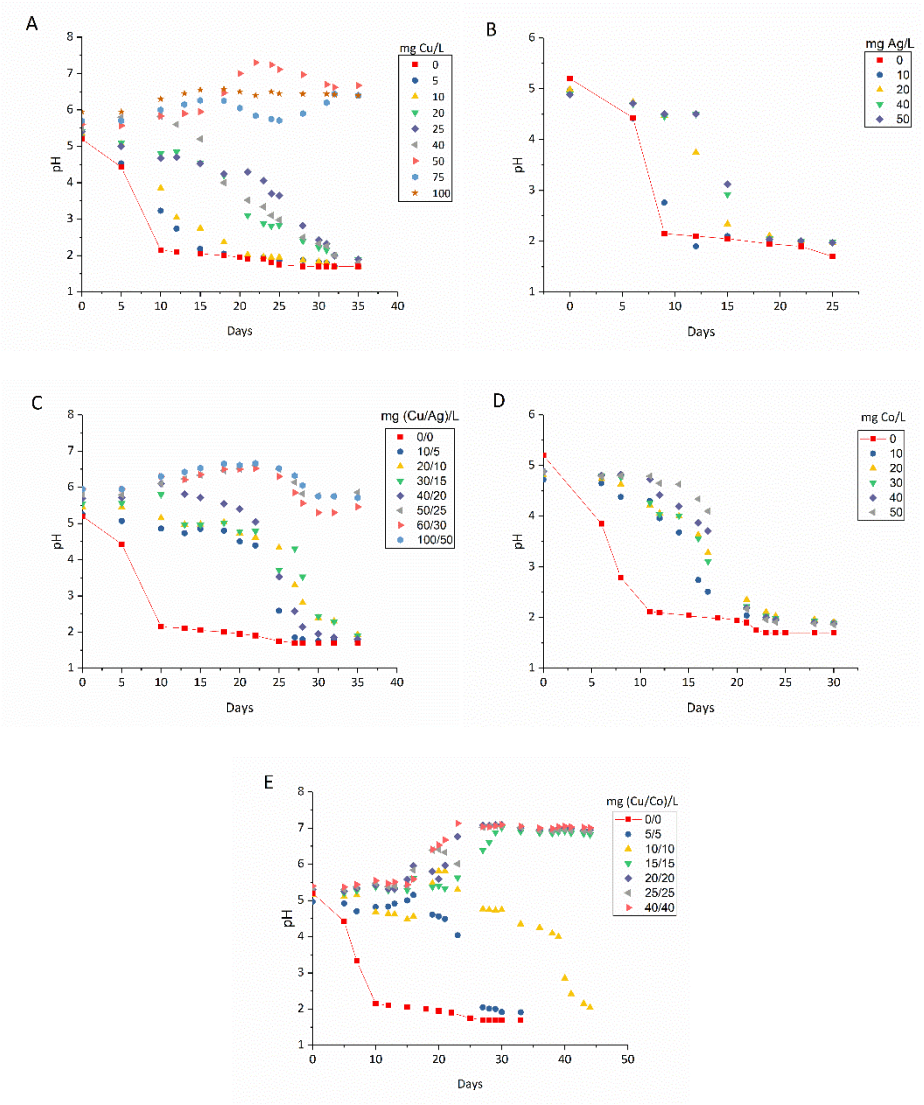

Figure 4-4. pH of enrichments including different levels of copper, cobalt, and silver, alone and in combinations. A: Cu^{2+}, B: Ag^{+}, C: Cu/Ag in combination at a ratio 2:1, D: Co^{2+}, and Cu/Co in combination at a ratio 1:1. Enrichments were inoculated with 150 µL of biofilm extract from a corroded site and dominated by Acidithiobacillus spp. (>95% relative abundance).

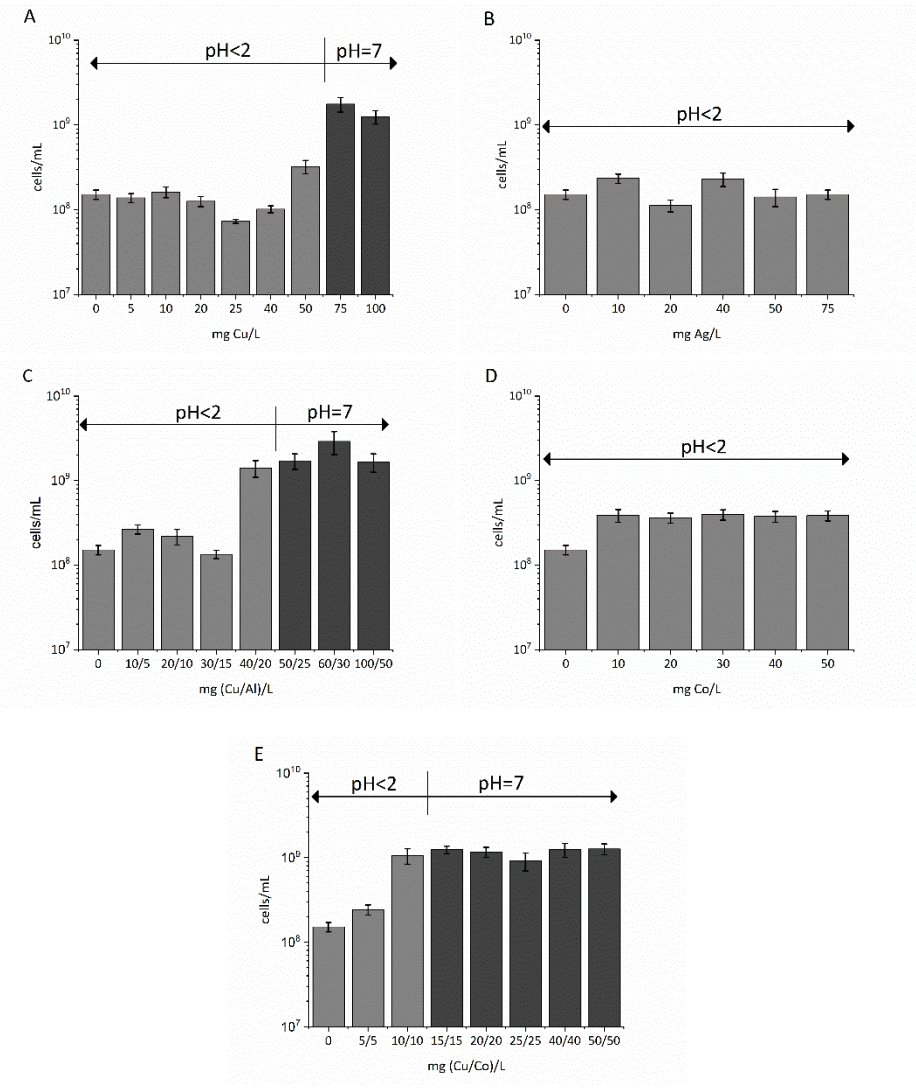

Figure 4-5. Cell densities (cells/mL) observed in sewer sourced enrichment cultures including copper, cobalt and silver, alone and in combinations. A: Cu^{2+}, B: Ag^{+}, C: Cu^{2+}/Ag^{+} in combination at a ratio 2:1, D: Co^{2+}, and Cu^{2+}/Co^{2+} in combination at a ratio 1:1. Light grey bars indicate enrichment cultures where pH dropped below 2. Dark grey bars indicate batches where pH approached neutrality. (n=3).

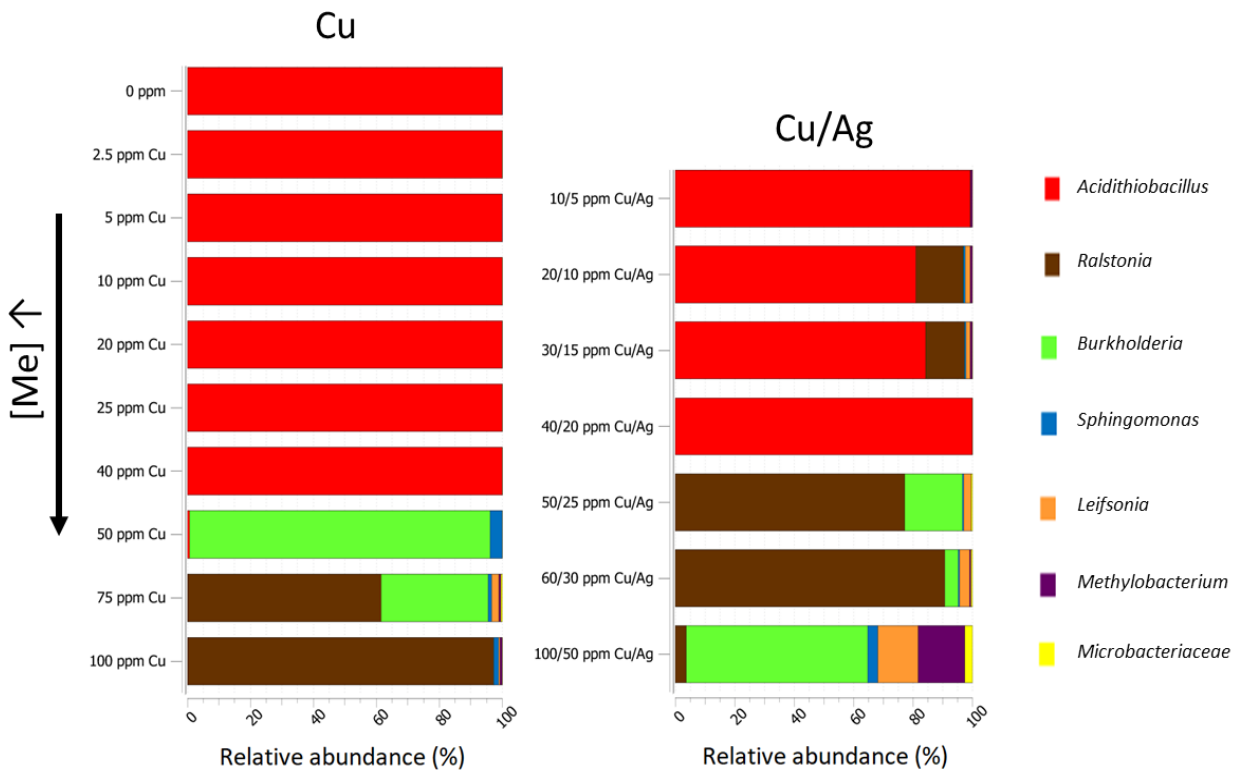

Figure 4-6. Relative abundance of bacterial taxa observed in sewer sourced enrichment cultures in the presence of copper, cobalt and silver, alone and in combinations.

Non-metric multidimensional scaling (NMDS) analysis correlates distance between matrix points with microbial composition similarity in a two axis format. Figure 4-7 displays an NMDS plot for selected enrichments. All enrichments which expressed pH depression exhibited high community similarity as judged by phylogenetic analysis. Community analyses suggests they were markedly different in enrichments where pH did not drop, regardless of the metal combinations used. No trends were observed that suggests association between metal combination (and concentration) with community similarity for the enrichment assemblages above the inhibition thresholds (≥ 50 mg Cu/L).

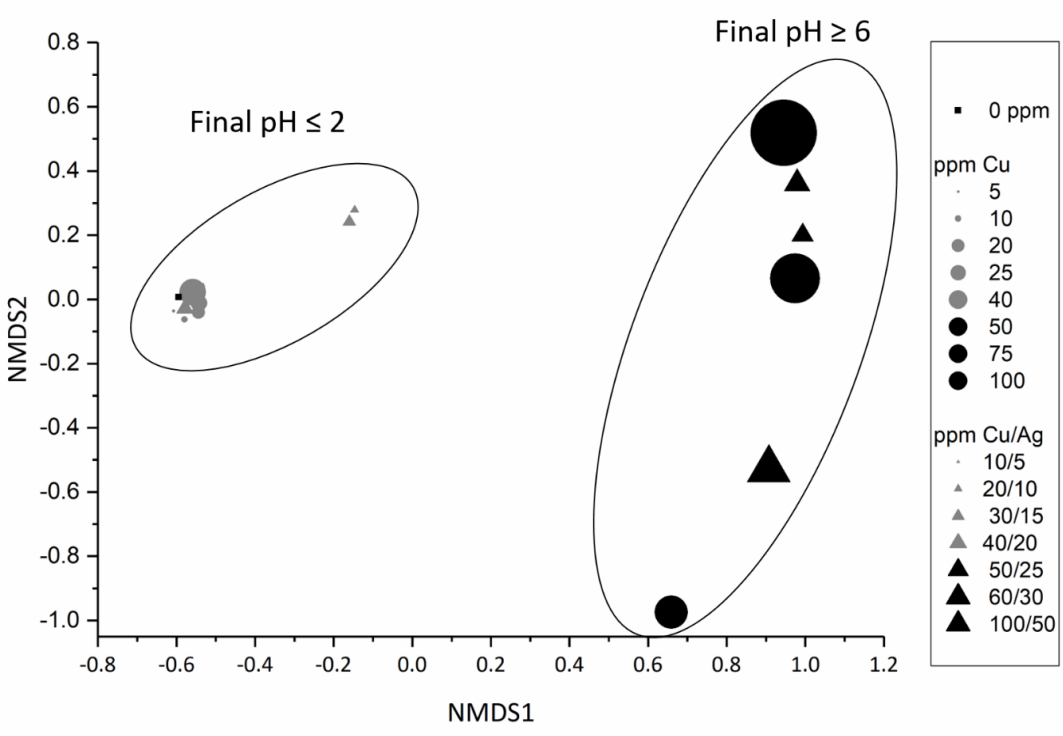

Figure 4-7. Non-metric multidimensional scaling (NMDS) analysis of metal exposed bacterial communities. Symbols represent metal combinations and are scaled with increasing concentration. Grey color indicates conditions were biogenic acid production depress pH below 2. Black color indicates batches where pH approaches neutrality. Circles denote major clusters of enrichments dominated by Acidithiobacillus (Left) and Burkholderiaceae (Right).

4.3 Sorbent sorption/desorption studies

Characterization of the sorbents used in the different mortar formulations were compiled through widely accepted material science techniques. This characterization was performed for the following reasons: i) to inform the designs of different corrosion-resisting mortars; ii) for elucidating possible interactions when combined with Portland cement; iii) to understand dominant sorption and desorption behavior of metal-impregnated sorbents; and iv) to investigate the fate of entrained when exposed to biogenic acids.

4.3.1 GAC characterization

The activated carbon used in these studies was characterized using the following metrics: total-, micropore- and external-surface areas, bulk- and specific gravity, water sorption, pH, and pH_{PZC} (Table

4-2). Calgon OL 20X50 was modified with hot acids as described in Section 3.3.1.1. Acidification resulted in approximately a 20% reduction of the BET surface area, micropore, and external surface areas; however, no significant changes in the micro- and mesopore distribution were observed. The bulk- and specific gravities were similar between the GACs tested here, with acid modification causing a small density reduction. Acid modification also caused a small reduction in water sorption capacity. Additionally, acidification resulted in a strong difference in pH and pH_{PZC} values. The raw GAC used (GAC-UNM) displayed alkaline behavior (pH 10.51, pH_{PZC}>8) while its acid modified counterpart (GAC-ACID) displayed acidic behavior (pH 4.62, pH_{PZC} 5.25) in unbuffered water. Acidification was designed for metal release at pH levels were *Acidithiobacillus spp*. start to dominate the microbial community in sewer crown environments.

Table 4-2. BET surface area, micropore area, external surface area, bulk specific gravity, water absorption, pH, and pH_{PZC} of Calgon OL 20X50 (GAC-UNM) and acid modified counterpart (GAC-ACID).

	BET surface area (m^2/g)	Micropore area (m^2/g)	External surface area (m^2/g)	Bulk specific gravity	Specific gravity	Water absorption (wt%)	pH	pH_{PZC}
GAC-UNM	1341.5	595.2	746.3	0.45	0.77	75.1	10.51	> 8
GAC-ACID	1073.6	479.5	594.1	0.43	0.75	74.2	4.62	5.25

The superficial chemical nature of the activated carbons used here was assessed through Boehm titration and FTIR. The oxygen-related functional group content of each carbon is presented in Figure 4-8**.** In both cases, the distribution of oxygen-containing functional groups correlated with their pH and pH_{PZC}. Unmodified GAC presented basic pH along with a dominance of phenolic-associated groups (57.8%), while the acid modified counterpart showed acid pH and dominance of carboxyl-associated groups (46.1 %). Additionally, the acidification process resulted in an increase of the total number of oxygen-related functionalities, by a factor of 7.1.

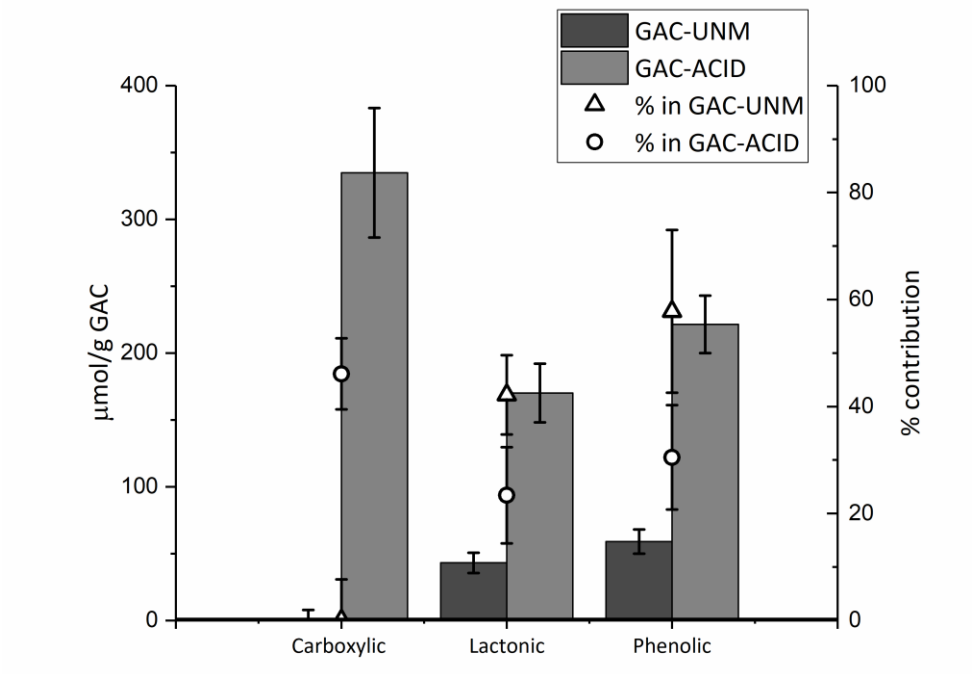

Figure 4-8. Oxygen-associated functional groups determined by Boehm titration. Bars indicate the concentration of functional groups in µmol/g GAC. Points indicate the relative contribution (%) of each functionality.

The 4,000-400 cm^{-1} infrared spectra (FTIR) of the GACs are presented in Figure 4-9. Assignment of observed bands on the different GACs was based on literature review and data published by different authors. GAC-UNM showed a faint O-H stretch of alcohol, phenols, and carboxylic acids, detected as a broad band signal between 3,200-3,700 cm^{-1} [199-201]. A possible band associated with stretch of C=O in cyclic amides at 1,546 cm^{-1} and hydroxyls absorbing at 1,118 cm^{-1} were also detected. Bands at 2,350 and 670 cm^{-1} indicated the presence of physisorbed gaseous carbon dioxide [218]. After acidification, major changes in the FTIR spectra were observed. Increased intensity of the band located between 3,200-3,700cm^{-1} (O-H stretch) was observed, while three new bands were detected at 1,220, 1,580, and 1,725 cm^{-1}. The first of the three bands (1,220 cm^{-1}) was attributed to a stretch in cyclic ethers attached to double bonds or asymmetrical stretch in either bridged group (-CO) [267]. The second band (1,580 cm^{-1}) was attributed to C=O containing groups, namely 1,3 diketone (enol form) or hydroxy aryl ketone groups [199, 200]. The band at 1,725 cm^{-1} was correlated with the presence of ketone, ester, and carboxylic acid in aromatic rings [199, 201].

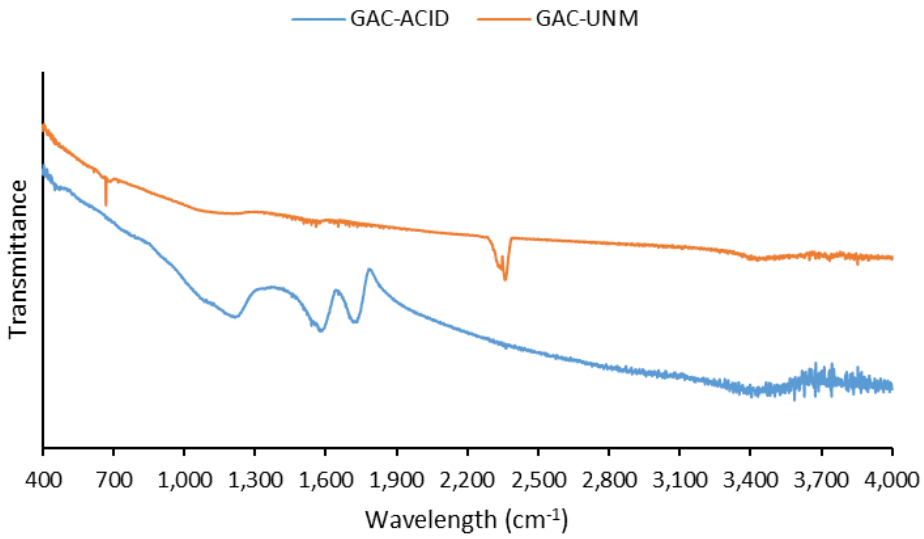

Band (this work)	Band (in reference)	Surface group	Assignment	Reference
3,450	3,200-3,700	OH	Alcohol, phenols and carboxylic acids	267
2,342	~ 2,350	CO_2	Physisorbed carbon dioxide	268
1,725	1,730	C=O	Stretch of C=O	268
1,580	1,558	C=O	Stretch of C=O	218
1,546	1,546	CONH	Stretch of C=O in cyclic amides	218
1,220	1,253	CO	Stretch in cyclic ethers attached to double bonds or asymmetrical stretch in ether bridged group	267
1,118	1,118	COH	OH stretch (Hydroxyl absorption)	269
672	~ 670	CO_2	Physisorbed carbon dioxide	268

Figure 4-9. Fourier Transformed Infrared Spectroscopy (FTIR) spectra of GAC-UNM and GAC-ACID. Assigned bands are summarized in the table below the spectra.

4.3.2 Steel slag characterization

Steel slag particles used in this study was characterized with the following metrics: bulk- and specific gravity, water sorption, and pH (Table 4-3). Basic oxygen furnace slag (BOF-S) was exclusively used and substituted for Ottawa sand in cement mortar formulations. The specific gravity was 1.79 times higher than the bulk gravity, and 1.2 times higher than the specific gravity of the Ottawa sand (2.65) it replaced. The water sorption capacity for the BOF-S was 3.1%, compared to 0.01% for Ottawa sand. The pH of the sorbent was 12.54, indicating a strong alkaline characteristic.

Table 4-3. Specific gravity, water absorption capacity, and pH of BOF-S and Ottawa sand used in mortar formulations.

	Bulk specific gravity	Specific gravity	Water absorption (wt%)	pH
BOF-S	1.78	3.18	3.1	12.54
Ottawa sand	1.73	2.65	0.01	-

Additionally, the chemical nature of the BOF-S was evaluated through determination of its major oxides and mineralogy. The oxide composition was obtained after digestion of a representative fraction of the BOF-S solids and performed by ICP-OES analysis (Table 4-4). Oxide abundance followed the series $CaO > Fe_2O_3 > SiO_2 > MgO > Al_2O_3 > MnO > P_2O_5 > SO_4 > Na_2O$. CaO (44.8 wt%) and Fe_2O_3 (35.1 wt%) accounted for more than 50% of the total oxide content.

Table 4-4. Major oxide composition of BOF-S in weight percent.

	SiO_2	Al_2O_3	CaO	SO_4	Fe_2O_3	K_2O	Na_2O	MgO	MnO	P_2O_5	Free CaO	
											Grain	Powder
BOF-S	14.7%	6.6%	31.7%	0.4%	25.8%	-	0.1%	10.8%	2.5%	0.7%	0.4%	1.5%

Mineral composition was obtained through peak analysis of the XRD diffractogram of the BOF-S, Figure 4-10. Major peaks identified corresponded to Larnite, Srebrodolskite, Mayenite, Wüstite, Merwinite, Periclase, and Quartz.

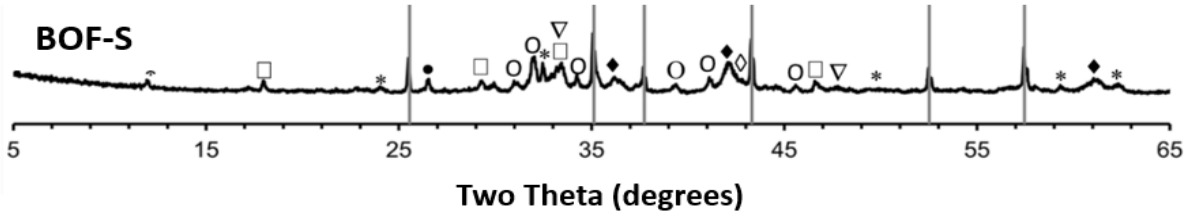

Mineral Name	Stoichiometry	Symbol	Unit Geometry	Unit Cell Volume (Å^3)	Density (g/cm^3)	PDF #
Larnite (Belite)	Ca_2SiO_4	O	Monoclinic	345.3	3.28	00-033-0302
Srebrodolskite	$Ca_2Fe_2O_5$	*	Orthorhombic	448	4.04	00-038-0408
Mayenite	$Ca_{12}Al_{14}O_{33}$	□	Cubic	1720.2	2.676	00-009-0413
Wüstite	$Fe_{0.9536}O$	♦	Cubic	78.5	5.613	01-074-1880
Merwinite	$Ca_3Mg(SiO_4)_2$	∇	Monoclinic	659.3	3.15	00-035-0591
Periclase	MgO	◊	Cubic	74.7	3.56	00-045-0946
Quartz	SiO_2	●	Hexagonal	113	2.66	00-046-1045

Figure 4-10. Raw diffraction pattern for BOF-S. Identified minerals are denoted with symbols as listed below the diffractogram. Mineral shapes, unit volumes, and densities have been obtained using Jade5 mineral database reference standard. Mineral identification according to their powder diffraction file number (PDF #).

4.3.3 Leaching studies

The three types of sorbents used in this study were loaded to saturation (in batch) using $Cu(NO_3)_2$ solutions, and solutions containing both $Cu(NO_3)_2$ and $Co(NO_3)_2$ (Table 4-5). In order to favor metal cation sorption on acid modified GAC (GAC-ACID), the solution pH was controlled at 5.75. Batches of unmodified GAC were adjusted to pH 8 to favor precipitate sorption. No pH-adjustments were undertaken for BOF-S batches. In all cases, metal uptake efficiency followed the series BOF-S > GAC-UNM > GAC-ACID, as defined by the amount of metal sorbed per unit mass of sorbent. A small reduction in copper loading was observed when added in combination with cobalt. Cobalt associated poorly with acid modified GAC in the presence of copper. When compared to the loads of cobalt sorbed on GAC-UNM and BOF-S, cobalt loaded on acid modified GAC was significantly lower, therefore was not considered for further study.

Table 4-5. Metal loads and selected characteristics of the sorbents used in this study. All sorbents were loaded to saturation, with the metals used in this study, either alone or in combinations.

Sorbent	Ph	pH_{PZC}	mg Cu/ g	(mg Cu/g)/(mg Co/g)	Mechanism
GAC-UNM	10.51	>8	14.2	13.8/4.5	Surface precipitation
GAC-ACID	4.62	5.25	8.5	8.3/0.03	Ionic exchange
BOF-S	12.54	-	17.9	16.8/8.5	Surface precipitation/ion exchange

Next, the metal laden sorbents were subjected to an Acid Neutralization Capacity (ANC) assay (Figure 4-11). As observed, the GAC-ACID-Cu rapidly transitioned from its natural pH of 4.8 (0 $eqHNO_3/kg$) to pH 2.12 (0.5 $eqHNO_3/kg$), exhibiting virtually no buffering capacity. GAC-UNM-Cu and GAC-UNM-Cu-Co exhibited similar trends, transitioning from pH 6.63 and 7 to pH 2.18 and 2, respectively. The two types of metal-laden slags differed from the carbons tested here as judged by their higher equilibrium pH and their markedly stronger alkaline buffering capacity. BOF slag particles loaded with copper (BOF-S-Cu) transitioned from pH 11.78 (0 $eqHNO_3/kg$) to pH 4.88 (4 $eqHNO_3/kg$). Similarly, BOF slag particles co-loaded with copper and cobalt (BOF-S-Cu-Co) transitioned from pH 11.78 (0 $eqHNO_3/kg$) to pH 4.47 (4 $eqHNO_3/kg$).

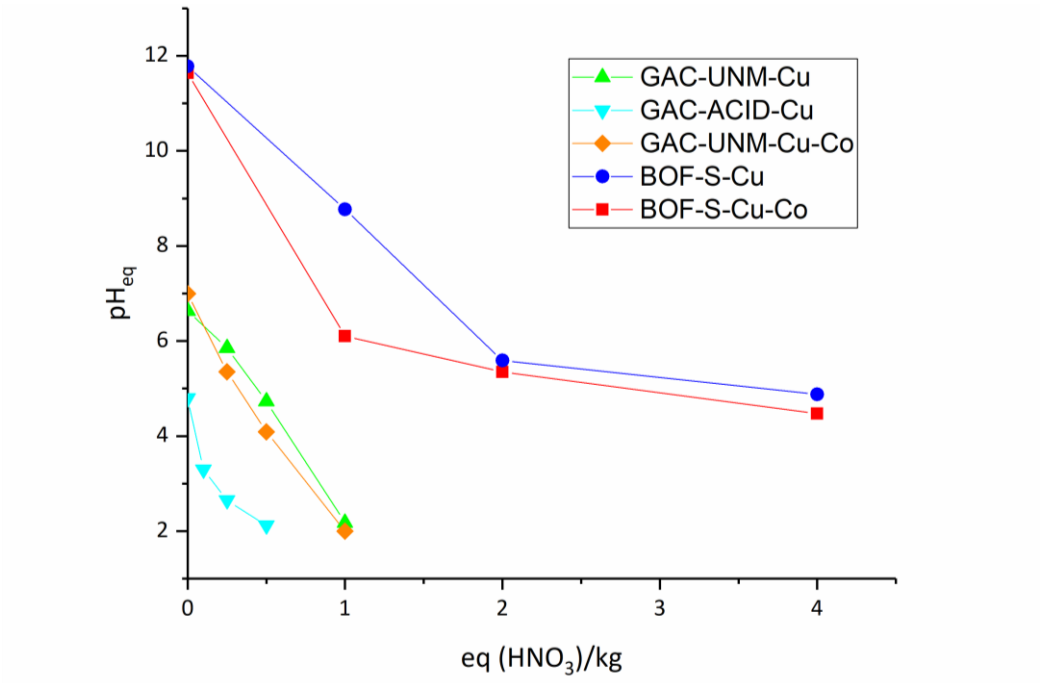

Figure 4-11. Equilibrium pH (pH_{eq}) of metal-laden sorbents exposed to increasing additions of acid (eq(HNO_3)/kg). Results are shown for a liquid:solid ratio of 1:20. GAC-UNM-Cu: Calgon 20x50 granular activated carbon loaded with copper; GAC-ACID-Cu: Acidified granular activated carbon loaded with copper; GAC-UNM-Cu-Co: Calgon 20x50 granular activated carbon co-loaded with copper and cobalt; BOF-S-Cu: BOF slag particles loaded with copper; BOF-S-Cu-Co: BOF slag particles co-loaded with copper and cobalt.

Aliquots were taken when equilibrium was reached and were then analyzed for soluble Cu and Co. The amount leached was normalized based on the total metal load per amount of sorbent used (Table 4-6). Visualization of both concentration and fraction leached at each acid addition and sorbent used is shown in Figure 4-11.

Table 4-6. Metal leached from sorbents exposed to the ANC test with HNO_3. Results expressed in weight % of the total metal loaded. Parentheses separate values for leached copper (left) and leached cobalt (right).

	Eq (HNO_3)/kg						
Sorbent	0	0.1	0.25	0.5	1	2	4
GAC-UNM-Cu	0.5	-	37.6	83.4	93.0	-	-
GAC-ACID-Cu	25.6	50.6	69.6	79.3	-	-	-
GAC-UNM-Cu-Co	0.1/35.4	-	31.0/76.8	75.8/88.3	87.3/86.8	-	-
BOF-S-Cu	0.1	-	-	-	0.3	19.2	50.70
B0F-S-Cu-Co	0/0	-	-	-	5.6/72.5	39.9/90.2	83.0/90.5

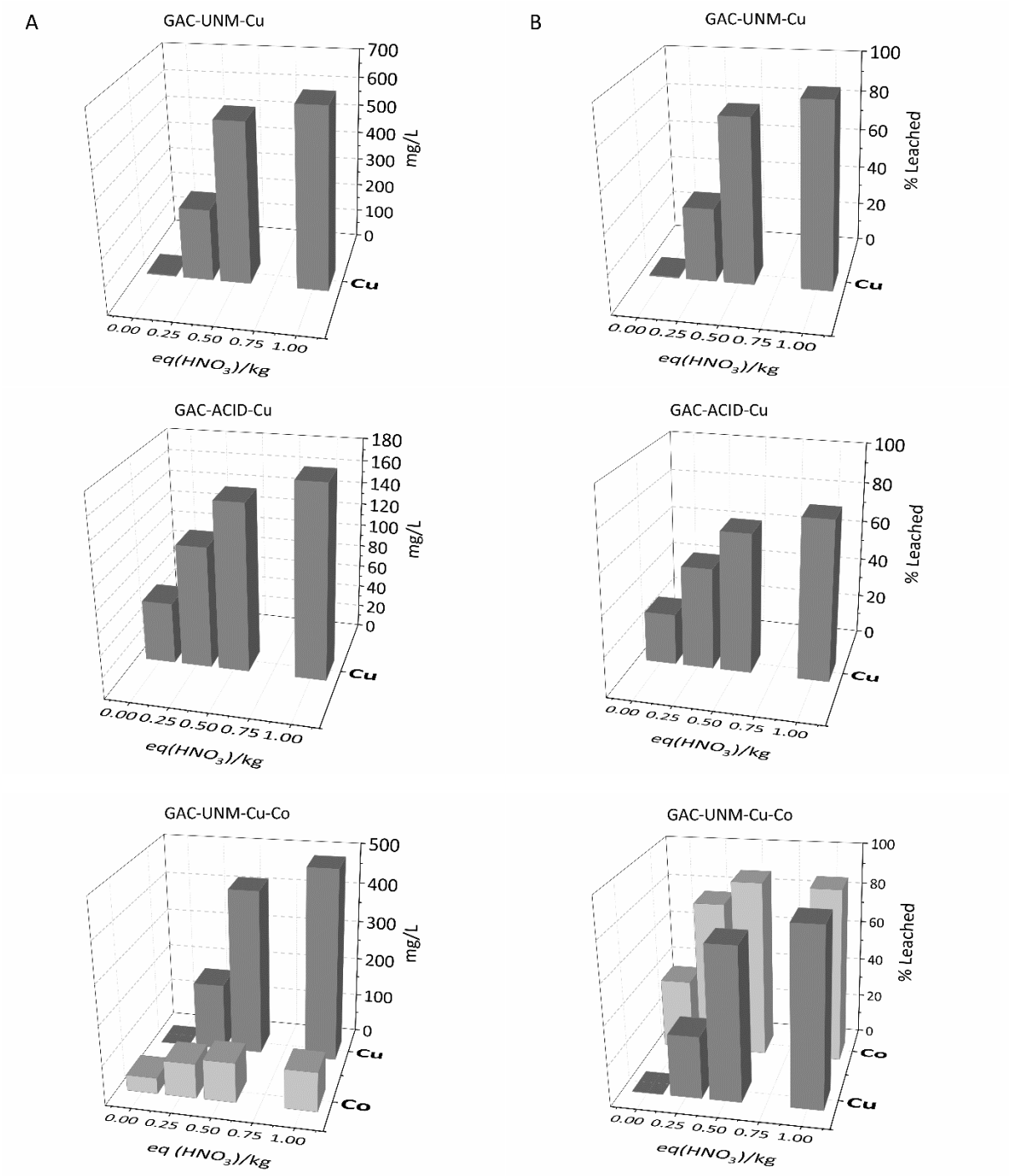

Figure 4-12. Solubilized metal from metal-loaded sorbents after exposure to increasing amounts of acid (eq HNO_3/kg). Column A: metal concentration (mg/L) at equilibrium in the liquid phase at each acid addition and sorbent. Column B: metal leached expressed as percentage of the total metal loaded on each sorbent. GAC-UNM-Cu: Calgon 20x50 granular activated carbon loaded with copper; GAC-ACID-Cu: Acidified granular activated carbon loaded with copper; GAC-UNM-Cu-Co: Calgon 20x50 granular activated carbon co-loaded with copper and cobalt; BOF-S-Cu: BOF slag particles loaded with copper; BOF-S-Cu-Co: BOF slag particles co-loaded with copper and cobalt.

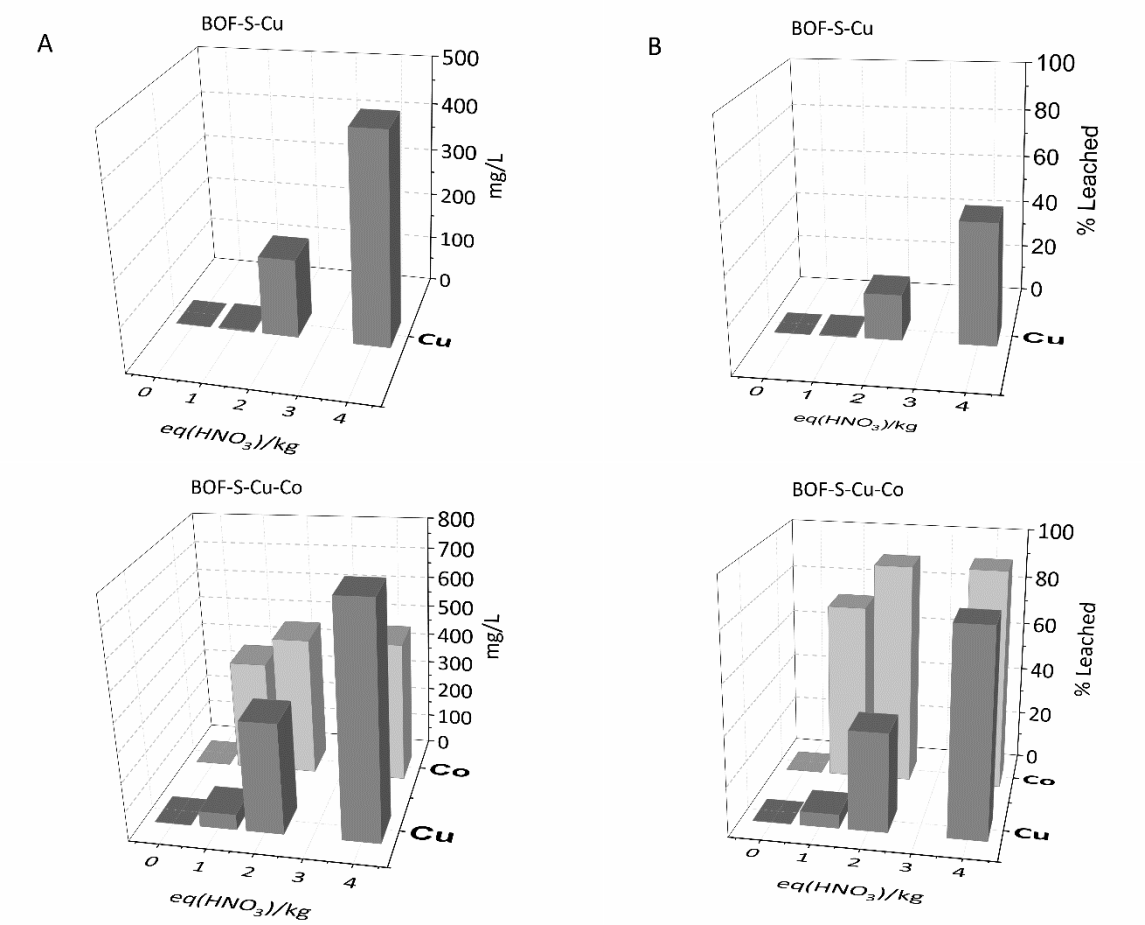

Figure 4-13. (Cont'd from Figure 4-12). Solubilized metal from metal-loaded sorbents after exposure to increasing amounts of acid (eq HNO_3/kg). Column A: metal concentration (mg/L) at equilibrium in the liquid phase at each acid addition and sorbent. Column B: metal leached expressed as percentage of the total metal loaded on each sorbent. GAC-UNM-Cu: Calgon 20x50 granular activated carbon loaded with copper; GAC-ACID-Cu: Acidified granular activated carbon loaded with copper; GAC-UNM-Cu-Co: Calgon 20x50 granular activated carbon co-loaded with copper and cobalt; BOF-S-Cu: BOF slag particles loaded with copper; BOF-S-Cu-Co: BOF slag particles co-loaded with copper and cobalt.

Leachate analysis showed different metal release behaviors for the sorbents used and the type of metal sorbed. GAC-UNM-Cu leachate analysis on Cu, indicated a change from 0.5% of the total Cu load at 0 eqHNO_3/kg to 93% at 1 eqHNO_3/kg. A maximum difference in leached Cu (45.9%) occurred between 0.25 and 0.5 eqHNO_3/kg. GAC-ACID-Cu leachate transitioned from 25.6% at 0 eqHNO_3/kg to 79.3% at 1 eqHNO_3/kg. A maximum difference in leached Cu (45.9%) occurred between 0 and 0.25 eqHNO_3/kg. GAC-UNM-Cu-Co leachate, normalized by the Cu mass, transitioned from 0.1% at 0 eqHNO_3/kg to 87.3% at 1 eqHNO_3/kg. As for GAC-UNM-Cu, the maximum difference in leached Cu (34.3%) occurred between 0.25 and 0.5 eqHNO_3/kg. On the other hand, Co transitioned from 35.4% at 0

eqHNO_3/kg to 86.8% at 1 eqHNO_3/kg. The maximum difference in leached Co (41.4%) was observed between 0 and 0.25 eqHNO_3/kg. BOF-S-Cu increased the amount of leached Cu from 0.1% at 0 eqHNO_3/kg to 50.7% at 4 eqHNO_3/kg. In this case, the maximum difference in leached Cu (31.5%) occurred between 2 and 4 eqHNO_3/kg. Finally, BOF-S-Cu-Co leachate, normalized by the Cu mass, increased from 0% at 0 eqHNO_3/kg to 83% at 4 eqHNO_3/kg. The maximum difference in leached Cu (43.2%) occurred between 2 and 4 eqHNO_3/kg**.** Co transitioned from 0% at 0 eqHNO_3/kg to 90.5% at 4 eqHNO_3/kg. The maximum difference in leached Co (72.5%) was observed between 0 and 1 eqHNO_3/kg.

An additional ANC assay was performed on the metal-laden sorbents after being mixed and cured with Portland cement (Figure 4-14). The goal was to elucidate the combined buffering capacity and leaching behavior when exposed to the most aggressive acid excreted by acidophilic bacteria (H_2SO_4). As observed, the amounts of acid delivered were increased to account for the buffering effect of the Ordinary Portland Cement (OPC). As for the sorbents, the acid-response could be divided between the formulations containing GAC and the formulations containing BOF-S. The mortar formulations containing GAC-UNM-Cu (CUP10), GAC-ACID-Cu (CHP10), and GAC-UNM-Cu-Co (CUCP10) transitioned from pH 10.58, 10.15, and 10.47 (4 eqH_2SO_4/kg), to pH 1.83, 163, and 1.72 (8 eqH_2SO_4/kg), respectively. While the starting an endpoint pH levels were similar, their difference was greater at 6 eqH_2SO_4/kg (5.81, 5.02, and 4.22). The formulations containing BOF-S-Cu (SP) and BOF-S-Cu-Co (SCP) transitioned from pH 11.23 and 11.37 (4 eqH_2SO_4/kg), to pH 5.79 and 4.90 (8 eqH_2SO_4/kg), respectively.

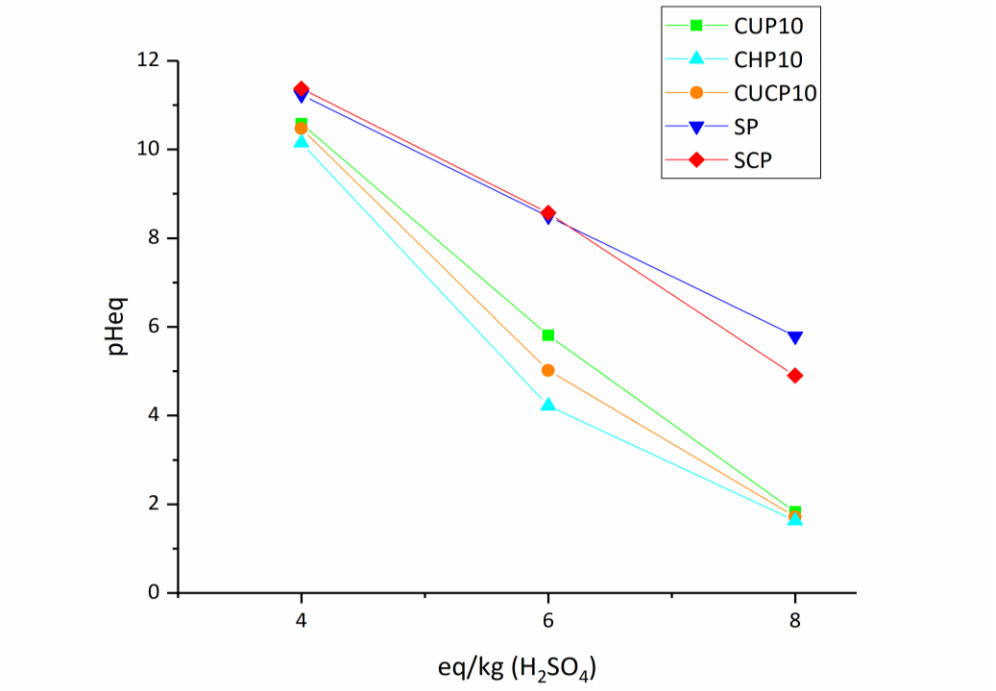

Figure 4-14. Equilibrium pH (pH_{eq}) of mortar formulations exposed to increasing additions of acid ($eq(H_2SO_4)/kg$). Results are shown for a liquid:solid ratio of 20:1. CUP10: mortar with 10% of sand replaced by GAC-UNM-Cu; CHP10: mortar with 10% of sand replaced by GAC-ACID-Cu; CUCP10: mortar with 10% of sand replaced by GAC-UNM-Cu-Co; SP: mortar with sand replaced by BOF-S-Cu, volumetrically equivalent to 10% GAC formulations; SCP: mortar with sand replaced by BOF-S-Cu-Co, volumetrically equivalent to 10% GAC formulations.

Leachate analysis and normalization was completed as previously described for metal-laden sorbent (Table 4-7) . Visualization of both concentration and fraction leached at each acid addition and sorbent used is shown in Figure 4-14.

Table 4-7. Metal leached from the mortar formulations exposed to the ANC test with H_2SO_4. Results are expressed in weight % of the total metal loaded. Parentheses separate values for leached Cu (left) and leached Co (right).

		Eq H_2SO_4/kg		
Mortars	Sand replacement (wt%)	4	6	8
CUP10	10	0	1.7	52.8
CHP10	10	0	66.1	96.6
CUCP10	10	0/1.3	32.9/84.2	100/100
SP	10-equivalent	0	0	9.0
SCP	10-equivalent	0/0.5	0.4/1.3	45.2/49.8

*10-equivalent: Volumetric BOF-S grain distribution in the mortar equal to the 10% GAC formulations.

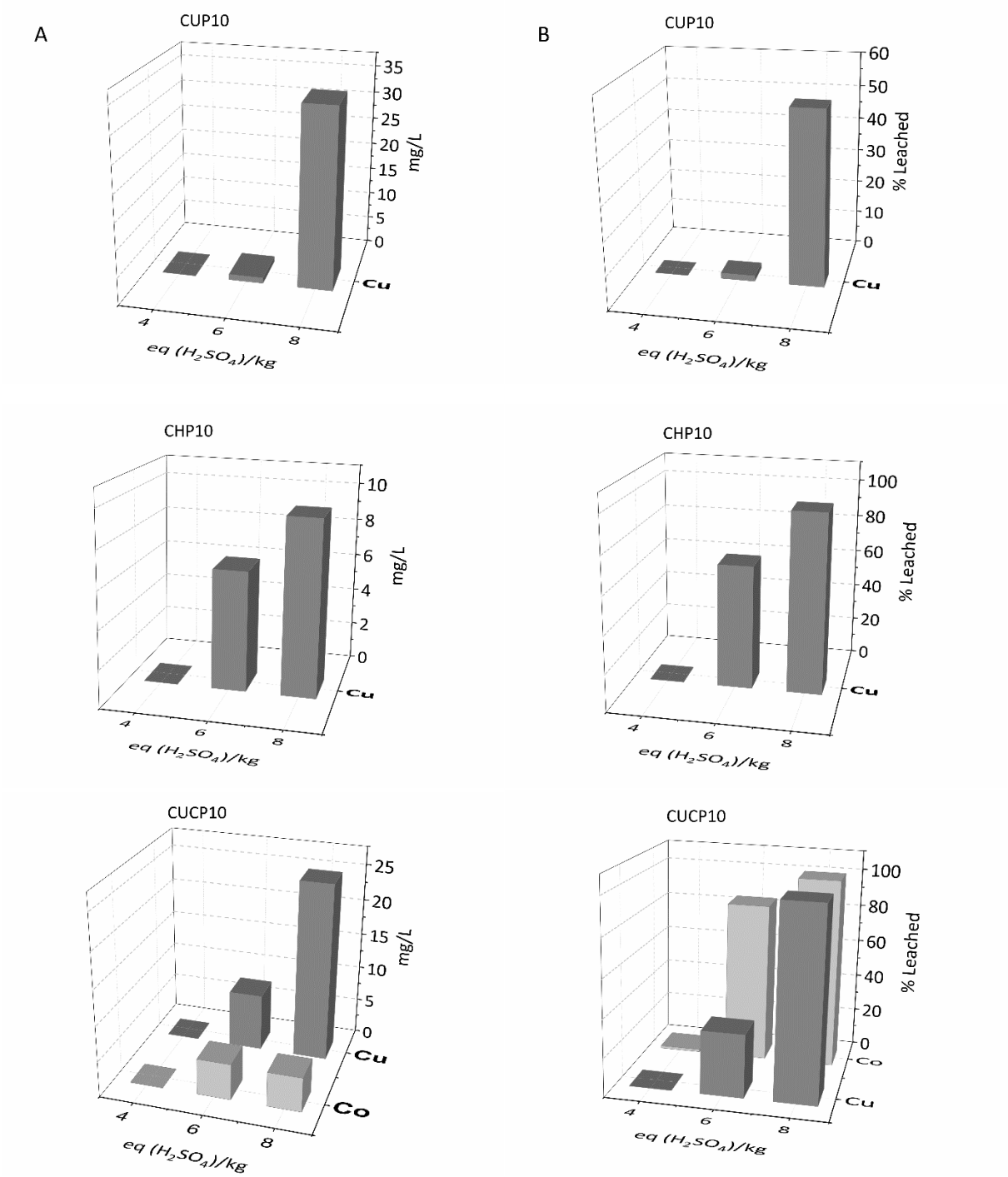

Figure 4-15. Solubilized metal from metal-loaded sorbents after exposure to increasing amounts of acid (eq(HNO_3)/kg). Column A: metal concentration (mg/L) at equilibrium in the liquid phase at each acid addition and mortar. Column B: metal leached expressed as percentage of the total metal loaded on each mortar. CUP10: mortar with 10% of sand replaced by GAC-UNM-Cu; CHP10: mortar with 10% of sand replaced by GAC-ACID-Cu; CUCP10: mortar with 10% of sand replaced by GAC-UNM-Cu-Co; SP: mortar with sand replaced by BOF-S-Cu, volumetrically equivalent to 10% GAC formulations; SCP: mortar with sand replaced by BOF-S-Cu-Co, volumetrically equivalent to 10% GAC formulations.

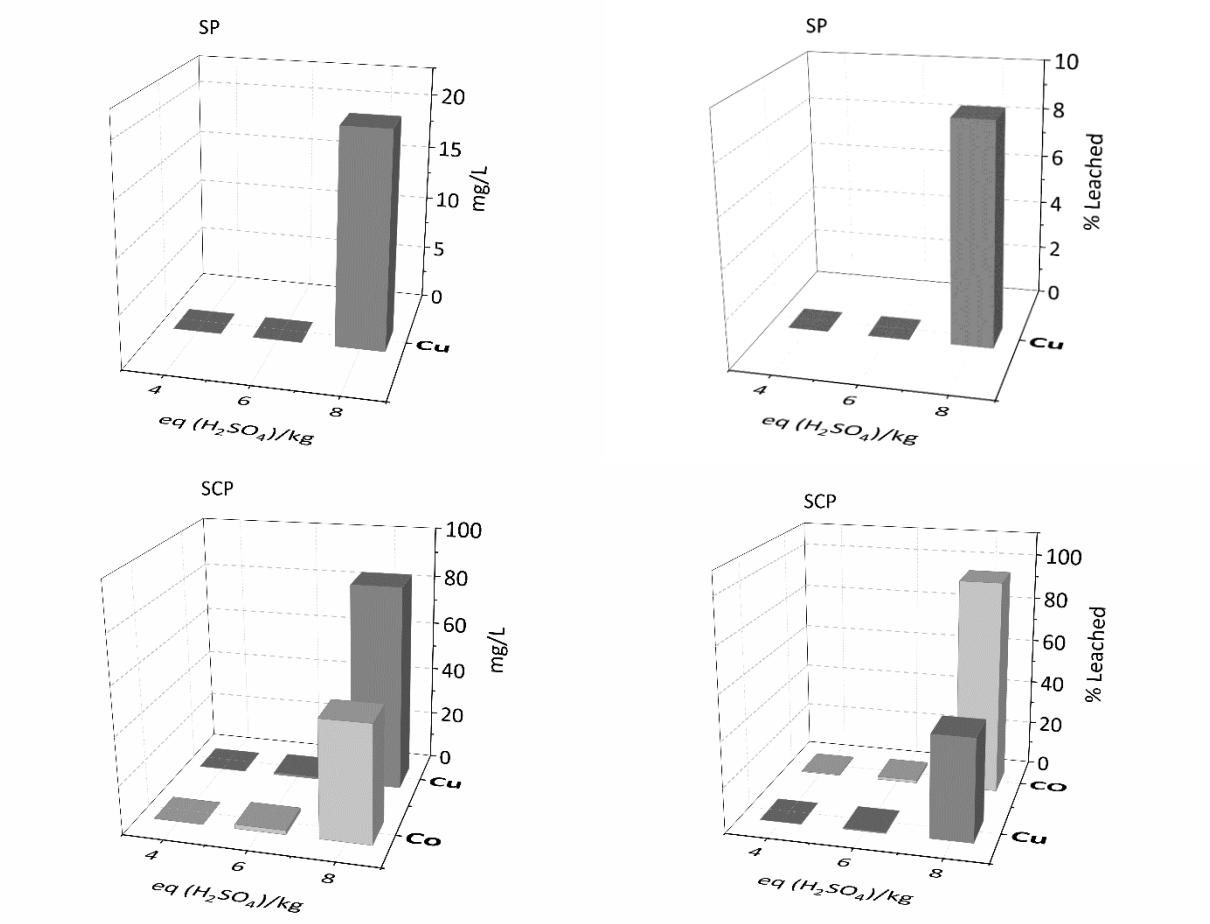

Figure 4-16.(Cont'd from Figure 4-15). Solubilized metal from metal-loaded sorbents after exposure to increasing amounts of acid (eq(HNO_3)/kg). Column A: metal concentration (mg/L) at equilibrium in the liquid phase at each acid addition and mortar. Column B: metal leached expressed as percentage of the total metal loaded on each mortar. CUP10: mortar with 10% of sand replaced by GAC-UNM-Cu; CHP10: mortar with 10% of sand replaced by GAC-ACID-Cu; CUCP10: mortar with 10% of sand replaced by GAC-UNM-Cu-Co; SP: mortar with sand replaced by BOF-S-Cu, volumetrically equivalent to 10% GAC formulations; SCP: mortar with sand replaced by BOF-S-Cu-Co, volumetrically equivalent to 10% GAC formulations.

CUP10 leachate analysis on Cu, indicated a change from 0% of the total Cu load at 4 eqH_2SO_4/kg to 52% at 8 eqH_2SO_4/kg. A maximum difference in leached Cu (50.3%) occurred between 8 and 6 eqH_2SO_4/kg. CHP10 leachate transitioned from 0% at 4 eqH_2SO_4/kg to 96% at 8 eqH_2SO_4/kg. A maximum difference in leached Cu (66.1%) occurred between 4 and 6 eqH_2SO_4/kg. CCP10U leachate, referred to Cu, transitioned from 0% at 4 eqH_2SO_4/kg to 100% at 8 eqH_2SO_4/kg. The maximum difference in leached Cu (67.1%) occurred between 6 and 8 eqH_2SO_4/kg. On the other hand, Co transitioned from 1.3% at 4 eqH_2SO_4/kg to 100% at 8 eqH_2SO_4/kg. The maximum difference in leached Co (82.9%) was observed

between 4 and 6 eqH_2SO_4/kg. SP increased the amount of leached Cu from 0% at 4 eqH_2SO_4/kg to 9% at 8 eqH_2SO_4/kg. In this case, the maximum difference in leached Cu (9%) occurred between 6 and 8 eqH_2SO_4/kg. Finally, SCP leachate, referenced to Cu, increased from 0% at 4 eqH_2SO_4/kg to 45.2% at 8 eqH_2SO_4/kg. The maximum difference in leached Cu (44.6%) occurred between 6 and 8 eqH_2SO_4/kg**.** Co transitioned from 0.5% at 4 eqH_2SO_4/kg to 49.8% at 8 eqH_2SO_{43}/kg. The maximum difference in leached Co (48.5%) was observed between 6 and 8 eqH_2SO_4/kg.

4.4 Mortar formulations effectiveness in bench scale bioreactor

The effectiveness of the mortar formulations in inhibiting acidophilic growth was evaluated in laboratory settings after simulating severe corrosion environments in an annular reactor. After 250 days of exposure, the tested mortar slides were recovered, extracted, and analyzed for microbial activity, bacterial enumeration, and acidophilic abundance through 16SrRNA gene analysis.

4.4.1 Microbial activity

Validation on the use of the NovaLUM luminometric readings as a surrogate for acidophilic activity was previously completed on laboratory cultures. For this purpose, *Acidithiobacillus* mixed cultures were prepared and monitored for temporal changes in bacterial abundance, microbial activity, and culture pH (Figure 4-17 (A,B,C)). The cell density followed a typical growth curve that correlated with the pH drop profile similar to that observed in liquid enrichments. A lag phase of 2 days preceded the exponential growth phase. pH slightly decreased during this time, dropping from 4.65 to 4.25. The exponential phase correlated with a significant pH drop, which transitioned from 4.25 to 2.15. After 9 days of incubation, the stationary phase was reached and minimum changes in total cell density were observed. pH continued dropping at a slower rate, stabilizing around 1.8 after 30 days of monitoring. No total RLU could be measured in the first 2 days. However, during the exponential growth the measured RLUs increased and plateau between 6 and 9 days after inoculation. After 9 days, the values continued

to increase, at a slower rate than the initially observed, and peaked at day 18. From this point, the readings started to decrease sharply, suggesting a senescing phase. The normalized RLU (on a cell density basis), showed two peaks, a small one at 6 days (3.08 RLU/(cells/mL)·10^3), and a larger one at day 18 (11.72 RLU/(cells/mL)·10^3). After the second peak the normalized values decreased sharply, with a final measurement, at 28 days, resembling that at 4 days. Finally, the effect of diluting the cultures on the RLU readings was study by preparing serial dilution in sterile *Thiobacillus* media of a stationary phase culture (day 18) (Figure 4-17(D)). A log-linear trend successfully described the relationship between cell density and acidophilic culture dilution between 10^5 and 10^9 cells/mL (R^2=0.99).

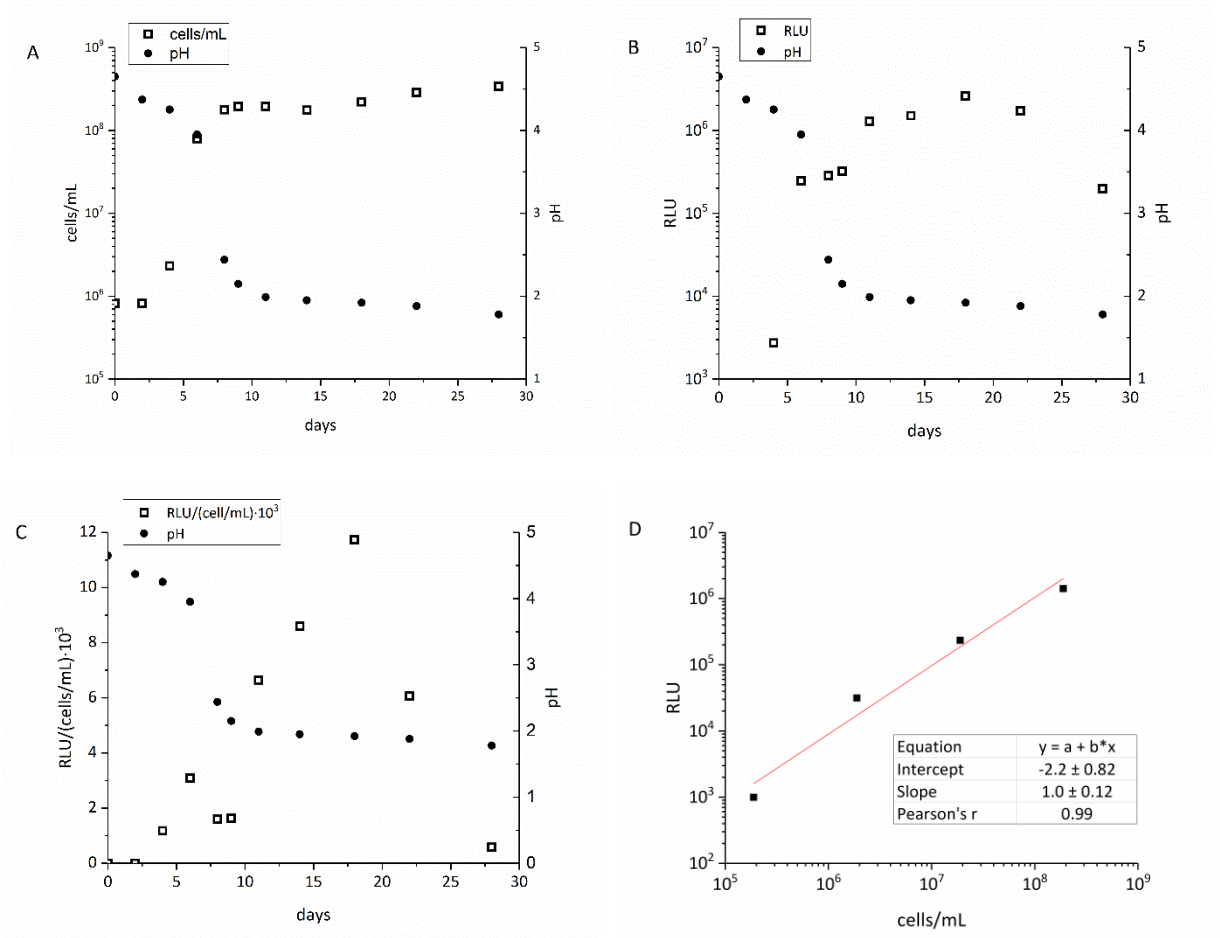

Figure 4-17. A) changes in cell density and pH; B) changes in microbial activity and pH; C) relative changes of microbial activity (on a cell density basis) over time; and, D) log-linear relationship between cell dilution and RLU. All observations were concurrently performed in enrichments inoculated with biofilm extracted from the crown of corroding sewers.

4.4.2 Suspension pH

The extracted corrosion product was suspended in 10mL of sterile saline solution, and is referred to as the corrosion eluate. For each sample, pH of the solution was measured and was used as an indicator of corrosion extent (Table 4-8).

Table 4-8. Measured pH and microbial activity (expressed as RLU) on the different corrosion eluates. Numbers in parenthesis indicate replicates for each formulation.

Formulation	pH	RLU
C0 (1)	3.93	481
C0 (2)	4.1	763
CNU10 (1)	3.34	782
CNU10 (2)	3.57	879
CPU10 (1)	4.5	6741
CPU10 (2)	4.3	5539
CHP10 (1)	3.35	2995
CHP10 (2)	4.81	3066
CUCP10 (1)	4.39	5274
CUCP10 (2)	3.88	12993
S0 (1)	3.9	466
S0 (2)	4.04	4049
SP (1)	5	5631
SP (2)	5.55	6076
SCP (1)	4.45	5308
SCP (2)	4.6	3309

4.4.3 Cell abundance

Dilutions of the corrosion suspensions were prepared in PBST (0.1 % Tween 20). Dilutions were sonicated for 90 seconds at 80W to facilitate cell detachment. Next, the larger and denser particles were allowed to settle for 30 minutes. Finally, aliquots taken, avoiding precipitates, were prepared for DAPI staining and microscope cell counts. While a simplified version of this method was successfully applied for cell enumeration of laboratory cultures, the cell detachment process from the mortar surfaces resulted in increased debris. The debris interacted with the DAPI stain and fluoresced when excited by ultraviolet light (Figure 4-18). This resulted in increased background brightness and the difficulty to

differentiate between bacterial cells and debris of similar size and shape. Therefore, cell enumeration was not performed on these samples.

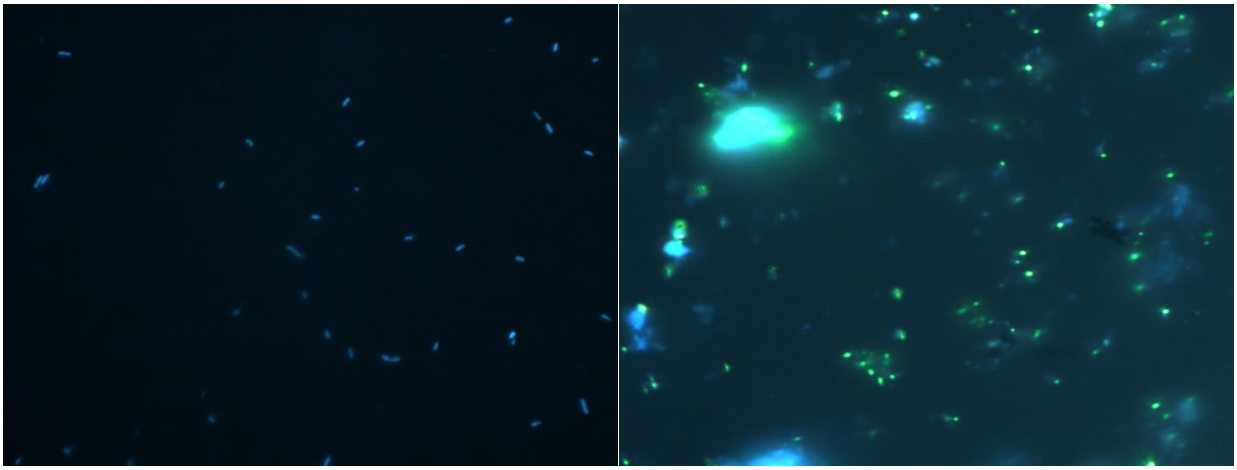

Figure 4-18. Epliflуorescence microscope images of DAPI stained bacteria at 100x magnification. (LEFT) Stained bacteria extracted from Acidithiobacillus cultures. (RIGHT) Stained bacteria (and debris) extracted from corroded mortar specimens.

4.4.4 Microbial activity

As judged by ATP, microbial activity in corrosion products was measured using the Luciferin-Luciferase reaction as described in Section 3.1.3. Swabs were immersed into each corrosion eluate for 30 seconds. Then, the correspondent Relative Light Units (RLU) were measured by inserting the swabs into a luminometer (Table 4-8).

4.4.5 16S rDNA analysis

Aliquots from the corrosion eluates were diluted for DNA extraction. Isolated and purified DNA were used to determine the relative recovery of universal and *Acidithiobacillus* 16S rRNA genes (Table 4-9). In all cases, the gene copy numbers recovered with universal primers were close or below the detection limit (100 copies/µL). *Acidithiobacillus* copy numbers were either undetected or ranged from <10 to 81 copies/ µL. PCR inhibition due to a preponderance of dissolved chemical species from the corrosion eluate was investigated through serial dilutions in TE buffer of selected samples (S0 and CNU10). Even after significant dilutions, positive amplification was obtained using universal primers only

after 40 cycles, but at or below 100 copies/µL. No amplification was obtained for *Acidithiobacillus* 16S rRNA gene, following serial dilutions.

Table 4-9. 16S rDNA copy numbers from undiluted corrosion eluates in bench-scale bioreactor using universal and Acidithiobacillus-specific primers. Numbers in parentheses correspond to duplicates of each formulation.

Formulation	Universal	*Acidithiobacillus*
C0 (1)	<100	n/a
C0 (2)	<100	n/a
CNU10 (1)	122	n/a
CNU10 (2)	110	n/a
CPU10 (1)	117	<10
CPU10 (2)	123	n/a
CHP10 (1)	140	<10
CHP10 (2)	129	n/a
CUCP10 (1)	105	n/a
CUCP10 (2)	106	<10
S0 (1)	110	<10
S0 (2)	120	<10
SP (1)	<100	n/a
SP (2)	<100	81
SCP (1)	123	n/a
SCP (2)	150	n/a

4.5 Field study

Cast mortar specimens were exposed to sewer headspace gases for a total of 11 months in a corroding manhole. During this time, headspace gas concentrations (H_2S and CO_2) were periodically observed and photographs of the samples' surface were archived (Figure 4-19). After exposure, samples were recovered and brought to the laboratory for further analysis. Different physical, chemical, and microbiological parameters were evaluated in order to assess the performance of the mortar formulations when subjected to biogenic corrosive environments.

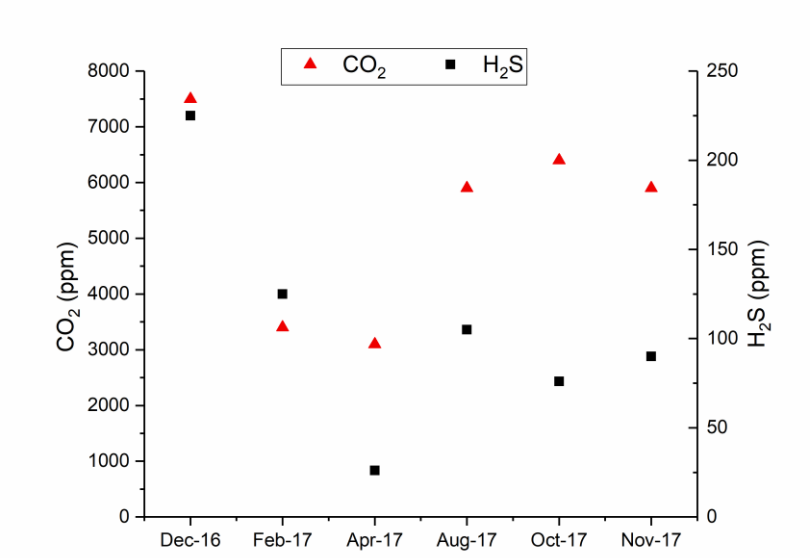

Figure 4-19. Concentrations of hydrogen sulfide(H_2S) and carbon dioxide (CO_2) in corroding manhole hosting test coupons.

4.5.1 Extent of corrosion

Samples were weighted before and after removal of soft corrosion products and were normalized to determine the percentage of cement mass lost (Figure 4-20). The control formulations (C0), which contained no carbon, slag, or metals, experienced mass losses between 2.7% and 3.2% after 11 months. GAC formulations without metals experienced different degrees of mass loss and no significant trends emerged in response to increasing the fractions of fine aggregate with GAC. Mass losses for these samples ranged between 2.1% (CHN2) and 9.4% (CHN10). Corrosive mass losses associated with cement hosting different amounts of metal-saturated GAC presented the following trend: samples at 2% and 5% sand replacement resulted in mass losses between 1.8% (CUCP2) and 9.8% (CHP5), and no trends emerged based on the type of GAC, or the metal combinations used. Formulations with 10% of sand replaced with metal-impregnated GAC had significantly lower mass losses, ranging from 0.4% (CUP10) 1.5% (CUCP10). At this substitution level, no trends were observed based on GAC type, or the metal combinations used. Overall, the slag-containing formulations experienced less mass losses than their GAC-containing counterparts. Formulations without any metal

content (S0) experienced significantly higher mass losses, between 2% and 2.1%, with respect to their metal-containing counterparts. For the latter, the mass losses ranged between 0.36% (SCP) and 0.98% (SCP) and no trends were observed based on the metal combinations used.

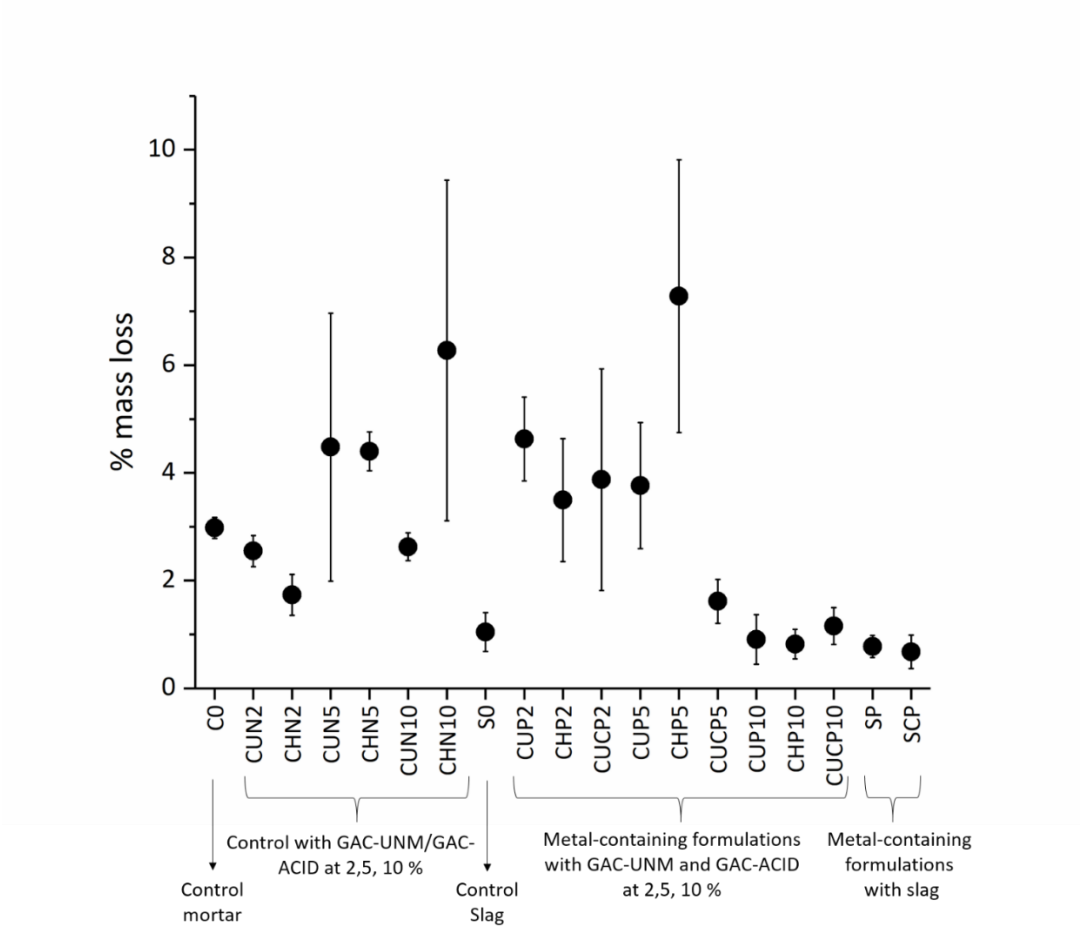

Figure 4-20. Mass losses on a percent basis (wt%) of different mortar formulations after exposure to corrosive environments. Bars indicate the range of observations. Control formulations include aggregates substitutions with no metal addition.

After removal of the corrosion product, the samples exhibited a characteristic radial corrosion front originating at the edges of the mortar surface and progressing into the center of the sample face (Figure 4-21). Different degrees of corrosion penetration were observe and quantification of corrosion extent for each sample was done by previously described imaging techniques (Figure 4-22). All formulations exhibited some degree of superficial corrosion. However, the samples containing the highest metal substitutions resulted in significantly lower corrosion penetration (<30% on CUP10,

CHP10, SP, and SCP mortar specimens). Formulations with uncorroded areas ranging between 50% and 70% included: CUCP10, CUCP5, and CHN2. The rest of the formulations experienced higher variability (e.g. S0), or consistently presented more than half of their exposed facial areas corroded.

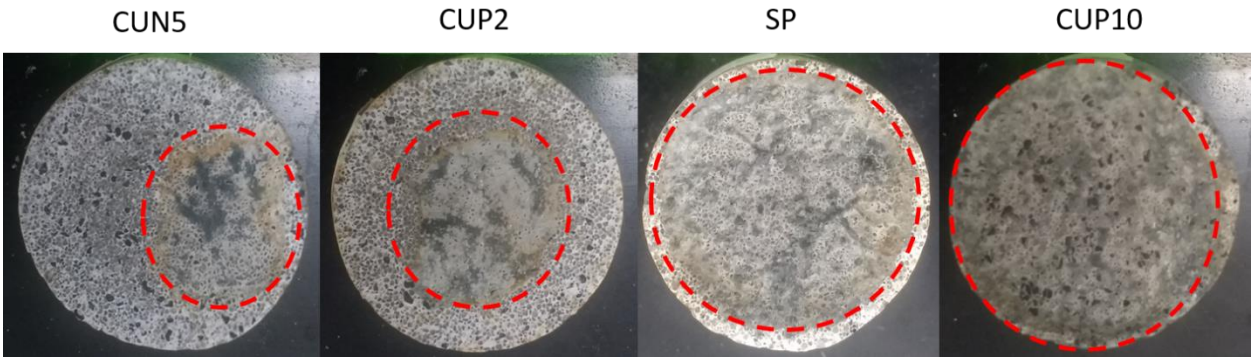

Figure 4-21. Top view of different mortar samples after removal of superficial corrosion products. The characteristic radial corrosion fronts can be visualized by the presence of gypsum/carbonate formation and exposure of internal aggregates. Corrosion front delimited with a red dashed line.

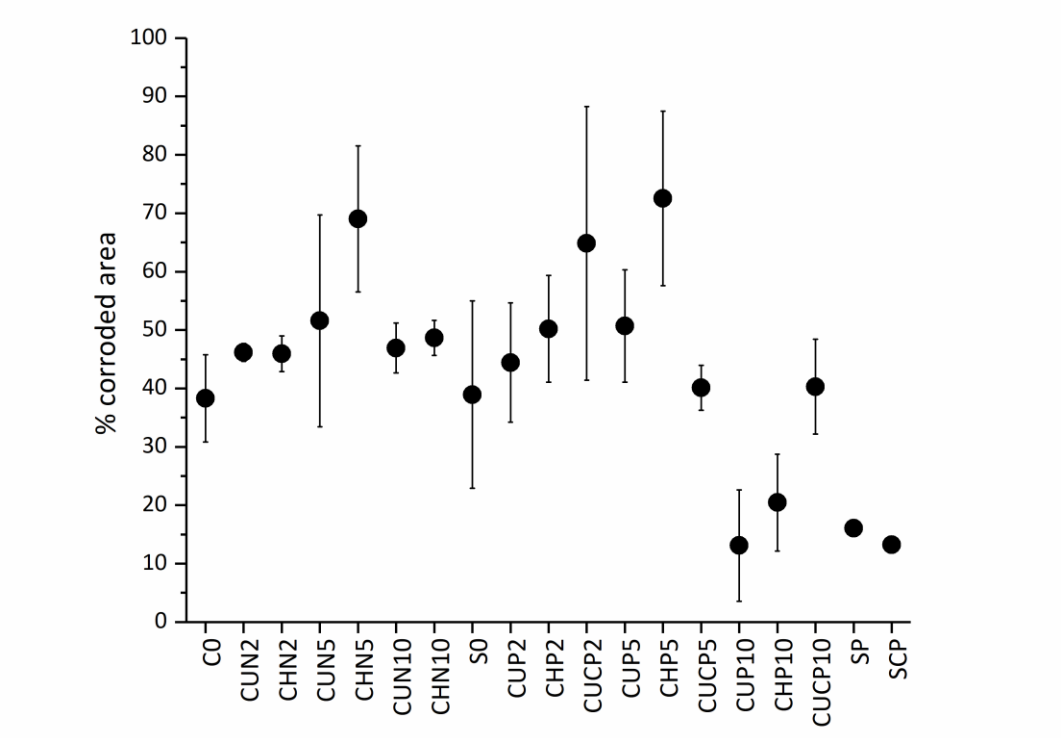

Figure 4-22. Corroded areas (%) for the different mortar samples after removal of superficial corrosion products. Bars indicate the range of observations.

The last analyzed parameters used to evaluate the corrosion extent of the samples were the pH of the suspended corrosion eluate and the assosiated pore water pH (Figure 4-23). pH was measured

after suspending the corrosion products in 10 mL of saline solution. The pore water pH was obtained by determining the moisture content of the corrosion products along with mass balance calculations for hydronium ion [4]. Moisture content was calculated for samples that presented at least 0.5 grams of corrosion product formation. Corrosion eluate pH ranged between 8.26 (SP) and 1.85 (CHP5). Pore water pH ranged between 6.95 (CHN10) and 1.13 (CHP5). In general, basic pH levels pHs (pH>7) were observed for samples containing the highest heavy metal doses (e.g. CUP10,CUCP10,SP, and SCP) with few exceptions that included replicates of CUN2, CHN2, CHN10, S0, and CUCP5. However, these formulations also included replicates that experienced low suspension pHs and considerable corrosion product formation (e.g. CUCP5).

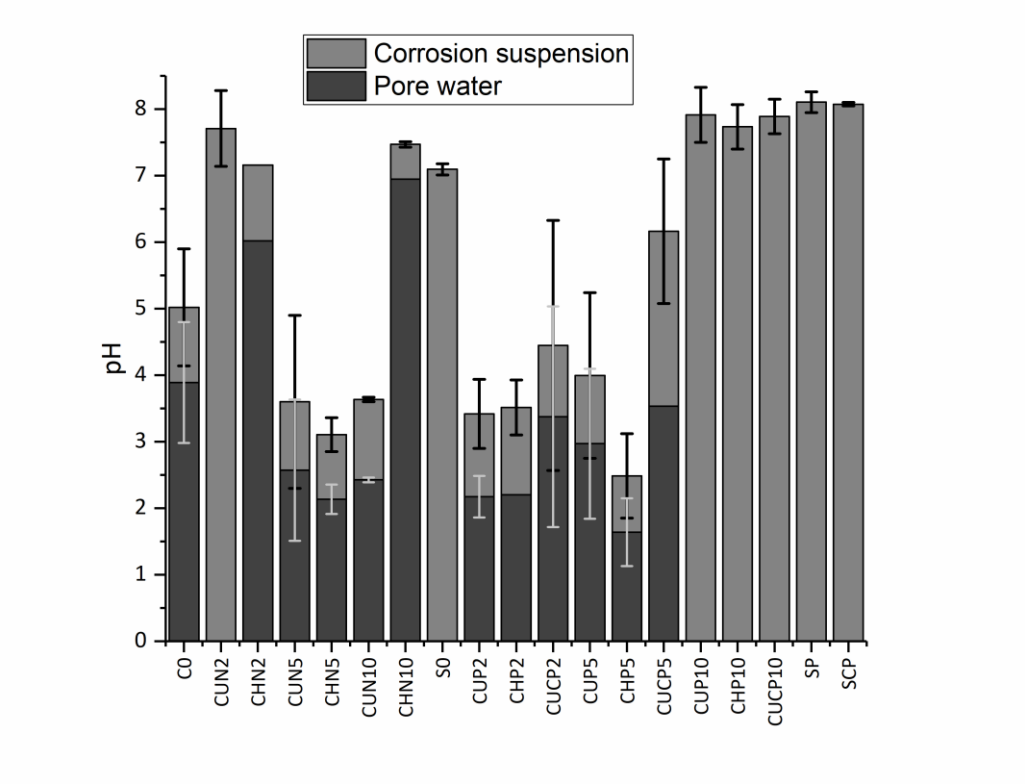

Figure 4-23. Corrosion suspension pH and water pore pH of the mortar samples after exposure to corrosive environments. Bars indicate the range of observations.

4.5.2 Microbial Analysis

Complimentary microbial analyses were used to evaluate the inhibitory potential of the mortar formulations against microbial growth, specifically *Acidithiobacillus spp.* growth. For that purpose, the mortar surfaces and corrosion products were analyzed for cell quantities, microbial activity, and abundance of universal and *Acidithiobacillus spp.* 16SrDNA copies. Direct cell counts were obtained through direct epifluorescence microscopy and normalized based by the amount of corrosion product and the original surface area of the coupons (Figure 4-24 and

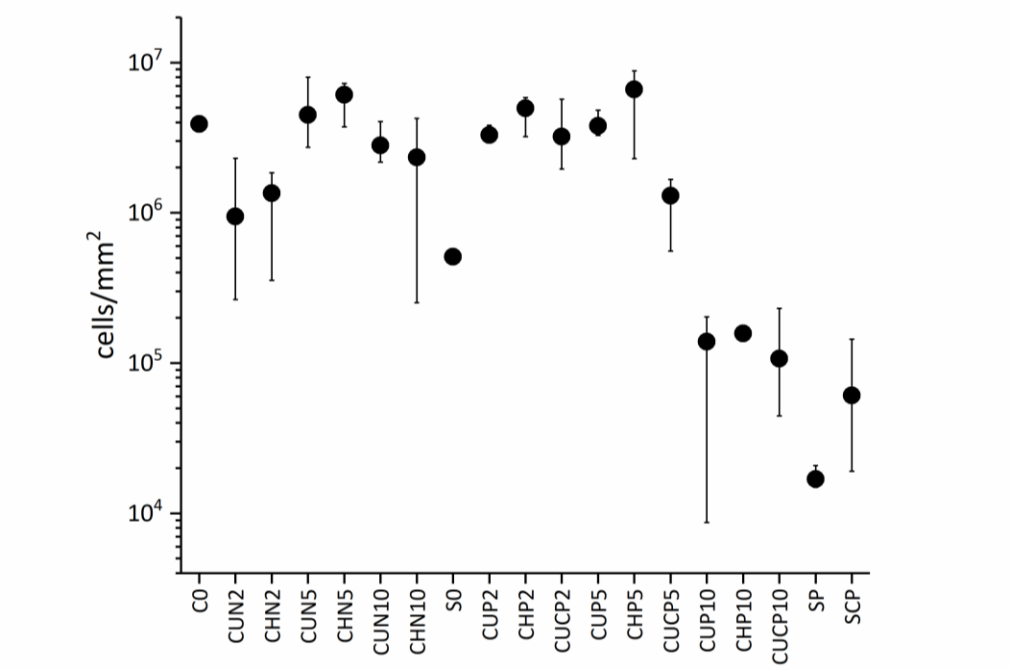

Figure 4-25). Surface cell densities decreased in response to increased substitution of fine aggregates with metal saturated sorbents, with the lowest values associated with CUP10, CHP10, CUCP10, SP, and SCP formulations. Cell abundance for these formulations ranged from $2.3 \cdot 10^7$ cells/g (SP) and $1.5 \cdot 10^5$ cells/mm^2 (SP), to $2.7 \cdot 10^8$ cells/g (SCP) and $2.3 \cdot 10^5$ cells/mm^2 (CUCP10). Formulations with fine aggregate substitutions less than 5% by mass lower metal content resulted in higher cell density values, ranging between $3.9 \cdot 10^8$ cells/g (CUN2) and $2.5 \cdot 10^5$ cells/mm^2 (CHN10) to $2.6 \cdot 10^9$ cells/g (CHN10) and $8.8 \cdot 10^5$ cells/mm^2 (CHP5).

Calibrated luciferase emissions were used to asses ATP content as a surrogate for microbial activity. Swabs immersed into corrosion eluates provided RLU readings that were normalized to total cell numbers obtained from the same corrosion product suspensions (Figure 4-26). In general, higher activity was observed for samples containing the highest metal loads (CUP10, CHP10, SP, and SCP). Normalized values for these samples ranged from 0.98 RLU/cells·10^{-3} (CHP10) to 3.82 RLU/cells·10^{-3} (CHP10). Formulations with lower metal content exhibited relatively lower specific RLU values; activity ranged between 0.39 RLU/cells·10^{-3} (CHP2) and 2.7 RLU/cells·10^{-3} (CHN5). A correlation emerged between the total cell densities (cells/mL) and the RLU emissions from the different corrosion product suspensions (R^2=0.93) (Figure 4-27).

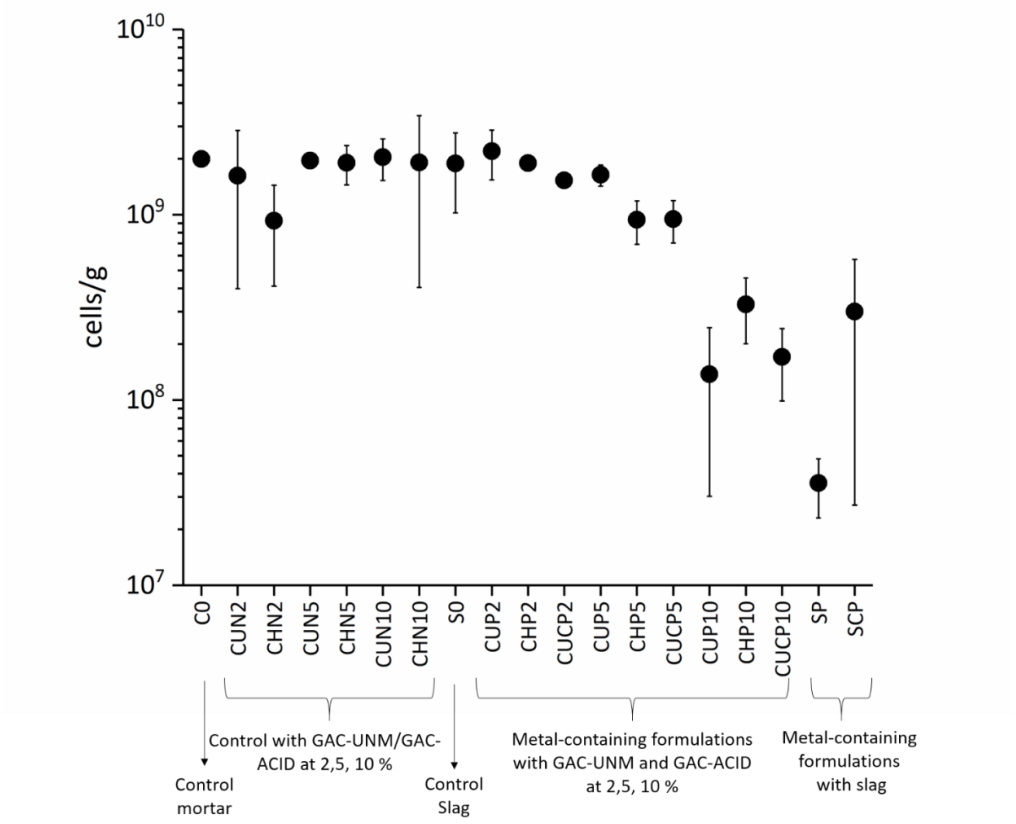

Figure 4-24. Mass normalized cell densities (cells/g) of different formulations after exposure to corrosive environments including cells recovered in corrosion products. Bars indicate the range of observations.

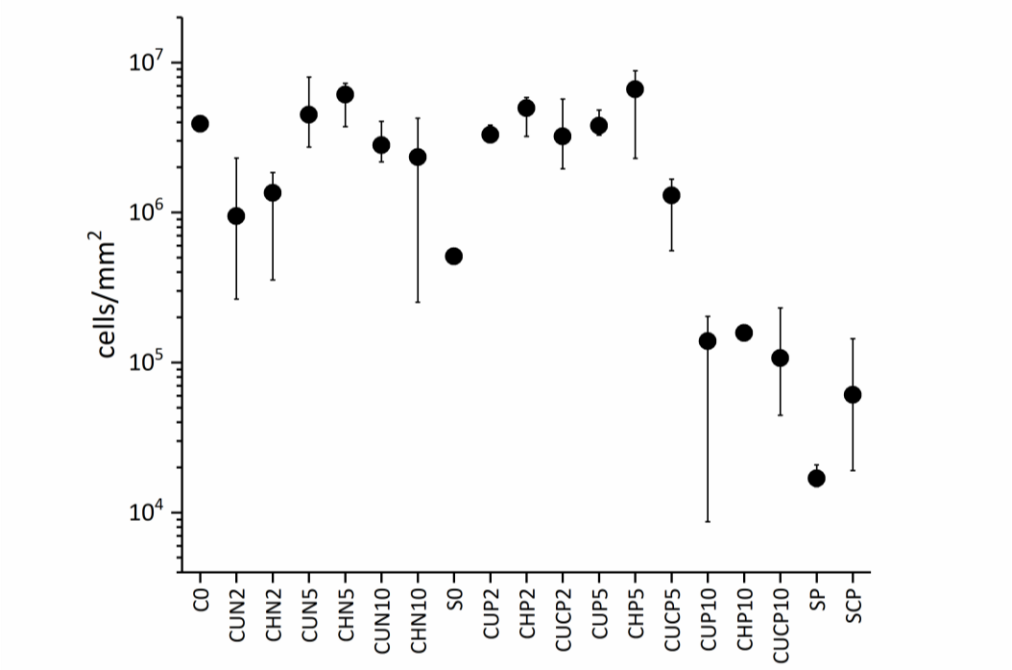

Figure 4-25. Surface normalized cell densities (cells/mm²) of different formulations after exposure to corrosive environments including cells recovered in corrosion products. Bars indicate the range of observations.

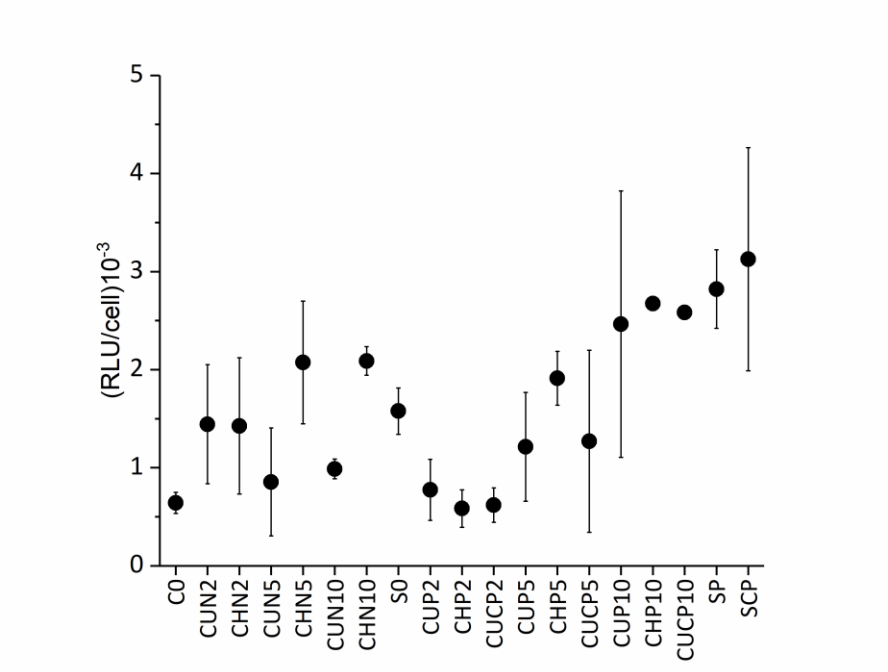

Figure 4-26. Specific microbial activity ((RLU/cell)·10^{-3}) of different formulations after exposure to corrosive environments including cells recovered in corrosion products. Bars indicate range of observations.

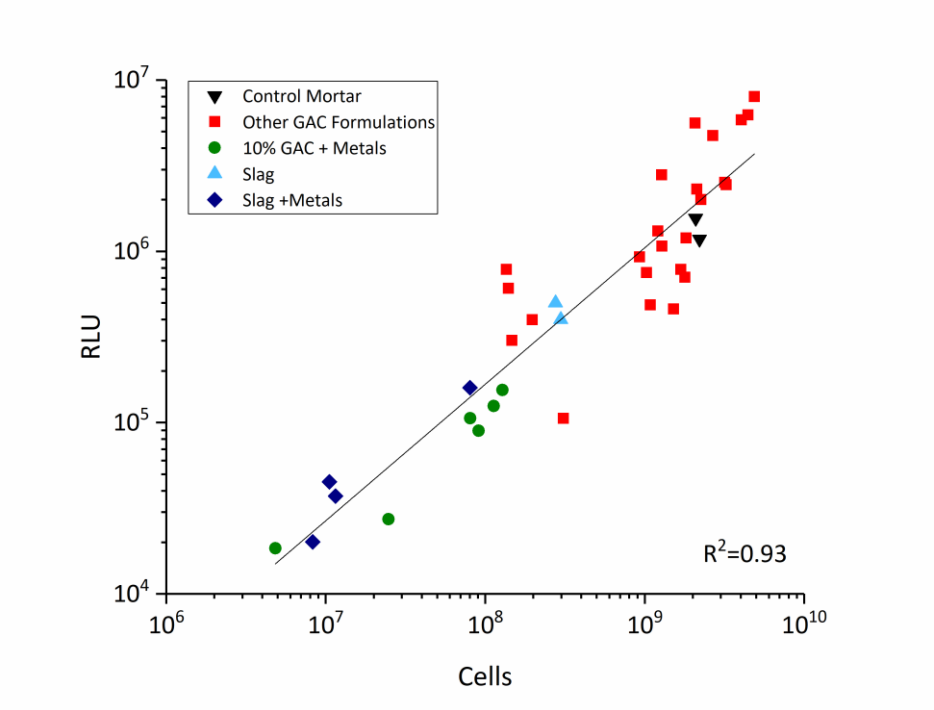

Figure 4-27. Regression of Luciferase emissions (expressed as RLU) against cell counts recovered from suspension for all the samples analyzed. Colors represent reference groups of interest.

16S rRNA gene analysis was used to determine the relative abundance of bacteria on coupon surfaces and associated to corrosion products. 16S genes were quantified with qPCR using universal primers and *Acidithiobacillus*-specific primers. Gene copy numbers were normalized to the corrosion product mass recovered and surface area of the samples (Figure 4-28 and Figure 4-29). Analogous to cell quantification, gene copies circumscribed by universal primers were significantly lower in the formulations with the highest metal loads (CUP10, CHP10, CUCP10, CUCP10, SP, SCP). Universal amplicons corresponded to the following: $9.5 \cdot 10^{9}$ copies/g (CUCP10(1)) and $4.3 \cdot 10^{6}$ copies/mm^2 (CUCP10(1)) to $1.8 \cdot 10^{9}$ copies/g (SCP(2)) and $6 \cdot 10^{7}$ copies/mm^2 (CUCP10(2)). CUN2(1), CHN10(2) and CHP5(1) also ranged between these values (where gene copies were normalized on a mass basis only). Universal copy numbers for the rest of the samples ranged between $2.2 \cdot 10^{11}$ copies/g (CUP2(1)) and $1.1 \cdot 10^{8}$ copies/mm^2 (CUN2(1)) to $3.7 \cdot 10^{14}$ copies/g (CUN10(2)) and $5.8 \cdot 10^{11}$ copies/mm^2 (CUN10(2)). *Acidithiobacillus* gene copy number exhibited similar trends to that of universal primers but resulted in

lower values than the universal copies. Formulations with the highest aggregate substitutions (and metal content) ranged between $6.6 \cdot 10^{8}$ copies/g (CUCP10(1)) and $3 \cdot 10^{5}$ copies/mm^2 (CUCP10(1)) to $1.1 \cdot 10^{10}$ copies/g (SCP(2)) and $2.7 \cdot 10^{6}$ copies/mm^2 (SCP(2)). Exceptions that also ranged between these values (on a mass basis) included: CHN10(2) and CHP5(1). *Acidithiobacillus* copies for the rest of the samples ranged between $2.3 \cdot 10^{11}$ copies/g (CUN2(1)) and $1.6 \cdot 10^{7}$ copies/mm^2 (CUN2(1)) to $1.1 \cdot 10^{14}$ copies/g (CUN10(2)) and $1.8 \cdot 10^{11}$ copies/mm^2 (CUN10(2)). The relative abundance of *Acidithiobacillus spp*. is indicated in Figure 4-30. Formulations with the highest aggregate substitution and metal content also had the lowest relative abundance of *Acidithiobacillus* 16S rRNA genes. Values ranged between 0.3% (CHP10(1)) and 3% (SP2). The rest of the samples displayed higher relative abundances, ranging between 13.8% (CHN5(2)) to 103.4% (CHP5(2)).

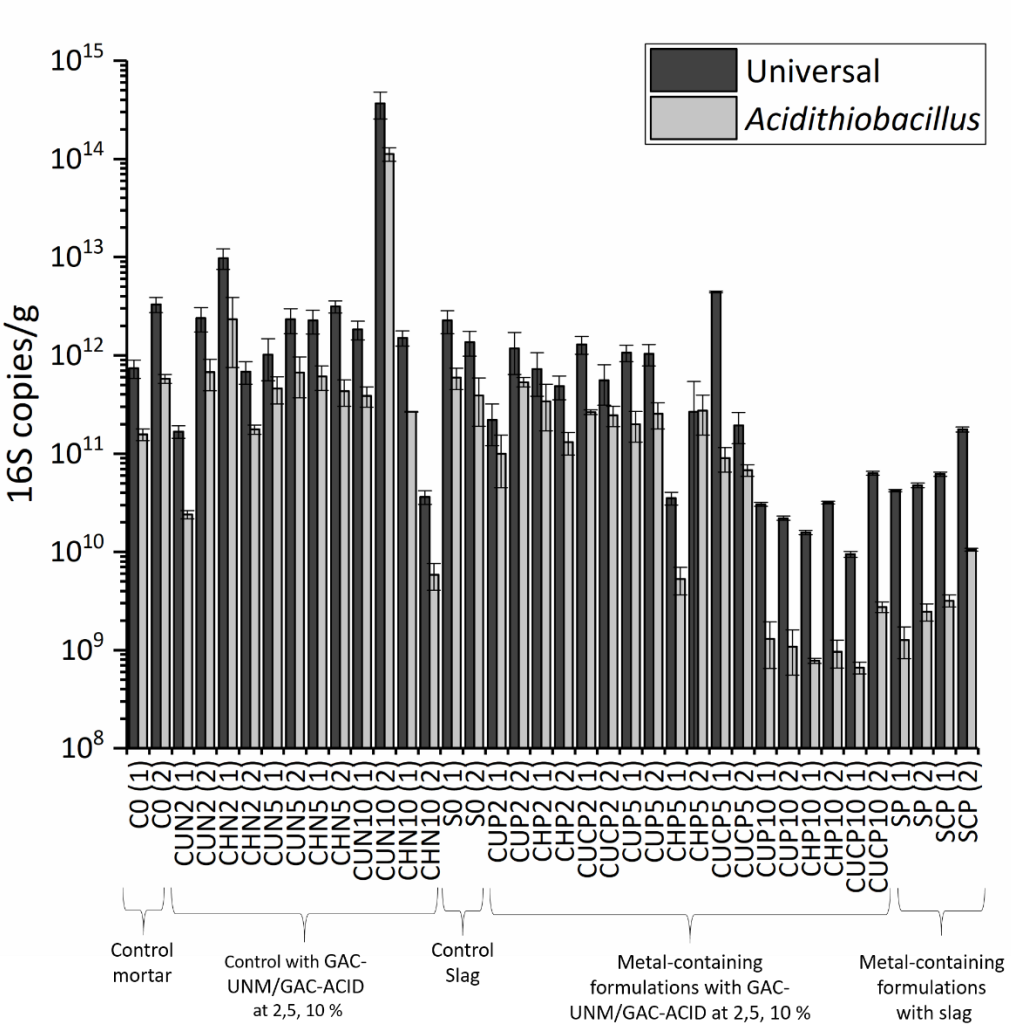

Figure 4-28. 16S rRNA gene copies per gram of corrosion product for all analyzed samples. Numbers in parentheses indicate replicates for each formulation. Dark grey columns represent average 16S gene copies circumscribed by universal primers. Light grey columns represent average 16S gene copies circumscribed by probes specific to the genus Acidithiobacillus. (n=3).

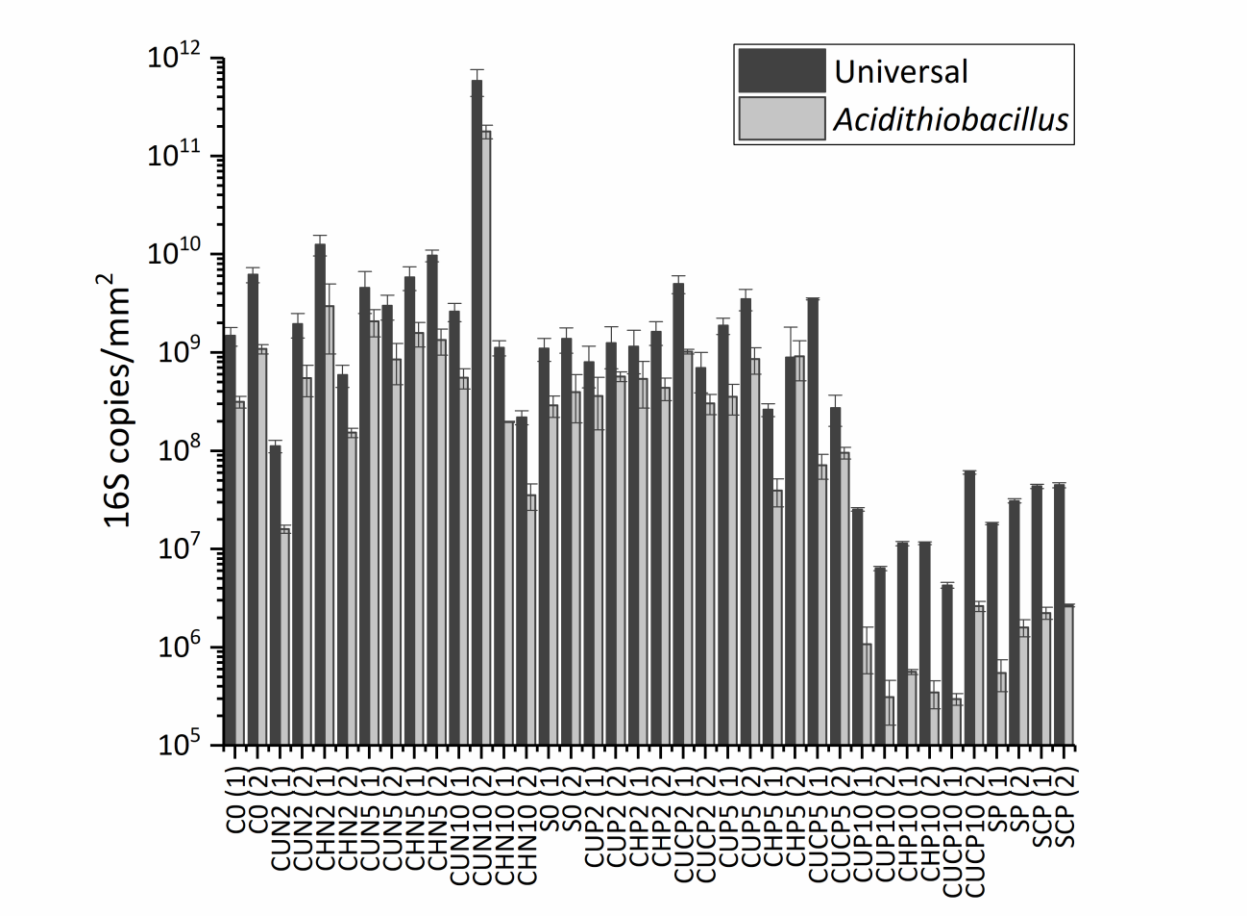

Figure 4-29. 16S rRNA gene copies per surface area of each sample. Numbers in parentheses indicate replicates for each formulation. Dark grey columns represent average 16S gene copies circumscribed by universal primers. Light grey columns represent average 16S gene copies circumscribed by probes specific to the genus Acidithiobacillus. (n=3).

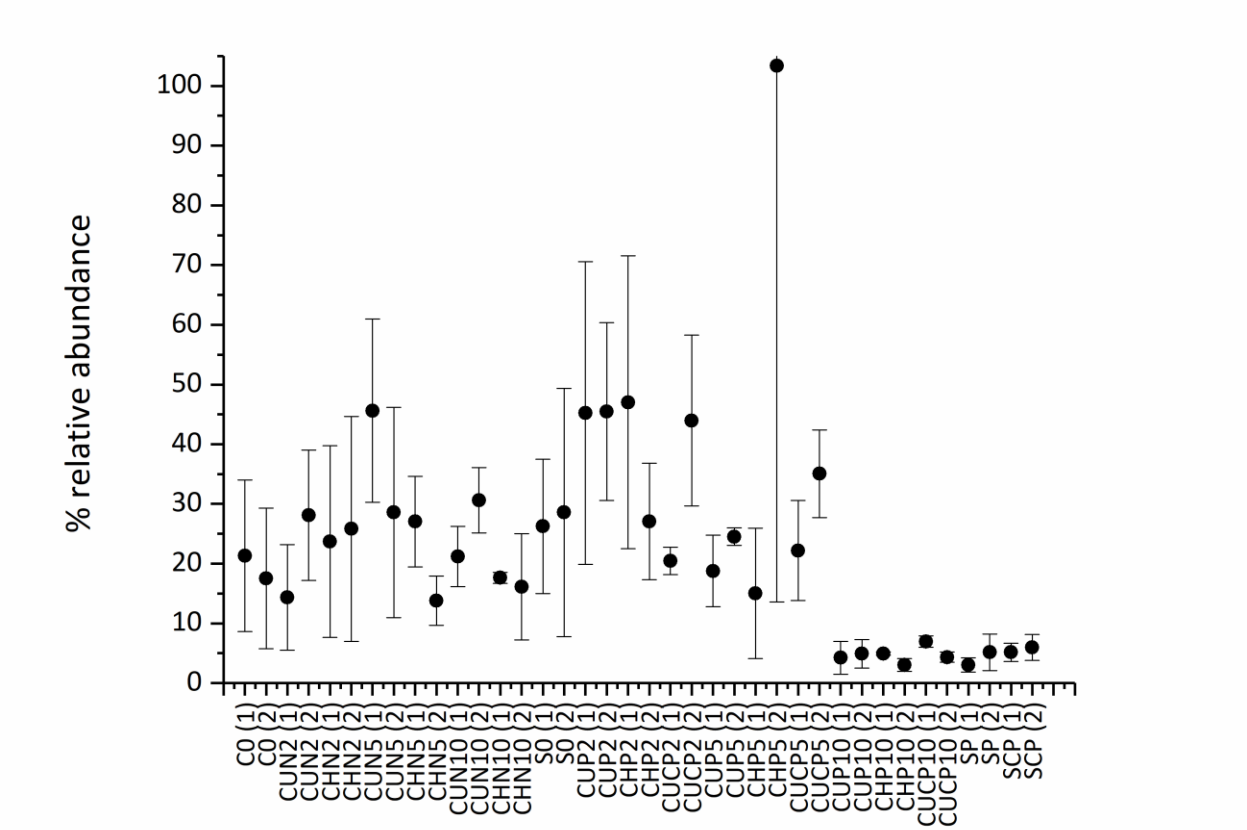

Figure 4-30. Relative abundance (%) of Acidithiobacillus-specific 16S rRNA gene copy numbers from the total universal 16S rRNA gene copy numbers. (n=3).

4.5.3 Chemical Analysis

Investigations of sentinel chemical transformations that occurred in the cement material after exposure to the corrosive environments were done through three complimentary approaches: i) analysis of sulfur and calcium abundance in the corrosion products, ii) sequential cation extraction on unexposed and corrosion-exposed formulation, and iii) electron microprobe mapping of cement surfaces challenged by corrosive sewer environments.

Abundance of sulfur, and its correlation with free calcium content in corrosion products was used as an indicator for sulfur-oxidizing metabolism and corrosion extent. The mass-normalized values for total sulfur and sulfur-to-calcium ratios are shown in Figure 4-31 and Figure 4-32. Following the trends observed in the microbial analyses, the specimens with the highest fine aggregate substitution (and metal content) (CUP10, CHP10, CUCP10, SP, and SCP) consistently exhibited the lowest sulfur values per gram of corrosion product, ranging between 0.14 mg S/g (SP) and 3.5 mg S/g (CUP10). Replicates for other formulations exhibited values within this range although with the exception of formulation CHN10. The rest of the formulations displayed higher and more variable sulfur loads, ranging between 0.8 mg S/g (CHN10) and 12.8 mg S/g (CUCP2).

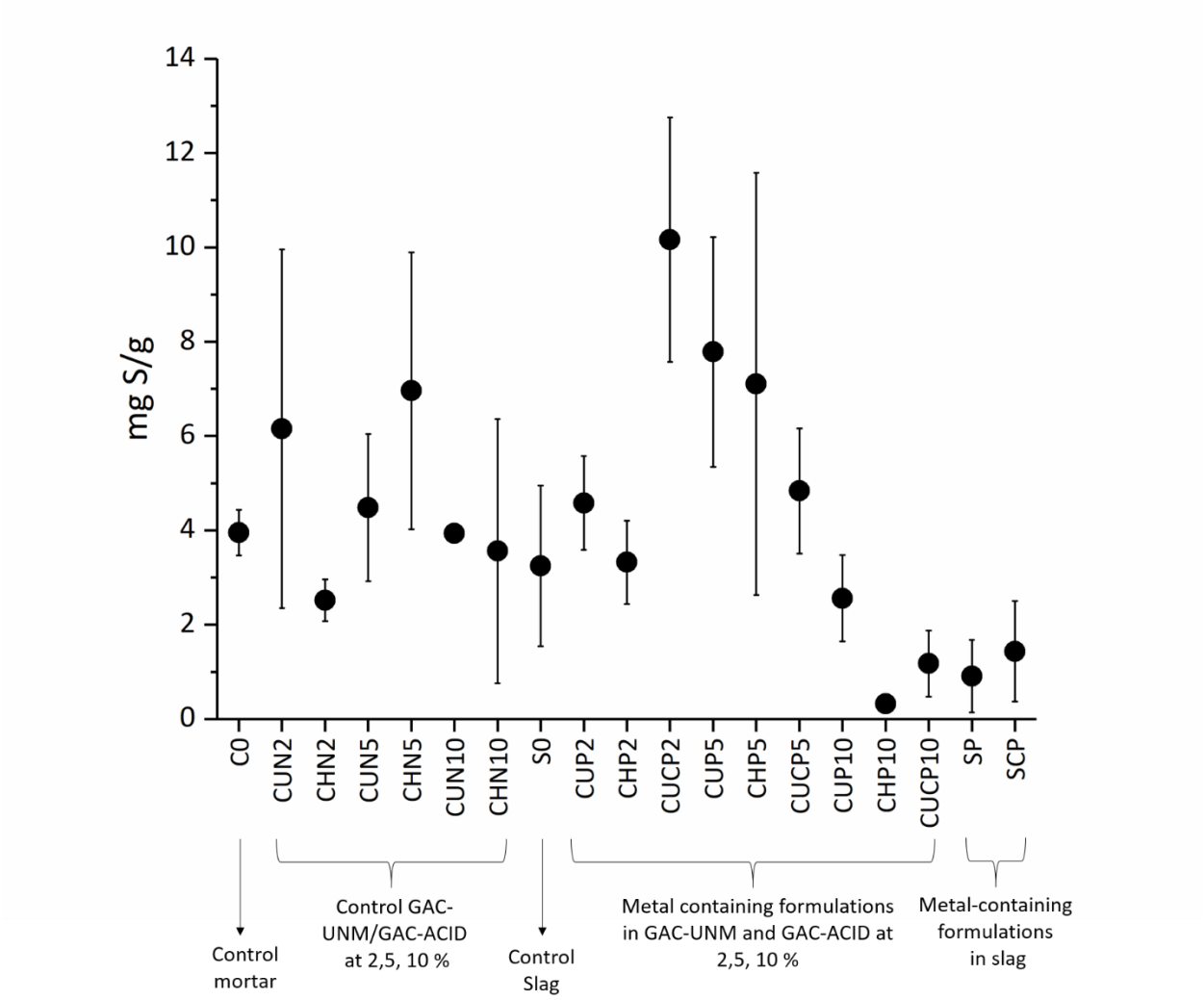

Figure 4-31. Total sulfur content (mg S) normalized by corrosion product mass obtained for each formulation after 11 months of exposure to a corrosive sewer environment. Bars indicate range of observations.

Sulfur-to-Calcium ratios followed a profile similar to that observed for total sulfur content.

Formulations with the highest aggregates substitutions (and highest metal loads) also presented the

lowest S:Ca ratios, along with the formulation containing unadulterated slag (S0), with values ranging between 0.11 to 0.55. The rest of the formulations ranged between 0.33 (S0) and 1.67 (CHN5).

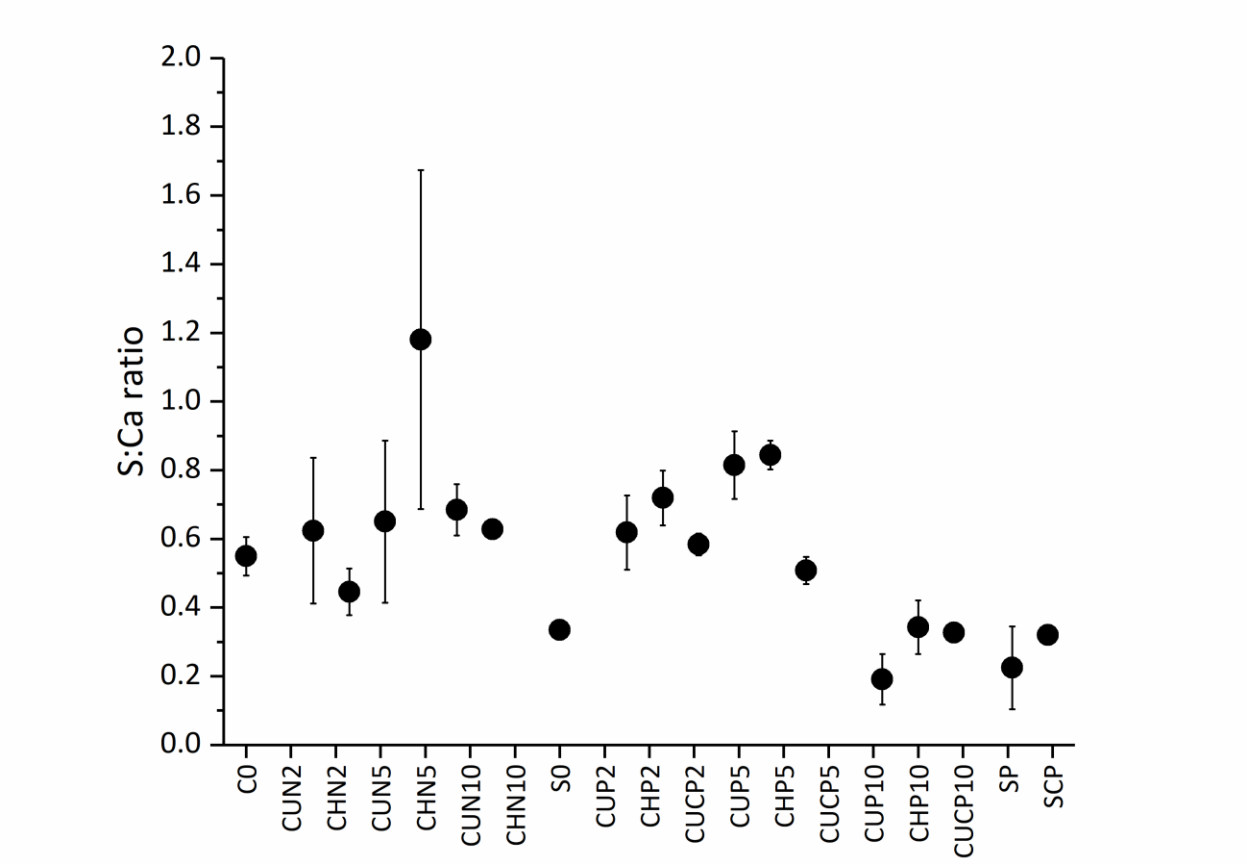

Figure 4-32. Sulfur-to-calcium ratios obtained from the corrosion suspensions for each formulation at the end of the experiment. Bars indicate range of observations.

To assess the potential mobility of inhibitory metals after field exposure, a series of sequential extractions were performed on the samples. The modified Tessier method [196] was applied partition aggregate-immobilized metals into the following five operationally defined categories:

Fraction 1 — Exchangeable. Changes in ionic strength drives metal sorption-desorption processes.

Fraction 2 — Bound to carbonates. Fraction susceptible to pH changes.

Fraction 3 — Bound to iron and manganese oxides. Fraction unstable under anoxic conditions.

Fraction 4 — Bound to sulfides and organic matter. Fraction susceptible to oxidizing conditions.

Fraction 5 — Residual. Fractions in which the metals may be found immobilized within the crystal structure of minerals.

Unexposed mortar cylinders, kept in ambient conditions for the length of the experiment (11 months), were pulverized and subjected to extraction. Mortar cylinders recovered from the sewer were cut longitudinally at the diameter, and transversally 3 mm from the most exposed face. The resulting mortar disk samples were pulverized and subjected to extraction. Formulations at 5% and 10% sand replaced with metal-laden GAC, and metal-laden slag formulations were used to evaluate metal mobility. Cement containing no antimicrobial aggregate and containing metal-free BOF-S (C0 and S0) were used as controls with no metals. Calcium was also analyzed and used as an indicator of corrosion extent. In general, calcium fractioning followed the series f2>f1>f3>f4>f5, with a slight difference in F1 and f2. Copper partitioning followed the series f2>f4≈f3>f1≈f5, with slight differences in F3 and F4. Finally, cobalt partitioning followed the series f2>f3>f1>f4≈f5.

Calcium within C0 displayed a decrease in F1 from 47.4% to 41.8%, and increase in F2 from 49.7% to 56.4%, after exposure to corrosive environments. Calcium in F3 experienced a decrease from 2.7% to 1.7%. S0 experienced minor changes in F1 from 30.7% to 30.4%, a slight increase in F2 from 58.6% to 61.3%, and a slight decrease in F3 10.4% to 8.2%. All 5%-GAC replacement samples (CUP5, CHP5, and CUCP5) shared the same calcium and copper partitioning trends. After exposure, calcium decreased in F1 11.9%, 17.7% and 12.1%, and increased in F2 12.1%, 18.1% and 12.1%. Copper increased in F2 6.5%, 3.4% and 4.8%, and decreased in F4 6.6%, 3.5% and 4.8%. After exposure, cobalt in CUCP5 experienced minor changes before and after exposure. All 10%-GAC replacement formulations (CUP10, CHP10, and CUCP10) shared metal partitioning profiles. After exposure, calcium decreased in F1 11.6%, 16.3% and 8.1%, respectively, and increased in F2 12.1%, 16.3%, and 8.5%, respectively. Copper

decreased in F2 0%, 3.9% and 5.4%, and F3 4.5%, 10.6% and 3.7%, and increased in F4 4.5%, 14.6% and 9.5%, respectively. Cobalt partitioning did not change in response to sewer exposure in CUCP10. Finally, both metal-laden slag formulations (SP and SCP) also presented similar metal partitioning behavior. After exposure, calcium decreased in F1 11.3% and 6.5%, and increased in F2 11.1% and 4.9%, respectively. Copper increased in F2 0% and 8.2%, and F4 3.5% and 0%, while it decreased in F3 3.9% and 8.4%, respectively. Cobalt in SCP increased in F2 4.6% while decreased in F3 4.5%.

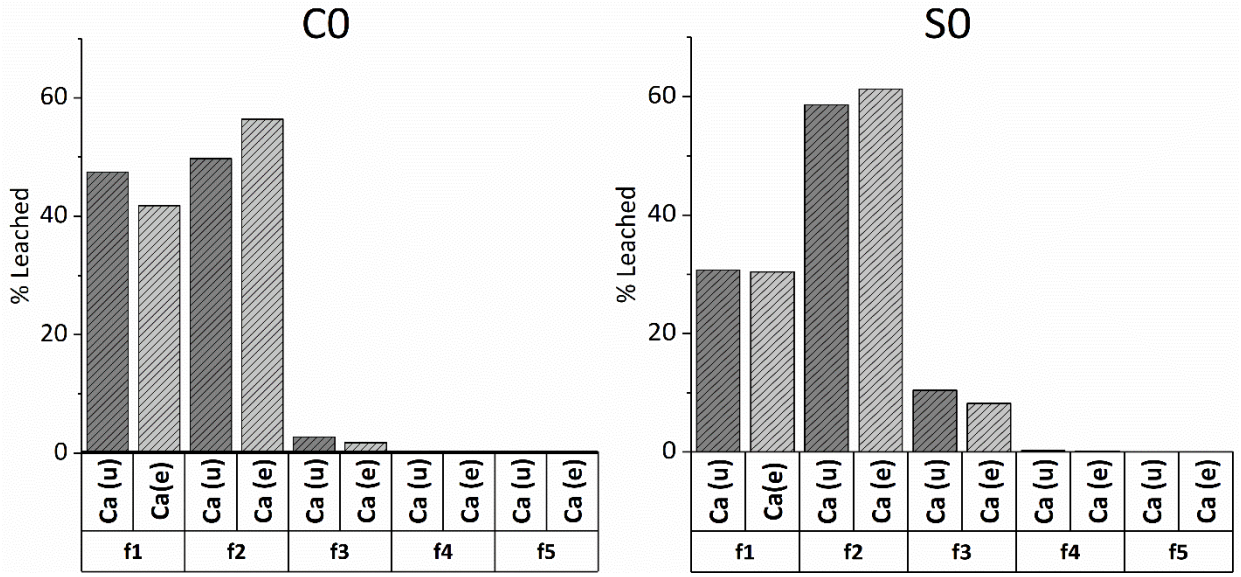

Figure 4-33. Calcium leached from mortar formulations (on a mass percent basis) after sequential extractions of pulverized mortar samples. (u): Calcium leached from corrosion unexposed formulations; (e): Calcium leached from formulations after exposure to sewer corrosion (11 months). C0: mortar without sand substitution by antimicrobial aggregates. S0: mortar with sand fractions substituted by BOF-S.

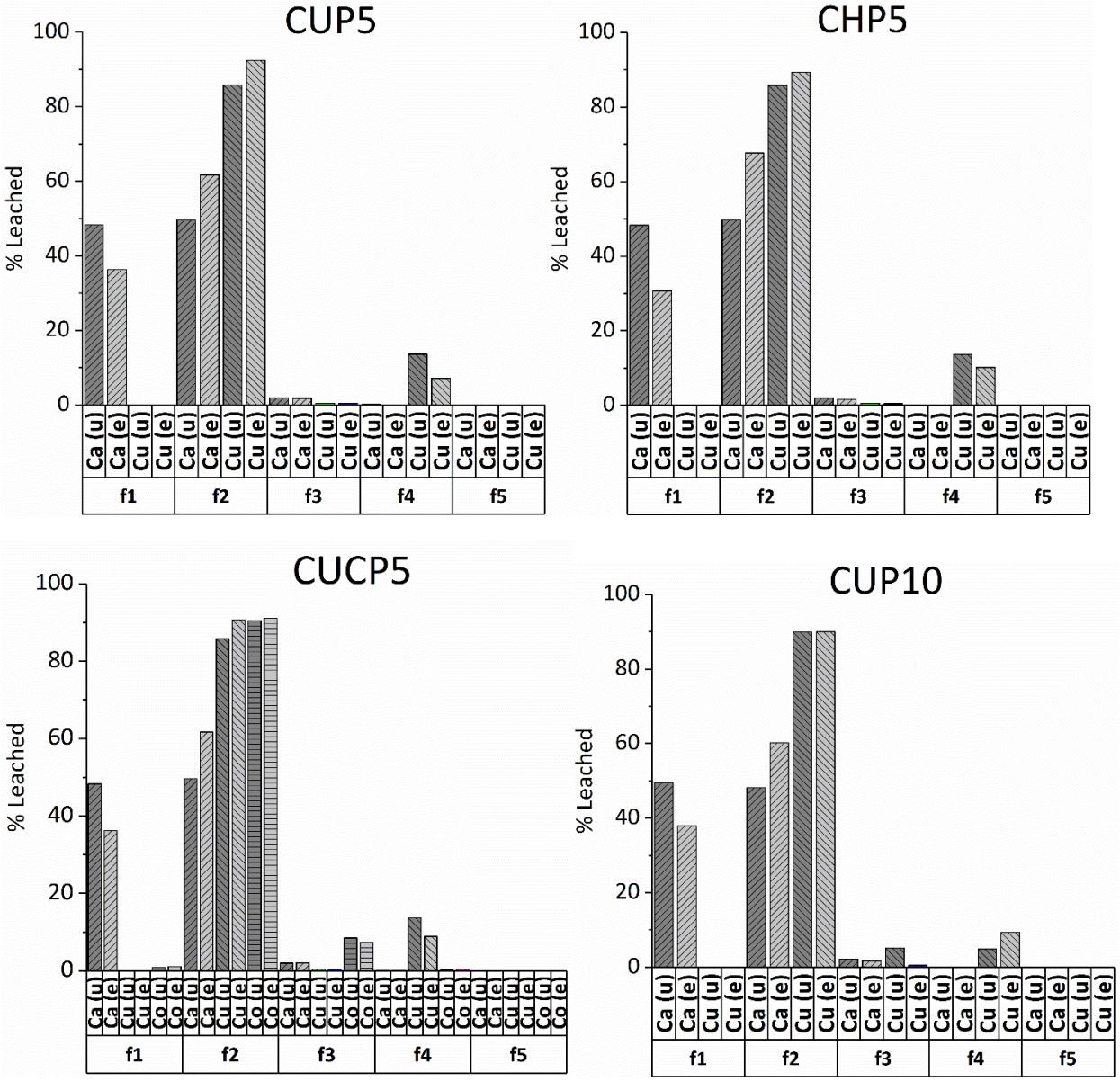

Figure 4-34. Calcium, Copper, and Cobalt leached from mortar formulations (on a mass percent basis) after sequential extractions of pulverized mortar samples. (u): metals leached from corrosion unexposed formulations; (e): metals leached from formulations after exposure to sewer corrosion (11 months); CUP5: mortar with 5% sand replaced by GAC-UNM-Cu; CHP5: mortar with 5% sand replaced by GAC-ACID-Cu; CUCP5: mortar with 5% sand replaced by GAC-UNM-Cu-Co; CUP10: mortar with 10% sand replaced by GAC-UNM-Cu.

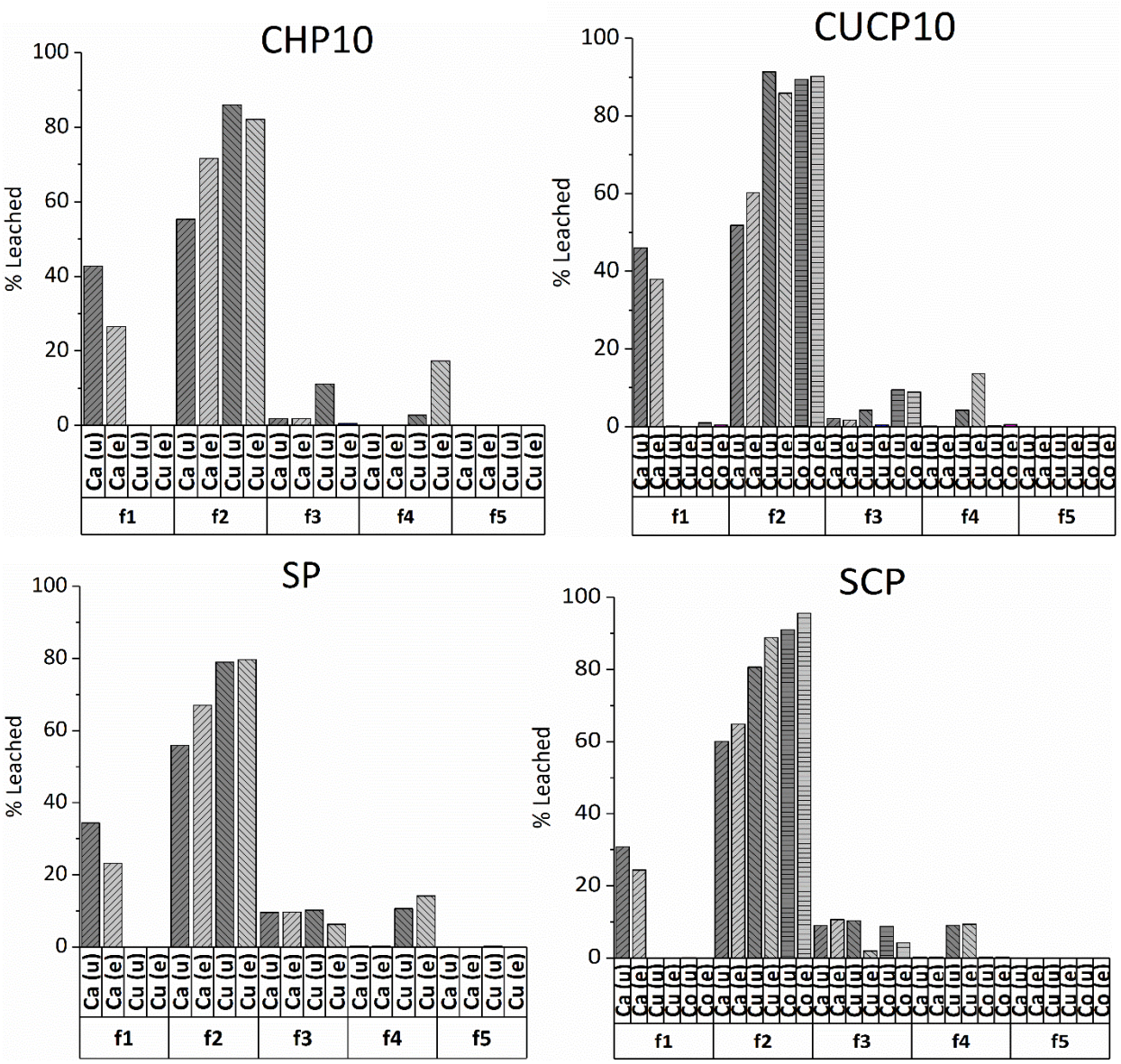

Figure 4-35. Calcium, Copper, and Cobalt leached from mortar formulations (on a mass percent basis) after sequential extractions of pulverized mortar samples. (u): metals leached from corrosion unexposed formulations; (e): metals leached from formulations after exposure to sewer corrosion (11 months); CHP10: mortar with 10% sand replaced by GAC-ACID-Cu; CUCP10: mortar with 10% sand replaced by GAC-UNM-Cu-Co; SP: mortar with fractions of sand replaced by BOF-S-Cu; SCP: mortar with fractions of sand replaced by BOF-S-Cu-Co.

The corrosion fronts of the different formulations were characterized by electron micro probe analysis (EMPA). Longitudinal cross sections of different mortar cylinders were immersed in epoxy, polished, and coated with silver prior to analysis. The most corroded regions in the polished sections were chosen for elemental mapping. The analytical depth for each mapping included the corroded area, corrosion front, and uncorroded matrix. Selected formulations included: C0, S0, CUCP10, SCP, and

CUCP5. Specific net intensity counts were obtained for: Si, Ca, Al, Fe, Mg, S, Cu, and Co (Figure 4-36). All samples presented silicon-rich nodules associated with sand grains. C0 and CUCP presented two distinct silicon regions within the mortar matrix, the regions near the sample's surface having less silicon net intensity counts, on average. Similarly, calcium in these two formulations presented the two regions. An additional calcium-rich band that separated these was observed. This front was also present at the surface of S0. CUCP10 and SCP showed little changes in calcium net intensity counts. Calcium-rich granules were observed within the matrix for S0 and SCP at different depths. Aluminum displayed a defined front in C0, CUCP10, and CUCP5. Absence of aluminum was observed passed the front and closer to the surface of the samples. S0 presented superficial dealumination near the surface. No significant trends were observed in the matrix of SCP. S0 and SCP presented aluminum-rich areas across the mapped region. Iron and magnesium presented similar trends as for aluminum. Iron- and magnesium-rich granules were also identified across S0 and SCP. Mappings of sulfur revealed a general negative correlation between this element and all the previously described. Sulfur in C0, CUCP10, and CUCP5 exhibited similar trends with different degrees of S intrusion into the matrix. Sulfur net intensity counts appeared to increase with depth, reaching the maximum at the corrosion front. Little sulfur was observed passed this front and at further depths. S0 presented a sulfur-rich superficial front, similar to the profile exhibited by calcium. SCP presented little sulfur across the mapped area. In general, net intensity counts for Cu and Co in the metal-containing formulations followed the series SCP>CUCP10>CUCP5. Cu and Co in SCP accumulated around specific granules and appeared to slightly diffuse into the cement matrix. Cu and Co in CUCP10 also appeared to accumulate around specific granules albeit by lesser net intensity counts. Absence of Cu and Co was observed passed the corrosion front and near the surface. Few net intensity counts for Cu in CUCP5 were observed across the mapped area. Richer areas appeared to concentrated around one grain (at the bottom of the image) and forming a thin line at the corrosion front. No significant Co was observed in this sample.

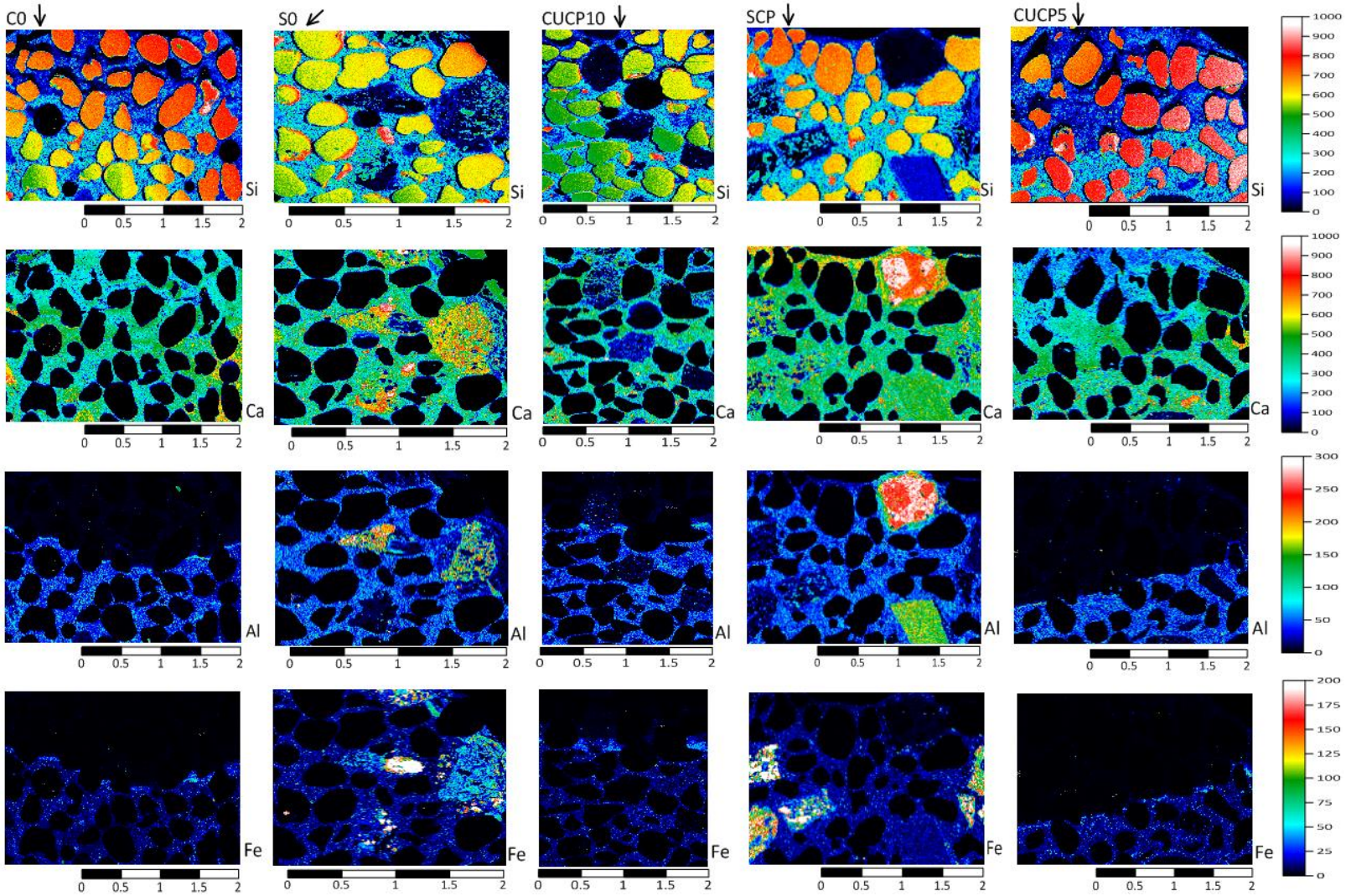

Figure 4-36. Elemental mapping of C0, S0, CUP10, SCP, and CUCP5 after exposure to sewer corrosion (11 months). Color scale represent net intensity counts obtained for each element. Arrows indicate the direction of the corrosion front. Scale bar = 2mm.

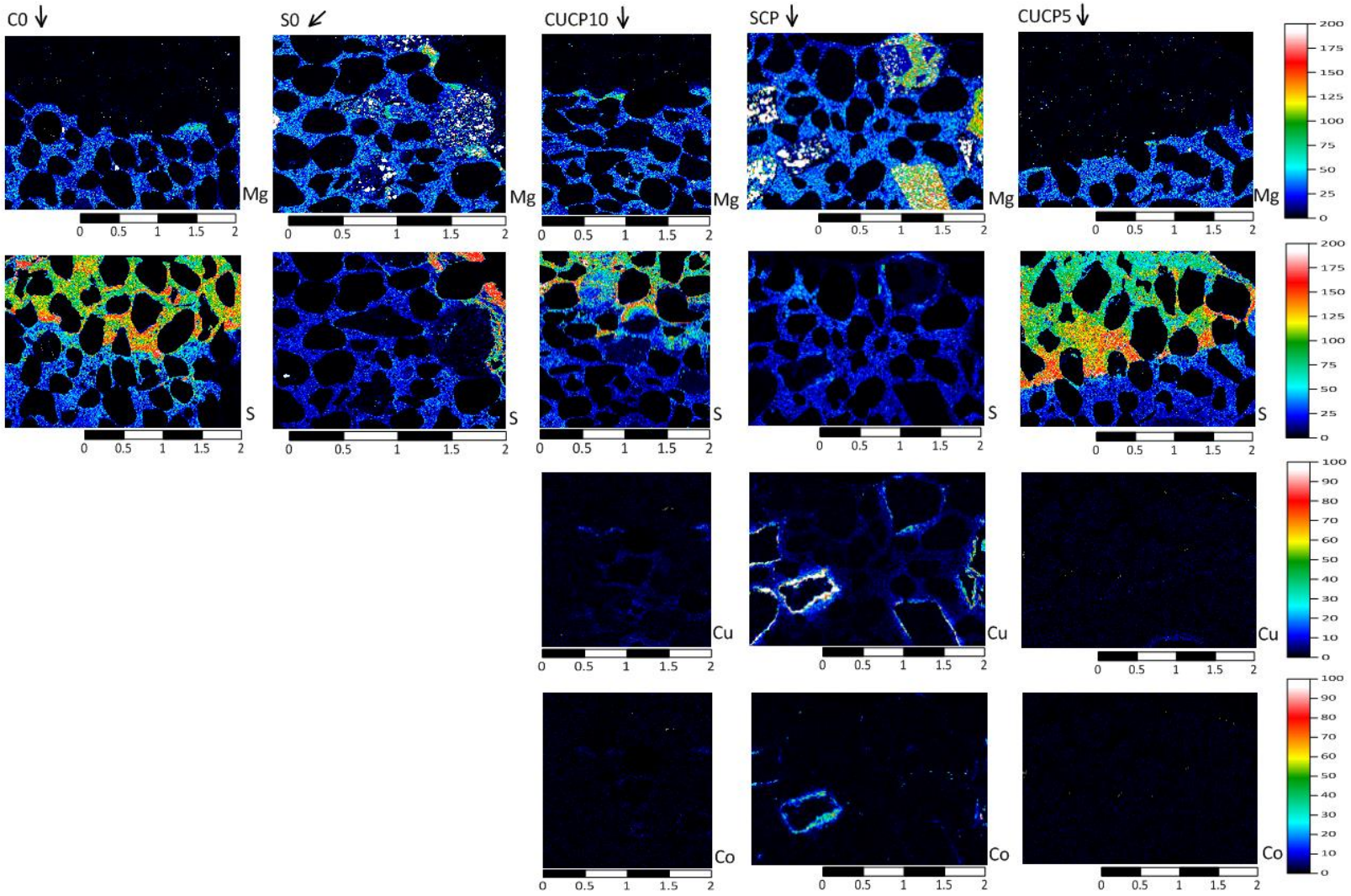

Figure 4-37. (Cont'd from Figure 4-36). Elemental mapping of C0, S0, CUP10, SCP, and CUCP5 after exposure to sewer corrosion (11 months). Color scale represent net intensity counts obtained for each element. Arrows indicate the direction of the corrosion front. Scale bar = 2mm.

Chapter 5 Discussion

5.1 Introduction

The results presented in the previous chapter provided information regarding the effect of different heavy metals on the inhibition of acidophilic sulfur oxidizing communities; the characterization and metal sorption/leaching behavior of fine aggregate substitutes and, the evaluation of antimicrobial mortar formulations of metal-impregnated sorbents in both simulated and real corrosive sewer environments. The discussions of these results are organized as follows: (i) the comparison of relevant findings in this study to those previously reported for acidophile inhibition, (ii) the converging lines of evidence on the specific antimicrobial materials response of new cement formulations; and, (iii) the perspective of how this research could influence the operating design and practices to minimize the effects of microbially induced concrete corrosion in sewers. The chapter is divided into four sections which correspond to the hypotheses presented (0).

5.2 Metal-Induced inhibition against acidophilic communities in solid and liquid media.

5.2.1 Inhibition studies in solid media

The results presented in this study, as well as, those previously reported ([18, 19],[111],[203, 204],[117]), support the hypothesis that different metal ions may have different inhibitory potential against *Acidithiobacillus spp*. enriched from sewer crown extracts. The inhibition potential observed (Cu>Co>Cd>Zn>Ni) generally agrees with some previous metal toxicity studies of pure microbial cultures [18, 19]. *Acidithiobacillus spp*. response to metal mixtures is limited, however, the synergy of binary and ternary metal solutions have been described [19, 117, 205]. In this study, a synergistic effect resulted from concurrent exposure to Cu and Co (Figure 4-2). The assay developed herein is the first of its kind for solid phase observations of metal inhibition of acidophilic communities. The classic Kirby-Bauer

antibiotic sensitivity test was adopted to assess diffusion inhibition of *Acidithiobacillus thiooxidans* growing on agar surfaces, in a longitudinal format. This method serves a simple and effective way to benchmark the inhibitory potential of leached metals by simple distance measurements.

Liquid inhibition assays require monitoring of multiple parameters such as pH, metabolite concentration, and cell numbers, to verify acidophile response, and are relatively labor intense and costly. This assay requires only visual inspection of the generated inhibition length on a macroscale, and the determination of the metal concentration at the interface (Figure 4-3). After incubation, the cell densities in the inhibition zone only increased by a maximum factor of 3 of the original inoculum density (control). Higher surface cell densities were consistently observed in the zones containing dispersed colonies. This might be attributed to the increased biofilm production which has been reported to help some bacteria select soluble metals, and sequester nutrients from competitors [206].

Metal inhibition studies of *Acidithiobacillus spp*. have predominantly studied pure *Acidithiobacillus ferrooxidans* strains as an environmental model organism. Additionally, *A. ferrooxidans* isolates use in many metal-tolerance studies were enriched from sites with relatively high heavy metal concentrations (e.g. acid mine drainage). The enrichments and inhibition assays developed here, are predominantly enriched *Acidithiobacillus thiooxidans* from corroded sewer crowns. While the enrichment origin did not impact the hierarchy of heavy metal inhibition potential observed, the results show *A. thiooxidans* enrichments from sewer crowns are significantly more sensitive to soluble heavy metals than *A. ferrooxidans* recovered from metal-contaminated sites.

5.2.2 Inhibition studies in liquid media

The inhibitory effects and minimum inhibitory concentration of Cu and Co were further assessed on mixed acidophilic cultures in a liquid format. Silver (Ag) was also included based on its literature history as broad-spectrum inhibitory metal. As for the solid inhibition assays, the results presented in

this study support the hypothesis that different metal may ions have markedly different inhibitory potential against *Acidithiobacillus spp*. extracted from sewer crowns. The temporal monitoring of pH used in this study proved to be a reliable and useful indicator for acidophilic activity and metabolism and metal sensitivity [18, 90, 115, 117]. The minimum inhibitory concentration (MIC) for acidophilic growth was repeatedly observed from enrichments that did not experience significant pH drop after 30 days of incubation. In thiosulfate-based media, stationary phase for *Acidithiobacillus* cultures was reached 8 days after inoculation. The relative duration of experiments highlighted metal-induced lag phases from stable inhibitory concentrations. MICs clearly emerged for Cu alone (50 mg Cu/L), and in mixtures of Cu/Ag (50 mg/L and 25 mg/L) and Cu/Co (15 mg/L and 15 mg/L). Enrichments with Ag and Co alone did not exhibit acute inhibition up to the highest concentrations tested (75 mg/L and 50 mg/L, respectively). No inhibitory synergism was observed when mixing Cu and Ag at a 2:1 ratio, when compared to any individual metal alone. However, synergistic inhibition was observed when Cu and Co were present at a 1:1 ratio. The MIC associated with Cu exposure dropped markedly from 50 mg/L to 15 mg/L, when mixed with Co at equal mass concentration. Similarly, the MIC of Co lowered from >50 mg/L, when individually added to 15 mg/L when added together with Cu. The literature is tenuous on this topic. Reported MIC values differ significantly across many studies on heavy metal-induced inhibition, some reporting values in the order of grams per liter. A study by Cho et al. on the toxicity response to metal mixtures by *Acidithiobacillus ferrooxidans* (ATCC 19859) extracted from pyrite-rich coal mines, indicated an elevated tolerance against heavy metals [19]. Single added metals that exhibited inhibitory response followed the sequence Cu (142 mM)>Cd (440 mM)>Zn (690 mM)>Ni (850 mM). Some binary, ternary, and quaternary systems resulted in metal synergy, while others resulted in competition for binding sites within the cell and consequent loss of inhibition. The lowest inhibitory concentration (referred to Cu) was obtained for a ternary system of Cu (47 mM), Cd (27 mM), and Zn (690 mM). A different study by Chen et al. on dose-response assessment to metal exposures upon indigenous *Acidithiobacillus*

thiooxidans BC1 extracted from a lead-contaminated site, also revealed increased tolerance against individual heavy metals [18]. The study reported effective inhibitory responses following the series Cd (300 mg/L)>Cu (400 mg/L)> Zn (>10,000 mg/L). Even though these authors reported lower inhibition values than their coworkers, the MIC for Cu was 8 times higher than the value reported here (50 mg Cu/L and 15 mg Cu/L).

Based on the literature review and the observations from this study, at least two considerations arise for MIC differences when comparing sewer-borne enrichments to those from metal-contaminated sites: metal tolerance of sewer crown isolates is not anticipated since they rarely encounter metals.

A majority of investigations on metal inhibition have been done on *Acidithiobacillus* species typically found in iron- and sulfide-rich mining ores, which usually contain elevated heavy metal levels. This condition likely exert selection pressure on these bacterial communities to tolerant different transition metals, as observed by the presence of "transferable genomic islands" [112, 114]. However, this study indicates that *A. thiooxidans* may be susceptible to lower heavy metal concentrations than mining-environments, particularly Cu. To date, there appears to be only one peer reviewed study assessing metal-associated inhibition of *A. thiooxidans* recovered from sewer crowns. Milner studied effects of different metal cations, anions, and chelators on the growth of sulfur oxidizing acidophile isolates from sewer crowns in Los Angeles [117]. In a manner similar to this study, Milner inoculated different cultures containing increasing amounts of single inhibitors and inhibitor combinations, then monitored the culture pH and cell numbers for up to 500 hours. Results derived from Milner's study include inhibition with single-added Hg exposure (10^{-4}M) and Cu (10^{-3}M); delayed lag effect with Co (10^{-3}M) and Ag exposures (10^{-3}M), and no inhibition observed in the presence of Cd and Zn. For binary mixtures, no significant synergistic effect was observed when combining Cu and Ag (10^{-3}M and 10^{-3}M, respectively) or Cu and Co (10^{-3}M and 10^{-3}M, respectively). Additionally, the author emphasized the importance of the initial culture pH on the toxicity of each metal species. The study concluded that

lower initial pH lowered the toxicity of cationic species, while increased the toxicity of anionic species. Although the monitoring of the cultures may have been too short to detect longer metal-induced lag effects, as seen in this study, the inhibitory concentrations and lag trends were within the limits observed here. These results suggest that *A. thiooxidans* growing in sewer crowns may be susceptible to doses of heavy metals that are markedly lower than mining environments. A broader survey on the inhibitory metal thresholds of different crown isolates is necessary to confirm this hypothesis.

A second, non-excluding, explanation for the lower MICs observed in this study, is the preferential growth of heterotrophic communities, found in acidophilic mixed cultures at low relative abundance, at metal concentrations above the MIC in carbon-limited media. Direct quantification at the end of the metal exposures, indicated elevated cellular abundance, independent of metal dose. Moreover, slightly higher cell densities were observed beyond metal inhibition thresholds. This lead to the investigation of microbial community composition at different metal exposures, when started from the identical inoculum. Copper alone, and the binary mixture of Cu and Ag, exhibited a pH-based inhibition threshold. 16S rDNA analysis revealed a transition from *Acidithiobacillus* dominance (<50 mg Cu/L) to a variety of oligotrophic communities (>50 mg Cu/L) above the MIC. At metal concentrations where *Acidithiobacillus* growth was inhibited, the bacterial community was dominated by *Burkholderia* and *Ralstonia*. These ubiquitous genera have been found in many environments: rivers, seas, soils, pure water systems, wastewater, and concrete corroded sewer systems [25, 91, 207]. Some species have been detected in acid mine drainage and heavy metal contaminated sites as well, indicating adaptability within a broad pH range and heavy metal concentration spectrum [208, 209]. Both genera are associated with heterotrophy and oligotrophy, which allows them to thrive in environments with low organic carbon load. Additionally, some species carry the genetic information for mediated assimilatory reduction of sulfate and thiosulfate [210, 211]. *Leifsonia spp.*, *Sphingomonas spp*., *Methylobacterium spp.*, and *Microbacterium spp*. were also in significant abundance at high metal concentrations. These

genera have also been found in a wide variety of environments, including wastewater [212, 213], and are able to use thiosulfate mixotrophically [214, 215]. Additionally, *Methylobacterium spp.* have been observed to mediate oxidation of reduced sulfur species [216].

The higher metal concentration dosages shifted the microbial community from less diverse acidophilic, autotrophic communities to more diverse neutrophilic communities able to survive in a thiosulfate enrichment. Two conditions may support this community response. It may be that the inhibition of *Acidithiobacillus thiooxidans* by heavy metal exposure reduces competition for ecological niches, otherwise to be colonized by other community members present in the inoculum. Another possibility is that the metal-induced reduction in the growth kinetics of *Acidithiobacillus* (increased lag phase) allows for other opportunistic, heterotrophic, neutrophilic, sulfur oxidizing members present in the inoculum to develop, in the absent of healthy *Acidithiobacillus.* Due to the fact that dominant communities are able to sustain neutral pH and use the reduced sulfur source in the media, *Acidithiobacillus* remains unable to develop in significant numbers. A study done by Padival et al., on the control of *Acidithiobacillus* by means of microbial competition, indicated the possibility to manipulate nutrient conditions in a CSTR to favor growth kinetics of certain yeasts and reduce the growth of these acidophiles [217].

5.3 Sorbent characterization and sorption/leaching behavior

5.3.1 GAC characterization

Two types of GAC were used as metal carriers in mortar formulations: steam-superheated bituminous coal, commercially referred as OL 20X50 GAC (GAC-UNM), and the same GAC after modification with hot nitric acid (GAC-ACID). Acid modifications of activated carbon have been extensively studied, documenting nitric acid as an effective agent for controlling some types of functional groups [128, 200, 219]. Thus, treatment with 5 % HNO_3 lead to a 20 % decrease in the specific

surface area of the carbon. The decrease in surface area was mainly ascribed to the equal destruction of both micro- and mesopores, as no significant changes in the pore size distribution were observed. Despite the loss in total specific surface area, no major differences in the water absorption capacity between unmodified and acid-modified carbons were observed. A possible explanation for this is the fact that a significant amount of new oxidized functional groups, with high hydrophilicity, were introduced to the carbon during acid exposure. Therefore, the acidified carbon may compensate for hygroscopic loss, in what would result in a decrease in water sorption capacity, with the presence of hydrophilic groups that can bind water through chemisorption and hydrogen bonding [220]. The acidification process lowered both pH and pHpzc, as expected for the HNO_3 treatment applied here. Additionally, the relative abundance of oxygen-containing functional groups shifted from Phenolic dominated towards carboxyl moieties in and on the acid-treated GAC. Additionally, the total number of surface functional groups increased, as a consequence of acid-enhanced oxidation as consistent with that observed by other GAC experimentalists [221-223]. Increased incorporation of carboxylic groups has been described as the major consequence of HNO_3 GAC treatment [200, 219, 221, 223]. FTIR analysis supported the increased oxidation of GAC surfaces by detection of previously absent ester-, ketone-, and carboxylic-related groups.

5.3.2 Steel slag characterization

Basic oxygen furnace steel slag (BOF-S) was also used as a metal carrier in mortar formulations. In contrast to carbon-based sorbents, BOF-S is mineral in nature. While its composition is similar to that of Portland cement, it differs significantly in the oxide proportions and the mineralogy [224]. The major oxide composition (>1%) of the BOF-S used in this study indicated an oxide abundance in the following series $CaO>Fe_2O_3>SiO_2>MgO>MnO>Al_2O_3$. Minor components included titanium, vanadium, and chromium. The mass percentages obtained were within those reported by different authors [134, 225]. The free lime content of the grains was assessed and compared to a pulverized format, where lime

comprised 0.04% and 1.5% of the total weight. In the context of durability, excess of free lime may lead to increased sulfate attack and cement paste deterioration, as hydrated $Ca(OH)_2$ will readily dissolve in the presence of sulfuric acid [44-46]. The fact that the BOF-S grains used in this study contribute to very small amounts of free lime indicates compatibility as a fine aggregate. The mineral composition of the slag used here exhibited major phases commonly found in different BOF-S (e.g. Larnite, Mayenite, Wüstite, and Srebrodolskite) [226, 227]. The specific water sorption of this material indicated low porosity. This material was not subject to BET analyses, because numerous studies have characterized the specific surface area of BOF slag fractions which may reach the tenths of m^2 per gram [227, 228].

5.3.3 Metal sorption/leaching

The physical chemistry of the sorbents dictated the dominant mechanism of metal sequestration both during impregnation and incorporation in cement. For unmodified GAC, the dominant mechanism was assumed to be the surface precipitation of metal hydroxides. Before GAC addition, the metal solutions were pH-adjusted to 8 to favor hydroxide complex formation. Then, GAC was added and the mixture was agitated overnight. At the end of the experiment, the solution contained a precipitate colloid "cloud" and GAC particles. After being separated from the loading suspension and dried, the resulted grains were covered with a green/grey layer. For high adsorbent/adsorbate ratios three factors may explain this behavior: 1) the carbon surface ($pH_{GAC\text{-}UNM}$=10.51) is higher than the solution pH; 2) the GAC surface behaves as a "nucleus" for metal hydroxide ($Me(OH)_{2(s)}$) formation; and, 3) a locally high concentration of metal may exist on the carbon surface, increasing the opportunity for precipitation to occur [229]. These mechanisms have been observed by different investigators studying the removal efficiency of aqueous cationic metals by activated carbon at high pH levels [130, 230, 231]. For acid-modified GAC, the mechanism was assumed to be ionic exchange. Due to the acidic nature of this modified GAC (pH_{PZC}= 5.25) and the initial solution pH (5.75), the dominant species to be adsorbed were mainly Cu^{2+}, $Cu(OH)^{+}$, and Co^{2+}. Studies on surface

functionalization have observed the improved cation adsorption of acid-treated GACs [12, 128]. For HNO_3-treated GAC, it is widely-accepted that acidification results in the incorporation of oxidized groups (e.g carboxylic) that can bind metals through ionic interactions [128, 200, 219]. Characterization of acid-treated GAC here, suggests that incorporation of such groups occurred, implying that a dominant sorption mechanism is through functional ionic associations. The dominant metal sorption mechanisms on BOF-S were assumed to be a combination of surface precipitation and surface complexation [232, 233]. Similar to GACs, metal sorption on slags is dependent on the type, the solution pH, the metal concentration, and the adsorbate/adsorbent ratio. Generally, under acidic conditions, surface complexation onto silicates, iron, and manganese oxides is favored, while at higher pH levels surface precipitation of hydroxide complexes dominate [15, 232, 233]. Additionally, at high metal concentrations (>0.1g/L), the equilibrium pH for metal hydroxide formation is significantly lower. Therefore, when adding highly alkaline slag into moderately concentrated metal solutions, formation of hydroxide complexes is favored, and may occur rapidly [233]. The sorption conditions established in this study involved concentrated metal solutions (10 g/L). Before slag addition (40 g/L), the metal solutions pH ranged between 5.75 and 6.3. After BOF-S addition and overnight mixing, the equilibrium pH ranged between 6.5 and 8. Higher equilibrium pH levels were not observed likely because hydroxide ion was consumed to form copper hydroxide (and cobalt hydroxide). At the end of slag loading, the contact solution contained a precipitate “colloidal cloud” separate from the slag grains, suggesting hydroxide precipitation. After being separated from the suspension and dried, the BOF-S grains were covered with a green/grey layer (slightly pink for cobalt-containing batches). These observations suggest that surface precipitation was a dominant sorption mechanism, as observed similarly by other investigations [15, 233]. However, the BOF-S used contained a significant proportion of SiO_2 (14.7%), Fe_2O_3 (25.8%), and MnO (2.5%), and heterogeneous grains were identified to be rich in these phases using EMPA. This suggests the possibility of metal sorption on these oxides as well [234].

The Acid Neutralization Capacity (ANC) test was performed in order to investigate the buffering and leachability potential of the metal-laden sorbents when exposed to increasing amounts of acid. Two types of ANC tests were performed: ANC on the metal-ladent sorbents, and ANC on the same when mixed and cured into Portland cement mortars.

With metal-laden sorbents, the ANC test indicated three distinct groups based on buffering capacity and metal release. The first group (GAC-ACID-Cu), showed little buffering effect with increasing acid addition. Before acid addition (0 eq/kg) the equilibrium pH was 4.8. This value was slightly higher than the measured pH of the carbon alone (pH=4.65), probably due to (deionized) water-induced leaching of Cu (25.6%). At 0.5 eq acid/kg, the solution pH had reached 2.12 and the Cu leached 79.3% of its sorbed mass. The second group was composed of GAC-UNM-Cu and GAC-UNM-Cu-Co. These two sorbents showed increased neutralization capacity and Cu retention. Before acid addition (0 eq/kg), the solution pH was circumneutral and minimal leaching of Cu occurred. In contrast to the acidified carbon, these sorbents required 1 eq/kg of acid to reach pH≈2, at which point the Cu leached was 93% and 87.3%, respectively. The changes in pH with increasing acid addition are within the ranges observed for different carbons [235], with small variations accounting for the buffering effects of the leached metals. An observation can also be made on the different Cu liberation profiles. GAC-ACID-Cu initially released significant amounts of Cu but delivered less metal into solution than the other two GACs with subsequent acid addition. This is because the leaching from GAC-ACID occurred through site-specific competition and displacement of Cu^{2+} by H^{+} from the acid, while leaching from GAC-UNM occurred by the (rapid) acid dissolution of hydroxide complexes. The last group included both BOF-S-Cu and BOF-S-Cu-Co. These materials exhibited the highest buffering effect and the highest metal retention capacity when challenged with acid. Before acid addition (0 eq/kg), the solution pH approached 12 and minuscule amounts of Cu were seen in solution. In contrast to the GACs, the high buffering effect provided by the slags resulted in higher resistance to pH depression in response to acid addition. At 4 eq

acid/kg, the solution pH approached 5 and the metal released was 50.7% for Cu and 83% for Co. The changes in pH with increasing acid addition are within the ranges previously observed for different slags [233, 236, 237]. For both GAC-UNM and BOF-S, cobalt showed higher mobility than Copper in response to acid additions. This is likely because in dilute solutions, Co^{2+} dominates aqueous speciation up to pH=8.2 [238]. Above this value, formation of the less soluble species $Co(OH)_2$ occurs. At 0 eq/kg, the solution pH of GAC-UNM already favors cobalt dissolution as Co^{2+}, while on BOF-S pH remains too high for Co^{2+} to dominate the aqueous speciation.

ANC performed on metal-laden sorbents mixed and cured with OPC differentiate two distinct groups, as shown in Figure 4-14. The amount of acid tested was increased to account for the additional alkalinity provided by cement. The first group included all the mortars with GAC. These mixtures resulted in similar solution pH (10.5) and Cu leached at 4 eq/kg (0%). The same group exhibited a common endpoint pH (2) after 8 eq/kg. In this case Cu leached increased following the series CUCP10≈CHP10>CUP10. The major differences in pH were observed at 6 eq/kg, indicating a leachability trend against acid addition following the series CHP10>CUCP10>CP10U. These results correlate well with the observations on the ANC of isolated metal-laden sorbents. The second group included the two slag-containing formulations. These sample exhibited increased ANC and higher metal retention than their GAC counterparts. The mixtures exhibited similar behaviors at 4 eq/kg with no detectable Cu leached. Significant Cu leaching was not observed until 8 eq/kg of acid addition, at which point SP leached 9% and SCP 45.2% of their total Cu load. The difference in Cu leached, on a percent basis, may be explained by their difference in solution pH at the end of the experiment. In CUCP10 and SCP, Co was observed more mobile than Cu, as also shown for individual metal sorbents.

5.4 Acidophile inhibition by mortar formulations in simulated corrosive environments

Analysis of extracted (and suspended) corrosion products from formulations challenged with H_2S and CO_2 in a bench-scale reactor were inconclusive. The pH of the corrosion products resulted in acidic values for all formulations. No trends were observed between formulations with tremendous variability between replicates. The acidification of these coupons may have been a result of the continuous inoculation of acidophilic cultures onto the mortar's surface, as well as the acidification due to acid gases (i.e. CO_2 and H_2S). However, few Universal and *Acidithiobacillus* qPCR amplicons were detected in the corrosion suspensions, indicating that all results relating to genetic observations were rendered indeterminate. Further, optical interferences made it impossible to detect; thus all bench scale reactor tests were abandoned.

5.5 Acidophile inhibition by mortar formulations under field conditions

Combinations of sewer gas concentrations serve as indicators of site corrosiveness [4]. Periodic monitoring of H_2S and CO_2 at the formulation challenge site indicated a moderate-to-severe corrosive environment, with H_2S concentrations ranging between 25 ppm_v and 225 ppm_v and CO_2 concentrations ranging between 3,000 ppm_v and 7,500 ppm_v. These ranges have been associated with increased corrosion rates in sewer appurtenances [4, 239-242].

5.5.1 Extent of corrosion

After 11 months of exposure, specimens with the highest metal-laden sorbent dosages (CUP10, CHP10, SP, and SCP) experienced the least corrosion as judged by wet mass loss, uncorroded surface area, and suspension pH (pore water pH). These formulations exhibited lower variability between samples and ranged within similar values, regardless of the sorbent. Significant corrosion was observed at lower fine aggregate substitution ratios despite presence of metals, in some cases resulting in more corrosion than their respective control materials. Analogous to the metal inhibition thresholds observed

in aqueous enrichments, these results suggest the existence of a solid phase inhibitory threshold below which significant corrosion can occur. In certain ranges, GAC can increase porosity, which may allow for increased acid diffusion into the cement matrix. Interestingly, the formulation incorporating slag grains with no metal associated (S0) resulted in mild corrosion. This may be attributed to an effect of the increased alkalinity provided by the BOF-S grains, which have a significantly higher acid neutralization capacity than GAC.

While numerous studies on concrete corrosion report degradation rates as linear penetration (mm/year) [21, 22, 56], this study used mass loss as the physical parameter describing corrosion extent. This physical assessment was selected for the following reasons: 1) corrosion products lead to expansive reactions that may influence corrosion depths on the scale of millimeters; 2) the corrosion products were uneven in every dimension with significant variability within the same formulation. Some studies have successfully employed mass loss for corrosion evaluation, reporting similar values for mild and highly corroded specimens [56, 243-245]. The corrosion profile was similar between mortar formulations. In most cases, corrosion was observed to penetrate into the coupon (depth) but also progressed to the center of the sample, radially. The radial degree of corrosion intrusion was significantly lower for the highest metal-containing formulations. The radial corrosion profiles are associated with the cylindrical geometry of mortar coupons, and their suspension and exposure to the sewer gas. The mortar samples were poured in conical plastic tubes and installed with-mold into the manhole, with the mortars only exposing a circular face to the headspace gases. This was done to minimize contact with untreated surfaces and unassociated acid dripping from these onto the mortar coupons, as observed in previous studies [4]. However, based on the obtained corrosion profiles, it is likely that acidophiles developing on the interior plastic wall of the molds produced acid that inadvertently contacted the exposed mortar surfaces. Nonetheless, this artifact was exploited in favor of quantifying corrosion progression, as different degrees of acid intrusion were clearly observed. Parallel

to the mass loss results, the formulations with highest metal-laden aggregate content consistently exhibited lower corroded areas than their counterparts.

The last parameter used to evaluate corrosion extent was the corrosion product pore water pH. The moist corrosion product fractions were used for moisture content determination, and the pore water pH was determined. The wet corrosion products were suspended in 10 mL of saline solution and pH was measured. However, corrosion product fractions were not available for fractionation and moisture content determination on formulations which significantly resist corrosion.

Most studies on biogenic concrete corrosion use pH as a major indicator of the deterioration degree of concrete samples. The three most common approaches to measure concrete pH are as follows: 1) use of flat-probe pH meters, or pH-strips, on affected surfaces, 2) determination of the pore water pH of the corrosion products, and 3) measurement of corrosion suspension pH [21, 243, 245, 246]. Flat-probe pH meters and pH strips are useful for non-destructive and on-site determination of surface pH. However, this surficial descriptive power is less useful when compared to that of the pore water pH. This comparison is especially problematic with extremely corroded surfaces that exhibit pH<1 [247]. In this study, suspension and water pore pH were useful for comparing the corrosion degree of the different formulations, and in agreement with other independent deterioration observations (i.e. mass loss). In general, samples exhibiting obvious corrosion resulted in suspension pH levels <7 with even lower water pore pH values. Exceptions where the mass lost did not correspond to corroded surface area and product pH included: CUN2, CHN2, CHN10, and S0. For the GAC-containing formulations, this might have been a result of the corrosion product extraction procedure. It is possible that the brushing used to remove corroded cement also removed unadulterated cement that, upon suspension, neutralized part of the acid from the corroded product. Sample S0 indicated a corrosion suspension pH near neutrality. This sample also exhibited reduced mass loss but increased corroded surface area. These results suggest that S0 was (slightly) affected by corrosion but offered some

protection due to the alkalinity provided by BOF-S grains. Samples with the highest metal dosages resulted in pH levels above neutrality. Overall, these samples consistently exhibit the lowest mass losses, highest uncorroded areas, and highest suspension pH levels, suggesting these fine aggregate substitutions provided metal-induced enhanced resistance against biogenic corrosion.

5.5.2 Microbial analysis

From a durability perspective, the mortar formulations were designed to find the sorbent substitution threshold which limits the development of acidophilic bacteria. After 11 months of field exposure, mortar specimens with the highest metal-laden sorbent dosages (CUP10, CHP10, SP, and SCP) experienced the lowest absolute cell abundance, microbial activity, and *Acidithiobacillus* relative abundance. The association of microbial cells were evaluated on a corrosion mass- and surface area basis. Cell abundance, activity and *Acidithiobacillus* associations exhibited a significant response to the different mortar formulations. For samples exhibiting lower mass losses (<1.5 wt%) it may be more appropriate the use of surface-normalized cell abundance, as cells would be mostly found attached to the undamaged mortar's surface. Alternatively, the microbial association with specimens experiencing significant corrosion (>1.5 wt%) may be better represented on a mass normalized basis, as cells would be found at the surface and in the soft corrosion material [90]. In either case, the normalized-abundance for corroded samples were within ranges reported by other investigators [48, 90, 153, 248].

Acidophile activity has traditionally been measured through changes in different metabolites (e.g. pH, sulfate, iron (III), enzymes) [90, 249, 250]. While less common, the specific use of rapid microbial activity detection systems has also been explored, suggesting good applicability for describing biogenic corrosion environments [251, 252]. These systems are preferred when easy and fast detection of microbial activity is desired. The relationship between *Acidithiobacillus* growth phases and cell density with specific activity, measured as Relative Light Units (RLU), was investigated in laboratory cultures. The

changes observed in activity correlated with cell densities and culture pH, and was useful for identifying lag, exponential, stationary, and (possibly) senescing phases. Logarithmic increases in activity were observed after a short lag phase, peaking in the stationary phase (18 days after inoculation), and significantly decreasing thereafter. The decrease in activity might be attributed to nutrient depletion and metabolite-induced inhibition (product toxicity) [253]. Additionally, a linear trend between RLU and cell dilutions was observed for a stationary-phase aliquot, validating the RLU observations as a surrogate for cell quantification when A*cidithiobacillus* dominates the microbial communities. These patterns have been observed in different bacterial strains, *Acidithiobacillus spp.* included [253-255]. A study by Pakostova et. al. [254], described the ATP changes in *A. ferrooxidans* using ferrous iron and elemental sulfur as nutrients. The authors observed similar patterns in RLU changes occurring at early periods of time and reaching lower RLU values. RLU values may differ as a result of the species investigated, the nutrients and media used, the growth conditions, and the luminometric assay used, among others. The investigators also observed a linear relationship between produced RLUs and cell concentration (R^2=0.996), suggesting its possible use for biomass quantification under defined conditions, as was the case with the field investigations performed here.

This luminometric detection system was used to evaluate the microbial activity associated with corrosion products after 11 months of sewer. Results indicate no clear trends in microbial activity where metal-laden sorbents replaced up to 5% of the fine sand aggregates, despite presence of metals. However, mass substitutions at 10% with metal-laden sorbents (CUP10, CHP10, CUCP10, SP, and SCP) impacted microbial activity as judged by absolute RLU values. These formulations also exhibited the highest cell-normalized RLU values among all mortar formulations. Absolute RLU values correlated well with the formulations exhibiting the least corrosion response, where microbial assemblages were not dominated by *Acidithiobacillus*. Finally, as observed for *Acidithiobacillus* liquid cultures, a linear relationship could be established between the observed cells in the corrosion products and associated

microbial activity (RLU), confirming the possibility to use microbial activity as a surrogate for cell abundance from corrosion extracts.

A critical aspect in the determination of corrosion resistant formulations is confirming inhibitory effects against *Acidithiobacillus spp*. For this purpose, universal and *Acidithiobacillus*-specific quantification of 16SrRNA genes was used. These observations were normalized based on the total mass of corrosion product and the surface area of the coupons. Results suggest a clear relationship between 16SrRNA genes and overall cell abundance. Samples with higher metal content (CUP10, CHP10, CUCP10, SP, and SCP) also had the lowest recovery of universal and *Acidithiobacillus*-specific 16S rRNA gene copies, with few exceptions. Samples CUN2(1), CHN10(2), and CHP5(1) recovered amplicon pools within the range of the higher metal doses. However, these samples presented relative abundances of *Acidithiobacillus spp*. within the observed range of lower metal doses. In this scenario, formulations with enhanced inhibition also carried the lowest absolute *Acidithiobacillus* 16S copies and the lowest relative abundance where normalized to universal 16SrRNA gene copies. The literature is tenuous with respect to the relative abundance of *Acidithiobacillus spp.* recovered from corroded concrete at similar exposure times. Okabe and coworkers [90] reported that approximately 50% of total DAPI-stained cells from corroded surfaces after 1 year (pH≈2) were other than SOB, notably including acid-tolerant heterotrophs. Alternatively, a study by Ling and coworkers [24] reported relative abundance of *Acidithiobacillus* on corroded surfaces >95% after 1 year of installation. Two reasons may account for such variability between studies: 1) it is possible that the headspace gases (and consequent acidophile development) were significantly different and, 2) the concrete exposure scenarios in this study (as well as in Okabe's study) exposed only one face of the field specimens to the headspace gases, offering enhanced protection against external sources of acid. The experimental design of this study differs from others where the concrete samples were entirely exposed to the surrounding sewer (gas) environment.

These observations may carry a potential bias on sample setup and installation, and the associated corrosion rates reported in these environments.

5.5.3 Chemical analysis

Once biogenic acids begin to degrade cement, soluble calcium is liberated into the corrosion product; the free calcium yield increases as corrosion progresses. Thus, the mass ratios of sulfur and calcium (S:Ca) in the corrosion products can be an indicator how much sulfur has been oxidized per unit mass of cement corroded. After 11 months of sewer exposure, formulations up to 5 % GAC replacement (including relevant controls) carried mass normalized free sulfur content between 0.76 mgS/g (CHN10) and 12.76 mgS/g (CUCP2), with notable variability. Where ≥10% of the fine aggregate was replaced with metal-bearing sorbents (CUP10, CHP10, CUCP10, SP, and SCP) free sulfur was significantly lower, ranging from 0.14 mgS/g (SP) to 2.50 mgS/g (SCP). With respect to fine aggregate substitutions ≤5% and 10% without metal-bearing sorbents, free sulfur was markedly less variable. When free sulfur was normalized by free calcium, ratios followed a similar trend. Formulations up to 5% fine aggregate (GAC) replacement ranged between 0.33 (S0) and 1.67 (CHN5) S:Ca. The mortars with 10% substitution (with metals) exhibited S:Ca ratios between 0.10 (SP) and 0.42 (CHP10). An exception included the mortar controls with slag (S0), which resulted in a relatively low Ca:S ratio, resembling the latter (higher-metal loading) formulations. Free S and Ca levels correlated well with corrosion extent observations and microbial analysis, which is consistent with a cementitious material that has enhanced resistance to biogenic corrosion after nearly a year of field exposure. A study by Ling [4] assessed the temporal changes in total sulfur content and S:Ca ratios of newly installed concrete in highly corrosive sewer environments. After one year of exposure, the samples exhibited between 2.5 mgS/g and 4 mgS/g, and S:Ca ratios between 1.78 and 3.16. The total sulfur values observed here were similar to the range observed by Ling. As a reference, the control mortar with no aggregate substitution (C0) contained nearly 4 mgS/g. However, the S:Ca ratios reported by Ling were significantly higher than the presented in this study. This may

indicate that the sites studied by Ling were more aggressively corrosive than the one used in this study. This is supported by the differences in relative abundance of *Acidithiobacillus spp*. mentioned previously, as well as the CO_2 and H_2S levels measured.

The mobility of calcium, copper and cobalt in the mortar mixes, before and after exposure to corrosive environments, was assessed through classic sequential cation extraction. A modified Tessier approach was used for this purpose. This is the first time this assay has been reportedly applied on mortar exposed to MICC. As judged by Tessier only, small variations in cation inventories were observed before and after exposure. It is possible that corrosion of the samples occurred superficially and did not penetrate further into the cement matrix, therefore leaving a significant portion of the sample unaffected by headspace gases and biogenic acid. Even though the differences were small, consistent results were observed between the different formulations. After curing, more than 80% of the total calcium was extracted within the first three Tessier fractions. This may be due to dissolution of calcium hydroxide, amorphous calcium silicate hydrate, and metal complexed calcium [196]. However, the distribution of other cations differed markedly between formulations containing GAC (control mortar included) and BOF-S. Calcium in GAC formulations was equally observed in the “exchangeable” and the “carbonate/sorption” fractions, with a residual fraction associated to “iron and manganese oxides”. This correlates well with the results observed by Li and coworkers [196]. On the other hand, slag cation eluates were mostly associated with “carbonate/sorption” fraction followed by the “exchangeable” fraction and where residual Calcium was associated to “iron and manganese oxides”. This is likely effect of the calcium present in the BOF-S grains, that are strongly associated to minerals and may not be easily solubilized by the Tessier reagents [134]. Copper in all formulations was observed mostly associated “carbonate/sorption” fraction. Considering the highly alkaline nature of cement, most of the Cu likely exist in hydrated metal phases, metal hydroxides and calcium complexes compounds near (nm-scale) or at the sorbent grains [256]. Roy and Cartledge [257] studied the speciation of Cu in

electroplating sludge stabilized with Portland cement. They found that the principal copper-bearing phase was a hydrated copper phase ($CuO{\cdot}3H_2O$) when Cu was added as copper nitrate in the cement. Cu may also exist as hydroxides or react with calcium to form simple divalent complexes. As judged by Tessier fractions, small differences between GAC and BOF-S formulations were observed. In GAC formulations, copper association was higher with "iron and manganese oxides" than with "sulfide" fractions. On the contrary, Cu was found equally in these fractions for BOF-S formulations, indicating stronger metal association between the metal and the mortar phases. Cobalt distribution presented similarities between sorbent types: Most Co was associated with "carbonate/soprtion" fraction, with minor association with "iron and manganese oxides". This suggests cobalt incorporation into the mortar is less dependent on the sorbent. After exposure, the control mortar and all GAC formulations experienced a decrease in Calcium in the "exchangeable" Tessier fraction and, experienced similar increases in the "carbonate/sorption", with a minor decrease in the association with "iron and manganese oxide" fraction. These changes are likely explained by the increased exposure to CO_2, and consequent accelerated carbonation of the calcium found at the sample surfaces [245]. A decrease in calcium mobilization was observed from highest to lowest in the following series of formulations: CHP5>CHP10>CUCP5=CUP5>CUCP10>C0. However, no trends were observed between the amount of calcium mobilized and the degree of corrosion (C0 and 5% GAC vs 10% GAC) or sorbent type used (GAC-ACID vs GAC-UNM)**.** The BOF-S formulations also experience a decrease in calcium in the "exchangeable" and the "iron and manganese" fractions, and an equivalent increase in the "carbonate/sorption" fraction. Carbonation also accounted for the major increase in the "carbonate" fraction. A decrease in calcium mobilization was observed following the series: SP>SCP>S0. Interestingly, Calcium in the slag control without metals (S0) was mostly mobilized from the "iron and manganese" fraction. This may be a result of the carbonation of calcium phases bound to iron and manganese present in the BOF-S grains near the mortar interface.

SP and SCP mortars may not experience the same degradation behavior as their GAC-containing counterparts because of the way the Cu and Co are held by slag grains, creating a passivation barrier and preventing calcium from react with local dissolved carbonates. Copper mobilized different between formulations that were significantly (5% GAC) and mildly (10% GAC) affected by corrosion. CUP5, CHP5, and CUCP5 experienced similar increases in the "carbonate/specifically adsorbed" fraction and equivalent decrease in the "iron and manganese oxides" fraction. The mobilization of aggregate bound Cu to more easily extractable fractions, may be a result of the increased corrosion rates observed in these samples and enhanced acid production, leading to increased Cu solubilization. In contrast, CUP10, CHP10, and CUCP10 experienced a decrease in copper from the "carbonate/specifically adsorbed" and "iron and manganese oxide" fractions, with an equivalent increase in the "sulfide" fraction. These observations, along with the improved performance of these formulations under corrosive environments, suggests that the mobilized Cu was associated to hydrogen sulfide dissolved near the solid phase boundary, and further immobilized as insoluble CuS. Decreased Cu mobilization followed the series: CHP10>CUCP10>CUP10. This behavior resembles that of the 10% GAC formulations exposed to the Acid Neutralization Capacity assay, indicating increased Cu mobilities when sorbed to acid-modified GAC (GAC-ACID), and to a lesser extent, when Cu and Co are concomitantly loaded on unmodified GAC (GAC-UNM). Both SP and SCP mortars experienced a decrease in copper in "iron and manganese oxide" fraction, while SP exhibited an equivalent increase in "sulfide" fraction, and SCP exhibited an equivalent increase in the "carbonate/sorption" fraction. These results agreed with the ANC assay, which resulted in higher mobility for Cu in SCP than SP formulations. Interestingly, SCP (slag with Cu and Co) exhibited similar Cu-mobility trends than significantly more corroded samples (5% GAC), yet this formulation experienced insignificant corrosion. As judged by elemental mappings, relatively little sulfur was deposited at the surface of SCP mortar specimens and therefore what little metal mobilization occurred was associated to carbonated species from the sewer gas (CO_2). Mobility of Cu (and Co) within SCP

formulations indicates most metal sorption is associated to iron oxide grains where any subsequent dissolution and metal mobilization likely occurs after carbonation (extended CO_2 exposure). For both types of sorbents used (GAC and BOF-S), there are indications of increased Cu mobility when concomitantly loaded with Co. Finally, Cobalt in both CUCP5 and CUCP10 presented minimal variations before and after extended exposure to a corrosive atmosphere. This suggests little effect of corrosion on the fate of Cobalt. However, SCP exhibited an increase in Cobalt in the "carbonate/sorption" fraction and an equivalent decrease in the "iron and manganese oxide" fraction. As mentioned previously, this may suggest specific metal sorption into iron oxide-rich phases present in the BOF-S.

Elemental mobility within formulations after extended exposure to a corrosive atmosphere was assessed through Electron Microprobe Analysis (EMPA). Areas selected for imaging included corrosion-affected and unaffected regions on a cross-sectional plane from the corrosion exposed surfaces. Sulfur intrusion was used as surrogate to estimate corrosion extent, with formulations succumbing to sulfur penetration in the following order: CUCP5>C0>CUCP10>S0>SCP. In most cases, corrosion fronts were well defined, distinguishing corroded and uncorroded areas. Using EMPA, corroded areas were characterized by lower calcium and silica x-ray intensities, as well as increased interstitial space between aggregates and the cement matrix. This is a consequence of C-S-H gel dissolution and calcium hydroxide phases by sulfuric acid, and the formation of expansive gypsum, as reported by several different investigators [258-260]. Silica-rich areas were associated with sand grains. Different studies independently reported that silica grains have no reactive potential with sewer gases or biogenic acids [258, 260]. In this study, the x-ray intensities of silica grains were a result of poorly polished samples, indicating preferential orientations that resulted in biased intensity variations within- and between grains. This effect was not observed in the cement, indicating a more homogeneous polishing preparation. GAC grains appeared as black areas in the EMPA maps that differed from air voids by the low presence of other elements (e.g. calcium), and clear indication of Cu and Co sorbed to grain edges.

BOF-S grains appeared more heterogeneous in nature, presenting different combinations of Ca-, Si-, Al-, Fe-, and Mg-rich phases, corresponding to what is typically found in steel slags [134], and distinctly different from the sand grains and the cement matrix. In general, uncorroded cement presented a homogeneous distribution of Ca, Si, Al, Fe, Mg, and S. Low intensities of sulfur in these areas corresponded to the original Portland cement mix, which included small amounts of gypsum necessary for the controlled hardening rates of hydrated cement [39]. As judged by EMPA, the corroded areas presented similar spatial spectra among corroded, with the major defining feature being the extent of sulfur intrusion (C0, CUCP5, CUCP10).

Corroded areas exhibited obvious decalcification, and desilication due to acid exposure. Additionally, depletion of aluminum, iron, and magnesium was noted in the corroded areas. Different electron microprobe studies of corroded concrete report this profile of mobile, where Fe-, Al-, and Mg-rich bands migrate to corrosion fronts [259, 260]. Mg-rich bands have been observed closer to uncorroded matrices; their formation attributed to Mg mobilization from the deeper uncorroded areas and subsequent precipitation with hydroxides $Mg(OH)_2$ at pH>9. Al-rich phases have also been identified, and attributed to the relatively low solubility of $Al(OH)_3$ between pH 9 and pH 4.

The most metal-rich outer bands have been associated with Fe, which are linked to precipitation of iron oxyhydroxides between pH 4 and pH 3. These outermost bands are suggested to play a key role in the microbial activity of *Acidithiobacillus ferrooxidans* and the mobilization of iron. Under anaerobic conditions, present at corrosion depths where oxygen cannot penetrate, *A. ferrooxidans* can reduce Fe^{3+} to a mobile Fe^{2+} species [258, 260-262].

In this study, formulations with significant sulfur intrusion experienced faint and thin Fe-, Al-, and Mg-rich bands located at the corrosion fronts. The presence and size of these bands indicated accelerated corrosion rates, limiting accumulation of Mg, Al, and Fe. Significantly corroded samples (C0

and CUCP5) exhibited increased sulfur gradients with depth, reaching maximum x-ray intensities at the respective corrosion fronts. This suggests accumulation of sulfate with deposited elements, predominantly with calcium as $CaSO_4$, as supported by the presence of an enriched calcium band at the corrosion front. CUCP10 exhibited moderate sulfur intrusion with shallower depth gradients than its corroded counterparts. This formulation experienced minimal corrosion, as indicated by mass loss and microbiological assays; the degree of sulfur intrusion indicates only superficial corrosion which progressed at markedly slower rates than the control formulation (C0) or lesser dosed counterparts (CUCP5). Sulfur intrusion may have been a result of the increased porosity of formulations containing 10% GAC, as observed by different studies on ion diffusion in mortars with high water-to-cement ratios and increased pore sizes exposed [263, 264].

The formulation containing only raw BOF-S (S0) experienced a thin sulfur-rich band at its surface, with minimal evidence of sulfur penetration into the mortar matrix. This sample also exhibited an enriched calcium band overlapping the sulfur band, also suggesting only superficial formation of $CaSO_4$. As observed by physical analysis, the slag control formulation without metals (S0) exhibited limited corrosion damage, which correlates with the surface accumulation of sulfur and its limited intrusion. Two hypothesis may account for the improved performance of formulations including slag in these corrosive environments: 1) fine aggregate substitution with BOF-S provided additional alkalinity to the cement matrix which in turn may have neutralized biogenic acids and, 2) BOF-S grains may have reacted with the cement matrix, resulting in the formation of a denser (and less porous) mortar paste. The latter hypothesis is less likely as the elemental mapping of the BOF-S-containing formulations did not indicate significant alkali-aggregate reactions. Sulfur was observed at very low intensities in SCP and no corrosion front was observed. Calcium was homogeneous across the cement matrix with higher intensities at the surface exposed to sewer gases. Silica, aluminum, iron, and magnesium were homogeneous across the cement matrix and no evidence for dissolution was observed. Exceptions to

the element homogeneities accounted for sand, and BOF-S grains. Together with physical and microbial assays of SCP, the observations suggest that this mortar formulation was not significantly affected by the corrosive atmosphere. Slight accumulation of calcium at the surface exposed to sewer gases was likely a combination of carbonation and sulfide precipitation. BOF-S particles were inert when mixed and cured with OPC; no changes in slag particles were observed when exposed to sewer gas (see S0).

As judged by EMPA, copper and cobalt x-ray intensities differed in the mortar formulations tested. CUCP5, a significantly corroded sample, exhibited low intensities of Cu in both the uncorroded and the corroded areas. A faint Cu band was observed at the corrosion front, indicating possible accumulation of Cu as $CuSO_4$. The highest Cu intensities were observed in the uncorroded area (bottom of the CUCP5 Cu map) surrounding unmodified GAC grains. Cobalt x-ray intensities were below detection limit and could not be identified surrounding co-loaded GAC grains. Formulation CUCP10 resulted in Cu and Co undetected in the corroded area and could only be detected on GAC grains. This suggests some increase in metal mobility near corroded areas, with a majority of metal associated with GAC grains in the uncorroded mortar. Finally, SCP exhibited the highest Cu and Co x-ray intensities of any mortar formulations. These metals were associated with the BOF-S grain surfaces, with little evidence for diffusion into the cement matrix. When impregnated with metals near their saturation thresholds, BOF-S grains exhibited higher Cu intensities than their GAC counterparts; a sentinel BOF-S grain accounted for the highest Cu and Co observed x-ray intensities. EMPA analysis identified Fe and Mg with BOF grains, providing optical evidence for a metal-oxide sorption mechanism that retain copper and cobalt on some of the heterogeneous slag aggregates. EMPA evidence for slag-transition metal sorption has also been reported by other researchers investigating the metal retention mechanisms of different steel making residuals[265, 266]. Copper and cobalt were also observed in/on grains exhibiting high calcium x-ray intensities. In these cases, metal precipitation around grains was likely responsible for this process. Metal-silicate interactions were also suggested by EMPA mapping of metal (Cu) association

with homogeneous silica phases [232]. EMPA mapping suggest metal immobilization in slag and GAC doped cements is a combination of adsorption on metal oxide surfaces and superficial precipitation. The improved antimicrobial performance of metal-BOF-S formulations may be a result of the increased specific metal loading offered by slag, creating a localized high metal concentration driving a stronger net inhibitory effect.

Chapter 6 Thesis Conclusions

6.1 Conclusions

The results presented, along with the reviewed literature, present independent lines of evidence that converge on the following conclusions. These are presented in the order of hypotheses presented.

Hypothesis I. Different metal ions have different inhibitory potential against acidophilic Sulfur Oxidizing Bacteria (SOB) present in sewer systems.

Hypothesis I a. A dose-response relationship can be established for selectively inhibiting acidophilic SOB. This manifests as dominance of neutrophilic communities sustaining a neutral pH range, when challenged under conditions that favor biogenic acid production.

Hypothesis I b. Metal association and release is a function of sorbent type and can be engineered to harbor a range of inhibitory metal species and host concentrations effective against the activities of planktonic and sessile SOB.

Conclusions: Acidophilic SOBs growing on agar surfaces were inhibited by the following transition metals, with relatively potency ordered as: Cu>Co>Cd>Ni=Zn. Metal impregnated GAC, embedded in agar demonstrate the potential use of metal-sorbent configurations against acidophile growth. Copper and cobalt can inhibit sulfur oxidizing acidophilic growth and thus maintaining neutrophilic communities. Binary mixtures of selected transition metals can be markedly more potent than the individual metals, as observed by the minimum inhibitory concentrations: 50 mg Cu/L, >50 mg Co/L, and 15 mg Cu/L and 15 mg Co/L when concomitantly added to liquid enrichments of SOB biofilms recovered from sewers. SOB inhibition was confirmed by pH monitoring and 16S rRNA gene analysis, which revealed diverse SOB community compositions sustaining neutral pH above the inhibitory thresholds. Copper was effectively immobilized on commercial GAC, acidified modified GAC, and BOF-S.

Cobalt could be co-loaded with copper in appreciable concentrations on commercial GAC and basic oxygen furnace slag (BOF-S). As opposed to GAC-U and BOF-S, acidic GAC cannot host cobalt when co-loaded with copper. This is an important consideration when assessing multi-metal induced inhibition of SOB.

Hypothesis II. Metals laden sorbents will remain immobilized when mixed and cured with Portland cements such that no metal will leach in into virgin cement mixtures at the pH of cement. However, inhibitory metal doses will be locally available - on a microscale - in response to biogenic acid production on cement surfaces, and metal exposures can be engineered to be pH responsive, locally bioavailable as pH drops below predetermined levels.

Hypothesis II a. Acid functionalized activated carbon will be more efficient at mediating inhibitory metal doses in pH ranges relevant to acidophilic microbial activities (pH<5) but have a similar sorption capacity than virgin activated carbon. Acid-modified activated carbon, impregnated with select metal ions, will bind/release metals in a pH dependent manner, preferably when SOBs become active, acting as long-term metal reservoir for antimicrobial, and thus anti-corrosive effect.

Hypothesis II b. Steel slag of similar grain size distribution as fine aggregates, can also host metals when entrained in cement and exposed to biogenic acid, although its specific metal loading profile will be different than activated carbons, regardless of modifications.

Conclusions: The response of the sorbents (GAC and BOF-S), regardless of aqueous suspension and incorporation into solid-phase of cement mortars, showed that BOF-S was able to retain higher metal loads than GAC-UNM and GAC-ACID, while simultaneously providing increased buffering capacity in response to (biogenic) acid attack. When challenged, metal bioavailability followed the series: GAC-ACID > GAC-UNM > BOF-S. After exposure to corrosive environments, only mortars with the highest metal-sorbent dosages exhibited significant biogenic corrosion resistance. Such resistance was described

by a clear dose-response to metal-impregnated sorbents, substituted for fine aggregate sand, exerting an inhibitory effect against *A.thiooxidans* growth, independently of the nature of the sorbent used (GAC-UNM, GAC-ACID or BOF-S) or the metals loaded (Cu or Cu/Co). Metal fate was influenced by the corrosion degree of the formulations. Most of the Cu and Co loaded was retained on/near the sorbent's surface, unless exposed to biogenic acid, in which case they associated with carbonates and sulfates *in-situ*.

6.2 Synthesis

The purpose of this research was to address the potential for new cement formulations, which mitigated microbially induced concrete corrosion, against *A.thiooxidans* found in sewer crowns. Through the combination of low-cost sorbents and metal solutions, it is possible to produce fine aggregates that can be incorporated into cement mixtures and host classic microbial biocides, which activate in response to acidophilic growth. Two key factors were considered when formulating such mixtures: the intrinsic inhibitory potential and the availability and abundance of the antimicrobial agents within cement. In this study, Cu and a mixture of Cu/Co resulted in enhanced inhibition potential against acidophilic SOB dominance, while a 10% GAC-Me replacement (and BOF-S-Me equivalent formulations) resulted in an optimal grain distribution to deliver a sustained biocidal effect (c.a. 1 year).

These factors were correlated to inhibition effectiveness in this thesis, as defined by pH, cement loss, corroded area, microbial abundance, microbial activity, and community composition. Concrete dissolution presents failure risk, as the corrosion byproducts that replace cement binder are structurally compromised in a way that they can easily be removed from concrete surfaces through sloughing and erosion. This thesis provided insights on the (re)use of low-cost materials for the purpose of limiting biogenic corrosion and extending the service life of affected infrastructure. Figure 6-1 provides an

overall synthesis of results as they pertain to the development of an effective, sustainable, and low-cost solution against MICC.

In a modified solid phase format, Cu and Co dose-response inhibition against sessile acidophilic SOB cultures enriched from a corroded site

In planktonic enrichments, minimum inhibitory concentration indicates specific synergy between Cu and Co, against acidophilic SOBs; Ag is ineffective

In field studies, corrosion-induced mass lost correlates with cement formulations including antimicrobial metals after *in situ* testing

Improved MICC resistance performance can be attributed to the specific inhibition of *A.thiooxidans* in corrosive atmospheres

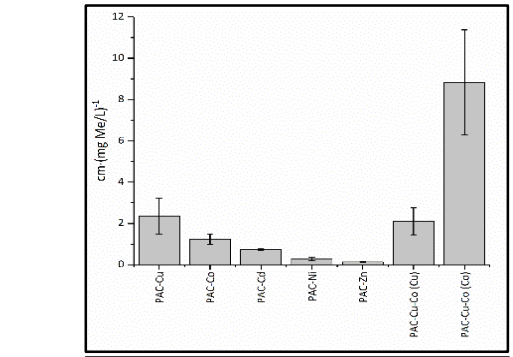

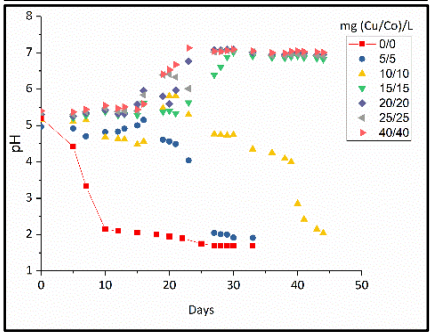

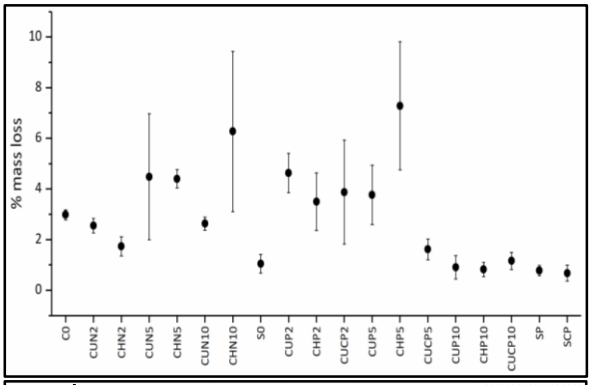

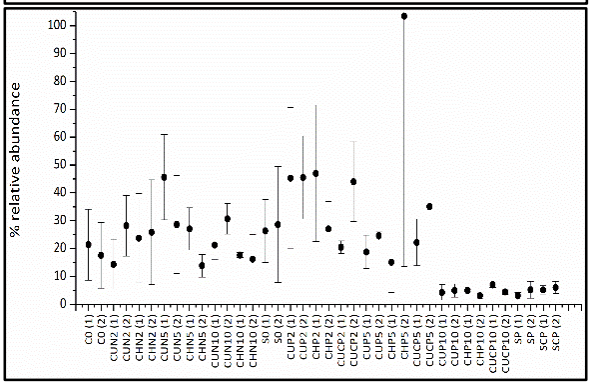

Figure 6-1. Synthesis of the effects of Cu and Co on the inhibition of A.thiooxidans. **Transition from lab scale tests to field tests indicate effectiveness of the metals against *A.thiooxidans* development, limiting consequent biogenic concrete corrosion in sewer systems.**

6.3 Applications to Practice

This research specifically addressed the root cause of concrete corrosion in sewer systems, *A.thiooxidans* activity. The focus of the work, evaluated the use of biocidal metal-sorbent complexes as substitutes for fine aggregate in standard cement mortar, with the purpose of inhibiting *A.thiooxidans* dominance in sewer crowns. Based on the results of this work, the following applications are suggested:

1) The Kirby-Bauer diffusion susceptibility assay can be modified for rapid screening of combinations of metals for their potential inhibitory impacts against environmental microbial enrichments, in a simple longitudinal format. For acidophilic culture applications, metal diffusion, and consequent inhibitory effect, was auto-induced by metabolic acidification which is easily monitored in the agar media.

2) Metal-sorbent particle distribution in a cement mortar mix is a critical variable in the production of effective antimicrobial mortar formulations. Only 10% GAC and BOF-S formulations indicated significant *A.thiooxidans* inhibition, probably due to the increased distribution of antimicrobial particles and the limited diffusivity of the active agent in solid cement.

3) Field trials must be performed in addition to laboratory simulations of corrosion; they offer a realistic environment that includes all necessary parameters (known and unknown) for durability studies. Survey on corrosion atmospheres (CO_2 and H_2S) at different appurtenances can result on the best location to perform accelerated MICC studies.

4) Sample testing in corrosive environments has to consider all possible sources of acidophilic growth other than the sample itself. Acid produced on external surfaces and dripping or contacting the sample of interest may lead to artifacts during field trials. This also suggests that for complete corrosion protection, all surfaces in the affected pipe or manhole must be coated with an antimicrobial cement formulation.

5) While some formulations exhibited improved durability after 11 months of exposure, their behavior under aggressive corrosion conditions for longer time periods remains unknown.

6.4 Future Recommendations

Microbially induced concrete corrosion is an expensive and widespread problem. Development of antimicrobial aggregates can be an effective, low-cost, and long-term solution for affected wastewater collection systems around the world. Based on the work presented herein, future research should focus on the following areas:

1) Detailed microbial community compositions on surfaces where *A.thiooxidans* has been significantly inhibited, and under this scenario, metagenomic studies of genes involved and surveys for heavy metal resistance should be conducted. Additionally, investigations on possible transfer of heavy metal resistance genes between microbial populations would give insights on the long term effectiveness of the proposed formulations.

2) Evaluation on the use of more sustainable precursors (e.g. biochar, metal plating wastes) for the development of sustainable antimicrobial aggregates, broader investigation on inhibitory agents and mixtures, and structural integrity of these.

3) Extended field assays to determine longer-term effectiveness in large-scale applications and across geographical locations.

4) Evaluation of the mechanical and structural properties of the mortar/concrete formulated with the antimicrobial aggregates, and their compatibility with common admixtures used in the field.

References

1. US Environmental Protection Agency, *Clean Watersheds Needs Survey (CWNS). Report to Congress*. EPA-830-R-15005. 2012.

2. Sterling, R., L. Wang, and R. Morrison, *Rehabilitation of wastewater collection and water distribution systems: State of technology review report.* US Environmental Protection Agency, 2009.

3. Carpenter, R., Fingers crossed: 15th Annual Municipal Survey. Underground Construction, 2012. Vol. 67 No2.

4. Ling, A.L., *Characterization and Control of Microbially Induced Concrete Corrosion, PhD dissertation.* University of Colorado at Boulder, 2013.

5. Parker, C., *Mechanics of corrosion of concrete sewers by hydrogen sulfide.* Sewage and Industrial Wastes, 1951. p. 1477-1485

6. Hashemi, B., T. Iseley, and J. Raulston, *Water pipeline renewal evaluation using AWWA class IV CIPP, pipe bursting, and open-cut*, in *ICPTT 2011: Sustainable Solutions For Water, Sewer, Gas, And Oil Pipelines*. 2011. p. 1257-1266.

7. De Muynck, W., N. De Belie, and W. Verstraete, *Effectiveness of admixtures, surface treatments and antimicrobial compounds against biogenic sulfuric acid corrosion of concrete.* Cement and Concrete Composites, 2009. **31**(3): p. 163-170.

8. Valix, M., Zamri, D., Mineyama, H., Cheung, W. H., Shi, J., and Bustamante, H., *Microbiologically Induced Corrosion of Concrete and Protective Coatings in Gravity Sewers.* Chinese Journal of Chemical Engineering, 2012. **20**: p. 433-438.

9. Haile, T., Nakhla, G., Allouche, E., & Vaidya, S., *Evaluation of the bactericidal characteristics of nano-copper oxide or functionalized zeolite coating for bio-corrosion control in concrete sewer pipes.* Corrosion Science, 2010. **52**: p. 45-53.

10. Roozbeh Hoseinzadeh Hesas, A.A.-N., Wan Mohd Ashri Wan Daud, J.N. Sahu, *Preparation and Characterization of Activated Carbon from Apple Waste by Microwave Assisted Phosphoric Acid Activation: Application in Methylene Blue Adsorption.* Bioresources, 2013. **8**(2): p. 2950-2966.

11. Maiti, S., Purakayastha, S., & Ghosh, B., *Production of low-cost carbon adsorbents from agricultural wastes and their impact on dye adsorption.* Chemical Engineering Communications, 2007. **195:4**: p. 386-403.

12. Kobya, M., Demirbas, E., Senturk, E., & Ince, M., *Adsorption of heavy metal ions from aqueous solutions by activated carbon prepared from apricot stone.* Bioresource technology, 2005. **96**: p. 1518-21.

13. Wahi, R., Ngaini, Z., & Jok, V. U., *Removal of Mercury, Lead and Copper from Aqueous Solution by Activated Carbon of Palm Oil Empty Fruit Bunch.* World Applied Sciences Journal, 2009. **5**: p. 84-91.

14. Patnukao, P., Kongsuwan, A., & Pavasant, P., *Batch studies of adsorption of copper and lead on activated carbon from Eucalyptus camaldulensis Dehn. bark.* Journal of environmental sciences, 2008. **20**(9): p. 1028-1034.

15. Kim, D. H., Shin, M. C., Choi, H. D., Seo, C. I., & Baek, K., *Removal mechanisms of copper using steel-making slag: adsorption and precipitation.* Desalination, 2008. **223**(1-3): p. 283-289.

16. Grubb, D., Jagupilla, S., and Wazne, M., *Immobilization of Cadmium (Cd) and Zinc (Zn) Using Steel Slag Fines*, in *Geo-Chicago, 2016*. p. 513-521.

17. Grubb, D., Jagupilla, S., Cummings, R., & Wazne, M., *Immobilization of Lead, Tungsten, and Phosphate by Steel Slag Fines: Metals Thresholding and Rate Studies.* Journal of Hazardous, Toxic, and Radioactive Waste, 2014. **18**(3): p. 04014017..

18. Chen, B. Y., Liu, H. L., Chen, Y. W., & Cheng, Y. C., *Dose–response assessment of metal toxicity upon indigenous Thiobacillus thiooxidans BC1.* Process Biochemistry, 2004. **39**: p. 737-748.

19. Cho, K.-S., H.W. Ryu, and H.-M. Choi, *Toxicity evaluation of complex metal mixtures using reduced metal concentrations: application to iron oxidation by Acidithiobacillus ferrooxidans.* Journal of microbiology and biotechnology, 2008. **18**(7): p. 1298-1307.

20. US Environmental Protection Agency, *Hydrogen sulfide corrosion in wastewater collection and treatment systems.* Report to Congress, 1991.

21. Mori, T., Nonaka, T., Tazaki, K., Koga, M., Hikosaka, Y., & Noda, S., *Interactions of nutrients, moisture, and pH on microbial corrosion of concrete sewer pipes.* Water Research, 1992. **26**(1): p. 29-37.

22. Zhang, L., De Schryver, P., De Gusseme, B., De Muynck, W., Boon, N., & Verstraete, W., *Chemical and biological technologies for hydrogen sulfide emission control in sewer systems: a review.* Water research, 2008. **42**: p. 1-12.

23. Robert L. Islander, R.L., Devinny, J.S., Mansfeld, F., Postyn, A.,& Shih, H., *Microbial ecology of crown corrosion in sewers.* Journal of Environmental Engineering, 1992. **117**: p. 751-770.

24. Ling, A. L., Robertson, C. E., Harris, J. K., Frank, D. N., Kotter, C. V., Stevens, M. J., Pace, N.R., & Hernandez, M. T., *High-Resolution Microbial Community Succession of Microbially Induced Concrete Corrosion in Working Sanitary Manholes.* PLoS ONE, 2015. **10**(3): p. e0116400.

25. Gomez-Alvarez, V.,Revetta R.P., & Domingo, J.W.S., *Metagenome analyses of corroded concrete wastewater pipe biofilms reveal a complex microbial system.* BMC Microbiology, 2012. **12**: p. 122-122.

26. Travisany, D., Cortés, M. P., Latorre, M., Di Genova, A., Budinich, M., Bobadilla-Fazzini, R. A., A., Parada, P.,Gonzalez, M., & Maass, A., *A new genome of Acidithiobacillus thiooxidans provides*

insights into adaptation to a bioleaching environment. Research in Microbiology, 2014. **165**(9): p. 743-752.

27. Valdés, J., Pedroso, I., Quatrini, R., Dodson, R. J., Tettelin, H., Blake, R., Eisen, J.A., & Holmes, D. S., *Acidithiobacillus ferrooxidans metabolism: from genome sequence to industrial applications.* BMC Genomics, 2008. **9**.

28. Madigan, M.T., Martinko, J.M., & Parker, J., *Brock Biology of Microorganisms*. 8th ed, 1997. Upper Saddle River,NJ: Simon and Schuster.

29. Atlas, R.M., *Principles of microbiology/by Ronald M. Atlas*. 1995. (No. 631.46 A8.).

30. Suzuki, I., *Oxidation of inorganic sulfur compounds: chemical and enzymatic reactions.* Canadian Journal of Microbiology, 1999. **45**(2): p. 97-105.

31. Trüper, H., *Microbial processes in the sulfur cycle through time*, in *Mineral Deposits and the Evolution of the Biosphere*, 1982, Springer. p. 5-30.

32. Bertini, I. (Ed.), *Biological inorganic chemistry: structure and reactivity*, 2007. University Science Books.

33. Finster, K., *Microbiological disproportionation of inorganic sulfur compounds.* Journal of Sulfur Chemistry, 2008. **29**(3-4): p. 281-292.

34. Burton, F. L., Stensel, H. D., & Tchobanoglous, G. (Eds.), *Wastewater Engineering: Treatment and Resource Recovery*, 2013. McGraw-Hill Education.

35. Nielsen, A. H., Vollertsen, J., Jensen, H. S., Madsen, H. I., & Hvitved-Jacobsen, T., *Aerobic and anaerobic transformations of sulfide in a sewer system--field study and model simulations.* Water Environment Research, 2008. **80**(1): p. 16-25.

36. Tanaka, N., Hvitved-Jacobsen, T., & Horie, T., *Transformations of carbon and sulfur wastewater components under aerobic–anaerobic transient conditions in sewer systems.* Water environment research, 2000. **72**(6): p. 651-664.

37. Thauer, R.K., Jungermann, K., & Decker, K., *Energy conservation in chemotrophic anaerobic bacteria.* Bacteriological reviews, 1977. **41**(1): p. 100.

38. Hvitved-Jacobsen, T., *Sewer Processes: Microbial and Chemical Process Engineering of Sewer Networks*, 2002. Boca Raton, FL: CRC Press.

39. Hewlett, P., *Lea's chemistry of cement and concrete*, 2003: Butterworth-Heinemann.

40. Kosmatka, S.H., Kerkhoff, B. & Panarese, W.C., *Design and control of concrete mixtures*, 2011: Portland Cement Assoc.

41. Bullard, J. W., Jennings, H. M., Livingston, R. A., Nonat, A., Scherer, G. W., Schweitzer, J. S., Karen, L.S. & Thomas, J. J., *Mechanisms of cement hydration.* Cement and Concrete Research, 2011. **41**(12): p. 1208-1223.

42. Richardson, I. G., Brough, A. R., Groves, G. W., & Dobson, C. M., *The characterization of hardened alkali-activated blast-furnace slag pastes and the nature of the calcium silicate hydrate (CSH) phase.* Cement and Concrete Research, 1994. **24**(5): p. 813-829.

43. Joseph, A. P., Keller, J., Bustamante, H., & Bond, P. L., *Surface neutralization and H(2)S oxidation at early stages of sewer corrosion: influence of temperature, relative humidity and H(2)S concentration.* Water research, 2012. **46**: p. 4235-45.

44. Gollop, R.S. & Taylor, H.F.W., *Microstructural and microanalytical studies of sulfate attack. I. Ordinary portland cement paste.* Cement and Concrete Research, 1992. **22**(6): p. 1027-1038.

45. Neville, A., *The confused world of sulfate attack on concrete.* Cement and Concrete Research, 2004. **34**(8): p. 1275-1296.

46. Marchand, J., Odler, I., & Skalny, J.P., *Sulfate attack on concrete*, 2003. CRC Press.

47. Beddoe, R.E. & Dorner, H.W., *Modelling acid attack on concrete: Part I. The essential mechanisms.* Cement and Concrete Research, 2005. **35**(12): p. 2333-2339.

48. Monteny, J., Vincke, E., Beeldens, A., De Belie, N., Taerwe, L., Van Gemert, D., & Verstraete, W., *Chemical, microbiological, and in situ test methods for biogenic sulfuric acid corrosion of concrete.* Cement and Concrete Research, 2000. **30**(4): p. 623-634.

49. Pikaar, I., Sharma, K. R., Hu, S., Gernjak, W., Keller, J., & Yuan, Z., *Reducing sewer corrosion through integrated urban water management.* Science, 2014. **345**(6198): p. 812-814.

50. Sun, J., Pikaar, I., Sharma, K. R., Keller, J., & Yuan, Z., *Feasibility of sulfide control in sewers by reuse of iron rich drinking water treatment sludge.* Water Research, 2015. **71**: p. 150-159.

51. Lin, H. W., Lu, Y., Ganigué, R., Sharma, K. R., Rabaey, K., Yuan, Z., & Pikaar, I., *Simultaneous use of caustic and oxygen for efficient sulfide control in sewers.* Science of The Total Environment, 2017. **601**: p. 776-783.

52. Dyer, T., *Biodeterioration of Concrete*, 2017. CRC Press.

53. Hewayde, E., Nehdi∗, M., Allouche, E., & Nakhla, G., *Neural network prediction of concrete degradation by sulphuric acid attack.* Structure and Infrastructure Engineering, 2007. **3**(1): p. 17-27.

54. Fattuhi, N. & Hughes, B., *The performance of cement paste and concrete subjected to sulphuric acid attack.* Cement and Concrete Research, 1988. **18**(4): p. 545-553.

55. Kawai, K., Yamaji, S., & Shinmi, T., *Concrete deterioration caused by sulfuric acid attack*, 2005. International Conference on Durability of Building Materials and Components. LYON [France].

56. Gutiérrez-Padilla, M. G. D., Bielefeldt, A., Ovtchinnikov, S., Hernandez, M., & Silverstein, J., *Biogenic sulfuric acid attack on different types of commercially produced concrete sewer pipes.* Cement and Concrete Research, 2010. **40**(2): p. 293-301.

57. Hewayde, E., Nehdi, M., Allouche, E., & Nakhla, G., *Effect of mixture design parameters and wetting-drying cycles on resistance of concrete to sulfuric acid attack.* Journal of materials in Civil Engineering, 2007. **19**(2): p. 155-163.

58. *ASTM C150 / C150M-17, Standard Specification for Portland Cement.* ASTM International, West Conshohocken, PA, 2017, www.astm.org, 2017.

59. Roy, D.M., Arjunan, P., & Silsbee, M.R., *Effect of silica fume, metakaolin, and low-calcium fly ash on chemical resistance of concrete.* Cement and Concrete Research, 2001. **31**(12): p. 1809-1813.

60. Bai, J., Wild, S., Sabir, B. B., & Kinuthia, J. M., *Workability of concrete incorporating pulverized fuel ash and metakaolin.* Magazine of Concrete Research, 1999. **51**(3): p. 207-216.

61. O'Connell, M., McNally, C., & Richardson, M.G., *Performance of concrete incorporating GGBS in aggressive wastewater environments.* Construction and Building Materials, 2012. **27**(1): p. 368-374.

62. Alexander, M.G. & Fourie, C., *Performance of sewer pipe concrete mixtures with portland and calcium aluminate cements subject to mineral and biogenic acid attack.* Materials and Structures, 2011. **44**(1): p. 313-330.

63. Torii, K. & Kawamura, M., *Effects of fly ash and silica fume on the resistance of mortar to sulfuric acid and sulfate attack.* Cement and Concrete Research, 1994. **24**(2): p. 361-370.

64. Lothenbach, B., Scrivener, K. & Hooton, R.D., *Supplementary cementitious materials.* Cement and Concrete Research, 2011. **41**(12): p. 1244-1256.

65. Sabir, B., Wild, S., & Bai, J., *Metakaolin and calcined clays as pozzolans for concrete: a review.* Cement and Concrete Composites, 2001. **23**(6): p. 441-454.

66. Bassuoni, M.T. & Nehdi, M.L., *Resistance of self-consolidating concrete to sulfuric acid attack with consecutive pH reduction.* Cement and Concrete Research, 2007. **37**(7): p. 1070-1084.

67. Scrivener, K.L., Cabiron, J.-L. & Letourneux, R., *High-performance concretes from calcium aluminate cements.* Cement and Concrete Research, 1999. **29**(8): p. 1215-1223.

68. Juenger, M. C. G., Winnefeld, F., Provis, J. L., & Ideker, J. H., *Advances in alternative cementitious binders.* Cement and Concrete Research, 2011. **41**(12): p. 1232-1243.

69. Arbi, K., Nedeljković, M., Zuo, Y., & Ye, G., *A review on the durability of alkali-activated fly ash/slag systems: advances, issues, and perspectives.* Industrial & Engineering Chemistry Research, 2016. **55**(19): p. 5439-5453.

70. Dimas, D., Giannopoulou, I. & Panias, D. *Polymerization in sodium silicate solutions: a fundamental process in geopolymerization technology.* Journal of Materials Science, 2009. **44**(14): p. 3719-3730.

71. Allahverdi, A. & Skvara, F., *Sulfuric acid attack on hardened paste of geopolymer cements-Part 1. Mechanism of corrosion at relatively high concentrations.* Ceramics Silikaty, 2005. **49**(4): p. 225.

72. Bakharev, T., *Resistance of geopolymer materials to acid attack.* Cement and Concrete Research, 2005. **35**(4): p. 658-670.

73. Lee, N. & Lee, H., *Influence of the slag content on the chloride and sulfuric acid resistances of alkali-activated fly ash/slag paste.* Cement and Concrete Composites, 2016. **72**: p. 168-179.

74. Sun, X., Jiang, G., Bond, P. L., Keller, J., & Yuan, Z., *A novel and simple treatment for control of sulfide induced sewer concrete corrosion using free nitrous acid.* Water Research, 2015. **70**: p. 279-287.

75. Negishi, A., Muraoka, T., Maeda, T., Takeuchi, F., Kanao, T., Kamimura, K., & Sugio, T., *Growth inhibition by tungsten in the sulfur-oxidizing bacterium Acidithiobacillus thiooxidans.* Bioscience, biotechnology, and biochemistry, 2005. **69**(11): p. 2073-2080.

76. Kong, L., Zhang, B., & Fang, J., *Study on the applicability of bactericides to prevent concrete microbial corrosion.* Construction and Building Materials, 2017. **149**: p. 1-8.

77. Haile, T. & Nakhla, G., *A Novel Zeolite Coating for Protection of Concrete Sewers from Biological Sulfuric Acid Attack.* Geomicrobiology Journal, 2008. **25**(6): p. 322-331.

78. Haile, T. & Nakhla, G., *The inhibitory effect of antimicrobial zeolite on the biofilm of Acidithiobacillus thiooxidans.* Biodegradation, 2010. **21**(1): p. 123-134.

79. Moore, S.L. & Payne, D.N., *Types of antimicrobial agents.* Principles and Practice of Disinfection, Preservation, and Sterilization, 2004. **4**: p. 8-97.

80. Gottenbos, B., van der Mei, H. C., Klatter, F., Nieuwenhuis, P., & Busscher, H. J., *In vitro and in vivo antimicrobial activity of covalently coupled quaternary ammonium silane coatings on silicone rubber.* Biomaterials, 2002. **23**(6): p. 1417-1423.

81. Isquith, A., Abbott E., & Walters, P., *Surface-bonded antimicrobial activity of an organosilicon quaternary ammonium chloride.* Applied microbiology, 1972. **24**(6): p. 859-863.

82. Abraham, D.M. & Gillani, S.A., *Innovations in materials for sewer system rehabilitation.* Tunnelling and Underground Space Technology, 1999. **14**: p. 43-56.

83. Garcia, C., Abraham, D. M., Gokhale, S., & Iseley, T., *Rehabilitation alternatives for concrete and brick sewers.* Practice Periodical on Structural Design and Construction, 2002. **7**(4): p. 164-173.

84. Ito, T., Nielsen, J. L., Okabe, S., Watanabe, Y., & Nielsen, P. H., *Phylogenetic identification and substrate uptake patterns of sulfate-reducing bacteria inhabiting an oxic-anoxic sewer biofilm*

determined by combining microautoradiography and fluorescent in situ hybridization. Applied and environmental microbiology, 2002. **68**(1): p. 356-364.

85. Santegoeds, C. M., Ferdelman, T. G., Muyzer, G., & de Beer, D., *Structural and functional dynamics of sulfate-reducing populations in bacterial biofilms.* Applied and Environmental Microbiology, 1998. **64**(10): p. 3731-3739.

86. Santo Domingo, J. W., Revetta, R. P., Iker, B., Gomez-Alvarez, V., Garcia, J., Sullivan, J., & Weast, J., *Molecular survey of concrete sewer biofilm microbial communities.* Biofouling, 2011. **27**(9): p. 993-1001.

87. Mizuno, K., Morishita, Y., Ando, A., Tsuchiya, N., Hirata, M., & Tanaka, K., *Genus-specific and phase-dependent effects of nitrate on a sulfate-reducing bacterial community as revealed by dsrB-based DGGE analyses of wastewater reactors.* World Journal of Microbiology and Biotechnology, 2012. **28**(2): p. 677-686.

88. Norsker, N.H., Nielsen, P.H. & Hvitved-Jacobsen, T., *Influence of oxygen on biofilm growth and potential sulfate reduction in gravity sewer biofilm.* Water Science and Technology, 1995. **31**(7): p. 159-167.

89. Liu, Y., Dong, Q., Wu, C., Zhou, X., & Shi, H., *Study of the succession of microbial communities for sulfur cycle response to ecological factors change in sediment of sewage system.* Environmental Science and Pollution Research, 2015. **22**(12): p. 9250-9259.

90. Okabe, S., Odagiri, M., Ito, T., & Satoh, H., *Succession of sulfur-oxidizing bacteria in the microbial community on corroding concrete in sewer systems.* Appl Environ Microbiol, 2007. **73**(3): p. 971-80.

91. Cayford, B. I., Dennis, P. G., Keller, J., Tyson, G. W., & Bond, P. L., *High-throughput amplicon sequencing reveals distinct communities within a corroding concrete sewer system.* Applied and Environmental Microbiology, 2012. **78**(19): p. 7160-7162.

92. Li, X., Kappler, U., Jiang, G., & Bond, P. L., *The ecology of acidophilic microorganisms in the corroding concrete sewer environment.* Frontiers in microbiology, 2017. **8**.

93. Gu, J. D., Ford, T. E., Berke, N. S., & Mitchell, R., *Biodeterioration of concrete by the fungus Fusarium.* International Biodeterioration and Biodegradation, 1998. **41**(2): p. 101-109.

94. Kyeoung-Suk, C., & Mori, T., *A newly isolated fungus participates in the corrosion of concrete sewer pipes.* Water Science and Technology, 1995. **31**(7): p. 263-271.

95. Tyson, G. W., Chapman, J., Hugenholtz, P., Allen, E. E., Ram, R. J., Richardson, P. M., ... & Banfield, J. F., *Community structure and metabolism through reconstruction of microbial genomes from the environment.* Nature, 2004. **428**: p. 37-43.

96. Ferrer, M., Golyshina, O. V., Beloqui, A., Golyshin, P. N., & Timmis, K. N., *The cellular machinery of Ferroplasma acidiphilum is iron-protein-dominated.* Nature, 2007. **445**(7123): p. 91-94.

97. Olmstead, W., & Hamlin, H., *Converting portions of the Los Angeles outfall sewer into a septic tank.* Engineering news, 1900. **44**(19): p. 317-318.

98. Waksman, S.A., *Microorganisms concerned in the oxidation of sulfur in the soil: a solid medium for the isolation and cultivation of Thiobacillus thiooxidans.* Journal of Bacteriology, 1922. **7**(6): p. 605-608.

99. Parker, C.D., *The corrosion of concrete: 1. The isolation of a species of bacterius associated with the corrosion of concrete exposed to atmospheres containing hydrogen sulphide.* Australian Journal of Experimental Biology and Medical Science, 1945. **23**: p. 81-90.

100. Vishniac, W., *The genus Thiobacillus.* Bergey's manual of determinative bacteriology, 1974.

101. Kelly, D.P., *Genus Thiobacillus.* Bergey's Manual of Systematic Bacteriology, 1989. **vol. 3**: p. 1842–1858.

102. Kelly, D.P., & Wood A.P., *Reclassification of some species of Thiobacillus to the newly designated genera Acidithiobacillus gen. nov., Halothiobacillus gen. nov. and Thermithiobacillus gen. nov.* International Journal of Systematic and Evolutionary Microbiology, 2000. **50**(2): p. 511-516.

103. Nuñez, H., Covarrubias, P. C., Moya-Beltrán, A., Issotta, F., Atavales, J., Acuña, L. G., ... & Quatrini, R., *Detection, identification and typing of Acidithiobacillus species and strains: a review.* Research in Microbiology, 2016. **167**(7): p. 555-567.

104. Nuñez, H., Moya-Beltrán, A., Covarrubias, P. C., Issotta, F., Cárdenas, J. P., González, M., ... & Quatrini, R., *Molecular systematics of the genus Acidithiobacillus: insights into the phylogenetic structure and diversification of the taxon.* Frontiers in microbiology, 2017. **8**.

105. Rawlings, D.E. & Johnson, D.B., *The microbiology of biomining: development and optimization of mineral-oxidizing microbial consortia.* Microbiology, 2007. **153**(2): p. 315-324.

106. Levicán, G., Ugalde, J. A., Ehrenfeld, N., Maass, A., & Parada, P., *Comparative genomic analysis of carbon and nitrogen assimilation mechanisms in three indigenous bioleaching bacteria: predictions and validations.* BMC genomics, 2008. **9**(1): p. 581.

107. Valdés, J., Pedroso, I., Quatrini, R., & Holmes, D. S., *Comparative genome analysis of Acidithiobacillus ferrooxidans, A. thiooxidans and A. caldus: Insights into their metabolism and ecophysiology.* Hydrometallurgy, 2008. **94**.

108. Yin, H., Zhang, X., Li, X., He, Z., Liang, Y., Guo, X., ... & Niu, J., *Whole-genome sequencing reveals novel insights into sulfur oxidation in the extremophile Acidithiobacillus thiooxidans.* BMC Microbiology, 2014. **14**(1): p. 179.

109. Bobadilla Fazzini, R. A., Cortés, M. P., Padilla, L., Maturana, D., Budinich, M., Maass, A., & Parada, P., *Stoichiometric modeling of oxidation of reduced inorganic sulfur compounds (Riscs) in Acidithiobacillus thiooxidans.* Biotechnol Bioeng, 2013. **110**.

110. Rohwerder, T., & Sand, W., *The sulfane sulfur of persulfides is the actual substrate of the sulfur-oxidizing enzymes from Acidithiobacillus and Acidiphilium spp.* Microbiology, 2003. **149**.

111. Leduc, L.G., Ferroni, G.D., & Trevors, J.T., *Resistance to heavy metals in different strains of Thiobacillus ferrooxidans.* World Journal of Microbiology and Biotechnology, 1997. **13**(4): p. 453-455.

112. Dopson, M., Baker-Austin, C., Koppineedi, P. R., & Bond, P. L., *Growth in sulfidic mineral environments: metal resistance mechanisms in acidophilic micro-organisms.* Microbiology, 2003. **149**(8): p. 1959-1970.

113. Das, A., Modak J., & Natarajan K., *Studies on multi-metal ion tolerance of Thiobacillus ferrooxidans.* Minerals Engineering, 1997. **10**(7): p. 743-749.

114. Navarro, C.A., von Bernath, D., & Jerez, C.A., *Heavy metal resistance strategies of acidophilic bacteria and their acquisition: importance for biomining and bioremediation.* Biological research, 2013. **46**(4): p. 363-371.

115. Barreira, R.P.R., Villar, L.D., & Garcia, O., *Tolerance to copper and zinc of Acidithiobacillus thiooxidans isolated from sewage sludge.* World Journal of Microbiology and Biotechnology, 2005. **21**(1): p. 89-91.

116. Caicedo-Ramirez, A., Ling, A.L. & Hernandez, M., *Diffusion susceptibility demonstrates relative inhibition potential of sorbent-immobilized heavy metals against sulfur oxidizing acidophiles.* Journal of Microbiological Methods, 2016. **131**: p. 42-44.

117. Milner, L.F., *Inhibition of sewer crown isolates (Acidophilic thiobacilli) by transition metals.* 1989.

118. Lemire, J. A., Harrison, J. J., & Turner, R. J., *Antimicrobial activity of metals: mechanisms, molecular targets and applications.* Nature Reviews Microbiology, 2013. **11**: p. 372-384.

119. Pham, A. N., Xing, G., Miller, C. J., & Waite, T. D., *Fenton-like copper redox chemistry revisited: Hydrogen peroxide and superoxide mediation of copper-catalyzed oxidant production.* Journal of Catalysis, 2013. **301**(Supplement C): p. 54-64.

120. Nies, D., *Microbial heavy-metal resistance.* Applied Microbiology and Biotechnology, 1999. **51**: p. 730-750.

121. Heuer, H., & Smalla, K., *Plasmids foster diversification and adaptation of bacterial populations in soil.* FEMS microbiology reviews, 2012. **36**(6): p. 1083-1104.

122. Nongkhlaw, M., Kumar, R., Acharya, C., & Joshi, S. R., *Occurrence of Horizontal Gene Transfer of PIB-type ATPase Genes among Bacteria Isolated from the Uranium Rich Deposit of Domiasiat in North East India.* PLOS ONE, 2012. **7**(10): p. e48199.

123. Orellana, L.H., & Jerez, C.A., *A genomic island provides Acidithiobacillus ferrooxidans ATCC 53993 additional copper resistance: a possible competitive advantage.* Applied Microbiology and Biotechnology, 2011. **92**(4): p. 761.

124. Sontheimer, H., Crittenden, J.C., & Summers, R.S., *Activated carbon for water treatment*. 1988: American Water Works Association.

125. Chen, X., Jeyaseelan S., & Graham N., *Physical and chemical properties study of the activated carbon made from sewage sludge.* Waste Management, 2002. **22**(7): p. 755-760.

126. Bandosz, T.J., & Ania, C.O., *Chapter 4 Surface chemistry of activated carbons and its characterization*, in *Interface Science and Technology*, T.J. Bandosz, Editor. 2006, Elsevier. p. 159-229.

127. Figueiredo, J.L. & Pereira, M.F.R., *The role of surface chemistry in catalysis with carbons.* Catalysis Today, 2010. **150**(1): p. 2-7.

128. Yin, C.Y., Aroua, M.K. & Daud, W.M.A.W., *Review of modifications of activated carbon for enhancing contaminant uptakes from aqueous solutions.* Separation and Purification Technology, 2007. **52**(3): p. 403-415.

129. Chen, J., Yiacoumi, S., & Blaydes, T.G., *Equilibrium and kinetic studies of copper adsorption by activated carbon.* Separations Technology, 1996. **6**(2): p. 133-146.

130. Marzal, P., Seco, A., & Gabaldon, C., *Cadmium and Zinc Adsorption onto Activated Carbon : Influence of Temperature , pH and Metal / Carbon Ratio.* 1996: p. 279-285.

131. Uchimiya, M., Lima, I. M., Thomas Klasson, K., Chang, S., Wartelle, L. H., & Rodgers, J. E., *Immobilization of heavy metal ions (CuII, CdII, NiII, and PbII) by broiler litter-derived biochars in water and soil.* Journal of Agricultural and Food Chemistry, 2010. **58**(9): p. 5538-5544.

132. Babić, B. M., Milonjić, S. K., Polovina, M. J., & Kaludierović, B. V., *Point of zero charge and intrinsic equilibrium constants of activated carbon cloth.* Carbon, 1999. **37**(3): p. 477-481.

133. Ober, J.A., *Mineral commodity summaries 2017*. 2017, US Geological Survey.

134. Yildirim, I.Z., & Prezzi, M., *Chemical, mineralogical, and morphological properties of steel slag.* Advances in Civil Engineering, 2011. **2011**.

135. Shi, C., *Steel slag—its production, processing, characteristics, and cementitious properties.* Journal of Materials in Civil Engineering, 2004. **16**(3): p. 230-236.

136. Lewis, D., *Properties and uses of iron and steel slags. National slag association report MF 182-6; Presentation at symposium on slag, South Africa*. 1982.

137. Proctor, D. M., Fehling, K. A., Shay, E. C., Wittenborn, J. L., Green, J. J., Avent, C., ... & Zak, M. A., *Physical and chemical characteristics of blast furnace, basic oxygen furnace, and electric arc furnace steel industry slags.* Environmental Science & Technology, 2000. **34**(8): p. 1576-1582.

138. Waligora, J., Bulteel, D., Degrugilliers, P., Damidot, D., Potdevin, J. L., & Measson, M., *Chemical and mineralogical characterizations of LD converter steel slags: A multi-analytical techniques approach.* Materials Characterization, 2010. **61**(1): p. 39-48.

139. Wang, G.W., *Properties and utilization of steel slag in engineering applications.* 1992.

140. Das, B., Prakash, S., Reddy, P. S. R., & Misra, V. N., *An overview of utilization of slag and sludge from steel industries.* Resources, Conservation and Recycling, 2007. **50**(1): p. 40-57.

141. Tsakiridis, P. E., Papadimitriou, G. D., Tsivilis, S., & Koroneos, C., *Utilization of steel slag for Portland cement clinker production.* Journal of Hazardous Materials, 2008. **152**(2): p. 805-811.

142. Yi, H., Xu, G., Cheng, H., Wang, J., Wan, Y., & Chen, H., *An Overview of Utilization of Steel Slag.* Procedia Environmental Sciences, 2012. **16**(Supplement C): p. 791-801.

143. Huijgen, W.J., Witkamp, G.-J., & Comans, R.N., *Mineral CO2 sequestration by steel slag carbonation.* Environmental Science & Technology, 2005. **39**(24): p. 9676-9682.

144. Ziemkiewicz, P., *Steel slag: Applications for AMD control*. in *Proceedings of the 1998 conference on Hazardous Waste Research*. 1998.

145. Bowden, L. I., Jarvis, A. P., Younger, P. L., & Johnson, K. L., *Phosphorus removal from waste waters using basic oxygen steel slag.* Environmental science & technology, 2009. **43**(7): p. 2476-2481.

146. Zhang, Y.J., & Chai, Q., *Alkali-activated blast furnace slag-based nanomaterial as a novel catalyst for synthesis of hydrogen fuel.* Fuel, 2014. **115**(Supplement C): p. 84-87.

147. Grubb, D. G., Wazne, M., S.C., Jagupilla, & N.E., Malasavage, *Beneficial use of steel slag fines to immobilize arsenite and arsenate: slag characterization and metal thresholding studies.* Journal of Hazardous, Toxic, and Radioactive Waste, 2011. **15**(3): p. 130-150.

148. Lee, J. M., Kim, J. H., Chang, Y. Y., & Chang, Y. S., *Steel dust catalysis for Fenton-like oxidation of polychlorinated dibenzo-p-dioxins.* Journal of Hazardous Materials, 2009. **163**(1): p. 222-230.

149. Zhang, Y. J., Liu, L. C., Xu, Y., & Wang, Y. C., *A new alkali-activated steel slag-based cementitious material for photocatalytic degradation of organic pollutant from waste water.* Journal of Hazardous Materials, 2012. **209**(Supplement C): p. 146-150.

150. Sarperi, L., A., Surbrenat, A., Kerihuel, & F., Chazarenc, The use of an industrial by-product as a sorbent to remove CO2 and H2S from biogas. Journal of Environmental Chemical Engineering, 2014. 2(2): p. 1207-1213.

151. Starosvetsky, J., Zukerman, U., & Armon, R.H., *A simple medium modification for isolation, growth and enumeration of Acidithiobacillus thiooxidans (syn. Thiobacillus thiooxidans) from water samples.* Journal of Microbiological Methods, 2013. **92**(2): p. 178-182.

152. Hobbie, J.E., Daley, R.J., & Jasper, S., *Use of nuclepore filters for counting bacteria by fluorescence microscopy.* Applied and Environmental Microbiology, 1977. **33**(5): p. 1225-1228.

153. Hernandez, M., Marchand, E. A., Roberts, D., & Peccia, J., *In situ assessment of active Thiobacillus species in corroding concrete sewers using fluorescent RNA probes.* International Biodeterioration & Biodegradation, 2002. **49**(4): p. 271-276.

154. Gould, S., Keller, G.-A., & Subramani, S., *Identification of a peroxisomal targeting signal at the carboxy terminus of firefly luciferase.* The Journal of cell biology, 1987. **105**(6): p. 2923-2931.

155. Dojka, M. A., Hugenholtz, P., Haack, S. K., & Pace, N. R., *Microbial diversity in a hydrocarbon-and chlorinated-solvent-contaminated aquifer undergoing intrinsic bioremediation.* Applied and Environmental Microbiology, 1998. **64**(10): p. 3869-3877.

156. Turner, S., Pryer, K. M., Miao, V. P., & Palmer, J. D., *Investigating deep phylogenetic relationships among cyanobacteria and plastids by small subunit rRNA sequence analysis.* Journal of Eukaryotic Microbiology, 1999. **46**(4): p. 327-338.

157. Ye, J., Coulouris, G., Zaretskaya, I., Cutcutache, I., Rozen, S., & Madden, T. L., *Primer-BLAST: a tool to design target-specific primers for polymerase chain reaction.* BMC bioinformatics, 2012. **13**(1): p. 134.

158. Hara, N., Alkanani, A. K., Ir, D., Robertson, C. E., Wagner, B. D., Frank, D. N., & Zipris, D., *Prevention of virus-induced type 1 diabetes with antibiotic therapy.* The Journal of Immunology, 2012. **189**(8): p. 3805-3814.

159. Markle, J. G., Frank, D. N., Mortin-Toth, S., Robertson, C. E., Feazel, L. M., Rolle-Kampczyk, U., ... & Danska, J. S.., *Sex differences in the gut microbiome drive hormone-dependent regulation of autoimmunity.* Science, 2013. **339**(6123): p. 1084-1088.

160. Ewing, B., Hillier, L., Wendl, M. C., & Green, P., *Base-calling of automated sequencer traces usingPhred. I. Accuracy assessment.* Genome research, 1998. **8**(3): p. 175-185.

161. Ewing, B., & Green, P., *Base-calling of automated sequencer traces using phred. II. Error probabilities.* Genome research, 1998. **8**(3): p. 186-194.

162. Edgar, R. C., Haas, B. J., Clemente, J. C., Quince, C., & Knight, R., *UCHIME improves sensitivity and speed of chimera detection.* Bioinformatics, 2011. **27**(16): p. 2194-2200.

163. Schloss, P. D., Gevers, D., & Westcott, S. L., *Reducing the Effects of PCR Amplification and Sequencing Artifacts on 16S rRNA-Based Studies.* PLoS ONE, 2011. **6**(12): p. e27310.

164. Pruesse, E., Peplies, J., & Glöckner, F.O., *SINA: accurate high-throughput multiple sequence alignment of ribosomal RNA genes.* Bioinformatics, 2012. **28**(14): p. 1823-1829.

165. Quast, C., Pruesse, E., Yilmaz, P., Gerken, J., Schweer, T., Yarza, P., ... & Glöckner, F. O., *The SILVA ribosomal RNA gene database project: improved data processing and web-based tools.* Nucleic acids research, 2013. **41**(D1): p. D590-D596.

166. Robertson, C. E., Harris, J. K., Wagner, B. D., Granger, D., Browne, K., Tatem, B., ... & Frank, D. N., *Explicet: Graphical user interface software for metadata-driven management, analysis, and visualization of microbiome data.* Bioinformatics, 2013. **doi: 10.1093/bioinformatics/btt526**.

167. Shepard, R.N., *The analysis of proximities: multidimensional scaling with an unknown distance function. I.* Psychometrika, 1962. **27**(2): p. 125-140.
168. Oksanen, J., et al., *vegan: Community Ecology Package. R package version 2.4-0.* https://CRAN.R-project.org/package=vegan, 2016.

169. Clarke, K. R., *Non-parametric multivariate analyses of changes in community structure.* Austral Ecology, 1993. **18**(1): p. 117-143.

170. Feinstein, L.M., Sul, W.J., & Blackwood, C.B., *Assessment of bias associated with incomplete extraction of microbial DNA from soil.* Applied and Environmental Microbiology, 2009. **75**(16): p. 5428-5433.

171. Martin-Laurent, F., Philippot, L., Hallet, S., Chaussod, R., Germon, J. C., Soulas, G., & Catroux, G., *DNA extraction from soils: old bias for new microbial diversity analysis methods.* Applied and Environmental Microbiology, 2001. **67**(5): p. 2354-2359.

172. Miller, D. N., Bryant, J. E., Madsen, E. L., & Ghiorse, W. C., *Evaluation and optimization of DNA extraction and purification procedures for soil and sediment samples.* Applied and Environmental Microbiology, 1999. **65**(11): p. 4715-4724.

173. Polz, M.F., & Cavanaugh, C.M., *Bias in template-to-product ratios in multitemplate PCR.* Applied and Environmental Microbiology, 1998. **64**(10): p. 3724-3730.

174. Kreader, C.A., *Relief of amplification inhibition in PCR with bovine serum albumin or T4 gene 32 protein.* Applied and Environmental Microbiology, 1996. **62**(3): p. 1102-1106.

175. Opel, K.L., Chung, D., & McCord, B.R., *A study of PCR inhibition mechanisms using real time PCR.* Journal of Forensic Sciences, 2010. **55**(1): p. 25-33.

176. Ross, M. G., Russ, C., Costello, M., Hollinger, A., Lennon, N. J., Hegarty, R., ... & Jaffe, D. B., *Characterizing and measuring bias in sequence data.* Genome Biology, 2013. **14**: p. R51.

177. Calgon Carbon Corporation, *Granular Activated Carbon OL 20x50 Data Sheet*. 2015: Pittsburg, PA, USA.

178. Aligizaki, K.K., *Pore structure of cement-based materials: testing, interpretation and requirements*. 2005: CRC Press.

179. Newcombe, G., Hayes, R., & Drikas, M., *Granular activated carbon: importance of surface properties in the adsorption of naturally occurring organics.* Colloids and Surfaces A: Physicochemical and Engineering Aspects, 1993. **78**: p. 65-71.

180. Prahas, D., Kartika, Y., Indraswati, N., & Ismadji, S., *Activated carbon from jackfruit peel waste by H3PO4 chemical activation: Pore structure and surface chemistry characterization.* Chemical Engineering Journal, 2008. **140**(1): p. 32-42.

181. Boehm, H., *Some aspects of the surface chemistry of carbon blacks and other carbons.* Carbon, 1994. **32**(5): p. 759-769.

182. Goertzen, S. L., Thériault, K. D., Oickle, A. M., Tarasuk, A. C., & Andreas, H. A., *Standardization of the Boehm titration. Part I. CO2 expulsion and endpoint determination.* Carbon, 2010. **48**(4): p. 1252-1261.

183. *ASTM Standard C128 - 15, 2015, Standard Test Method for Relative Density (Specific Gravity) and Absorption of Fine Aggregate, ASTM International, West Conshohocken, PA, 2015, DOI: 10.1520/C0128-15, www.astm.org.*

184. Farrell, R.F., Matthes, S.A., & Mackie, A.J.*, A simple low-cost method for the dissolution of metal and mineral samples in plastic pressure vessels.* Report of Investigations - Bureau of Mines, 1980. **8480**.

185. Eberl, D., *User guide to RockJock-A program for determining quantitative mineralogy from X-ray diffraction data*. 2003, US Geological Survey.

186. Javellana, M. & Jawed, I., *Extraction of free lime in Portland cement and clinker by ethylene glycol.* Cement and concrete research, 1982. **12**(3): p. 399-403.

187. Bauer, A. W., Kirby, W. M., Sherris, J. C., & Turck, M., *Antibiotic susceptibility testing by a standardized single disk method.* American journal of clinical pathology, 1966. **45**(4): p. 493.

188. Lansdown, A., *Silver in health care: antimicrobial effects and safety in use*, in *Biofunctional textiles and the skin*. 2006, Karger Publishers. p. 17-34.

189. Patel, A.K., *Isolation and Characterization of Thiobacillus ferrooxidans from Coal Acid Mine Drainage* International Journal of Applied Agricultural Research, 2010. **5**(1): p. 73-85.

190. Ryu, H. W., Moon, H. S., Lee, E. Y., Cho, K. S., & Choi, H., *Leaching Characteristics of Heavy Metals from Sewage Sludge by Acidithiobacillus thiooxidans MET.* Journal of Environmental Quality, 2003. **32**(3): p. 751-759.

191. American Water Works Association, *Cement-mortar lining for ductile-iron pipe and fittings for water*, in *AWWA standards*. 1996.

192. ASTM C778-17, Standard Specification for Standard Sand, ASTM International, West Conshohocken, PA, 2017, DOI: 10.1520/C0778-17. www.astm.org.

193. Schneider, C.A., Rasband, W.S., & Eliceiri, K.W., *NIH Image to ImageJ: 25 years of image analysis.* Nature methods, 2012. **9**(7): p. 671-675.

194. Schindelin, J., Rueden, C. T., Hiner, M. C., & Eliceiri, K. W., *The ImageJ ecosystem: An open platform for biomedical image analysis.* Molecular reproduction and development, 2015. **82**(7-8): p. 518-529.

195. Tessier, A., Campbell, P.G., & Bisson, M., *Sequential extraction procedure for the speciation of particulate trace metals.* Analytical chemistry, 1979. **51**(7): p. 844-851.

196. Li, X. D., Poon, C. S., Sun, H., Lo, I. M. C., & Kirk, D. W., *Heavy metal speciation and leaching behaviors in cement based solidified/stabilized waste materials.* Journal of Hazardous Materials, 2001. **82**(3): p. 215-230.

197. Donovan, J.J., & Tingle, T.N., *An improved mean atomic number background correction for quantitative microanalysis.* Microscopy and Microanalysis, 1996. **2**(1): p. 1-7.

198. Bruun, S. W., Kohler, A., Adt, I., Sockalingum, G. D., Manfait, M., & Martens, H., *Correcting Attenuated Total Reflection–Fourier Transform Infrared Spectra for Water Vapor and Carbon Dioxide.* Applied spectroscopy, 2006. **60**(9): p. 1029-1039.

199. Silverstein, R. M., Webster, F. X., Kiemle, D. J., & Bryce, D. L., *Spectrometric identification of organic compounds*. 2014: John wiley & sons.

200. Moreno-Castilla, C., Ferro-Garcia, M. A., Joly, J. P., Bautista-Toledo, I., Carrasco-Marin, F., & Rivera-Utrilla, J., *Activated carbon surface modifications by nitric acid, hydrogen peroxide, and ammonium peroxydisulfate treatments.* Langmuir, 1995. **11**(11): p. 4386-4392.

201. Dandekar, A., Baker, R., & Vannice, M., *Characterization of activated carbon, graphitized carbon fibers and synthetic diamond powder using TPD and DRIFTS.* Carbon, 1998. **36**(12): p. 1821-1831.

202. Socrates, G., *"Infrared Characteristic Group Frequencies", Wiley-Interscience, Chichester, 1980.*

203. Cabrera, G., Gómez, J.M., & Cantero, D., *Influence of heavy metals on growth and ferrous sulphate oxidation by Acidithiobacillus ferrooxidans in pure and mixed cultures.* Process Biochemistry, 2005. **40**(8): p. 2683-2687.

204. Cabrera, G., Gómez, J.M., & Cantero, D., *Kinetic study of ferrous sulphate oxidation of Acidithiobacillus ferrooxidans in the presence of heavy metal ions.* Enzyme and Microbial Technology, 2005. **36**(2–3): p. 301-306.

205. Barbič, F.F., *Effects of different compounds of metals and of their mixtures on the growth and survival of Thiobacillus ferrooxidans.* Zeitschrift für allgemeine Mikrobiologie, 1977. **17**(4): p. 277-281.

206. Huirong Lin, G.C., Zhu, S., Chen, Y., Chen, D., Xu, W., Yun, X., & Shi, J., *The Interaction of CuS and Halothiobacillus HT1 Biofilm inMicroscale Using Synchrotron Radiation-Based Techniques.* International Journal of Molecular Sciences, 2013. **14**(6): p. 11113-11124.

207. Bramucci, M., Kane, H., Chen, M., & Nagarajan, V., *Bacterial diversity in an industrial wastewater bioreactor.* Applied Microbiology and Biotechnology, 2003. **62**(5): p. 594-600.

208. Jiang, C. Y., Sheng, X. F., Qian, M., & Wang, Q. Y., *Isolation and characterization of a heavy metal-resistant Burkholderia sp. from heavy metal-contaminated paddy field soil and its potential in promoting plant growth and heavy metal accumulation in metal-polluted soil.* Chemosphere, 2008. **72**(2): p. 157-164.

209. Méndez-García, C., Peláez, A. I., Mesa, V., Sánchez, J., Golyshina, O. V., & Ferrer, M., *Microbial diversity and metabolic networks in acid mine drainage habitats.* Frontiers in Microbiology, 2015. **6**: p. 475.

210. Bhowal, S., & Chakraborty, R., *Five novel acid-tolerant oligotrophic thiosulfate-metabolizing chemolithotrophic acid mine drainage strains affiliated with the genus Burkholderia of Betaproteobacteria and identification of two novel soxB gene homologues.* Research in microbiology, 2011. **162**(4): p. 436-445.

211. Bick, J. A., Dennis, J. J., Zylstra, G. J., Nowack, J., & Leustek, T., *Identification of a new class of 5'-adenylylsulfate (APS) reductases from sulfate-assimilating bacteria.* Journal of Bacteriology, 2000. **182**(1): p. 135-142.

212. Durska, G., *Some properties of methylotrophic bacteria isolated from sewage sludges derived from mechanical and biological sewage treatment plants.* Polish Journal of Microbiology, 2007. **56**(4): p. 251.

213. VVela-Cano, M., Castellano-Hinojosa, A., Vivas, A. F., & Toledo, M. V. M., *Effect of heavy metals on the growth of bacteria isolated from sewage sludge compost tea.* Advances in Microbiology, 2014. **2014**.

214. Anandham, R., Indiragandhi, P., Madhaiyan, M., Kim, K., Yim, W., Saravanan, V. S., ... & Sa, T., *Thiosulfate oxidation and mixotrophic growth of Methylobacterium goesingense and Methylobacterium fujisawaense.* J Microbiol Biotechnol, 2009. **19**(1): p. 17-22.

215. Anandham, R., Indiragandhi, P., Madhaiyan, M., Ryu, K. Y., Jee, H. J., & Sa, T. M., *Chemolithoautotrophic oxidation of thiosulfate and phylogenetic distribution of sulfur oxidation gene (soxB) in rhizobacteria isolated from crop plants.* Research in Microbiology, 2008. **159**(9–10): p. 579-589.

216. Friedrich, C. G., Rother, D., Bardischewsky, F., Quentmeier, A., & Fischer, J., *Oxidation of reduced inorganic sulfur compounds by bacteria: Emergence of a common mechanism?* Applied and Environmental Microbiology, 2001. **67**(7): p. 2873-2882.

217. Padival, N.A., Weiss, J.S., & Arnold, R.G., *Control of Thiobacillus by means of microbial competition: Implications for corrosion of concrete sewers.* Water environment research, 1995. **67**(2): p. 201-205.

218. Socrates, G., *"Infrared Characteristic Group Frequencies", Wiley-Interscience, Chichester, 1980.*

219. Gokce, Y., & Aktas, Z., *Nitric acid modification of activated carbon produced from waste tea and adsorption of methylene blue and phenol.* Applied Surface Science, 2014. **313**(Supplement C): p. 352-359.

220. Do, D.D., & Do, H.D., *A model for water adsorption in activated carbon.* Carbon, 2000. **38**(5): p. 767-773.

221. Moreno-Piraján, J. C., Tirano, J., Salamanca, B., & Giraldo, L., *Activated Carbon Modified with Copper for Adsorption of Propanethiol.* International Journal of Molecular Sciences, 2010. **11**(3): p. 927.

222. Edwin Vasu, A., *Surface Modification of Activated Carbon for enhancement of Nickel (II) adsorption.* Journal of Chemistry, 2008. **5**(4): p. 814-819.

223. Shim, J.-W., Park,, S.-J. & Ryu, S.-K., *Effect of modification with HNO3 and NaOH on metal adsorption by pitch-based activated carbon fibers.* Carbon, 2001. **39**(11): p. 1635-1642.

224. Zhang, T., Yu, Q., Wei, J., Li, J., & Zhang, P., *Preparation of high performance blended cements and reclamation of iron concentrate from basic oxygen furnace steel slag.* Resources, Conservation and Recycling, 2011. **56**(1): p. 48-55.

225. Yildirim, I.Z., & Prezzi, M., *Geotechnical properties of fresh and aged basic oxygen furnace steel slag.* Journal of Materials in Civil Engineering, 2015. **27**(12): p. 04015046.

226. Reddy, A.S., Pradhan, R., & Chandra, S., *Utilization of basic oxygen furnace (BOF) slag in the production of a hydraulic cement binder.* International journal of mineral processing, 2006. **79**(2): p. 98-105.

227. Tossavainen, M., Engstrom, F., Yang, Q., Menad, N., Larsson, M. L., & Bjorkman, B., *Characteristics of steel slag under different cooling conditions.* Waste management, 2007. **27**(10): p. 1335-1344.

228. Ortiz, N., Pires, M., & Bressiani, J., *Use of steel converter slag as nickel adsorber to wastewater treatment.* Waste management, 2001. **21**(7): p. 631-635.

229. Sengupta, A.K., *Environmental separation of heavy metals: engineering processes*. 2001: CRC Press.

230. Inyang, M., Gao, B., Yao, Y., Xue, Y., Zimmerman, A. R., Pullammanappallil, P., & Cao, X., *Removal of heavy metals from aqueous solution by biochars derived from anaerobically digested biomass.* Bioresource technology, 2012. **110**: p. 50-56.

231. Romero, L.C., Bonomo, A., & Gonzo, E.E., *Peanut shell activated carbon: Adsorption capacities for copper (II), zinc (II), nickel (II) and chromium (VI) ions from aqueous solutions.* Adsorption Science & Technology, 2004. **22**(3): p. 237-243.

232. Dimitrova, S., *Metal sorption on blast-furnace slag.* Water Research, 1996. **30**(1): p. 228-232.

233. Xue, Y., Wu, S., & Zhou, M., *Adsorption characterization of Cu (II) from aqueous solution onto basic oxygen furnace slag.* Chemical engineering journal, 2013. **231**: p. 355-364.

234. Smith, K.S., *Metal sorption on mineral surfaces: an overview with examples relating to mineral deposits.* Reviews in economic geology, 1999. **6**: p. 161-182.

235. Contescu, A., Vass, M., Contescu, C., Putyera, K., & Schwarz, J. A., *Acid buffering capacity of basic carbons revealed by their continuous pK distribution.* Carbon, 1998. **36**(3): p. 247-258.

236. Kostura, B., Kulveitova, H., & Leško, J., *Blast furnace slags as sorbents of phosphate from water solutions.* Water research, 2005. **39**(9): p. 1795-1802.

237. Yan, J., Moreno, L., & Neretnieks, I., *The long-term acid neutralizing capacity of steel slag.* Waste Management, 2000. **20**(2-3): p. 217-223.

238. Yüzer, H., Kara, M., Sabah, E., & Çelik, M. S., *Contribution of cobalt ion precipitation to adsorption in ion exchange dominant systems.* Journal of hazardous materials, 2008. **151**(1): p. 33-37.

239. Nielsen, A.H., Hvitved-Jacobsen, T., and Vollertsen, J., *Effect of sewer headspace air-flow on hydrogen sulfide removal by corroding concrete surfaces.* Water Environment Research, 2012. **84**(3): p. 265-273.

240. Wells, T., & Melchers, R., *A collaborative investigation of microbial corrosion of Concrete Sewer Pipe in Australia OzWater 2012 Conference.* Sydney, May, 2012.

241. Cesca, J., Sharma, K., Vuong, L., Yuan, Z., Hamer, G., & McDonald, A., *South Australia Water Corporation's Pro-active Corrosion and Odour Management Strategy Development.* Proceedings of the Water Environment Federation, 2015. **2015**(9): p. 919-935.

242. Grengg, C., Mittermayr, F., Baldermann, A., Böttcher, M. E., Leis, A., Koraimann, G., & Dietzel, M., *Stable isotope signatures within microbial induced concrete corrosion: A field study.* Procedia Earth and Planetary Science, 2015. **13**: p. 68-71.

243. Vincke, E., Verstichel, S., Monteny, J., & Verstraete, W., A new test procedure for biogenic sulfuric acid corrosion of concrete.*Biodegradation*, 1999, *10*(6), 421-428.

244. Herisson, J., van Hullebusch, E. D., Moletta-Denat, M., Taquet, P., & Chaussadent, T., *Toward an accelerated biodeterioration test to understand the behavior of Portland and calcium aluminate cementitious materials in sewer networks.* International Biodeterioration & Biodegradation, 2013. **84**: p. 236-243.

245. Ismail, N., Nonaka, T., Noda, S., & Mori, T., *Effect of carbonation on microbial corrosion of concretes.* Journal of Construction Management and Engineering, 1993. **474**(20): p. 133-138.

246. Jiang, G., Sun, X., Keller, J., & Bond, P. L., *Identification of controlling factors for the initiation of corrosion of fresh concrete sewers.* Water research, 2015. **80**: p. 30-40.

247. Cheng, K., & Zhu, D.-M., *On calibration of pH meters.* Sensors, 2005. **5**(4): p. 209-219.

248. Wei, S., Sanchez, M., Trejo, D., & Gillis, C., *Microbial mediated deterioration of reinforced concrete structures.* International biodeterioration & biodegradation, 2010. **64**(8): p. 748-754.

249. Haile, T., Nakhla, G., Zhu, J., Zhang, H., & Shugg, J., *Mechanistic study of the bactericidal action of silver-loaded chabasite on Acidithiobacillus thiooxidans.* Microporous and Mesoporous Materials, 2010. **127**(1-2): p. 32-40.

250. Wakai, S., Kikumoto, M., Kanao, T., & Kamimura, K., *Involvement of sulfide: quinone oxidoreductase in sulfur oxidation of an acidophilic iron-oxidizing bacterium, Acidithiobacillus ferrooxidans NASF-1.* Bioscience, biotechnology, and biochemistry, 2004. **68**(12): p. 2519-2528.

251. Herisson, J., Guéguen-Minerbe, M., Van Hullebusch, E. D., & Chaussadent, T., *Behaviour of different cementitious material formulations in sewer networks.* Water Science and Technology, 2014. **69**(7): p. 1502-1508.

252. Soleimani, S., Ormeci, B., & Isgor, O.B., *Growth and characterization of Escherichia coli DH5α biofilm on concrete surfaces as a protective layer against microbiologically influenced concrete deterioration (MICD).* Applied microbiology and biotechnology, 2013. **97**(3): p. 1093-1102.

253. Mandl, M., Markova, R., & Lojek, A., *ATP measurements in iron-oxidizing Acidithiobacillus ferrooxidans*. in *Advanced Materials Research*. 2009. Trans Tech Publ.

254. Pakostova, E., Mandl, M., Pokorna, B. O., Diviskova, E., & Lojek, A., *Cellular ATP changes in Acidithiobacillus ferrooxidans cultures oxidizing ferrous iron and elemental sulfur.* Geomicrobiology Journal, 2013. **30**(1): p. 1-7.

255. Mempin, R., Tran, H., Chen, C., Gong, H., Ho, K. K., & Lu, S., *Release of extracellular ATP by bacteria during growth.* BMC microbiology, 2013. **13**(1): p. 301.

256. Johnson, C. A., Kersten, M., Ziegler, F., & Moor, H. C., *Leaching behaviour and solubility—Controlling solid phases of heavy metals in municipal solid waste incinerator ash.* Waste Management, 1996. **16**(1-3): p. 129-134.

257. Roy, A., & Cartledge, F.K., *Long-term behavior of a portland cement-electroplating sludge waste form in presence of copper nitrate.* Journal of Hazardous Materials, 1997. **52**(2–3): p. 265-286.

258. Jiang, G., Wightman, E., Donose, B. C., Yuan, Z., Bond, P. L., & Keller, J., *The role of iron in sulfide induced corrosion of sewer concrete.* Water research, 2014. **49**: p. 166-174.

259. Grengg, C., Baldermann, A., Dietzel, M., Mittermayr, F., Böttcher, M. E., & Leis, A., *Concrete corrosion in an Austrian sewer system*. in *Concrete Repair, Rehabilitation and Retrofitting IV: Proceedings of the 4th International Conference on Concrete Repair, Rehabilitation and Retrofitting (ICCRRR-4), 5-7 October 2015, Leipzig, Germany*. 2015. CRC Press.

260. Grengg, C., Mittermayr, F., Koraimann, G., Konrad, F., Szabó, M., Demeny, A., & Dietzel, M., *The decisive role of acidophilic bacteria in concrete sewer networks: A new model for fast progressing microbial concrete corrosion.* Cement and Concrete Research, 2017. **101**: p. 93-101.

261. Satoh, H., Odagiri, M., Ito, T., & Okabe, S., *Microbial community structures and in situ sulfate-reducing and sulfur-oxidizing activities in biofilms developed on mortar specimens in a corroded sewer system.* Water research, 2009. **43**: p. 4729-39.

262. Okabe, S., Ito, T., Sugita, K., & Satoh, H., *Succession of internal sulfur cycles and sulfur-oxidizing bacterial communities in microaerophilic wastewater biofilms.* Applied and Environmental Microbiology, 2005. **71**(5): p. 2520-2529.

263. Halamickova, P., Detwiler, R. J., Bentz, D. P., & Garboczi, E. J., *Water permeability and chloride ion diffusion in Portland cement mortars: relationship to sand content and critical pore diameter.* Cement and concrete research, 1995. **25**(4): p. 790-802.

264. Kim, Y. Y., Lee, K. M., Bang, J. W., & Kwon, S. J., *Effect of W/C ratio on durability and porosity in cement mortar with constant cement amount.* Advances in Materials Science and Engineering, 2014.

265. Benjamin, M. M., Sletten, R. S., Bailey, R. P., & Bennett, T., *Sorption and filtration of metals using iron-oxide-coated sand.* Water research, 1996. **30**(11): p. 2609-2620.

266. Madzokere, T.C., & Karthigeyan, A., *Heavy Metal Ion Effluent Discharge Containment Using Magnesium Oxide (MgO) Nanoparticles.* Materials Today: Proceedings, 2017. **4**(1): p. 9-18.

267. Rios, R. R. A., Alves, D. E., Dalmázio, I., Bento, S. F. V., Donnici, C. L., & Lago, R. M., *Tailoring activated carbon by surface chemical modification with O, S, and N containing molecules.* Materials Research, 2003. **6**(2): p. 129-135.

268. Terzyk, A.P., *The influence of activated carbon surface chemical composition on the adsorption of acetaminophen (paracetamol) in vitro: Part II. TG, FTIR, and XPS analysis of carbons and the temperature dependence of adsorption kinetics at the neutral pH.* Colloids and Surfaces A: Physicochemical and Engineering Aspects, 2001. **177**(1): p. 23-45.

269. Solum, M. S., R. J. Pugmire, M. Jagtoyen, and F. Derbyshire., *Evolution of carbon structure in chemically activated wood.* Carbon, 1995. **33**(9): p. 1247-1254.